

Synthesis, Characterization, and Applications of Free-base and Metal complexes of β -Thiocyanatocorroles

By

KASTURI SAHU

CHEM11201604018

**National Institute of Science Education and Research,
Bhubaneswar, Odisha**

*A thesis submitted to the
Board of Studies in Chemical Sciences
In partial fulfilment of requirements
for the Degree of*

DOCTOR OF PHILOSOPHY

Of

HOMI BHABHA NATIONAL INSTITUTE

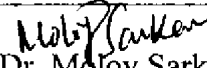


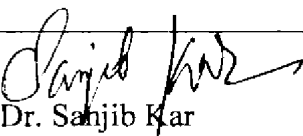
May 2022

Homi Bhabha National Institute¹

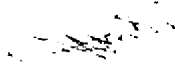
Recommendations of the Viva Voce Committee

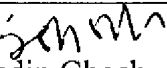
As members of the Viva Voce Committee, we certify that we have read the dissertation prepared by **Ms. Kasturi Sahu** entitled “**Synthesis, Characterization, and Applications of Free-base and Metal complexes of β -Thiocyanatocorroles**” and recommend that it may be accepted as fulfilling the thesis requirement for the award of Degree of Doctor of Philosophy.

Chairman - 
<Name> Dr. Moloj Sarkar Date: 01.09.2022

Guide / Convener - 
<Name> Dr. Sanjib Kar Date: 01.09.2022

Co-guide -

Examiner - 
<Name> Prof. Debabrata Maiti Date: 01.09.2022

Member 1- 
<Name> Dr. Subhadip Ghosh Date: 01.09.2022

Member 2- 
<Name> Dr. C.S Purohit Date: 01.09.22

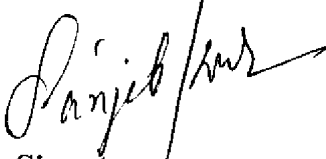
Member 3- 
<Name> Dr. Shantanu Pal Date: 01/09/22

Final approval and acceptance of this thesis is contingent upon the candidate's submission of the final copies of the thesis to HBNI.

I/We hereby certify that I/we have read this thesis prepared under my/our direction and recommend that it may be accepted as fulfilling the thesis requirement.

Date: 01.09.2022

Place: Bhubaneswar, Signature Co-guide (if any)


Signature
Guide

¹ This page is to be included only for final submission after successful completion of viva voce.

STATEMENT BY AUTHOR

This dissertation has been submitted in partial fulfilment of requirements for an advanced degree at Homi Bhabha National Institute (HBNI) and is deposited in the library to be made available to borrowers under rules of the HBNI.

Brief quotations from this dissertation are allowable without special permission, provided that accurate acknowledgement of source is made. Requests for permission for extended quotation from or reproduction of this manuscript in whole or in part may be granted by the Competent Authority of HBNI when in his or her judgment the proposed use of the material is in the interests of scholarship. In all other instances, however, permission must be obtained from the author.

Kasturi Sahu

Kasturi Sahu

DECLARATION

I, hereby declare that the investigation presented in the thesis has been carried out by me.
The work is original and has not been submitted earlier as a whole or in part for a degree/
diploma at this or any other Institution / University.

Kasturi Sahu

Kasturi Sahu

PUBLICATIONS

- #1."Regioselective thiocyanation of corroles and the synthesis of gold nanoparticle–corrole assemblies." **Kasturi Sahu**, Sruti Mondal, Bratati Patra, Tanmoy Pain, Sajal Kumar Patra, Carsten Dosche, and Sanjib Kar. *Nanoscale Adv.*, **2020**, 2, 166-170.
- #2."Photocatalytic C–H thiocyanation of corroles: development of near-infrared (NIR)-emissive dyes." **Kasturi Sahu**, Sruti Mondal, Shaikh M. Mobin, and Sanjib Kar, *J. Org. Chem.*, **2021**, 86, 3324-3333.
- #3."Investigation of the Nature of Intermolecular Interactions in Tetra(thiocyanato)corrolato-Ag(III) Complexes: Agostic or Hydrogen bonded?" **Kasturi Sahu**, Juhi Dutta, Srimoy Nayak, Panisha Nayak, Himansu S. Biswal and Sanjib Kar. *Inorg. Chem*,**2022**,61,6539-46.
- #4. "NIR-Emissive, Singlet-Oxygen–Sensitizing Gold Tetra(thiocyano)corroles. " **Kasturi Sahu**, Sara Angeloni, Jeanet Conradie Marco Villa, Manisha Nayak, Abhik Ghosh, Paola Ceroni, and Sanjib Kar." *DaltonTrans.*, **2022**.
5. "Synthesis of urea derivatives via reductive carbon dioxide fixation into contracted porphyrin analogs." Sajal Kumar Patra, **Kasturi Sahu**, Bratati Patra, Dipak Kumar Sahoo, Sruti Mondal, Payel Mukherjee, Himansu S. Biswal, and Sanjib Kar. *Green Chem.*, **2017**, 19, 5772-5776.
6. "An N, N'-Bridged Corrole" First Example of a N21, N22-Methylene-Bridged Corrole Derivative." Sajal Kumar Patra, **Kasturi Sahu**, Bratati Patra, Sruti Mondal, and Sanjib Kar, *Eur. J. Org. Chem.*, **2018**, 47, 6764-6767.

7. "A new synthesis of porphyrins via a putative trans-manganese (iv)-dihydroxide intermediate." Sruti Mondal, **Kasturi Sahu**, Bratati Patra, Subhrakant Jena, Himansu S. Biswal, and Sanjib Kar. *Dalton Trans.*, **2020**, 49,1424-32.
8. "Large-Scale Green Synthesis of Porphyrins." Sruti Mondal, Tanmoy Pain, **Kasturi Sahu**, and Sanjib Kar, *ACS omega*, **2021**, 6, 22922-22936.
9. "Synthesis, characterization, and application of oxo-molybdenum (V)-Corrolato complexes in epoxidation reactions." Manisha Nayak, Panisha Nayak, **Kasturi Sahu**, and Sanjib Kar, *J. Org. Chem*, **2020**, 85, 11654-11662.

List of publications pertaining to the thesis.

CONFERENCES

1. "N, N' -Bridged corrole: First example of a N^{21} , N^{22} -Methylene-Bridged Corrole Derivative." **Kasturi Sahu** and Sajal Kumar Patra, Sanjib Kar*, National Bioorganic Chemistry Conference (NBCC) held on 22 -24th December, 2018, NISER, Bhubaneswar (**Poster Presentation**)
2. "First example of a N^{21} , N^{22} -Methylene-Bridged Corrole Derivative." **Kasturi Sahu** and Dr. Sanjib Kar*, "Advances in Materials Chemistry and Applications." (AMAC-2019), National Conference held on February 23-24th, 2019, Utkal University, Bhubaneswar. (**Oral Presentation**)
3. "Regioselective thiocyanation of corroles and the synthesis of gold nanoparticle–corrole assemblies." **Kasturi Sahu**, Dr. Sanjib Kar* "Recent Advances in Material Chemistry." (RAMC 2021), National Conference held on 8-9th March, 2021, Utkal University, Bhubaneswar. (**Oral Presentation, Online**)
4. "Photocatalytic C–H thiocyanation of corroles: development of near-infrared (NIR)-emissive dyes." **Kasturi Sahu**, Dr Sanjib Kar*, 2nd International Conference on Main group Molecules to Materials (MMM-II) held on 13-15th December 2021, NISER, Bhubaneswar. (**Poster Presentation, Online**)

Dedicated to...

My Family

ACKNOWLEDGEMENTS

This is a very small way to show my heartfelt gratitude through the expression of thankfulness by words written through each corner of my heart and mind for those who were my companions throughout this whole long journey.

I am grateful to the **Almighty** for beholding me and blessings me giving strength at each step of my life.

The struggles of my **parents** for helping me to grow to this level were much more tedious than my own path of hurdles for which I bow my head for them. The unconditional love, blessings and inspiration from my **family** was more than what one would expect which has strengthened me to face all the hurdles in my journey of life.

I would like to express my gratitude and respect to my supervisor, **Dr. Sanjib Kar**, NISER, for continuous support and kind-heartedness. He gave full freedom for free thinking and work out the problems, which helped me a lot in my research career. His constant support throughout the entire phase of my PhD will be remembered life-long.

I am thankful to the Director, **Prof. S. Panda**, NISER, for providing the laboratory facilities, which help me to complete my research work.

I thank my Doctoral committee members, Chairman **Dr. Moloy Sarkar**, **Dr. Chandra Sekhar Purohit**, **Dr. Subhadip Ghosh**, **Dr. Shantanu Pal** and all other faculties in SCS NISER, especially **Dr. Chandra Sekhar Purohit** for their useful suggestions regarding crystallography and scientific officer **Dr. Arun Kumar** for his support on numerous occasions.

I owe my sincere thanks to my collaborator, **Dr. Himansu Sekhar Biswal**, SCS, NISER for his valuable assistance regarding theoretical studies described in the thesis.

I also want to thank my other collaborators, **Prof. P. Ceroni**, **Prof. A. Ghosh**, and **Dr. C. Dosche**, for helping me explore and expand various aspects of research.

I sincerely thank **Dr. Mriganka**, **Mr. Deepak**, **Mr. Amit**, **Mr. Prakash**, and **Mr. Sanjaya** NISER for performing characterization of my samples.

I am immensely obliged to **all my teachers** of school, graduation and post-graduation who inculcated knowledge, discipline and inspiration for Chemistry.

It gives me enormous pleasure to thank all those seniors, friends and juniors who made my life at NISER certainly gratifying and memorable. Special mention must be made of my lab mates, and special thanks to my seniors **Dr. Bratati Patra, Dr. Sajal Kumar Patra**, and my Junior **Manisha Nayak, Panisha Nayak, Tanmoy Pain, Srimoy Nayak** for their help, support and guidance. No words are enough for my pillar of strength during my Ph.D tenure, my bosom friends **Sagarika Meher, Dr. Syamasrit Dash, Dr. Manjari Chakraborty** and my lab mate **Sruti Mondal**. Thanks a million! My sincere thanks to all my hostel mates, in particular **Prajnashree Panda, Amita Mohapatra, Naupada Priyanka, Dr. Ankita Bal** their friendship and support in all deeds. My special thanks to **Rakesh Ranjan Behera (NISER)** who helped me in most of the GCMS related problems. Also, I would like to acknowledge my special friend **Dr. Belarani Ojha (IIT Bombay)** for her support. Her company will be remembered forever.

I am greatly thankful to all of my family members, particularly my father **Abhaya Kumar Sahu** and my mother **Mrs. Santilata Sahu** and Bada papa **Krushna Chandra Sahu** for their support, suggestions and care.

I am privileged to stay strongly bonded to my beloved brother **Soubhagya Kumar Sahu**, who cared and stood with me whenever I got stuck in any kind of snags.

Finally, I would like to express my earnest gratitude to everyone who contributed for the accomplishment of my course and I express my apology for those whom I could not mention here.

Kasturi Sahu

Kasturi Sahu

CONTENTS

	Page No.
Synopsis	X
List of Tables	XIX
List of Schemes	XX
List of Figures	XXIX
List of Abbreviations	XXVII
Chapter 1	1-49
Chapter 2	50-74
Chapter 3	75-125
Chapter 4	126-156
Chapter 5	157-196

SYNOPSIS

Porphyrins and their generic derivatives (porphyrinoids) are pyrrole-containing macrocycles with intricate pi-conjugation pathways that follow Hückel aromatic character. They regulate vital biological processes like oxygen transport, electron transfer, and photosynthesis in the form of heme and chlorophyll.^{1,2} Porphyrins and their modified derivatives are popular topics of research due to their huge biological significance and varied applications. Increasing or decreasing an atom or *meso* carbon in the inner core leads to expanded or contracted porphyrinoids. Corrole was first reported in 1965 as a contracted porphyrin analog.³ It shares a similar skeletal structure with corrin, along with a 18π electron aromatic system like porphyrin. In 1999, facile synthetic protocols started to be used in corrole research.^{4,5} This led to a lot of new research in the field. Corroles act as trianionic ligands and stabilizes the higher oxidation state of metal. Corroles have numerous other applications besides stabilizing the higher oxidation states of metals. The absorption and emission spectrum of these macrocycles lies in the visible region of the spectrum. These properties enable the use of corroles in a wide variety of applications, including anticancer therapy, as well as photovoltaic research.⁶ With all these diverse applications of corroles, it is clear that they constitute a very important class of compounds.

Scope and Organization of Present Thesis

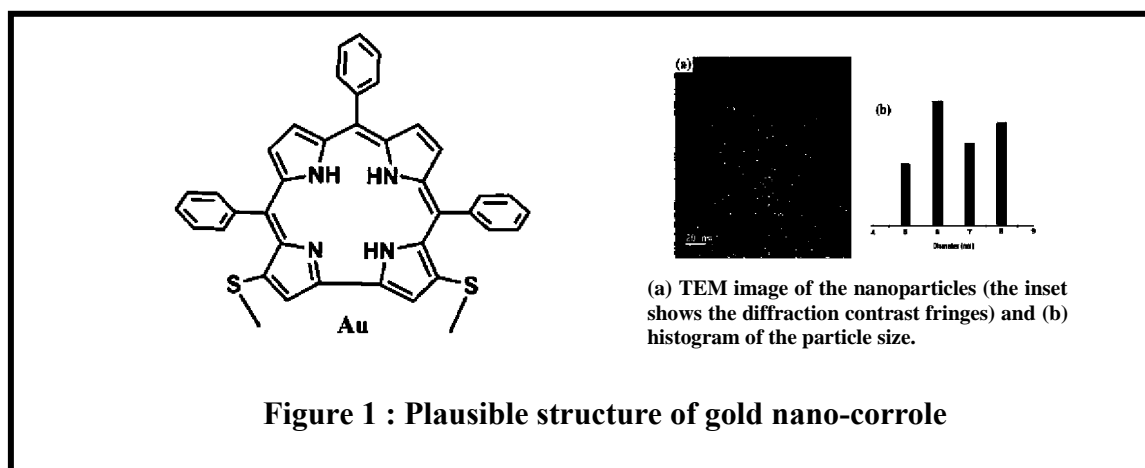
The present thesis describes the new synthetic protocols for corrole functionalization *via* the photo-catalytic process and also *via* the nucleophilic substitution reaction. The newly synthesized corroles have been thoroughly characterized by various spectroscopic techniques including single-crystal XRD analysis. The mechanistic pathway and applications of these free base- corroles and their metallated derivatives have been thoroughly explored. The present thesis contains five chapters, and each chapter has been briefly described below.

CHAPTER 1 Evolution of Corrole its Functionalization and Applications

The first chapter is on modified porphyrinoids corrole, which is a contracted form of the porphyrin macrocycle.^{1,2} Various synthetic procedures and functionalizations are detailed in this section. The different coordination modes of corrole, as well as its capacity to bind metal in higher oxidation states, have been discussed. The diverse uses in catalysis, medicinal chemistry, dye sensitizers in solar cells, and particularly in photodynamic therapy, have been highlighted.⁶

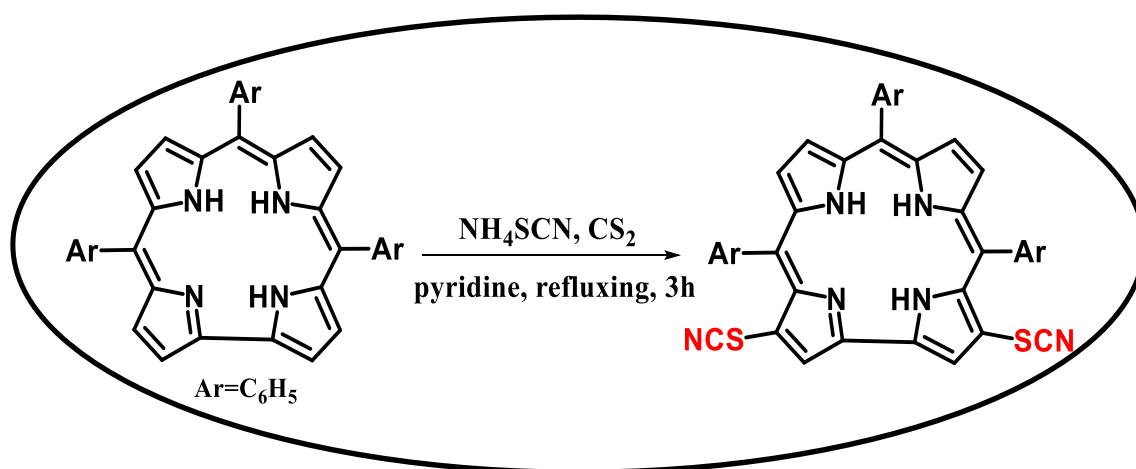
CHAPTER 2 Regioselective thiocyanation of corrole and synthesis of gold nanoparticles and corrole assemblies

Gold nanoparticles (Au NPs) are extensively used in various areas like catalysis, medicine, sensors, fuel cells, surface enhanced Raman spectroscopy, probes for transmission electron microscopy, and antibiotics. One can easily coat the surface of Au NPs with various molecules, either small or big, and thus can fine tune their physical and chemical properties.⁷ In this context, Au NPs bearing π -conjugated molecules are ideal platforms for various nanoelectronic devices.⁸ Thus there is widespread research interest in studying porphyrinoid coated gold nanoparticles.



Corrole, a ring contracted version of porphyrin, has interesting and different photo-physical properties in comparison to porphyrin. Thus, it is expected that corrole coated Au NPs will show great promise in designing newer varieties of functional materials having diverse applications. Tour et al. reported that organic thiocyanates can easily form assemblies on gold surfaces without the help of any external agent and have several

advantages over free thiols or other thiol-based precursors.⁹ Their observations have prompted us to choose the thiocyanato appended corrole as a possible precursor for the synthesis of gold nanoparticle–corrole assemblies. The existing literature reports that *meso*-substituted porphyrinoids are used exclusively as binders for gold nanoparticles, and the related β -substituted derivatives are rarely used for this purpose. As β -substitution has a more pronounced effect on the electronic structure, we have chosen β -substitution at the corrole periphery.



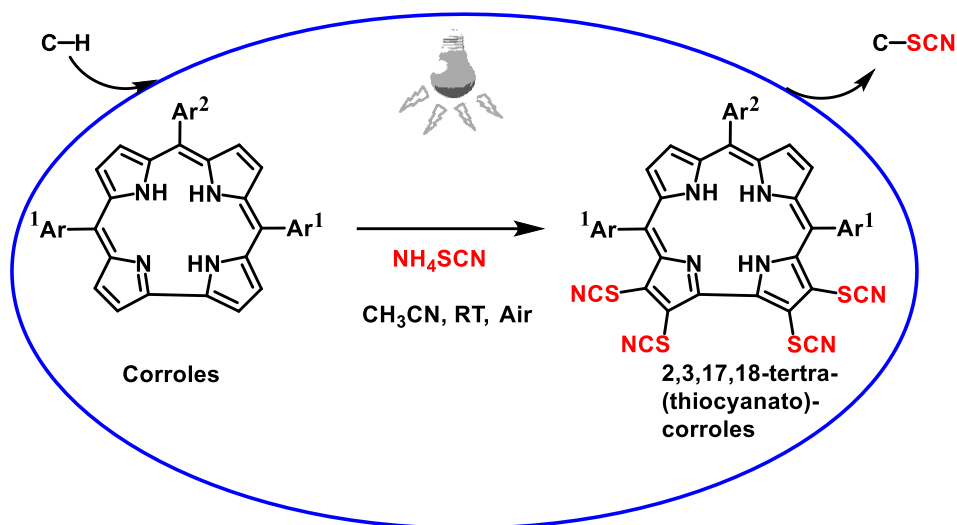
Scheme 1 : Synthetic route to 3,17-bis(thiocyanato)-5,10,15-triphenylcorrole, 1.

5,10,15-triphenylcorrole (TPC) in a carbon disulfide solution was treated with an excess amount of NH₄SCN and excess pyridine. Refluxing for 3 hours resulted in the formation of **1** in good yields (Scheme 1). The thiocyanato appended corrole **1** acts as a stabilizer for gold nanoparticles.

The corrole **1** and the Au nanoparticle hybrid exhibits interesting photo physical properties. The changes in absorption and emission spectra are remarkable and these also clearly indicate that a strong electronic interaction exists between the corrole and the Au nanoparticles. These studies will certainly be helpful in designing various multidentate corrole based ligands in order to stabilize Au nanoparticles with a specific size and functions depending on the choice of corrole framework.

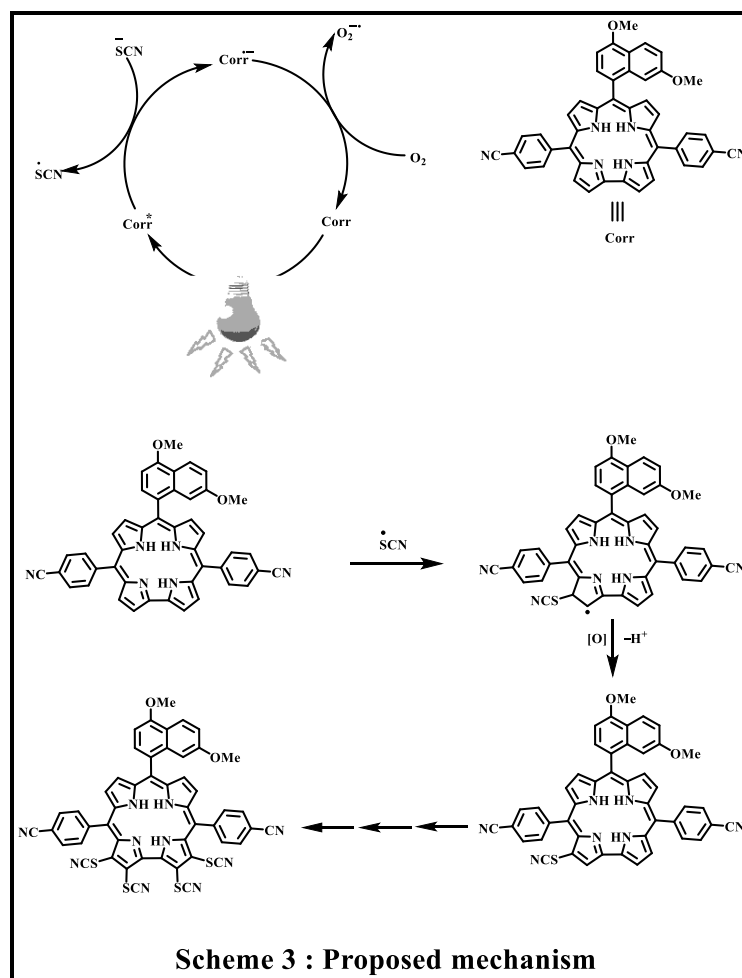
CHAPTER 3 Photocatalytic C–H Thiocyanation of Corroles: Near-Infrared (NIR)

Emissive Dyes.



Scheme 2 : C–H to C–SCN bond conversion

Porphyrinoids are traditionally used as photosensitizers in singlet oxygen generation reactions. However, the applications of porphyrinoids in photo-redox reactions are rather limited. Corrole, a contracted version of porphyrin having 18π -electron has many similarities with porphyrins. The triplet state lifetime of corroles is in the range of 10^{-4} to 10^{-5} s. Similar to porphyrin, corroles also act as a photosensitizer.¹⁰ Although there are few examples of porphyrin as in photo-redox catalysis, similar studies in corroles are still rare. Herein we have reported the application of corroles in photo-catalysis reaction. A unique reaction has been designed, in which corrole acts as a self-catalyst and introduces four thiocyanato groups in the β -pyrrolic positions and thus resulted in the formation of tetrathiocyanato corroles. In order to generalize this photochemical thiocyanation reaction, the substituents at the *meso*-phenyl rings of corroles were varied from electron withdrawing groups to electron donating groups including the unsubstituted phenyl ring.



The newly synthesized corroles have been characterised through various spectroscopic techniques. The mechanistic pathways have been studied thoroughly. The absorption feature of these modified corrole derivatives (both position and intensity) bears a nice similarity with the naturally occurring chromophore, chlorophyll-*a*. Thus, these newly synthesized molecules can be considered as a spectroscopic model for chlorophyll-*a* pigments.¹¹

CHAPTER 4 Investigation of the Nature of Intermolecular Interactions

Tetra(thiocyanato)corrolato-Ag(III) Complexes: Agostic or Hydrogen bonded?

The nature of metal-hydrogen interactions depend on the electronic nature of the metal ion and also on the electronic and steric nature of the coordinated ligands.

Tetra(thiocyanato)corrolato-Ag(III) complexes presented here constitute a new class of

metallo-corrole complexes. The spectroscopic properties of these complexes are quite unusual and interesting. For example, the absorption spectra of these β -substituted corrolato-Ag(III) complexes are very different from the β -unsubstituted corrolato-Ag(III) derivatives. Single-crystal XRD analysis of a representative tetra(thiocyanato)corrolato-Ag(III) derivative reveals C-H...Ag interactions.¹² The C-H...Ag interactions are rarely demonstrated in the crystal lattice of a discrete coordination/organometallic compound. Optimization of the hydrogen positions of the crystal structure discloses the geometrical parameters of the said interaction as Ag...H distance of 2.597 Å and \angle C-H...Ag of 109.62°.¹³ The NBO analysis provides information about the donor-acceptor orbitals involved in the interactions and their interaction energies. It was observed that the $\sigma_{\text{C-H}}$ orbital overlaps with the vacant d-orbital of Ag with an interaction energy of 17.93 kJ/mol. The filled d-orbital of Ag overlaps with the $\sigma^*_{\text{C-H}}$ orbital with interaction energy of 4.79 kJ/mol. The highlights of this work are that the H...Ag distance is outside of the distance range for the typical agostic interaction but fitted with the weak H-bond distance. However, the \angle C-H...Ag angle is within the range of the agostic interaction. Both crystallographic data and electronic structure calculations reveal that these kinds of intermolecular interactions in square-planar d⁸ Ag(III) complexes are intermediate in nature. Thus, they cannot be categorically called either hydrogen bonding or agostic interaction.

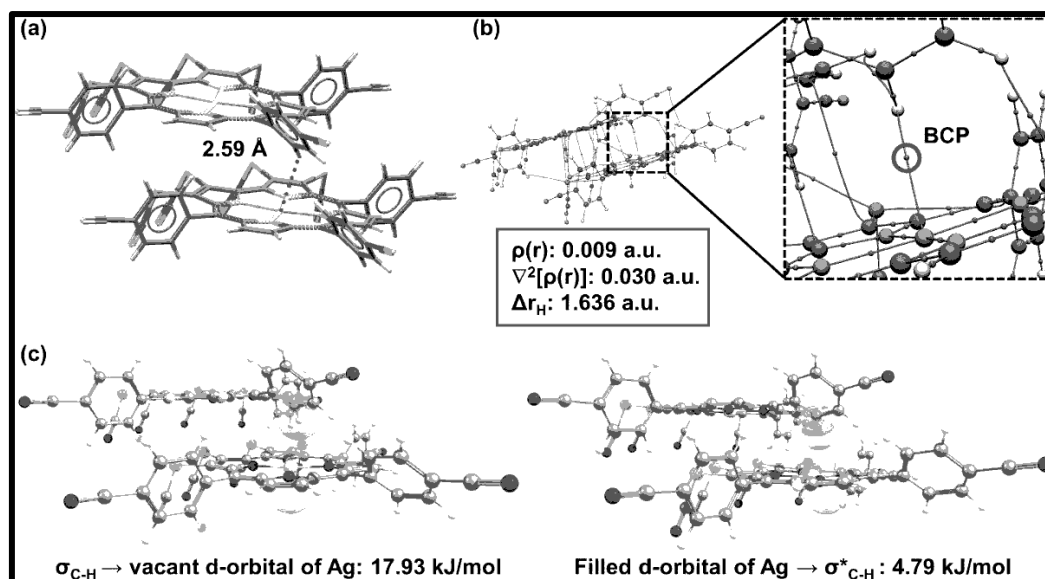


Figure 2 : (a) Hydrogen position optimized structure of dimer of **1** revealing $d_{Ag \cdots H}$ value of 2.59 Å. (b) Noncovalent (c) The Natural Bond Orbital (NBO) analysis of the dimer divulges the orbital overlap between the filled bonding σ_{C-H} orbital and vacant d-orbital of silver atom (σ -donation) along with the overlap between the filled d-orbital of Ag and the vacant antibonding orbital of C-H bond (π -back donation), which gives rise to the total donor-acceptor energy of 22.72 kJ/mol.

CHAPTER 5 Synthesis, Characterization, NIR- Emissive Properties and Singlet oxygen sensitization by Tetra(thiocyanato)corrolato-Au(III) derivatives

The metalloporphyrinoids frequently showed phosphorescence at longer wavelengths and had relatively shorter lifetimes. Due to their superior photophysical properties, they are often used as phosphorescent markers of biomolecules.¹⁴ One of the notable uses of these classes of molecules is in oxygen sensing applications, which arises due to the favourable energy transfer from the triplet state of the metalloporphyrinoid to the ground state of the molecular oxygen. The photosensitizers having superior performance have extensive applications in photodynamic therapy (PDT).¹⁵ Among the various metalloporphyrinoid derivatives, metallo corroles show distinct photophysical properties. In this context, gold corroles are recently attracting considerable research interest. Having a long triplet state lifetime and phosphorescence at ambient temperatures makes them ideal for photoactive

material with emerging applications in various areas. It is worth mentioning that the photophysical properties of gold corroles bearing various substitutions at the *meso*- and β -positions have been described recently. In this context, we have recently reported the synthesis of 2,3,17,18-*tetra*-SCN-substituted corroles. The preliminary photophysical properties of 2,3,17,18-*tetra*-SCN-substituted corroles have demonstrated that their absorption and emission properties are drastically altered while comparing to the unsubstituted parent free-base (FB) corroles.

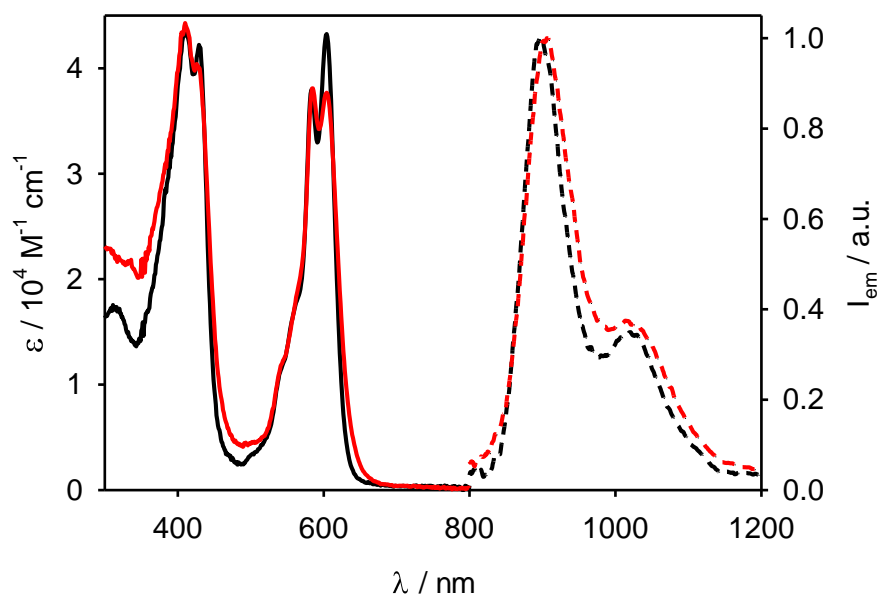


Figure 3: Absorption (solid lines) and normalized phosphorescence spectra (dashed lines) of compounds **1** (black lines) and **2** (red lines) in degassed toluene solution at 298 K. $\lambda_{exc}=410\text{nm}$.

Herein, we have described the synthesis and spectroscopic characterization of two new gold corrole complexes, namely, 2,3,17,18 tetra(thiocyanato)-10-(4-bromophenyl) - 5,15- bis(4- cyanophenyl)corrolato-Au(III)}, **1** and 2,3,17,18-tetrathiocyanato-10-(4,7- dimethoxynaphthalen-1-yl)-5,15- bis(4- cyanophenyl)corrolato-Au(III)}, **2** (Scheme 1). The full spectroscopic and structural characterization of newly synthesized 2,3,17,18-tetrathiocyanato-corrolato-Au(III)

complexes were reported herein. Single-crystal XRD analysis of a representative Au(III) derivative is also presented. The photophysical studies of the newly synthesized 2,3,17,18-tetrathiocyanato-corrolato-Au(III) complexes and their suitability as room temperature near-infrared phosphor is also described. The potential of these complexes in singlet oxygen sensitization is also highlighted.

References

- [1] A. R. Battersby, C. J. R. Fookes, G. W. J. Matcham, E. McDonald, *Nature* **1980**, 285, 17–21.
- [2] R. Kadish, K. M.; Smith, K. M.; Guillard, *The Porphyrin Handbook*, Elsevier, **2003**.
- [3] A. W. Johnson, I. T. Kay, *J. Chem. Soc.* **1965**, 1620–1629.
- [4] Z. Gross, N. Galili, L. Simkhovich, I. Saltsman, M. Botoshansky, D. Bläser, R. Boese, I. Goldberg, *Org. Lett.* **1999**, 1, 599–602.
- [5] R. Paolesse, S. Mini, F. Sagone, T. Boschi, L. Jaquinod, D. J. Nurco, K. M. Smith, *Chem. Commun.* **1999**, 1307–1308.
- [6] I. Aviv-Harel, Z. Gross, *Chem. Eur. J.* **2009**, 15, 8382–8394.
- [7] E. C. Dreaden, A. M. Alkilany, X. Huang, C. J. Murphy, M. A. El-Sayed, *Chem. Soc. Rev.* **2012**, 41, 2740–2779.
- [8] B. C. Sih, M. O. Wolf, *Chem. Commun.* **2005**, 3375–3384.
- [9] G. H. Woehrle, L. O. Brown, J. E. Hutchison, *J. Am. Chem. Soc.* **2005**, 127, 2172–2183.
- [10] A. Mahammed, Z. Gross, *Coord. Chem. Rev.* **2019**, 379, 121–132.
- [11] C. M. Lemon, R. L. Halbach, M. Huynh, D. G. Nocera, *Inorg. Chem.* **2015**, 54, 2713–2725.
- [12] S. Hiroto, K. Furukawa, H. Shinokubo, A. Osuka, *J. Am. Chem. Soc.* **2006**, 128, 12380–12381.
- [13] C. Brückner, *J. Chem. Educ.* **2004**, 81, 1665.
- [14] A. P. Savitsky, A. V Savitskaja, E. A. Lukyanets, S. N. Dashkevich, E. A. Makarova, in *Adv. Fluoresc. Sens. Technol. III*, SPIE, **1997**, 352–357.
- [15] R. W.-Y. Sun, C.-M. Che, *Coord. Chem. Rev.* **2009**, 253, 1682–1691.

LIST OF TABLES

Tables	Description	Page No.
Table 2.1	Crystallographic Data for 1 .	56
Table 3.1	Yield in Different Solvents.	81
Table 3.2	Percentage of Yield.	81
Table 3.3	UV–Vis data ^a in acetonitrile ^b and dichloromethane ^c .	97
Table 3.4	Crystallographic Data for 2 .	101
Table 3.5	Crystallographic Data for 2-Au .	103
Table 4.1	UV–Vis data in dichloromethane.	135
Table 4.2	Crystallographic Data for 1 .	
Table 5.1	Crystallographic Data for 2	166
Table 5.2	UV–Vis and electrochemical data of compounds 1 , 2 , 1a (β -unsubstituted corrolato-Au(III) analogue of compound 1), and 2a (β -unsubstituted corrolato-Au(III) analogue of compound 2) in dichloromethane.	168
Table 5.3	UV–Vis data in dichloromethane.	170
Table 5.4	Most important photophysical data of compounds 1 and 2 in toluene solution at 298 K, unless otherwise noted.	171
Table 5.5	Calculated IPs and EAs (eV).	174
Table 5.6	B3LYP*/ZORA-STO-TZ2P TDDFT results, including transition energies (E) and wavelengths(λ), oscillator strengths (f), MO compositions, and excited state irreps.	175

LIST OF SCHEMES

Scheme	Description	Page No.
Scheme 1.1	a,c-biladienes cyclization to 10-substituted corroles.	9
Scheme 1.2	Tetramerization of pyrrole.	10
Scheme 1.3	Generation of the β -substituted corroles through dipyrranes and bipyrrrole condensation.	11
Scheme 1.4	β -substituted corrole synthesis through desulfuration of thiaphlorin.	11
Scheme 1.5	Synthesis <i>via</i> ring contraction of porphyrin.	12
Scheme 1.6	One pot synthetic route of 5,10,15-triphenyl corrole.	13
Scheme 1.7	Solvent free synthetic route of 5,10,15-tris(pentafluorophenyl) corrole.	14
Scheme 1.8a	Meso-substituted A ₃ -corrole in water-methanol mixture by Gryko <i>et al.</i>	15
Scheme 1.8b	Synthesis of Trans A ₂ B corrole <i>via</i> dipyrromethane and aldehyde.	15
Scheme 1.9	Synthetic route of Palladium metalated 10-azacorrole.	17
Scheme 1.10	Synthetic route of 10-azacorroles by Buchwald-Hartwig reaction.	18
Scheme 1.11	Synthetic route of 21-oxacorrole.	19
Scheme 1.12	Synthetic route of 22-oxacorrole.	19
Scheme 1.13	Synthetic route of 21-thiacorrole.	20
Scheme 1.14	Synthetic route of 21, 24-dioxacorrole.	21
Scheme 1.15	Synthetic route of 10-hetrocorrole with S, Se, O in core position.	22
Scheme 1.16	Synthesis of norcorrole via oxidation.	22
Scheme 1.17	Synthetic Route of Ni(II) norcorrole through intramolecular homocoupling.	23
Scheme 1.18	Synthesis of N-confused corrole and norrole.	24
Scheme 1.19	Synthesis of isocorrole by Vogel and co-workers.	24
Scheme 1.20	Synthetic scheme for chlorination of corrole.	25
Scheme 1.21	Synthesis of β -carboxy triaryl corrole.	26
Scheme 1.22	Formylation of corrole <i>via</i> Vilsmeier reagent.	26
Scheme 1.23	Sulfonation of H ₃ TPFC <i>via</i> sulfuric acid.	28
Scheme 1.24	Synthetic route of vinyl corrole derivative.	29
Scheme 1.25	N-alkylation of β -substituted corrole.	32
Scheme 1.26	Preparation of chiral corroles derivative.	33
Scheme 1.27	Hydroxylation catalysed by Metallocorrole.	35

Scheme	Description	Page No.
Scheme 1.28	Symmetric sulfoxidation by albumin conjugated Metalloporphyrin.	36
Scheme 2.1	Synthetic route to 3, 17- bis (thiocyanato)-5, 10, 15-triphenylporphyrin, 1 .	53
Scheme 3.1.	Structures of the porphyrins 1A-6A and the corresponding 2,3,17,18- tetrathiocyanatoporphyrin derivatives 1-6 .	79
Scheme 3.2	Synthetic application of 2,3,17,18-tetrathiocyanatoporphyrin.	80
Scheme 3.3	Proposed mechanism.	106
Scheme 3.4	Radical trapping reaction with TEMPO.	107
Scheme 3.5	Radical trapping reaction with BHT.	108
Scheme 3.6	Reaction with NH ₄ SCN.	109
Scheme 4.1	Structures of the 2,3,17,18-tetra (thiocyanato) porphyrinato-Ag(III)derivatives (a) 2,3,17,18-tetra (thiocyanato)-5,10,15-tris(4-cyanophenyl) porphyrinato-Ag(III), 1 and (b) 2,3,17,18-tetra (thiocyanato)-10- (4-bromophenyl)-5,15-bis(4-cyanophenyl) porphyrinato-Ag(III), 2 .	129
Scheme 4.2	Synthetic application of 2,3,17,18-tetrathiocyanatoporphyrins Ag(III)	130
Scheme 5.1	(a) 2,3,17,18-tetra(thiocyanato)-10-(4-bromophenyl)-5,15-bis(4-cyanophenyl) porphyrinato-Au(III)}, 1 and (b) 2,3,17,18-tetrathiocyanato-10-(4,7-dimethoxynaphthalen-1-yl)-5,15-bis(4-cyanophenyl) porphyrinato-Au(III)}, 2 .	160
Scheme 5.2	Synthetic application of 2,3,17,18-tetrathiocyanatoporphyrins Au(III).	160

LIST OF FIGURES

Figure	Description	Page No.
Figure 1.1	Various positions of porphyrin.	
Figure 1.2	Structure of porphyrin pigments in biological process.	3
Figure 1.3	Porphyrin with various structural diversity.	4
Figure 1.4	Numbering scheme of porphyrin, corrole, corrin.	7
Figure 1.5	Structure of vitamin B ₁₂ .	6
Figure 1.6	Acid -base tautomerisation.	7
Figure 1.7	Substituted <i>meso</i> -corrole in different category.	13
Figure 1.8	Examples of some heterocorrole macrocycles.	16
Figure 1.9	The products formed when H ₃ TTC reacts with AgNO ₂ /NaNO ₂ .	27
Figure 1.10	Tricationic corrole derivative.	29
Figure 1.11	Cycloaddition product <i>via</i> Diel-Alder reaction.	30
Figure 1.12	Palladium catalysed products.	31
Figure 1.13	Different coordination mode of metallocorrole.	34
Figure 1.14	Metallocorrole used in different catalytic processes.	38
Figure 1.15	Structure of Au (III) corrole and the brominated derivatives as oxygen sensors.	39
Figure 1.16	Ga(III) metalated corrole used as anticancer drugs.	40
Figure 1.17	structures of cationic Ga corrolates.	41
Figure 1.18	Metal complexes used in dye sensitized solar cells.	42
Figure 2.1	¹ H NMR spectrum of 3,17-bis(thiocyanato)-5,10,15-triphenylcorrole, 1 in CDCl ₃ .	53
Figure 2.2	ESI-MS spectrum of 3,17-bis(thiocyanato)-5,10,15-triphenylcorrole, 1 in CH ₃ CN shows (a) the measured spectrum and (b) with isotopic distribution pattern.	54
Figure 2.3	FT-IR spectrum of 1 (---) and Gold nanoparticle-Corrole assemblies (---) as KBr pellet.	54
Figure 2.4	Perspective view of 1 . Hydrogen atoms are omitted for clarity.	55
Figure 2.5	Electronic absorption spectrum of 1 in dichloromethane.	57
Figure 2.6	Electronic emission spectrum (excited at the Soret band) of 1 in CH ₂ Cl ₂ .	57
Figure 2.7	Electronic absorption spectrum of 1 powder.	58
Figure 2.8	Time evolution UV-vis spectra of a mixture of 1 (~10 ⁻⁶ M), NaBH ₄ (~10 ⁻⁴ M), and HAuCl ₄ (~10 ⁻⁵ M) in DMF.	59

Figure	Description	Page No.
Figure 2.9	Plausible structure of gold nano-corrole assemblies.	60
Figure 2.10	Time evolution emission spectra of a mixture of 1 ($\sim 10^{-6}$ M), NaBH ₄ ($\sim 10^{-4}$ M), and HAuCl ₄ ($\sim 10^{-5}$ M) in DMF.	61
Figure 2.11	Fluorescence decay profiles of (a) 1 (-); $\lambda_{em} = 672$ nm and (b) 1-Au NPs (----); $\lambda_{em} = 672$ nm. The red line represents the IRF.	61
Figure 2.12	TEM image of the nanoparticles (the inset shows the diffraction contrast fringes) and (b) histograms of the particle size.	62
Figure 2.13	TEM image of nanoparticle.	62
Figure 2.14	EDS spectrum of 1-Au NP shows the presence of the entire constituent elements: Au, N, and S.	63
Figure 2.15	Electronic absorption spectrum for 1-Au NP .	63
Figure 2.16	N 1s XP spectrum of 1-Au NPs on a Si substrate. Measured data are in black, fitted components are in orange, the background is in green and the sum is in red.	64
Figure 2.17	S 2p spectrum of 1-Au NPs on a Si substrate. Measured data are in black, the fit for bound thiol is in orange, the fit for free thiol is in blue, the fit for oxidized thiol is in dark green, the background is in green and the sum is in red.	65
Figure 3.1	¹ H NMR (400 MHz) spectrum of 1 in CDCl ₃ .	82
Figure 3.2	¹ H NMR (400 MHz) spectrum of 2 in CD ₃ CN.	82
Figure 3.3	¹³ C { ¹ H} NMR (101 MHz) spectrum of 2 in CD ₃ CN.	83
Figure 3.4	¹ H NMR ((400 MHz) spectrum of 3 in CD ₃ CN.	83
Figure 3.5	¹³ C { ¹ H} NMR (101 MHz) spectrum of 3 in CD ₃ CN.	84
Figure 3.6	¹ H NMR (400 MHz) spectrum of 4 in CDCl ₃ .	84
Figure 3.7	¹⁹ F { ¹ H} NMR (377 MHz) spectrum of 4 in CDCl ₃ .	85
Figure 3.8	¹ H NMR (400 MHz) spectrum of 5 in CD ₃ CN.	85
Figure 3.9	¹³ C { ¹ H} NMR (101 MHz) spectrum of 5 in CD ₃ CN.	86
Figure 3.10	¹ H NMR (400 MHz) spectrum of 6 in CD ₃ CN.	86
Figure 3.11	¹³ C { ¹ H} NMR (101 MHz) spectrum of 6 in CD ₃ CN.	87
Figure 3.12	¹ H NMR (400 MHz) spectrum of 2-Au in CDCl ₃ .	87
Figure 3.13	¹³ C { ¹ H} NMR (101 MHz) spectrum of 2-Au in CDCl ₃ .	88
Figure 3.14	FT-IR spectrum of 1(a) , 2(b) and as a KBr pellet.	88
Figure 3.15	FT-IR spectrum of 3(a) , 5(b) and 5(c) as a KBr pellet.	89
Figure 3.16	FT-IR spectrum of 6 (a) and 2-Au(b) as a KBr pellet.	90
Figure 3.17	ESI- MS spectrum of 1 in CH ₃ CN shows the measured spectrum with isotopic distribution pattern.	91
Figure 3.18	ESI- MS spectrum of 2 in CH ₃ CN shows the measured spectrum with isotopic distribution pattern.	91

Figure	Description	Page No.
Figure 3.19	ESI-MS spectrum of 3 in CH ₃ CN shows the measured spectrum with isotopic distribution pattern.	91
Figure 3.20	ESI-MS spectrum of 4 in CH ₃ CN shows the measured spectrum with isotopic distribution pattern.	92
Figure 3.21	ESI-MS spectrum of 5 in CH ₃ CN shows the measured spectrum with isotopic distribution pattern.	92
Figure 3.22	ESI-MS spectrum of 6 in CH ₃ CN shows the measured spectrum with isotopic distribution pattern.	93
Figure 3.23	ESI-MS spectrum of 2-Au in CH ₃ CN shows the measured spectrum with isotopic distribution pattern.	93
Figure 3.24	UV-vis absorption spectra of 5,10,15-tris(pentafluorophenyl) corrole, 4A (green line) and 2,3,17,18-tetrathiocyanato-5,10,15-tris(pentafluorophenyl) corrole, 4 (blue line) in acetonitrile.	94
Figure 3.25	Electronic absorption spectrum of 1 in dichloromethane.	94
Figure 3.26	Electronic absorption spectrum of 2(a) , 3(b) and 4(c) in acetonitrile.	95
Figure 3.27	Electronic absorption spectrum of 5(a) , 6(b) in CH ₃ CN and 2-Au(c) in CH ₂ Cl ₂ .	96
Figure 3.28	Electronic emission spectrum (excited at 687 nm) of 1(a) in dichloromethane and 2(b) (excited at 671 nm) in acetonitrile.	98
Figure 3.29	Electronic emission spectrum of 4(a) (excited at 651 nm), 5(b) (excited at 673 nm) and 6(c) (excited at 670 nm) in acetonitrile.	98
Figure 3.30	Single-crystal X-ray structure of 2 . Hydrogen atoms are omitted for clarity.	100
Figure 3.31	Single-crystal X-ray structure of 2-Au . Hydrogen atoms are omitted for clarity.	102
Figure 3.32	X-ray single-crystal structure analysis of 2-Au , showing C-H...Au interactions [\angle C-H...Au = 108.42° and C-H...Au = 2.838 Å] between neighbouring molecules. The entry in square brackets is the angle and distance.	102
Figure 3.33	EPR spectrum of a mixture of 5,10,15-tris(4-cyanophenyl)corrole and NH ₄ SCN in CH ₃ CN solution under the irradiation of a CFL lamp (20 watts) at 298 K.	105
Figure 3.34	ESI-MS spectrum of the crude reaction mixture in CH ₃ CN shows the (a) measured spectrum with isotopic distribution pattern (experimental) and (b) isotopic distribution pattern (simulated).	108
Figure 3.35	ESI-MS Spectra of the reaction mixture. The peak corresponds to (SCN) ₂ .	109

Figure	Description	Page No.
Figure 3.36	Electronic excitation (black line) and emission (red line) spectra of 5,10,15-tris(4-cyanophenyl)corrole in acetonitrile.	110
Figure 3.37	Cyclic voltammogram (black solid line) of 5,10,15-tris(4-cyanophenyl)corrole in CH ₃ CN. The potentials are vs. SCE.	110
Figure 3.38	Cyclic voltammogram (black solid line) of NH ₄ SCN in CH ₃ CN. The oxidation occurred at 0.65V. The potentials are vs. SCE.	111
Figure 4.1	¹ H NMR (400 MHz) spectrum of 1 in CDCl ₃ .	131
Figure 4.2	¹ H NMR (400 MHz) spectrum of 2 in CDCl ₃ .	131
Figure 4.3	ESI- MS spectrum of 1 in CH ₃ CN shows the measured spectrum with the isotopic distribution pattern.	132
Figure 4.4	ESI- MS spectrum of 2 in CH ₃ CN shows the measured spectrum with the isotopic distribution pattern.	132
Figure 4.5	FT-IR spectrum of 1 and 2 as a KBr pellet.	133
Figure 4.6	Electronic absorption spectrum of 1 in dichloromethane.	134
Figure 4.7	Electronic absorption spectrum of 2 in dichloromethane.	134
Figure 4.8	Single-crystal X-ray structure of 1 . Hydrogen atoms are omitted for clarity.	135
Figure 4.9	Two adjacent molecules in the molecular stack of complex 1 (highlighting the C-H...Ag interactions). Selected bond distance (Å) and angle (°): C28-H28...Ag1 = 2.608 Å and <C28-H28...Ag1 = 108.1°. All hydrogen atoms, except the one in close contact with the Ag(III), have been omitted for clarity.	135
Figure 4.10	ORTEP diagram of 1 . Hydrogen atoms are omitted for clarity. Ellipsoids are drawn at 50% probability.	137
Figure 4.11	(a) Hydrogen position optimized structure of dimer of 1 revealing d Ag...H value of 2.59 Å. (b) Noncovalent (c) The Natural Bond Orbital (NBO) analysis of the dimer divulges the orbital overlap between the filled bonding σ _{C-H} orbital and vacant d-orbital of silver atom (σ-donation) along with the overlap between the filled d-orbital of Ag and the vacant antibonding orbital of C-H bond (π-back donation), which gives rise to the total donor-acceptor energy of 22.72 kJ/mol.	140
Figure 5.1	¹ H NMR (400 MHz) spectrum of 1 in CDCl ₃ .	161
Figure 5.2	¹ H NMR (400 MHz) spectrum of 2 in CDCl ₃ .	162
Figure 5.3	ESI- MS spectrum of 1 in CH ₃ CN shows the measured spectrum with isotopic distribution pattern.	163
Figure 5.4	ESI- MS spectrum of 2 in CH ₃ CN shows the measured spectrum with isotopic distribution pattern.	163
Figure 5.5	FT-IR spectrum of 1 and 2 as a KBr pellet.	164

Figure	Description	Page No.
Figure 5.6	Single-crystal X-ray structure of 2 . Hydrogen atoms are omitted for clarity.	165
Figure 5.7	ORTEP diagram of 2 . Hydrogen atoms are omitted for clarity. Ellipsoids are drawn at 50% probability.	165
Figure 5.8	Cyclic voltammogram (black solid line) and differential pulse voltammogram (black dash-dot line) of 2 in CH ₂ Cl ₂ under a nitrogen atmosphere. The potentials are vs. Ag/AgCl.	167
Figure 5.9	(a) Electronic absorption spectra of compounds 1 and 1a (β -unsubstituted corrolato-Au(III) analogue of compound 1)	169
Figure 5.10	(b) Electronic absorption spectra of compounds 2 and 2a (β -unsubstituted corrolato-Au(III) analogue of compound 2)	169
Figure 5.11	Excitation (dashed line) and absorption spectra (solid line) of compound 1 (a) and 2 (b) in deaerated toluene solution ($\lambda_{em}=900$ nm).	170
Figure 5.12	Absorption (solid lines) and normalized phosphorescence spectra(dashed lines) of compounds 1 (black lines) and 2 (red lines) in degassed toluene solution at 298 K. $\lambda_{exc}=410$ nm.	172
Figure 5.13	Selected distances (Å) in the optimized geometries of Au[TPC] and Au[TPC(SCN) ₄].	173
Figure 5.14	Simulated TD-B3LYP*-COSMO optical spectra Au[TPC] and Au[TPC(SCN) ₄] in dichloromethane.The vertical lines represent calculated transitions which have then been broadened with Gaussians to generate the simulated spectra.	175
Figure 5.15	Selected frontier MOs, along with their irreps and orbital energies, of Au[TPC] and Au[TPC(SCN) ₄].	176
Figure 5.16	B3LYP*-D3/STO-TZ2P Kohn-Sham MO energy (eV) level diagram of Au[TPC] and Au[TPC(SCN) ₄], in dichloromethane modelled with COSMO. Selected frontier MOs, along with their irreps and orbital energies shown. Unoccupied MOs are shown in red and occupied MOs in blue	177

LIST OF ABBREVIATIONS

^1H NMR	Proton Nuclear Magnetic Resonance
^{13}C NMR	Carbon-13 Nuclear Magnetic Resonance
^{19}F NMR	Fluorine-19 Nuclear Magnetic Resonance
UV-Vis	Ultraviolet–Visible
ESI	Electrospray Ionization
GOF	Goodness of Fit
CCDC	Cambridge Crystallographic Data Centre
DFT	Density Functional Theory
TD-DFT	Time-Dependent Density Functional Theory
DDQ	2,3-Dichloro-5,6-dicyano-1,4-benzoquinone
CH_2Cl_2	Dichloromethane
CHCl_3	Chloroform
EtOAc	Ethyl acetate
CH_3CN	Acetonitrile
CH_3OH	Methanol
THF	Tetrahydrofuran
TBAP	Tetrabutylammonium perchlorate
DMF	Dimethylformamide
Chloranil	Tetrachloro-1,4-benzoquinone
NaBH_4	Sodium borohydride
$\text{C}_6\text{F}_5\text{CHO}$	Pentafluoro benzaldehyde
NEt_3	Triethylamine
HOMO	Highest Occupied Molecular Orbital
HBr	Hydrogen Bromide
LUMO	Lowest Unoccupied Molecular Orbital
CO	Carbon monoxide
HCl	Hydrogen chloride
TFA	Trifluoroacetic acid
KOH	Potassium Hydroxide
CaH_2	Calcium Hydride
TMS	Tetramethylsilane

CDCl ₃	Deuterated chloroform
CD ₂ Cl ₂	Dideuteromethylenechloride
CD ₃ CN	Deuterated acetonitrile
Φ	Quantum Yield
ε	Molar absorption coefficient
FB	Free-Base
TLC	Thin Layer Chromatography
Na ₂ SO ₄	Sodium sulphate
Pd(OAc) ₂	Palladium acetate
FeCl ₃	Iron(III) chloride
Anal.Calc	Analytically calculated

Evolution of Corrole: its Functionalization and Applications

1.1 Porphyrin

1.2 Structural Modifications of Porphyrin

1.3 Corrole

1.3.1 Spectroscopic and Structural Properties of Corroles

1.3.2 General Synthetic Protocol for Corrole Synthesis

1.3.2.1 From a,c-biladienes

1.3.2.2 Pyrrole Tetramerization

1.3.2.3 Synthesis via 2, 2'- Bipyrrrole and Dipyrranes

1.3.2.4 From ring-contraction of macrocycles

1.3.2.5 One-pot synthesis

1.3.2.6 A modified synthetic pathway *via* water -methanol-acid system

1.4.1 Heterocorrole

1.4.2 Norcorrole

1.4.3 N-confused and Neo-confused Corroles

1.4.4 Isocorroles

1.5 Functionalization of Corrole

1.5.1 Peripheral Functionalization

1.5.2 Corrole Post-Functionalization

1.5.3 Inner Core Positions Functionalization

1.6 Metalloporroles

1.6.1 Coordination Mode of Metalloporrole

1.7 Corrole and Metalloporrole Applications

1.1 Porphyrin

Porphyrins are naturally occurring tetrapyrrolic macrocycles regarded as "Pigments of Life."^[1] The tetrapyrrolic moiety consists of two amine and two imine nitrogens connected by four methine/*meso* carbon bridges. The inner core contains 16 atoms in a macrocyclic framework, with 18π conjugated electrons exhibiting aromatic features. Porphyrins and the related macrocyclic compounds (chlorin and corrin) act as cofactors in various biological functions. Hemes, **2**, are the important bio-catalyst^[2,3] and oxygen carriers in blood, **3**,^[4,5] while chlorophylls, **1**,^[6,7] (Figure 1.2) play a vital role in photosynthesis. Indeed, several biological processes are performed or catalysed by heme-containing proteins, **4**. Hence porphyrin research has a wide variety of applications in natural sciences, organic photovoltaic cells, bioimaging probes, chemo sensors, conductive organic materials, light-emitting diodes, NIR dyes, molecular wires, and so forth. They have lately been employed as efficient sensitizers for photodynamic therapy (PDT) and photosensitizing drug for cancer treatment.^[8] The word porphyrin is derived from the Greek word "Porphyra" which means purple colour due to the intense purple colour of porphyrins and porphyrin derivatives. Porphyrins show remarkable absorption spectra in the blue (Soret bands) and red part (Q-band) of the visible spectrum. Their properties can be tuned up by synthetic modifications at the periphery (*meso*- and β -positions). (Figure 1.1) The NMR spectrum analysis shows the diamagnetic current outside the cavity, which results in the deshielding of the pyrrolic β -CH protons and *meso* protons. In contrast, the inner NH proton is shielded due to the paramagnetic ring current. The versatility of porphyrin chemistry and its diverse applications has inspired researchers to synthesize new derivatives of porphyrins and their analogues for the past three decades.

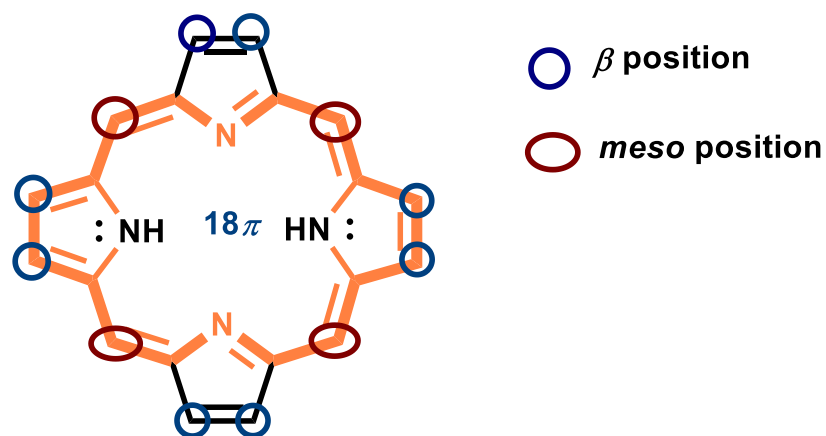
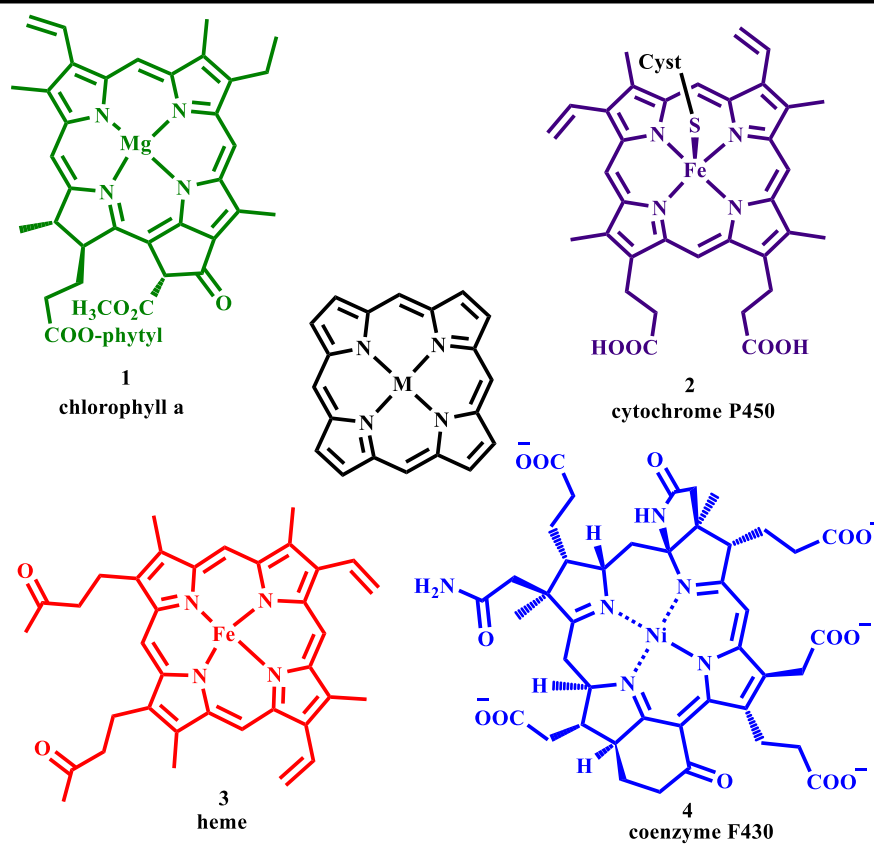
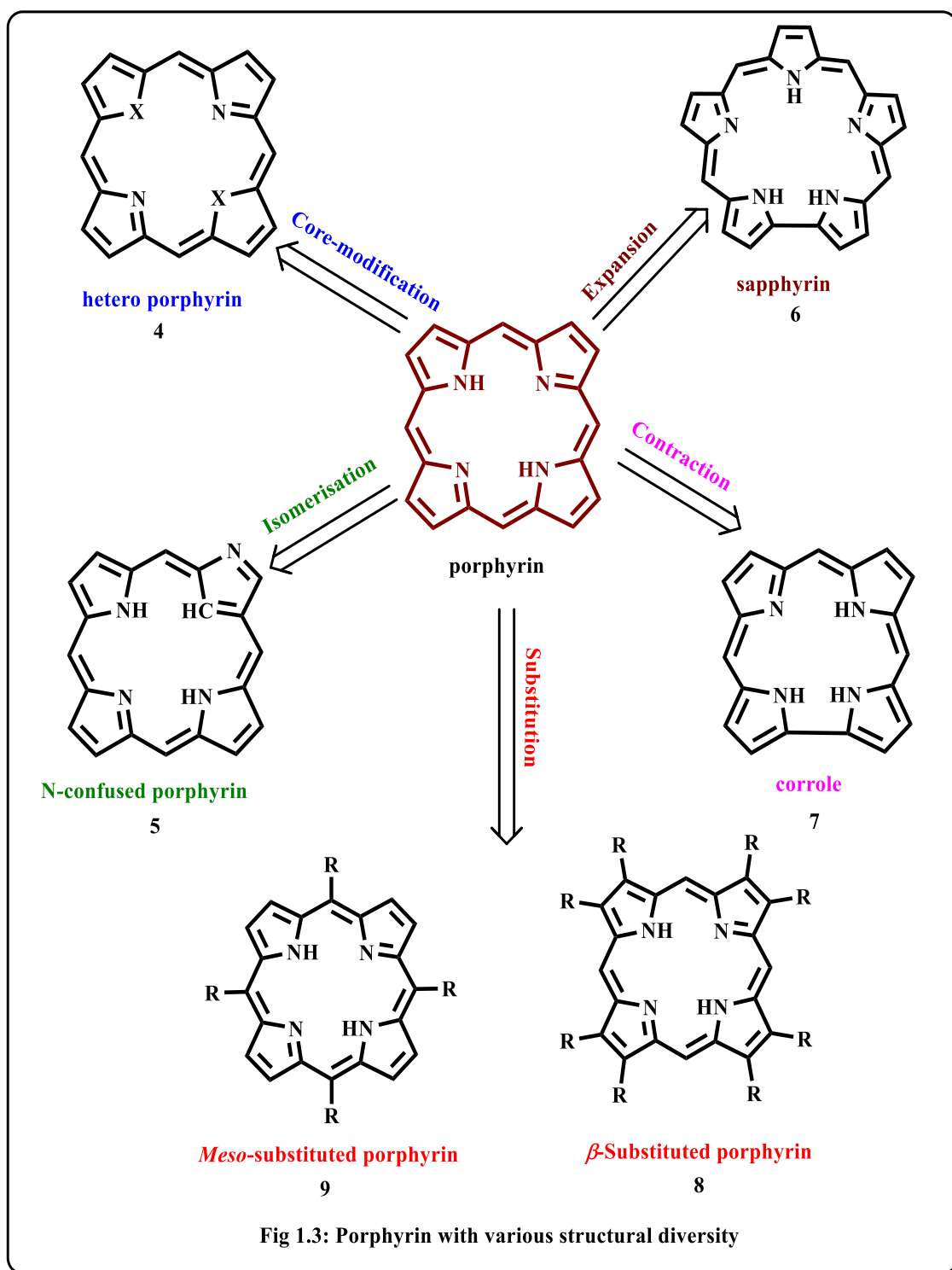


Fig 1.1: Various positions of porphyrin

Fig 1.2: Structure of porphyrin pigments in biological process^{2,3}



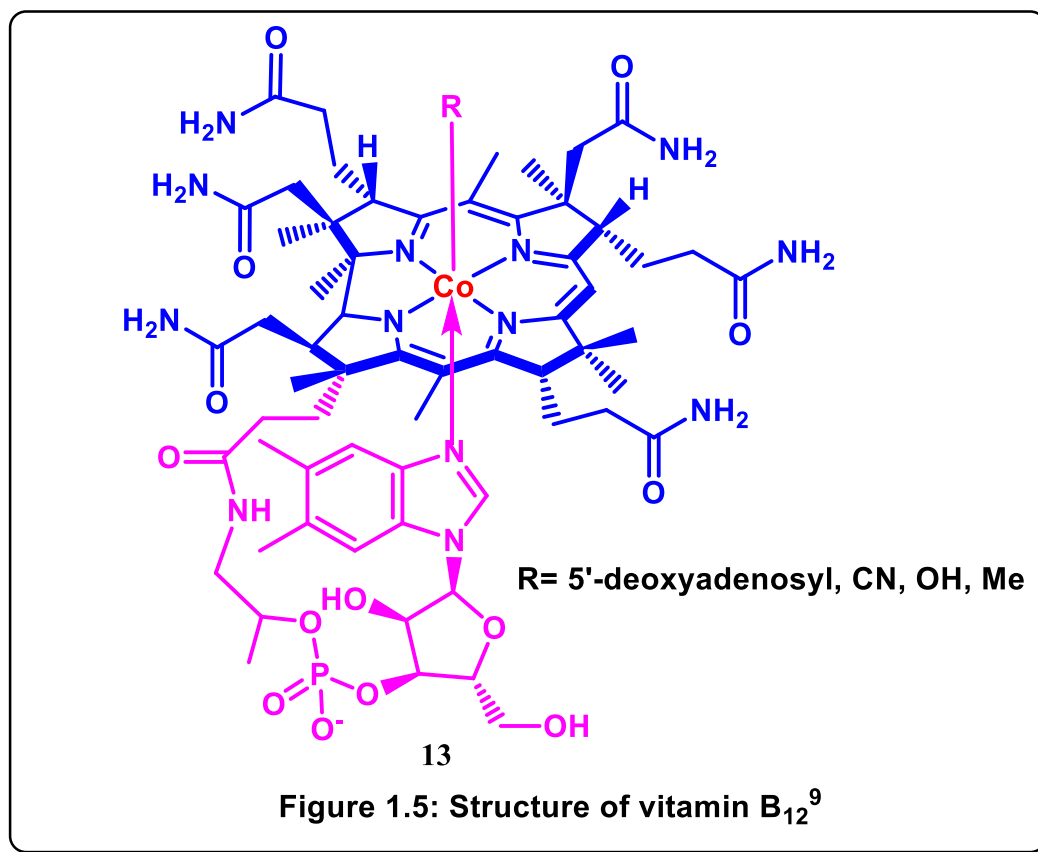
1.2 Structural Modifications of Porphyrin

Several modifications such as; contraction of the ring by decreasing the number of pyrrole rings,^[9] expansion of the ring by adding more pyrrole rings in conjugation,^[10] replacement of one or more pyrrole rings by other heterocyclic rings such as furan and

thiophene, and new isomers of porphyrins have been done to exploit their rich chemistry as well as their diverse functional applications. These types of porphyrinoids are classified into various categories, as shown in Figure 1.3. Expanded porphyrins are the synthetic analogues of porphyrins possessing a large central core with more than 16 atoms in their conjugated structural framework.^[11] The chemistry of expanded derivatives has flourished in recent years with the goal of investigating the possibility of stabilising higher oxidation states of metal ions, studying the change in their aromatic behaviour, and also of determining their binding affinities to anionic and neutral species. In contrast, contracted porphyrins are formed by decreasing one or more pyrrolic units or some *meso* carbon units in the porphyrin framework, leading to an increase in the π electron conjugation.^[10]

1.3 Corrole

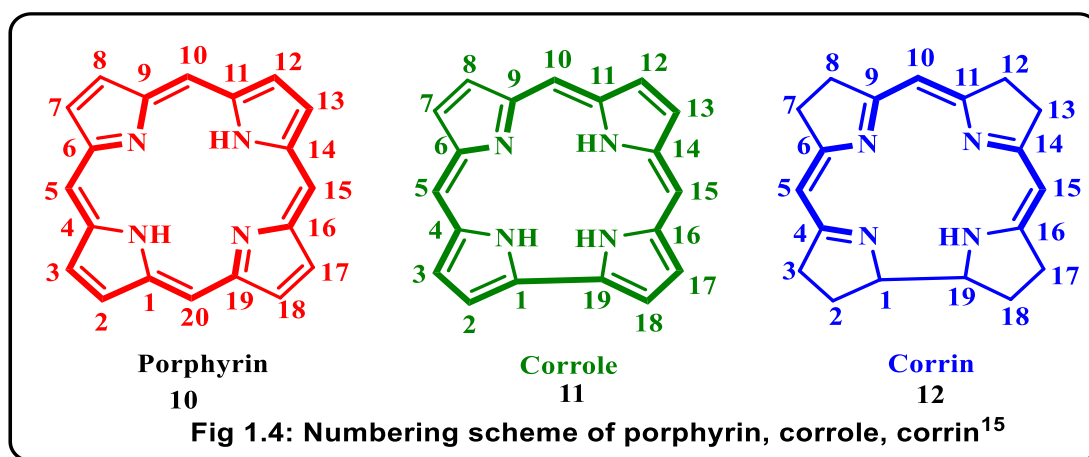
Corroles are tetrapyrrolic macrocycles with a straight pyrrole-pyrrole connection and a structural framework containing 19 atoms, resulting in a contracted cavity in comparison to porphyrin.^[12] The similarity of corrole with the cobalt chelating corrin ring in vitamin B₁₂. (Figure 1.5) was the apparent motivation for its synthesis by Johnson and Kay in 1964.^[13] The free base corrole structure was established by Hodgkin and co-workers through X-ray crystallography in 1971.^[14] Numerous studies have been conducted since Gross *et al.*, and Paolesse *et al.*, have introduced simple one-pot synthetic procedures. Both the technique involves the direct reaction between aldehyde and pyrrole; the only difference is that the Gross method consists of the solvent-free reaction with basic alumina as a catalyst, while in the Paolesse process, acid is used as a solvent. Since then, for almost 15 years, corrole chemistry has been studied, along with porphyrin, exploring its potential applications.



Corroles and porphyrins have many similarities, like both the compounds are 18π conjugated aromatic systems and share similar photophysical properties. The IUPAC numbering of both the structure with corrin ring is shown in Figure 1.4. In the case of corrole, one of the *meso*-carbons, C-20, is missing, and because of that, two pyrrole rings at that position are directly connected by a bond between C-1 and C-19 (Figure 1.4). The numbering of the corrole ring structure is derived from the porphyrin ring.^[15] The inner core of the corrole ring contains three amino nitrogens and one imino nitrogen, and these NH protons tautomerize very rapidly in the freebase corrole.^[16]

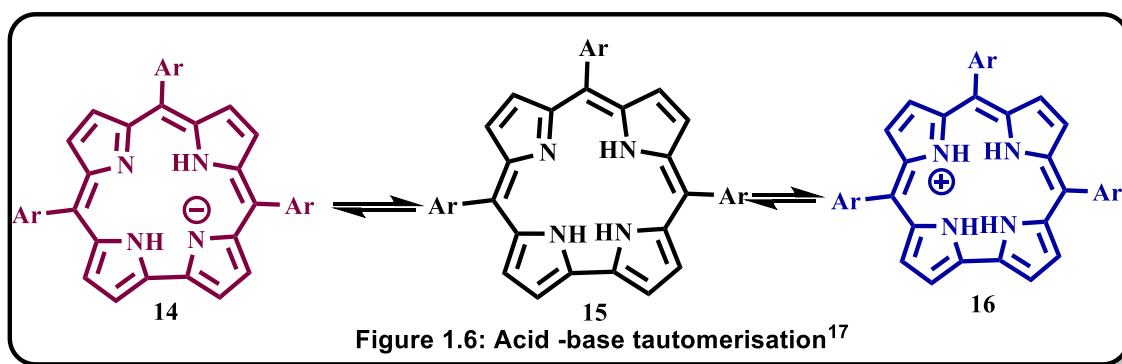
1.3.1 Spectroscopic and Structural Properties of Corroles

The primary structural distinction between corroles and porphyrins is that the former has a somewhat smaller N₄ coordination core, acting as a trianionic instead of dianionic ligand.



This leads to a decrease in the symmetry of corrole. Thus, corrole is more acidic than porphyrin; hence the anionic species of corrole is easily formed in organic solvents with the addition of the bases (Figure 1.6).^[12] However, in the reaction with dilute acid, they generate mono protonated species.^[13,17] Both the monoanionic and monoprotonated forms of corroles are found to retain aromaticity as indicated by the presence of Soret bands in their electronic absorption spectrum.

The structure of corrole synthesized by Johnson *et al.*, was finally elucidated in 1971 by Hodgkin and co-workers.^[14] The 8,12-diethyl-2,3,7,13,17,18-hexamethyl corrole that was studied was found not to be strictly planar. The deviation from planarity is due to the short N-N distance because of direct C(1)-C(19) connection. Most accurate structural data were obtained in 1999, from the XRD data analysis of 5,10,15-tris(pentafluorophenyl) corrole.^[18]



The X-ray data of crystals were collected at low temperatures (116 K), which offer the hydrogen atoms' precise location in the reported corrole. The pyrrole rings are slightly altered from the mean plane with the angles of 4.4- 19.5°. Only one NH is almost in the mean plane in the inner cavity, while the other two are present above and below the plane.

The electronic spectra of corroles are pretty similar to the porphyrins. Both display intense blue band called Soret band that appears around 400 nm and several Q-bands around 500-650 nm.^[13,19] The fluorescence intensity of the several corroles is much higher than porphyrins, and the lifetime falls in the range of 3.3-3.9 ns. The emission spectrum of corroles is present in the visible range.^[19]

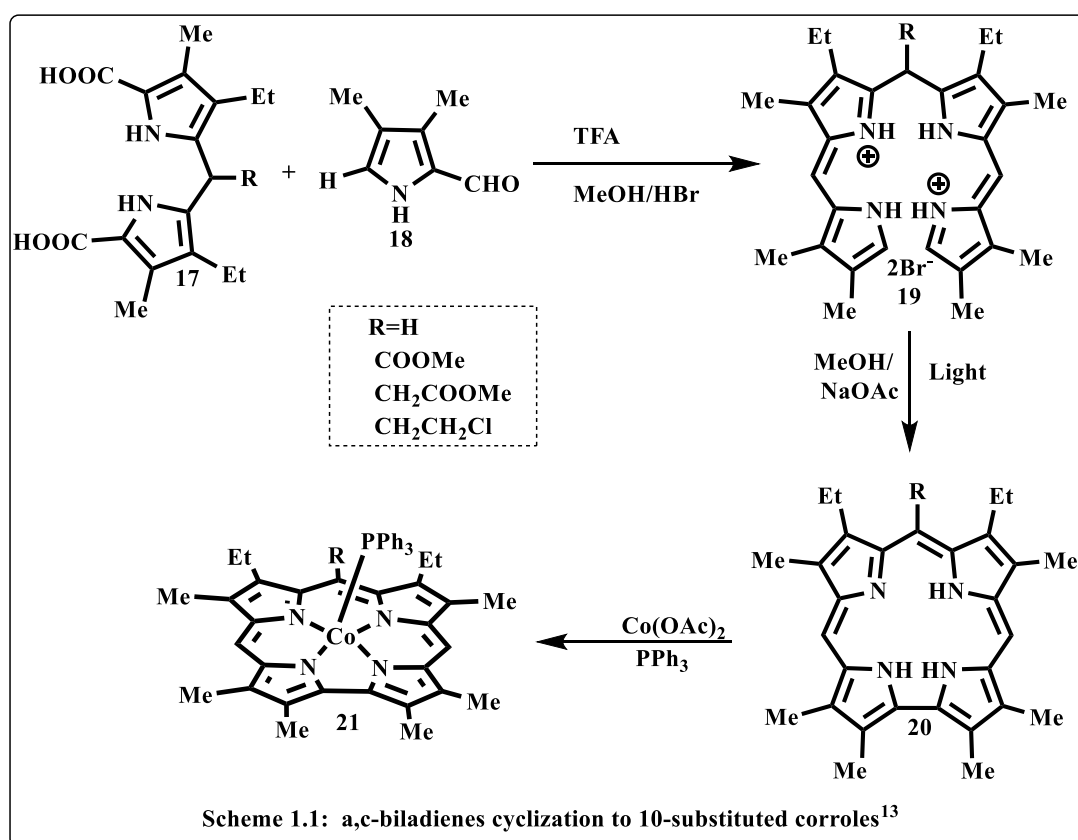
¹H NMR spectra of corroles exhibit a strong deshielding for *meso* and the β - substituted protons. The peaks of *meso* protons lie in the ranges 8-9 ppm, and β - protons appear at ~10 ppm. This diatropic ring current indicates the aromatic nature of the ring. Since the imino protons of the inner core fall in the shielding region of the ring current, they appear upfield with respect to TMS, in the region of -2.00 to -3.00 ppm, as a broad singlet. The broadness has been assigned due to two reasons: non-identical tautomers and the highly acidic nature of the corrole core.^[20] However, three distinct singlets corresponding to the three different types of NH protons have been observed at low temperatures (below 226 K) in some of the cases.

1.3.2 General Synthetic Protocol for Corrole Synthesis

The first corrole was accidentally synthesized by Johnson and Kay while they were trying to synthesize the corrin ring of vitamin B₁₂ via cyclization of a,c-biladienes. This synthetic method was frequently used for the synthesis of corrole until 1999.^[13] The process is quite tedious, precursors preparation is quite lengthy, and the yield is unsatisfactory.

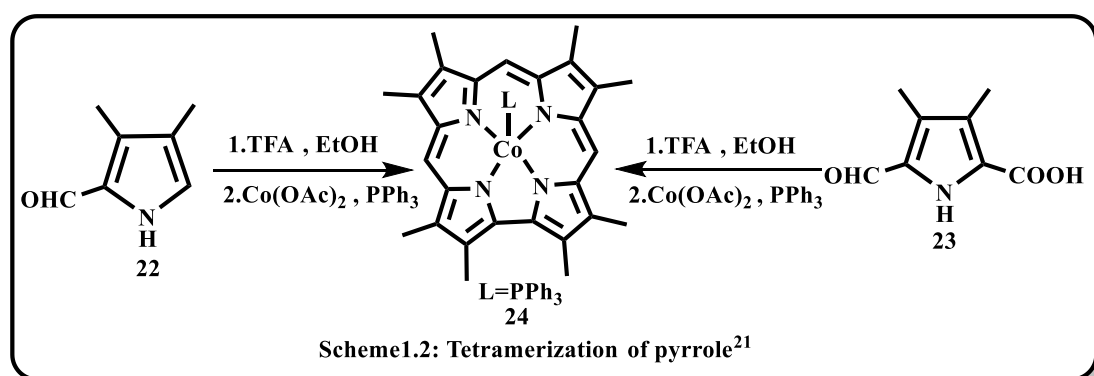
1.3.2.1 From a,c-biladienes

The first corrole synthetic route involves the photochemical cyclization of a,c-biladienes in the presence of a weak base such as ammonium hydroxide or sodium acetate methanolic solution.^[13] The photo-oxidation step was carried out in the presence of light from a 200W tungsten bulb or mercury lamp. Corrole, **21**, was obtained with a yield of about 20%-60%. The precursor a,c-biladienes, **19**, are tetrapyrrolic molecules prepared by the condensation of dipyrromethene dicarboxylic acid with 2-formyl pyrrole in a 1:2 ratio (Scheme 1.1). The freebases were usually transformed into their cobalt (III) derivatives to sort out NMR broadening issues. Later, the irradiation phase could be successfully substituted with a variety of oxidizing agents, including iron (III) chloride, cerium (IV) sulphate, potassium hexacyanoferrate (III), benzyl peroxide, or hydrogen peroxide, while retaining the primary condition.



1.3.2.2 Pyrrole Tetramerization

The direct tetramerization of pyrrole results in the formation of corrole; this synthetic protocol was first reported by Paolesse *et al.* in 1996.^[21] The *meso* free β -substituted corrole synthesized by the tetramerization of 3,4-dimethyl-pyrrole-2-carbaldehyde, **22**, and the yield of the product is about 10%. If the starting material changed to 3,4-dimethyl-2-formylpyrrole-5-carboxylic acid, **23**, a similar corrole, **24**, was obtained (Scheme 1.2). This occurs most likely as a result of fast decarboxylation of the reactant pyrrole in acidic circumstances. The chemical process entails a fast Friedel-Crafts reaction, followed by metal complex formation, cyclization, and lastly, displacement of one *meso* carbon atom.

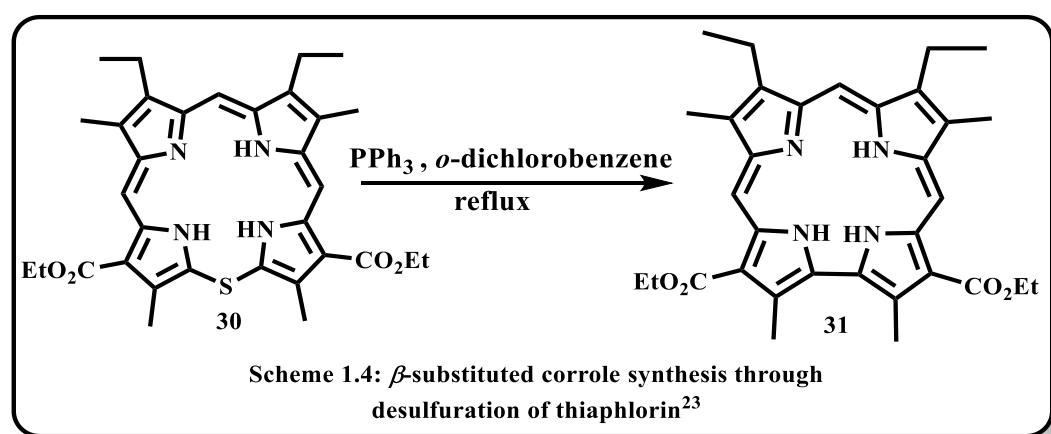
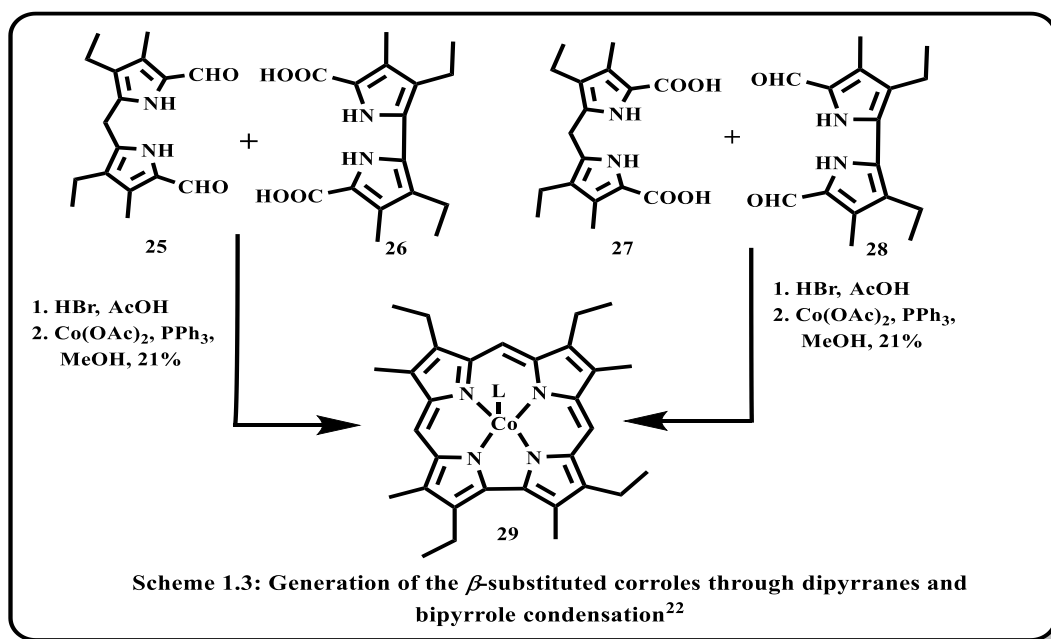


1.3.2.3 Synthesis via 2, 2'- Bipyrrrole and Dipyrranes

Another suitable corrole synthetic protocol can be recommended from the structure of corrole macrocycle, which is by the addition of substituted dipyrane with 2, 2'-bipyrrrole, **26** (Scheme 1.3). In the year of 1973, Conlon *et al.* first reported this procedure.^[22] The reaction between bipyrrrole and dipyrane in an acidic medium led to the formation of a red precipitate. The residue was then heated with cobalt (II) acetate and triphenylphosphine to convert into a corrole complex, **29**, with moderate yield (21%). The cobalt (II) acetate is used to increase the reaction yield, and the most likely activity of cobalt cation is to stabilize the tetrapyrrolic intermediate.

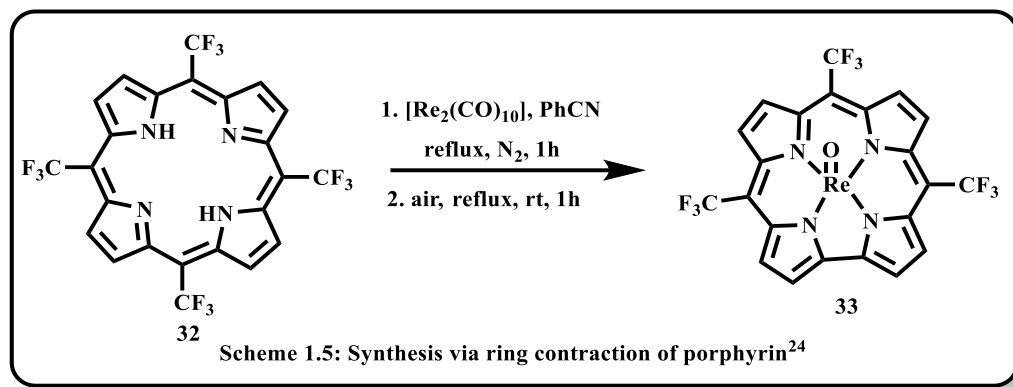
1.3.2.4 From ring-contraction of macrocycles

Synthesis of corroles by atom-extrusion was performed by Johnson and co-worker^[23] using a nonaromatic intermediate, *meso*-thiaphlorin, **30**. The *meso*-thiaphlorin was either heated in dichlorobenzene (yield=40%) for two hours or treated with triphenylphosphine (yield=60%), leading to the removal of the bridging sulphur atom in the final product, **31** (Scheme 1.4).



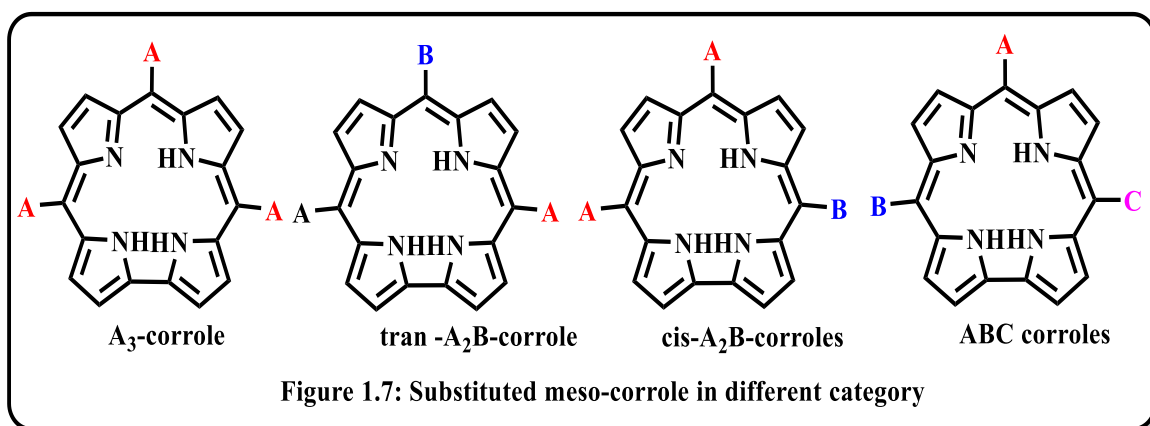
Synthesis via ring contraction of porphyrin: The extremely electron-poor porphyrin, **32**, upon refluxing with $\text{Re}_2(\text{CO})_{10}$ resulted in the formation oxorhenium(V) corrole, **33**, complexes. This is the first time Chan *et.al* ^[24] have disclosed a synthetic procedure for

corrole using porphyrin ring contraction. The A₃-corrole was obtained with a 9% yield (Scheme 1.5).



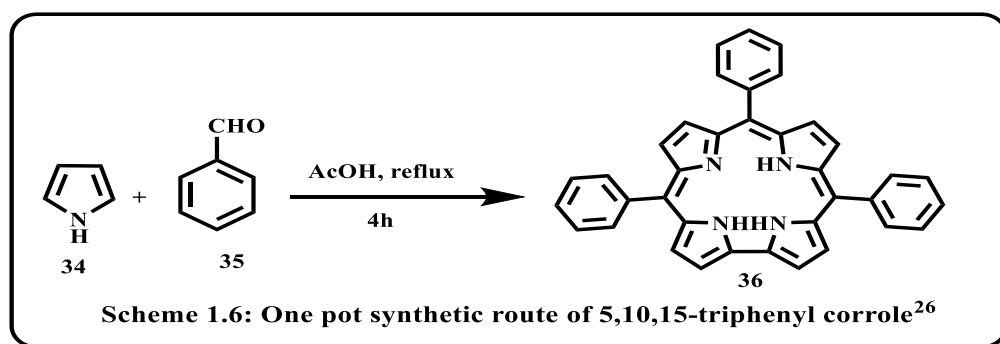
Meso-substituted A₃-corroles synthesis

Prior to 1999, just two *meso*-substituted corroles had been reported, but the revelation of the one-pot synthesis method altered the landscape. The *meso*-substituted corrole gained more attention due to their easy synthesis and higher stability. Recently the most approved methods for synthesis of *meso*-substituted corroles are i) direct condensation of aldehyde and pyrrole leading to bilanes which undergo oxidative cyclization *via p*-chloranil or DDQ; ii) condensation of dipyrroles and aldehydes. Much like with *meso*-substituted porphyrins, *meso*-substituted corroles fall into four separate categories (Figure 1.7).^[25] The important distinction between the synthetic routes for *meso*-substituted corroles and porphyrins is that the precursor formed in case of porphyrin is macrocyclic. Still, the bilane intermediate for corrole is non-macrocyclic.^[25]

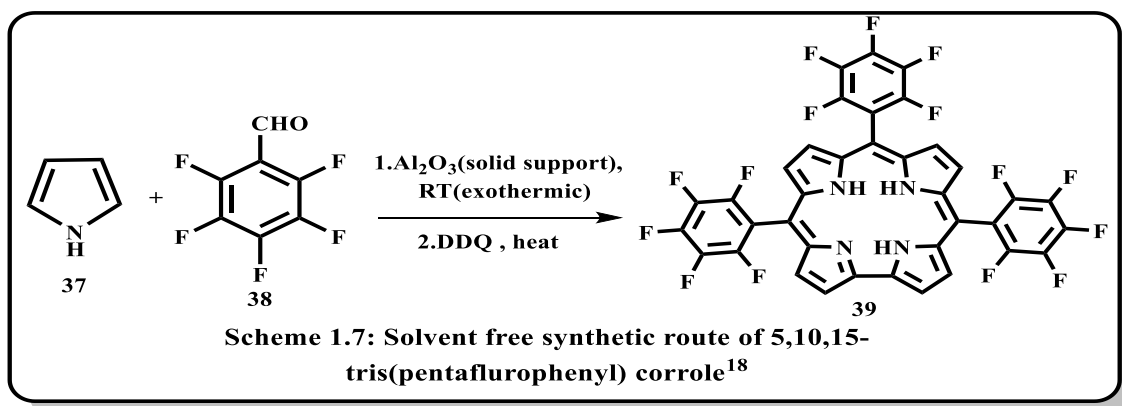


1.3.2.5 One-pot synthesis

The first A₃ corrole was reported by Paolesse and groups in 1999 via a one-pot synthetic route.^[26] The synthesis involves the reaction between aldehyde and pyrrole in 1:3 ratio refluxing in acetic acid medium. The A₃-corrole, **36**, was obtained with a 9% yield. The major limitation of the method was the formation of porphyrin as the side product of the reaction (Scheme 1.6).

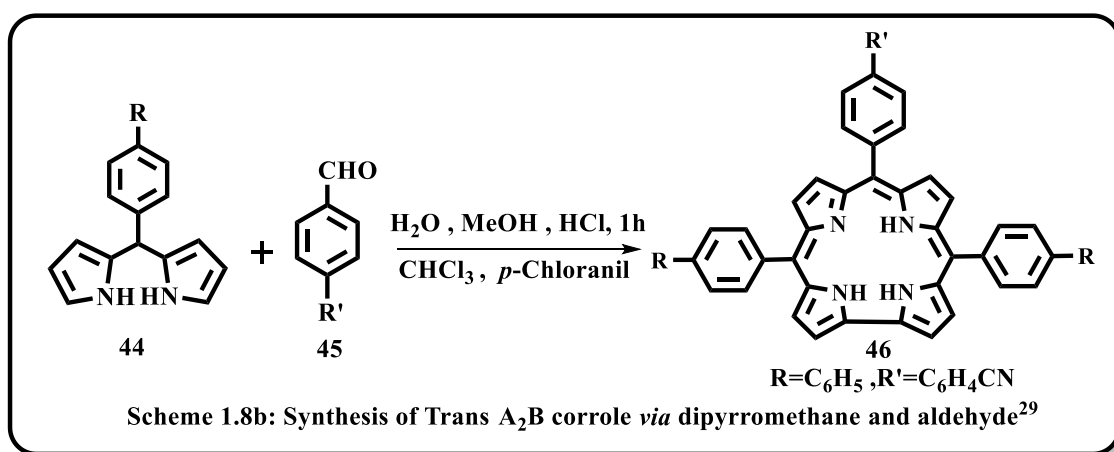
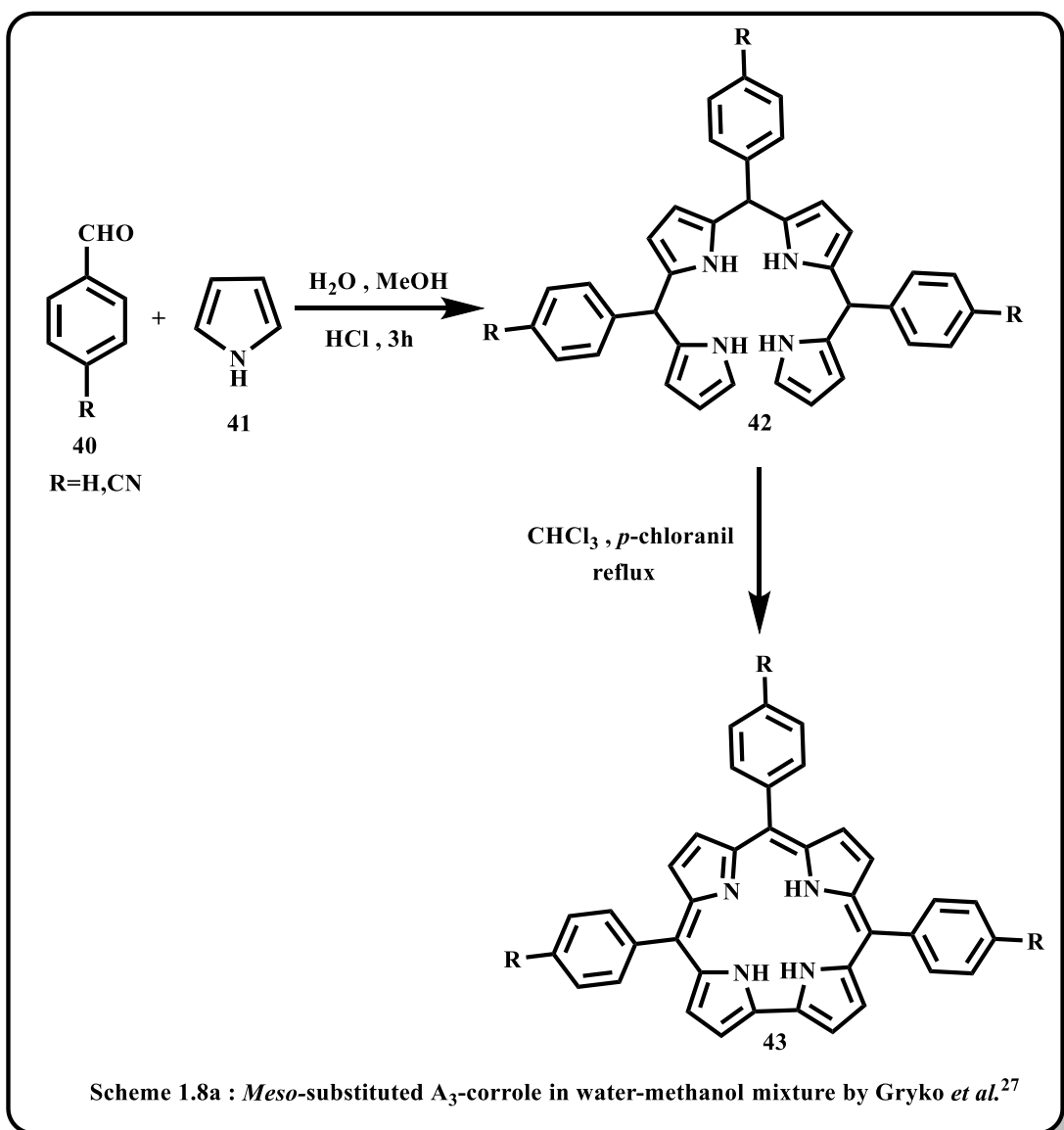


One important solvent-free one-pot corrole synthesis was reported by Gross and co-workers. The condensation reaction of pentafluoro benzaldehyde with pyrrole under the neat condition with solid support resulted in the formation of bilane, which upon oxidation in the presence of DDQ gave tris(pentafluorophenyl) corrole, **39**, in 8-11% yield.^[18] The best part of the reaction was no porphyrin was obtained as a side product (Scheme 1.7). The reaction is particularly substrate-specific; mainly, the aldehydes with electron-withdrawing groups give a better result.



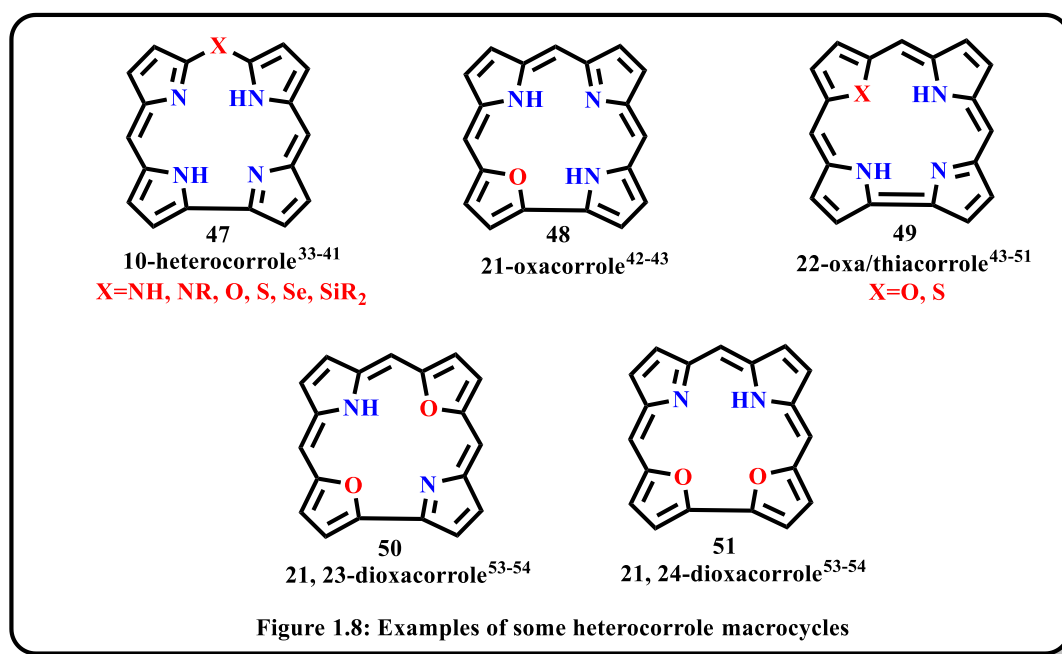
1.3.2.6 A modified synthetic pathway *via* water -methanol-acid system

In the year 2006, Gryko *et.al* reported the most widely used protocol for corrole synthesis.^[27] The inspiration behind the work came from Karl and co-workers,^[28] that describe the synthesis of dipyrromethene in a water medium. The first synthesis step involves the acid-catalysed electrophilic substitution reaction of aldehyde and pyrrole in a mixture of methanol and water. The reaction produces several types of oligocondensates, such as tetrapyrane/ bilane (unconjugated open-chain corrole precursor), dipyrromethane, tripyrrane, *etc.* and were then extracted through CHCl_3 ; the second step includes the macrocyclic oxidation in the presence of DDQ (Scheme 1.8a). The procedure proved very selective for relatively reactive aldehydes, particularly those with electron-donating groups. Geier and co-workers later revealed that DDQ is not the best oxidizing agent for the synthesis of certain corroles because it causes partial decomposition of the product. Hence, instead of DDQ, *p*-chloranil can be used as an oxidizing agent, which gives a better yield than previous. The result (32%) was better when the aldehyde and pyrrole were present in a 1:2 ratio. In addition to A_3 corrole, the synthetic procedure is also efficient for the synthesis of A_2B corrole. The only difference is, instead of pyrrole, dipyrromethene undergoes electrophilic substitution reaction with aldehyde, producing over 50% product (Scheme 1.8b).^[29]



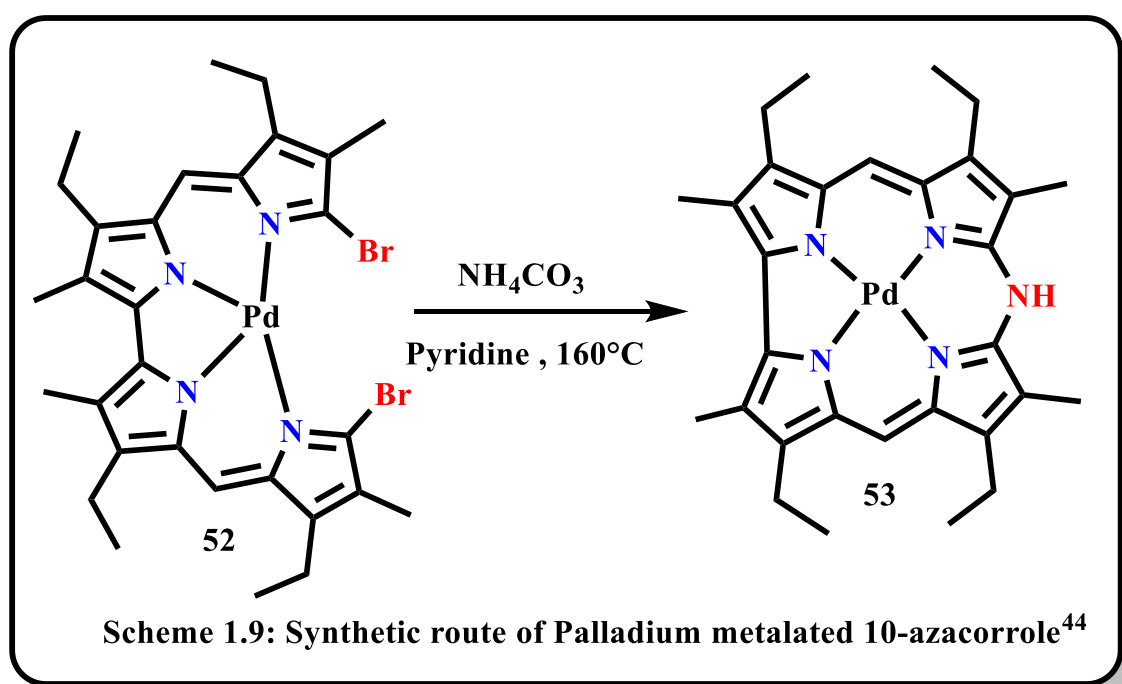
1.4.1 Heterocorrole

Heterocorroles are the class of corrinoids that can be achieved by introducing the heteroatom into the corrole cavity either in the *meso* position or on their conjugative framework.^[25,30] The replacement of one or two corrole nitrogen atom(s) by sulphur or oxygen atom and *meso* modification replaces the *meso* carbon at 10-position by the groups or atoms like NH, NR, Se, S, O, and including Si involved in core modification strategy.(Figure 1.8)^[31–37] Despite their dianionic structure and confined cavity, heterocorroles are an excellent ligand for studying the coordinating property of corrole.^[36–52] When N-confused corroles^[55] and its isomers, norrole,^[56] are investigated, they exhibit peculiar coordination behaviour attributed to the existence of a carbon atom in the core of the macrocycle. The emission and absorption properties of 10-silacorroles in the near-infrared region make them attractive alternatives for light-harvesting applications. This section summarises the advancements made in heterocorrole chemistry, including their synthesis, fundamental structural traits, and properties.

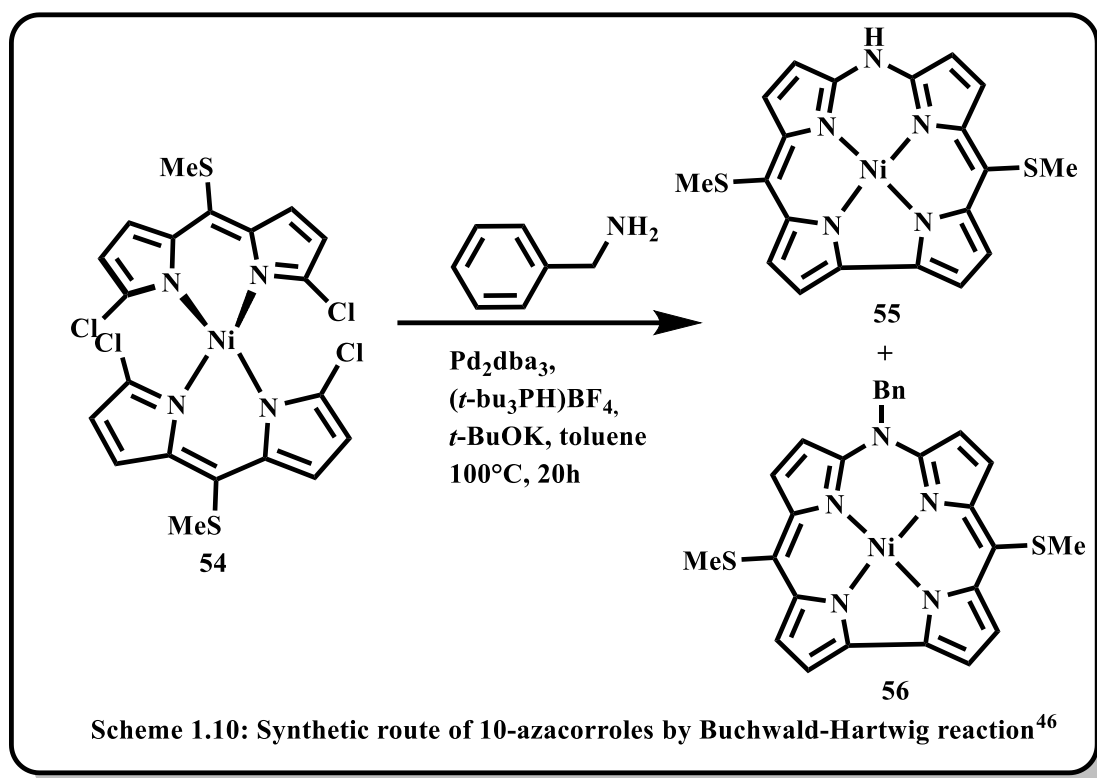


Meso-modified heterocorrole

The first β -substituted *meso*-heterocorrole was reported in 1960 by Johnson and Kay, in which one of the *meso* carbon is replaced by a nitrogen atom, hence called 10-azacorrole. The palladium (II) chelated azacorrole, **53**, was synthesized through metalated dibromo-5,5'-bi(dipyrromethene), **52**, (Scheme 1.9).^[44] Later the group was unsuccessful in isolating the demetalated product through acid treatment. Although the structure is relatively simple, the procedure they developed is quite tedious.



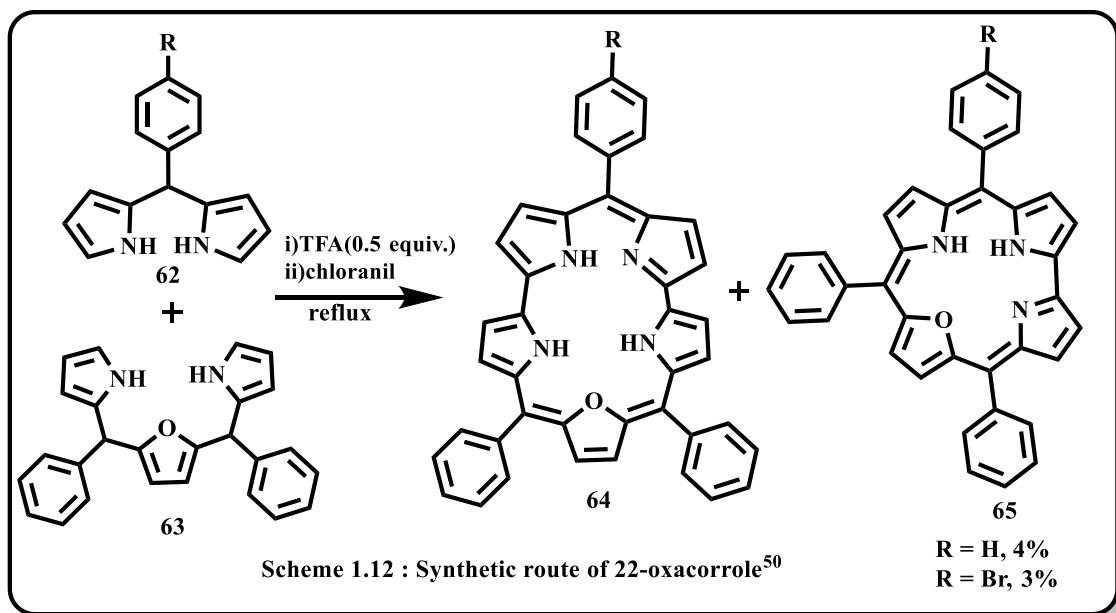
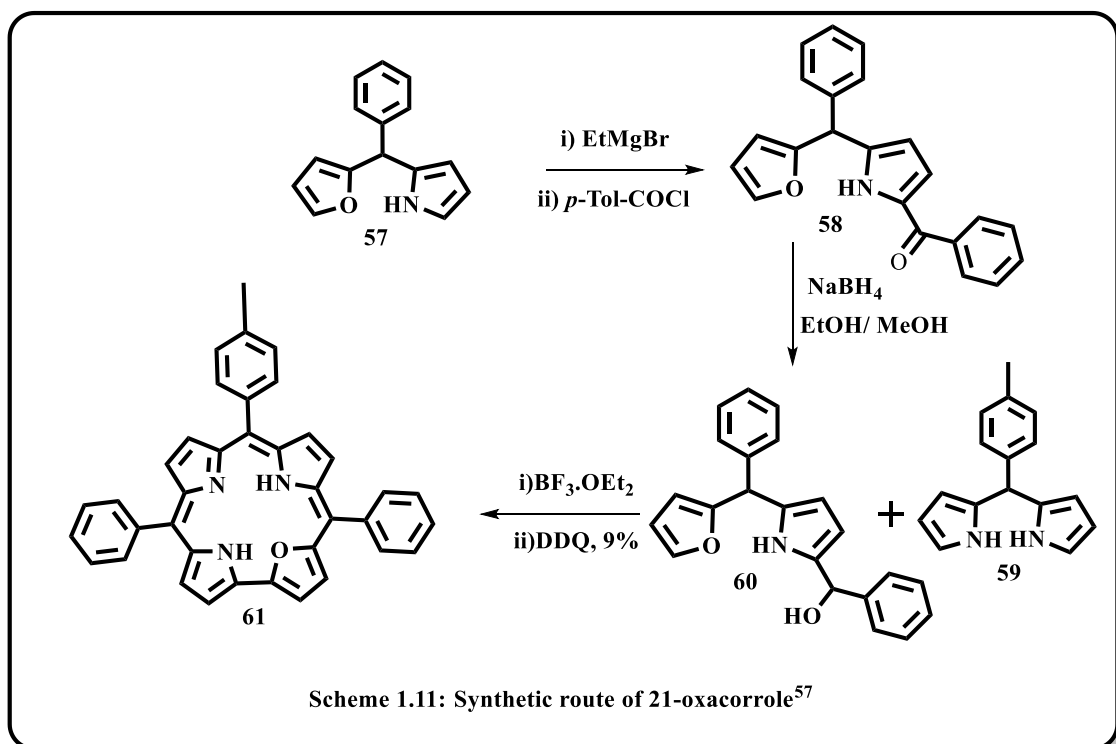
Later, Shinokubo *et. al.* developed a new synthetic protocol that improved the yield of azacorrole.^[46] The reaction condition involves α , α' -dichlorodipyrin Ni (II), **54**, with benzylamine undergoing Hartwig-Buchwald amination, to form azacorrole, **55**, and N-benzylazacorrole, **56**, as nickel metalated complexes, in 8% and 27% yield, respectively (Scheme 1.10). The azacorrole, **55**, is a planar compound with a low oxidation potential compared to diazaporphyrins.



21-Oxacorrole: The first example of 21-oxacorrole, **61**, was reported by Lee and co-workers with 9% yield by acid-catalyzed condensation of furyl-pyrrolyl mono-ol, **60**, with *meso*-aryl dipyrromethene, **59** (Scheme 1.11).^[57] The pyrrole acylated product was obtained in the first step when *p*-tolyl-(furan-2-yl) -(pyrrol-2-yl) methane, **57**, reacted with EtMgBr in THF followed by *p*-toluoyl chloride. The acylated pyrrole, **58**, upon reduction with NaBH₄ gives the desired furyl-pyrrolyl mono-ol, **60**, which later undergoes acid-catalysed reaction with **59**. In comparison to 21-oxaporphyrin *meso*-tetra aryl, the 21-oxacorrole, **60**, exhibited a nearly planar shape due to the existence of a direct furan-pyrrole link.

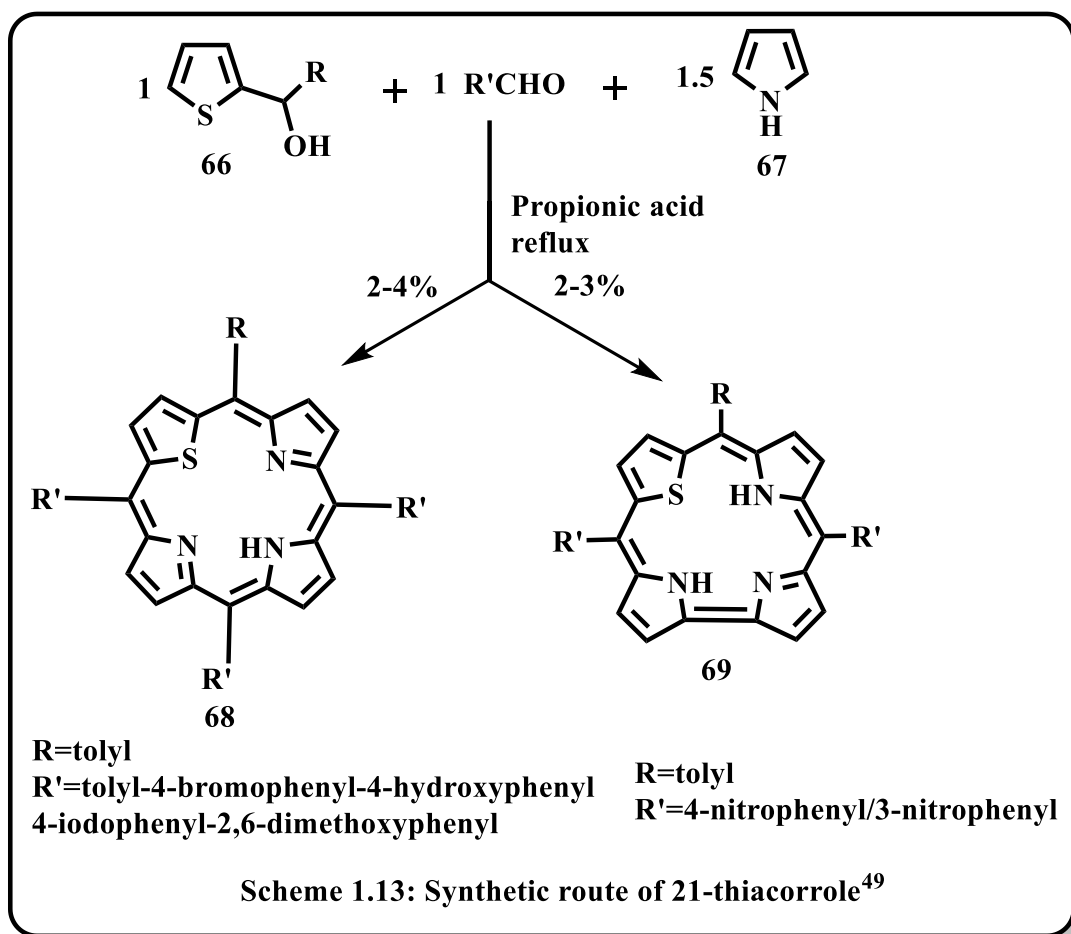
22-Oxacorrole: Chandrashekar and groups^[50] first reported the synthesis of 22-oxacorrole as a minor by product during their extended porphyrin synthesis. The oxidative coupling reaction among the 16-oxatripyrrane, **63**, and *meso*-aryl dipyrromethene, **62**, catalyzed by TFA, afterward oxidation with chloranil yielded 25-

oxasmaragdyrin, **64**, (50% yield) as a major product with 22-oxacorrole, **65**, in 3-4% yield (Scheme 1.12).



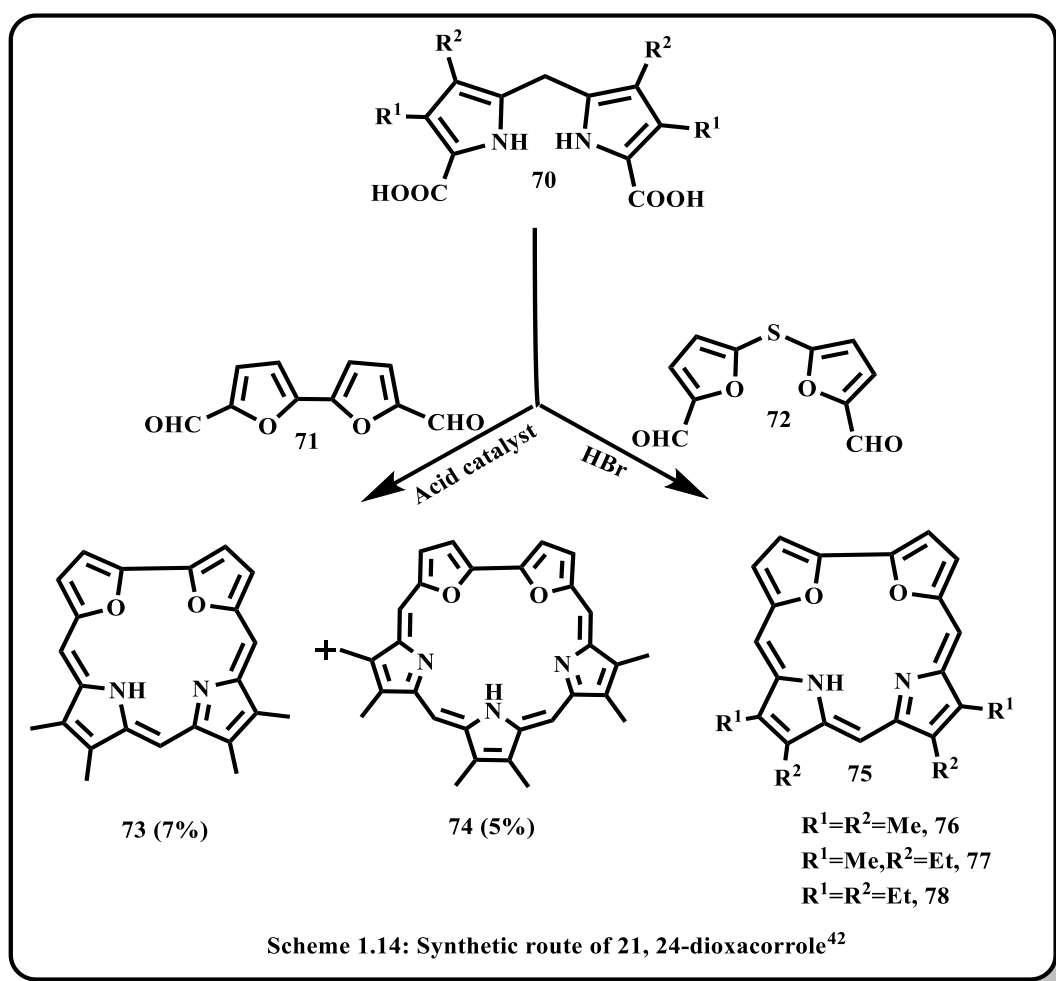
22-Thiacorrole: Ravikanth and groups tried to synthesize 21-thiacorrole by condensing pyrrole, thiophene mono-carbinol, **66**, and aromatic aldehyde refluxing in propionic acid (Scheme 1.13).^[49] The resulting major product was thiaporphyrin but the thiacorroles

were formed only in few cases, which they could not isolate because of their low stability. Later, they were successful in recovering the stable thiacorrole, **69**, when 4-/3-nitobenzaldehyde was used in the condensation in a similar condition that described above.



Dioxacorrole: The *meso*-free 21, 24-dioxacorrole, **75**, was first reported by Broadhurst *et.al* ^[42] in 1969. The synthetic route involves the acid catalyzed condensation of β -substituted dipyrrolylmethane diacids, **70**, with either diformyl-difuryl sulphide, **72**, or bifuran dialdehyde, **71**. The condensation of diformyl-difuryl sulphide, **72**, with dipyrrolylmethane diacids, **70**, gave only dioxacorrole, **75** (**76-78**) while the other condensation, of β -substituted dipyrrolylmethane diacids, **70**, with bifuran dialdehyde, **71**, yielded dioxacorrole, **73**, together with heterosapphyrin, **74** (Scheme 1.14).

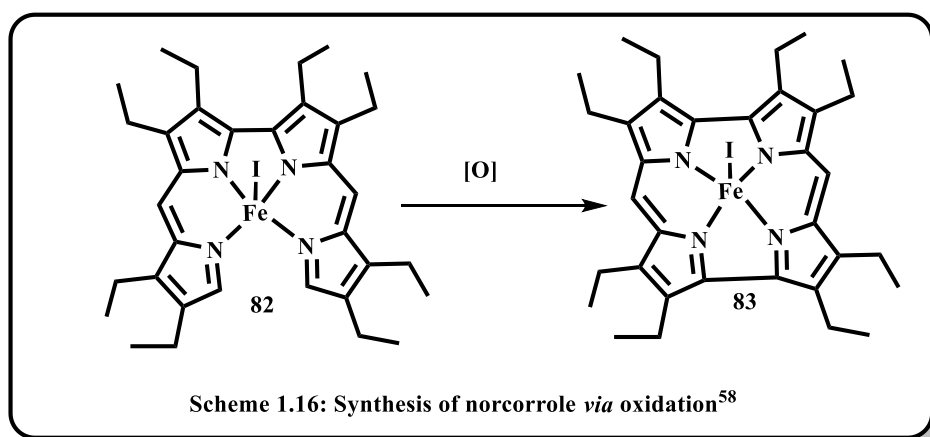
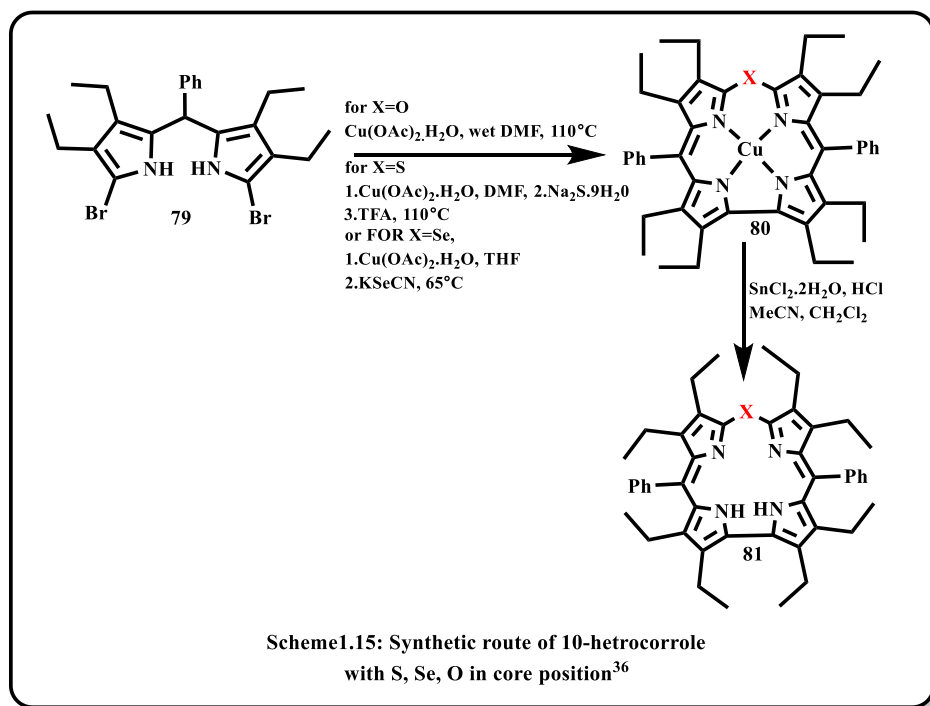
10-Heterocorrole: 10-heterocorrole having O, S, Se in their core was reported by Bröring *et. al.*^[36] The cyclization reaction of α, α' -dibromodipyrin, **79**, with copper (II) salt yielded the 10-oxacorrole copper complex (Scheme 1.15). Later the demetallation was proceed through tin (II) chloride, and HCl resulted the free base corrole, **81** in good yield. The compound, **79**, upon reaction with KSeCN or Na₂S yielded the 10-selena- and 10-thiacorrole, respectively.



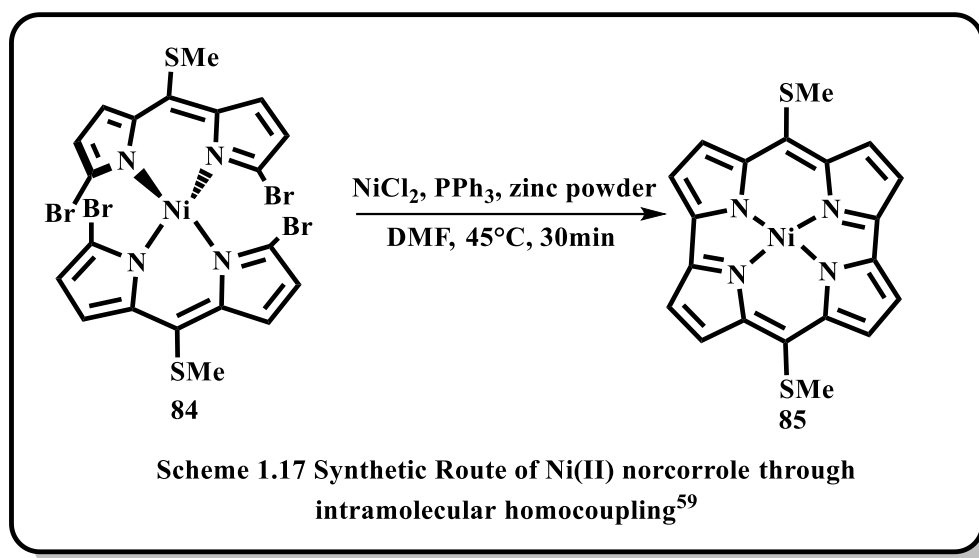
1.4.2 Norcorrole:

The norcorrole is a ring contracted version of corrole in which one of the *meso* carbon is missing. According to Huckel aromaticity, this macrocycle type is antiaromatic because it contains 16π conjugated systems. The first synthetic route for norcorrole was reported

by Bröring and co-workers in 2008.^[58] The oxidation of the 2,2'-bidipyrin iron complexes, **82**, results in norcorrole, **83**, formation, which was confirmed through NMR and MALDI-TOF experiment (Scheme 1.16). The isolation of compounds was not possible due to their low stability and dimerization.



Later, Shinokubo and co-workers successfully isolated the Ni (II) norcorrole, **85**, through intramolecular homocoupling of α , α' -dibromodipyrin, **84**.^[59] The green coloured compound is air stable and is obtained with 90% yield. The product is strongly antiaromatic, which is confirmed through NMR and NICS measurement (Scheme 1.17).

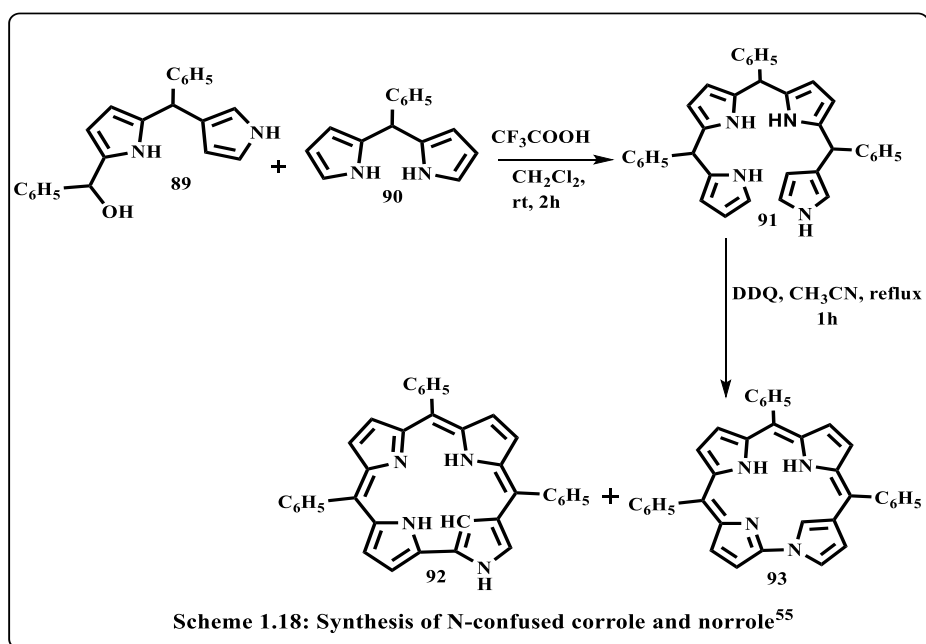


1.4.3 N-confused and Neo-confused Corroles:

Despite the fact that N-confused porphyrins have been reported since 1994, Furuta and co-workers first synthesized novel N-confused corroles in 2011.^[55] After DDQ oxidation and refluxing in acetonitrile, 2-aza-21-carbabilane, **91**, yielded N-confused corroles **92**, and **93** (Scheme 1.18). X-ray crystallographic analysis and NMR data demonstrated that these corrole moieties adopted the 3H form while retaining aromaticity. These corroles have lower aromaticity than the regular corrole because the confused pyrrole ring is considerably tilted away from the plane.^[60]

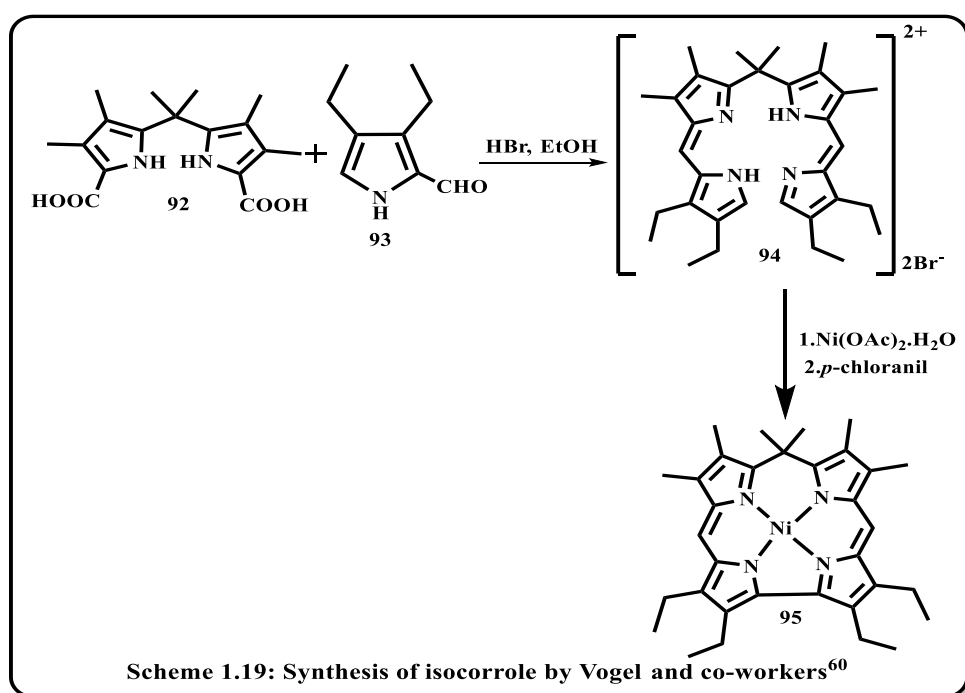
1.4.4 Isocorroles:

Isocorrole is one of the corrole macrocycles that has a sp^3 hybridised *meso* carbon atom. Hence, these corroles are nonaromatic in nature, having two ionizable N-pyrrolic protons. They can exist as 5- or 10-isocorroles, depending on where the sp^3 -hybridized carbon atom is located. Vogel and co-workers^[60] reported the synthesis of isocorrole by condensation of α -formyl pyrrole, **93**, with dipyrane, **92**, to form a linear intermediate, **94**, that undergoes Ni (II) assisted oxidative cyclisation to give the desired product, **95** (Scheme 1.19).



1.5 Functionalization of Corrole:

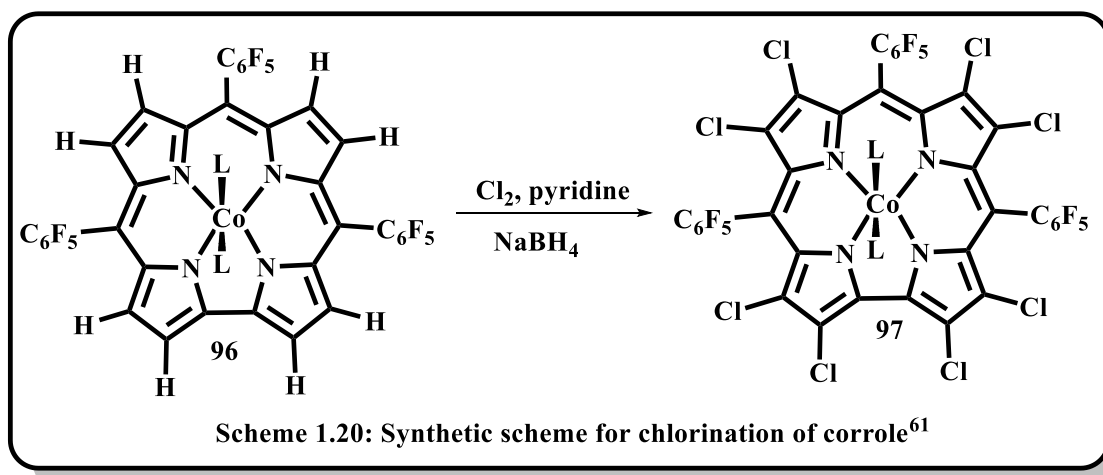
The high acidity of inner imine hydrogen makes corrole more reactive than the porphyrin. The corrole functionalization can be divided into three stages: inner core functionalization, peripheral functionalization (carboxylation, nitration, sulfonation, halogenation, and formylation), and post functionalization, which can include nucleophilic substitution reactions and witting reactions.^[15]



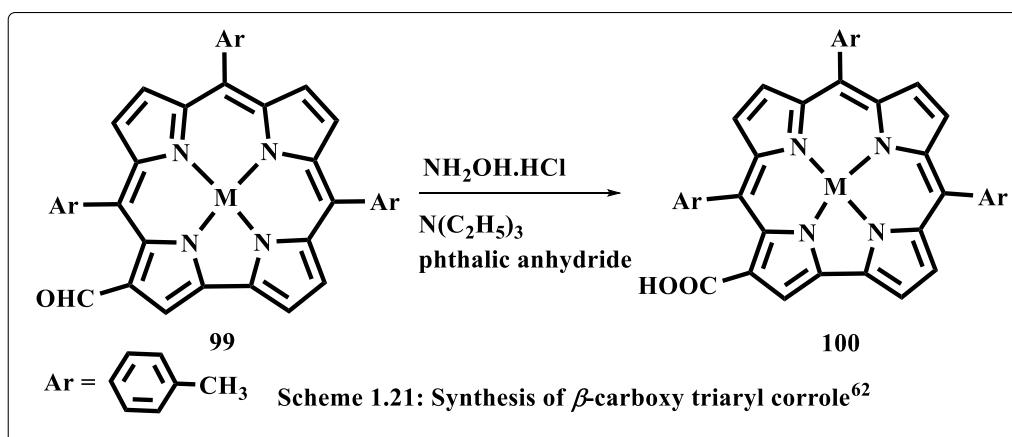
1.5.1 Peripheral Functionalization:

The scheme mentioned in below sections are associated with the evolution of new protocols for directly introducing major primary groups positioned at corrole periphery. These reactions are distinctly regioselective. The significant variation in reactivity among the atoms of carbon on the corrole framework is because of electronic instead than steric effects.

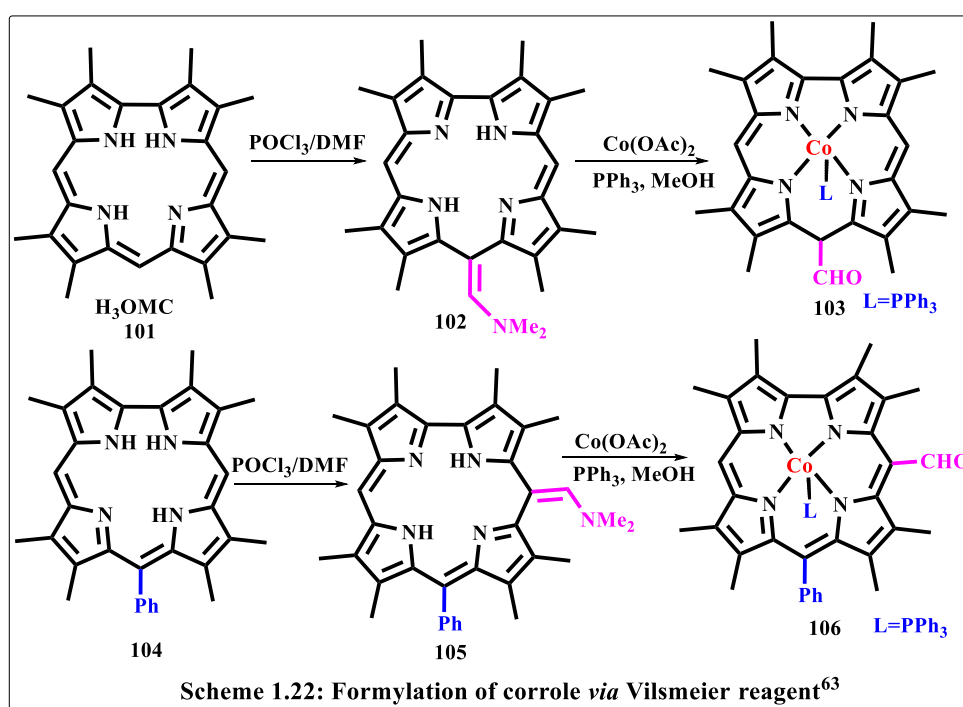
Halogenation: Halogenation of corroles involves the reactions like chlorination, bromination, and iodination, mainly on the β -positions of the macrocycles. A suitable procedure for fluorination is not yet developed. There are several procedures have been reported in the literature regarding the halogenation of corrole. Gross and groups^[61] described the chlorination of metalated Co (III) corrole, **96**, with Cl_2 (Scheme 1.20). The completely halogenated (chlorination) Co (III) corrole, **97**, (90%) was produced following the addition of NaBH_4 and pyridine to the reaction medium.



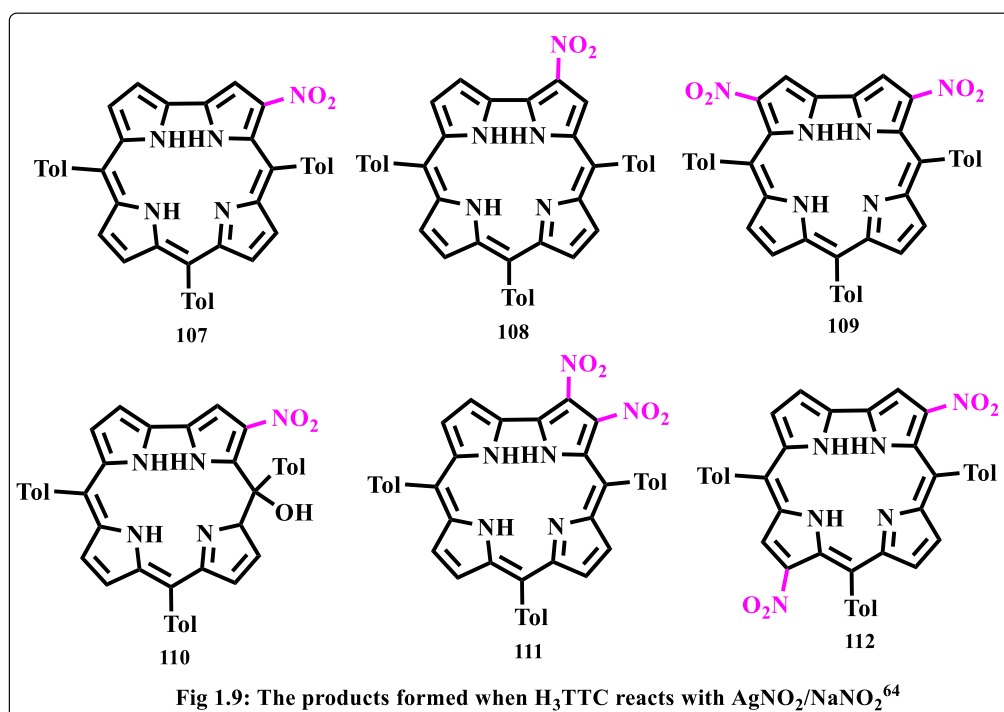
Carboxylation: Giribabu and co-workers^[62] reported a protocol for carboxylation of corrole that involves reacting FB carbaldehyde corrole, **99**, or the analogous copper complexes, with phthalic anhydride and $\text{NH}_2\text{OH}\cdot\text{HCl}$ in dry CH_3CN at reflux (Scheme 1.21). This protocol was expanded to create FB and copper derivatives of triarylamine-substituted -3-carboxylic acids corrole, which can be utilised in dye-sensitized solar cells.



Formylation: The Vilsmeier-Haas reaction on metallo-corrole and freebase can yield corrole with a formyl moiety attached to the β -pyrrolic or *meso* position. Paolesse *et. al.*,^[63] have reported the first example of corrole ring formylation, in 1997. The reaction of H₃OMC, **101**, with the Vilsmeier reagent, yielded corroles (**102**, **105**) rather than the expected 5-formyl or 10-formyl corrole derivatives. The compound **102** or **105** refluxed with PPh₃ and Co(OAc)₂ in methanol causes both hydrolysis/ tautomerisation to the respective *meso*-formyl Co (III) corrolato complexes **103** and **106** in almost quantifiable yield (Scheme 1.22).

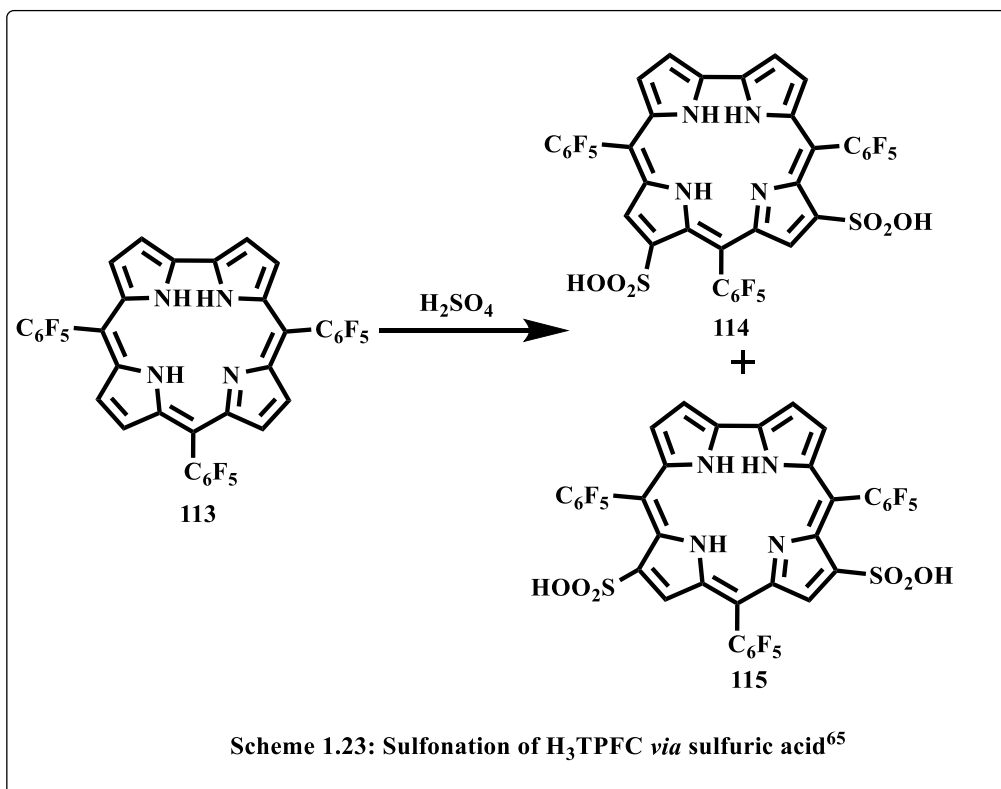


Nitration: Numerous techniques have been developed to facilitate the isolation of corroles containing one or more nitro groups directly connected to peripheral (β -pyrrolic) locations. In 2007, Paolesse and co-workers^[64] started providing meaningful contributions on the efficacy of various reactants for the nitration of metallocorroles and FB corroles. One methodology involves converting corroles into the 3-nitro silver corrole complexes by using a nitrating agent such as AgNO_2 . The reaction of nitrate (NO_2^-) to the π -radical cation of the silver (III) corrole (produced by reaction with excessive Ag^+) is the crucial step in the reaction (Figure 1.9). Further research found that when the stoichiometry was carefully regulated, the reaction of FB corroles with the $\text{NaNO}_2/\text{AgNO}_2$ was regioselective, produced di- and mono-nitro-corrole derivatives. The 3-nitrocorrole, **107**, was synthesised as the principal product with a 52% yield using a corrole/ $\text{AgNO}_2/\text{NaNO}_2$ molar ratio of 1:1:9, whereas the 2-nitrocorrole, **108**, was synthesised as a minor product. When the ratio is changed to 1:2:8 (corrole/ $\text{AgNO}_2/\text{NaNO}_2$), the primary products is 3,17-dinitrocorroles, **109** (20%) (Figure 1.4). A small amount of NO_2 -isocorrole **110** (9%) as well as the 2,3- and 3,12-dinitro derivatives of corroles (**111** and **112**) were isolated from the same reaction.



Sulfonation: At room temperature sulfonation of **113**, with concentrated sulfuric acid yielded a 9:1 combination of the 2,17- and the 3,17-bis (sulfonic acid) corrole isomer,

114, 115 respectively (Scheme 1.23).^[65] The two sulfonato substitution increases the water solubility and amphipolarity of corroles.



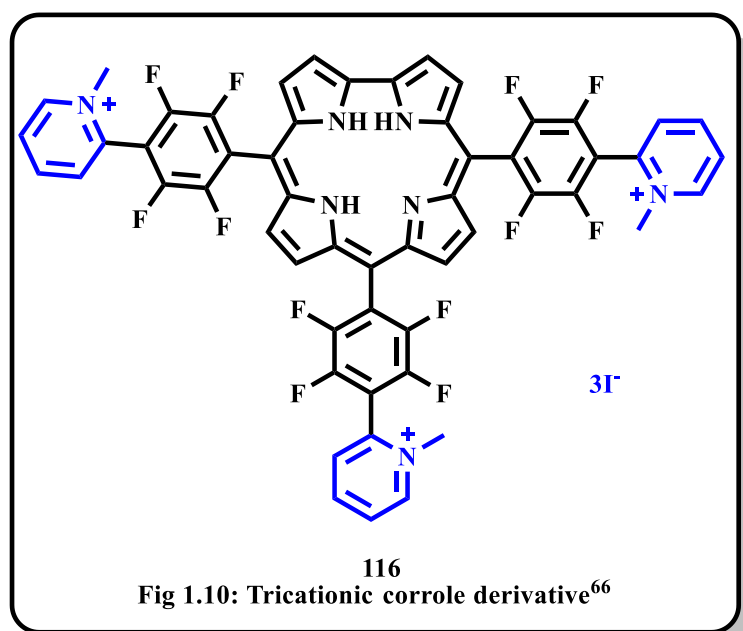
1.5.2 Corrole Post-Functionalization

The availability of suitable groups at the corrole macrocycle's peripheral sites allows them to be converted into additional corrole derivatives via "simple" organic processes. The organic reactions involve the conversion of a selected functional group in an adaptable method to form newly synthesised corrole analogues. The nucleophilic substitution reaction of *meso*-substituted pentafluorophenyl groups of corrole by O, S, N-nucleophiles, or another example that include the formyl corrole as a key component for post-functionalization of corrole. Cycloaddition processes or metal catalysed reactions can also be used to modify the substituted corroles. All of these sorts of reactions have been utilised to post-functionalize the corroles.

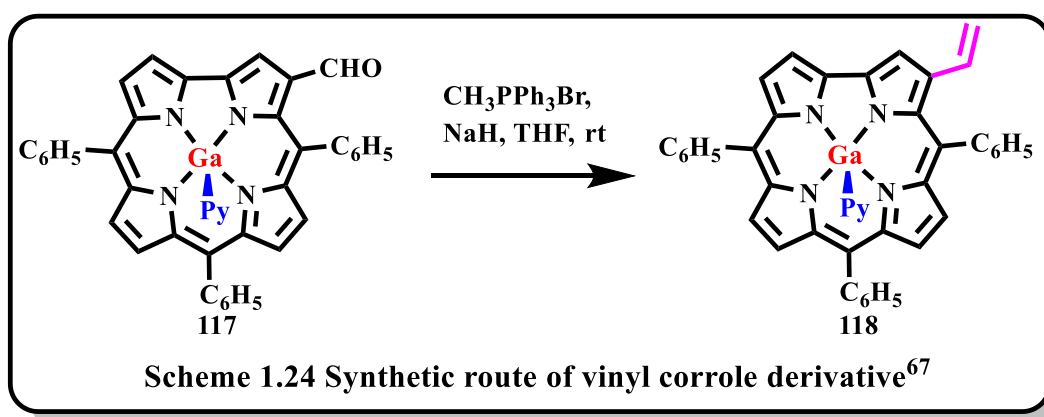
Post Functionalization *via* Nucleophilic Aromatic Substitutions:

Strong electron-withdrawing groups connected to the aromatic ring play an important role in nucleophilic substitution processes. In 1999, the first reports of corrole S_NAr reactions

surfaced. Gross *et.al* ^[66] reported that treating corrole with 2-pyridyllithium; subsequently, the addition of iodomethane produces the tri-cationic macrocycle of corrole, **116** (Figure 1.10). This product is found to be more effective than a wide range of porphyrins at inhibiting endothelial cell proliferation, tumour development, and metastasis.

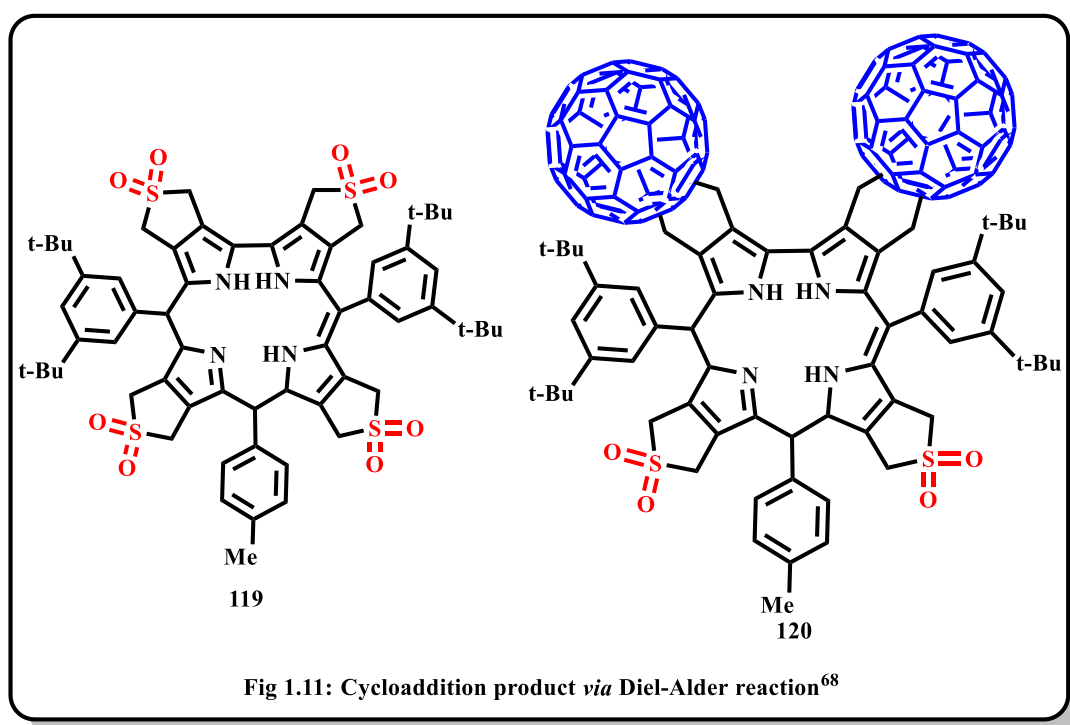


Functionalization through Wittig Reaction: Neves and groups^[67] used the Wittig reaction for the first time in the corrole functionalization. The resulting 3-vinylcorrole formed *via* the reaction of 3-formylcorrole, **118**, with sodium hydride and methyltriphenylphosphonium bromide. In Diels-Alder reactions, corrole **118** was successfully utilised as either the dienophile or diene (Scheme 1.24).



Cycloaddition reaction *via* corrole: According to research, corroles, like porphyrins, can act as dienes, dienophiles, 1,3-dipoles, or dipolarophiles, in cycloaddition reactions. Occasionally, unusual reactivity is noticed due to peculiar properties of the corrole. The tetra sulfano-fused corrole, **119**, used as diene react with C_{60} in Diels- Alder reaction reported by Krautler and group^[68]. The difullereno-corrole, **120**, (Figure 1.11) was obtained in 83% yield by thermal displacement of SO_2 at $140^\circ C$ in the vicinity of an excess fullerene in 1,2-dichlorobenzene as solvent.

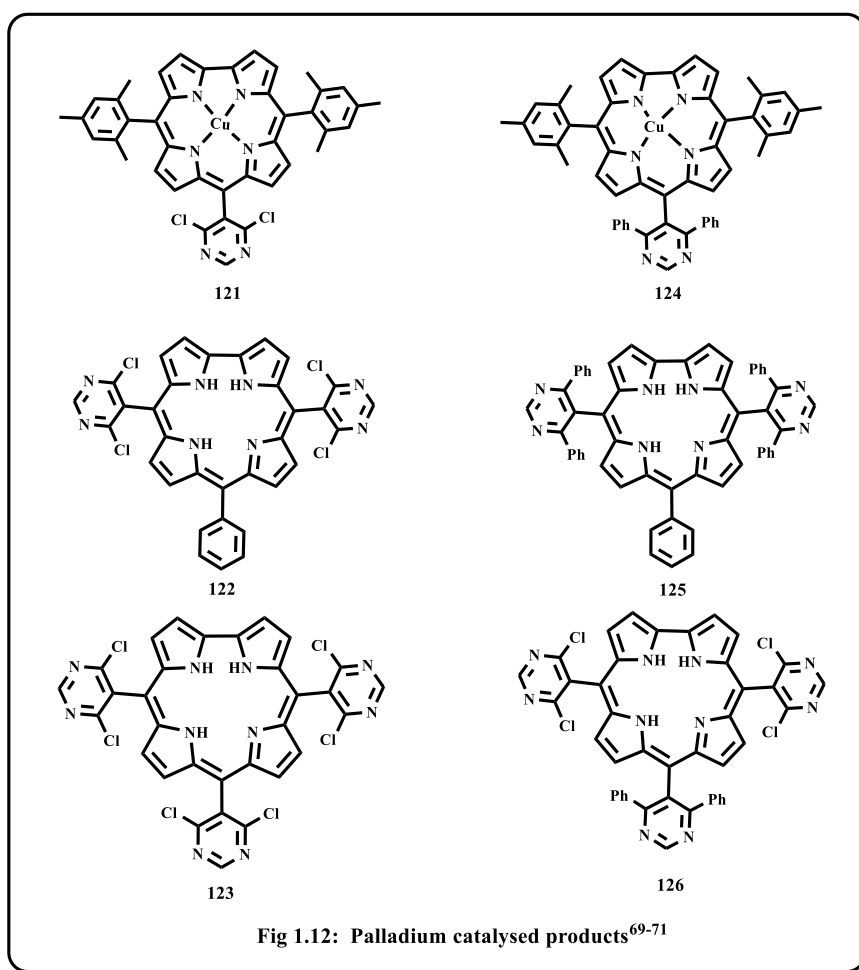
Metal Catalysed Post Functionalization: There are several metals catalyzed coupling reactions involved in the post-functionalization of corrole. In most of the cases, Pd(0) is used to catalyse the reaction of corrole containing Br atom in *meso* or β -pyrrolic positions. Maes *et.al* described a Pd-catalyzed cross-coupling process in which *meso*-pyrimidinyl substituents of corroles were employed. Using the Suzuki-Miyaura procedure and beginning with the free bases **122**, **123**, or the copper corrole, **121**, the authors were able to produce sterically crowded aryl corroles **124-126**.^[69-71](Figure 1.12)



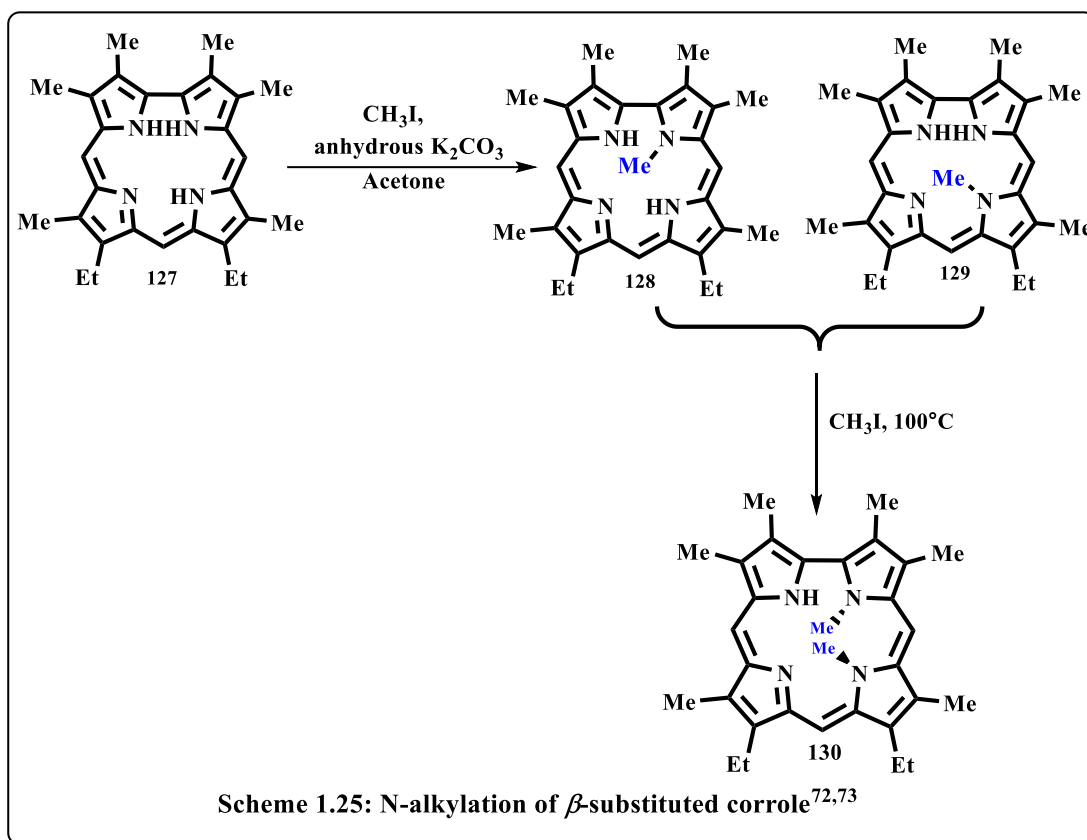
1.5.3 Inner Core Positions Functionalization:

Corroles, like porphyrins, undergo several reactions at the inner centre locations, including deprotonation, protonation, metal coordination, N-acylation, and N-alkylation. Corrole is more acidic than porphyrin and acts as trianionic rather than dianionic, unlike porphyrin. Because of this significant difference, corroles may coordinate high-valent metal ions.

In 1965, Johnson and Kay described the N-alkylation of corroles. The reaction of CH_3I to the corrole and refluxing in acetone in the presence of anhydrous K_2CO_3 results in a mixture of two isomeric N-methylated corroles **128** and **129**. Later, it was revealed that both the N (21)- and N (22)-methylated corroles react further with CH_3I at 100°C (sealed tube, 15 h) to generate, the N (21), N (22)-dimethyl corrole isomer, **130**.^[72,73] Under identical circumstances, the same dimethylcorrole was produced (71%), **130**, along with the starting material (14%) from the parent corrole **127** (Scheme 1.25).



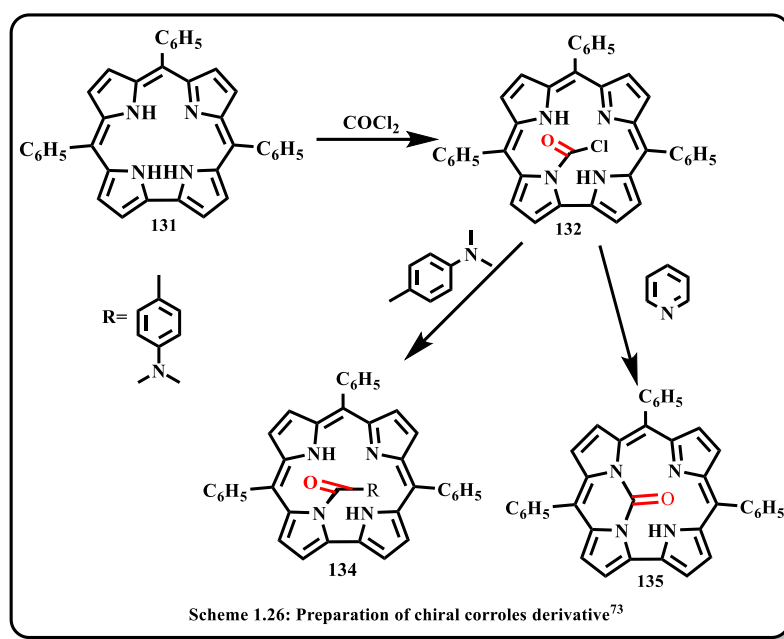
In addition to N-substitution, unexpected reactivity of the inner nitrogen atoms was observed while trying carboxylation with phosgene.^[73] Instead of peripheral N-acylated carboxylation product, N-21, N-22 urea derivatives, **134**, **135** were produced as a result of the reaction (Scheme 1.26).



1.6 Metallocorroles:

In the previous section, we have already discussed the acidity of the inner NH proton of corrole. The acidity is sufficiently high because of steric reasons hence susceptible to deprotonation and easily coordinated to the metal ion. Shortly after the discovery of free base corroles, researchers began investigating the chemistry of metallocorroles. The synthesis of metallic derivatives of corroles can be broadly classified into two types: i) macrocyclization using a metal ion as a mould and ii) the incorporation of metal of in the internal cavity of the corrole. The first methodology was discussed to some extent in the

previous section (Scheme 1.2). In the next section, we will discuss the different methods of introducing metal into the corrole cavity and its structure with varying coordination modes.



1.6.1 Coordination Mode of Metallocorrole:

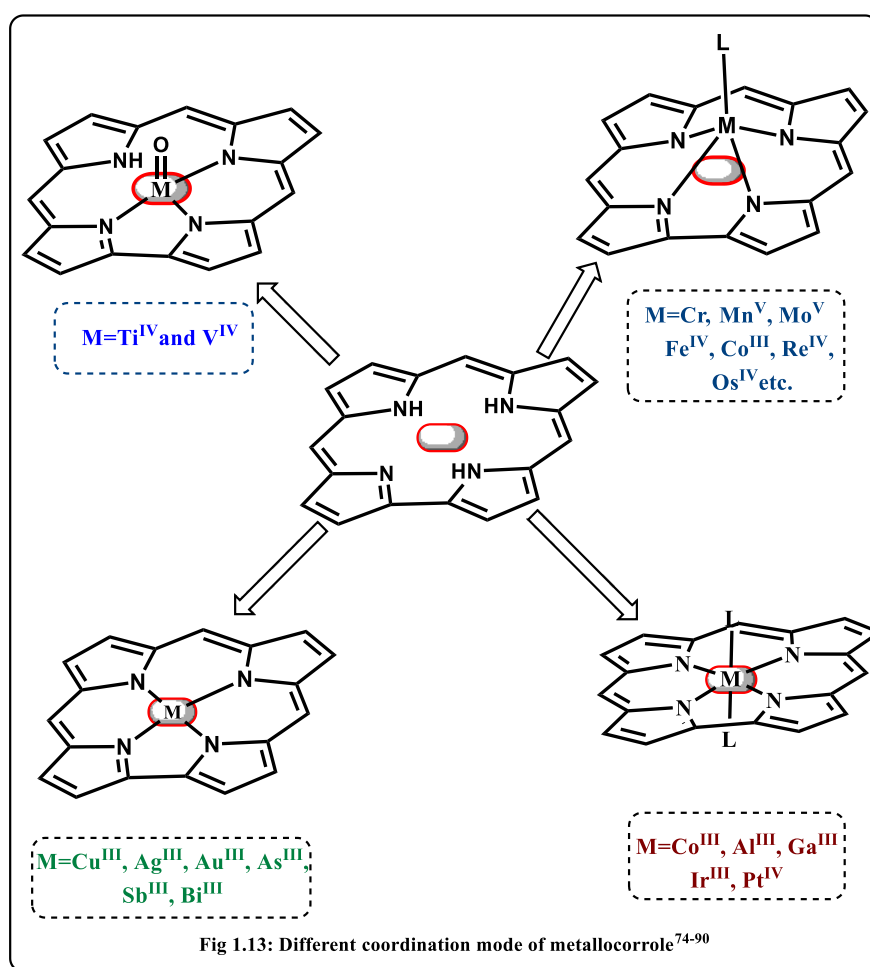
A wide variety of metallocorroles have already been explored due to their large application in different fields. The fundamental properties of corroles demand that the complexes having trivalent metal ions be neutral, and are frequently four-coordinated. This expectation, however, is only met on rare occasions, mostly with the d^8 Au (III) and Ag (III), and Cu (III) complexes.^[74–78] The other metal complexes that adopt such type of coordination mode are In^{III} , As^{III} , Sb^{III} , Bi^{III} , etc. In the absence of any coordinating solvents, this geometry is also adopted by corrole complexes of Co^{III} , Mn^{III} , and also Ru^{III} where two Ru centers are connected by triple bonds (Figure 1.13).^[79–84]

The pentacoordination mode is by far the maximum typically followed coordination mode of corroles. The corrole structure is domed in five-coordinate complexes, and each metal ion for its particular oxidation state has optimal bond lengths which favours the geometry. This sort of geometry is seen in complexes with Cr, Mo, Mn, Fe, Co, Rh, Ge, Sn, or P that have neutral as well as anionic axial ligands such as triphenylphosphine,

pyridine, or halides (F^- , Cl^- , Br^- , I^-), phenyl, methyl, and they also exist as oxo, nitride, and nitrosyl complexes (Figure 1.13).^[85–87]

Another mode of coordination for metalloporphyrins is to act as six coordinated complexes with octahedral geometry. Such octahedral geometry is observed in the axially coordinated pyridine complexes of cobalt (III), aluminium (III), gallium (III) and iridium (III) complexes. As we previously discussed the most common mode of coordination for porphyrins is to behave as trianionic and tetradentate ligands. In rare cases, they act as tridentate and dianionic ligands, such as in oxovanadium (IV) and oxotitanium (IV) complexes of porphyrins (Figure 1.13).^[88]

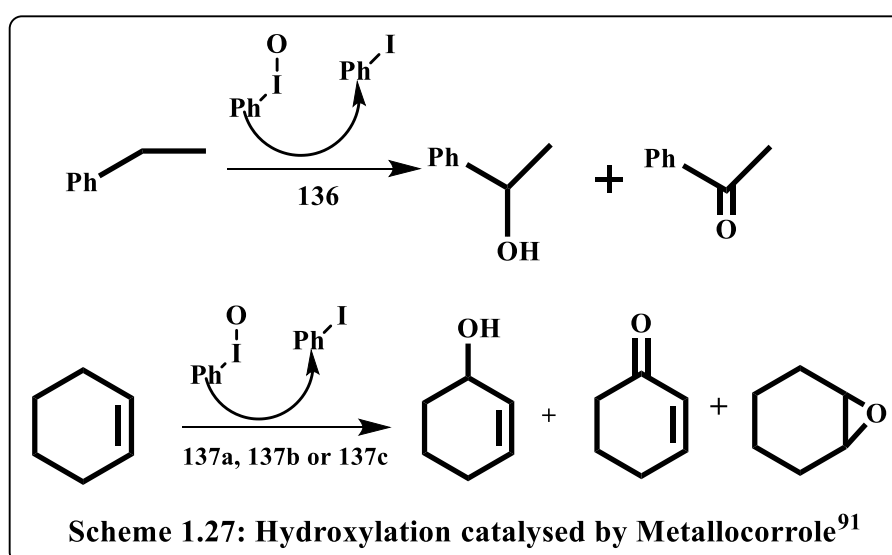
In view of the interest shown in the coordination chemistry of porphyrin, it is remarkable that the synthesis of *f*-block elemental porphyrin is still considerably underdeveloped.^[89,90] The low toxicity and unusual electronic properties have put the lanthanide in good use in biological imaging and single molecular magnets.



1.7 Corrole and Metalloporrole Applications:

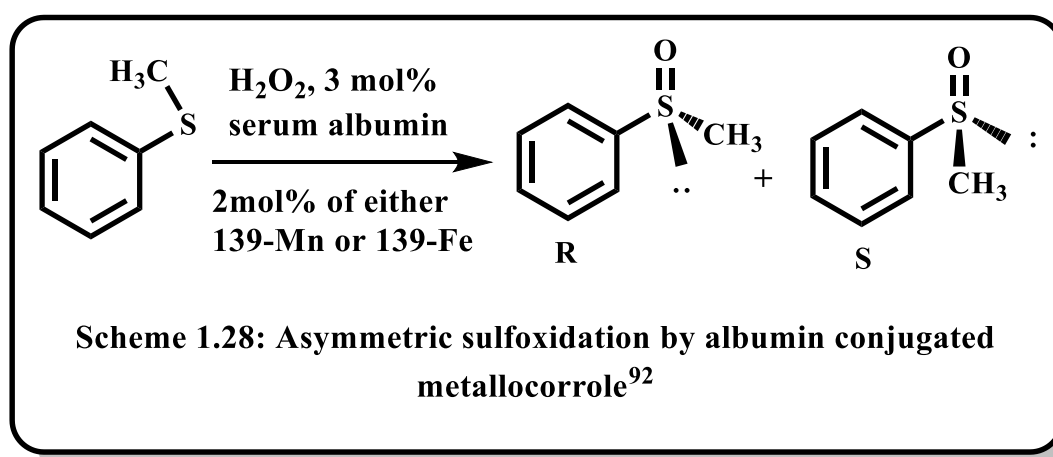
Over the last two decades, there has been a considerable growth in the chemistry of corrole derivatives, and this interest is continuously refreshed by new discoveries, which have allowed for their use in a variety of areas. In this section, we will discuss several examples of corroles being employed as essential components in gaseous molecule detection, catalysis, and bio-medical-related research.

A catalyst in oxidation reaction: The hydroxylation of ethylbenzene by iodosyl benzene to produce the corresponding alcohol and ketone is catalyzed by Fe (tpfc) Cl, **136**, (Scheme 1.27, Figure 1.14).^[91] However, the catalytic activity and yield of the equivalent porphyrin [Fe(tpfp)Cl] derivative are significantly higher. Following that, this hydroxylation reaction was further investigated, employing manganese corrole, **137**, as a catalyst to convert cyclohexene to corresponding products, demonstrating its advantage over the former iron complex, **136**, in terms of product yield, turnover frequency, and reaction stability (Scheme 1.27).



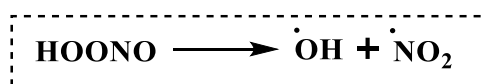
Later, Luobeznova *et. al.*^[92] reported antimony corroles, **138**, as an excellent catalyst to promote the aerobic oxidation reaction of hydrocarbon to corresponding peroxides

(Figure 1.14). The *trans*-difluoroantimony(V) corrole, **138a**, demonstrated exceptional reactivity and selectivity for the aerobic oxidation as compare to others metallo-corroles. The bis-sulfonated Mn(III), Fe(III), **139**, corrole complexes interact non-covalently with serum albumins, help in enantioselective oxidation of sulphides by H₂O₂ (Scheme 1.28). The kinetic study of the experiment clearly indicates that catalysis was dependent on metallo-corrole complexes.



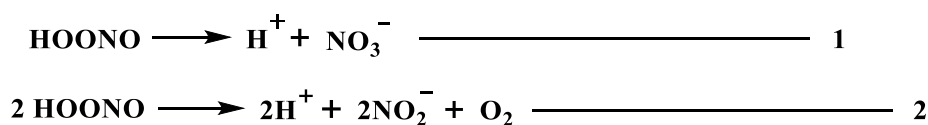
A Catalysis in Reduction Reaction:

Because corroles may stabilize higher oxidation states of metals, low-valent metallocorroles are predicted to be very reactive. The metallocorroles can show strong catalase-like activity, were investigated as catalysts for the breakdown of another ROS: peroxynitrite (PN), the nitrogen-containing analogue of hydrogen peroxide (H₂O₂). Because of its spontaneous degradation by homolytic bond cleavage to OH[•] and NO₂[•], PN may be regarded the most damaging ROS.



During environmental stress, reactive oxygen species levels can rise, causing damage to cellular molecules such as DNA, proteins, peptides, lipids, and carbohydrates, leading to

a variety of neurodegenerative diseases such as Huntington's, Alzheimer's, and Parkinson's diseases. Unfortunately, no such enzyme was available to mitigate its damaging effects on live cells. Gross et al.,^[93,94] were the first to describe the two amphiphilic metallocorroles, **139a** and **139b**, in 2006. Both the studied metallocorroles, **139a** and **139b**, were found to be efficient catalysts for the detoxification of peroxyxynitrites. The half-life duration of peroxyxynitrite, for instance, was substantially reduced from 1.8s to 0.025s and 0.31s with 4 mol% **139a** and **139b**, respectively (Figure 1.14). The Fe-corrole complex catalyses the breakdown process *via* isomerization (Equation 1) and forms nitrate anion with more efficiency than the equivalent porphyrin derivative. Mn-corrole, on the other hand, exhibits catalytic activity *via* the disproportionation process (Equation 2) and does not create any radical species.

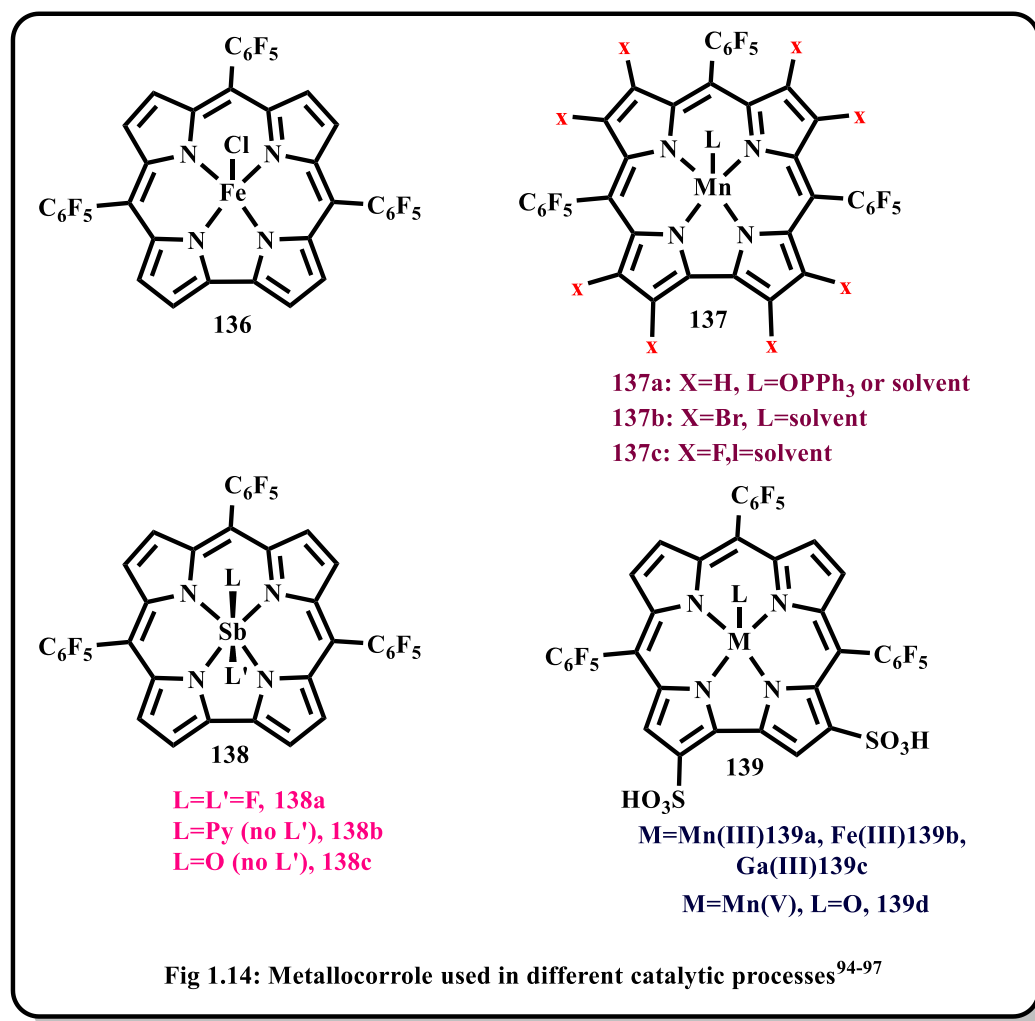


Chemical Sensors

The unique coordination mechanism of metallocorrole compounds promotes this macrocycle for the development of chemical sensors. The recent development of corrole as chemical-sensors will be discussed in below section.^[95]

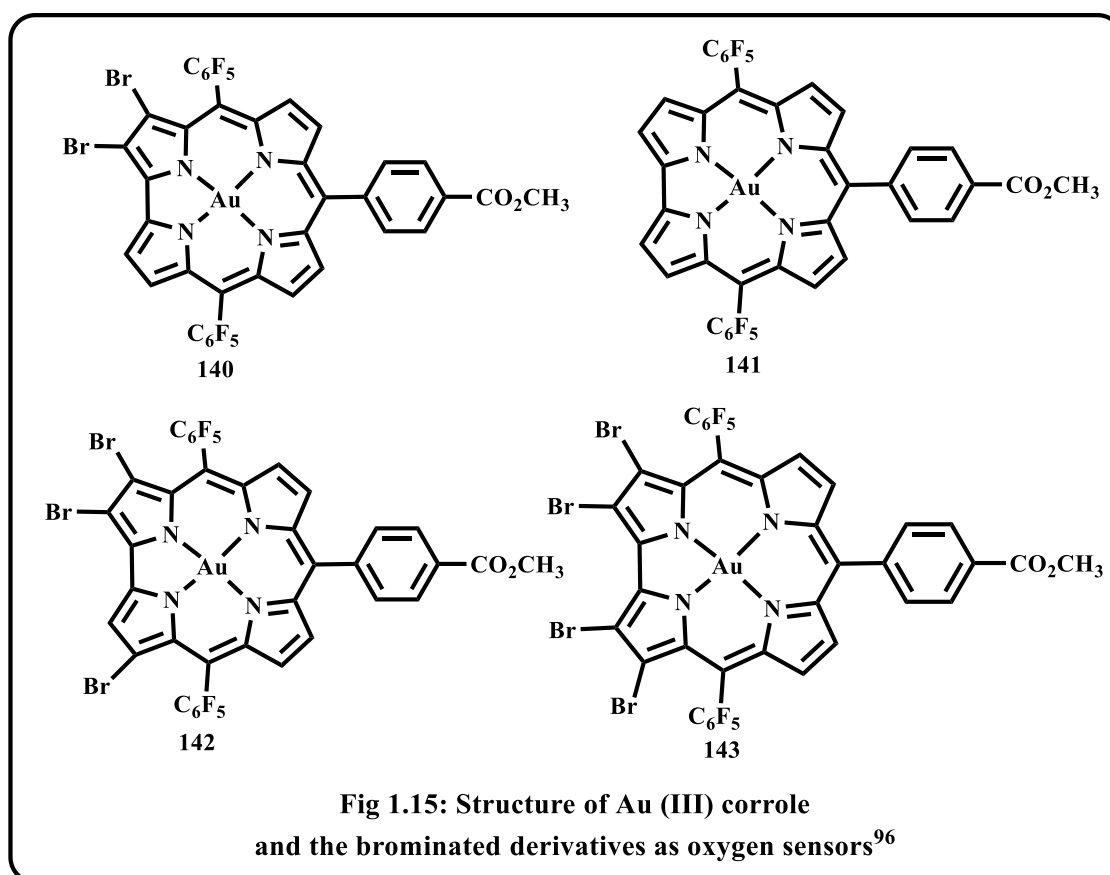
Oxygen detection has been one of the most extensively researched sensor applications, owing to the critical nature of molecular oxygen detection in a variety of disciplines. These oxygen sensing tools based on sensing mechanism of Pd and Pt porphyrin macrocycle phosphorescence quenching. Due to the fact that gold corroles emit a near-infrared phosphorescence, they may be useful for developing optical oxygen sensors in biological materials. Nocera and groups^[96] described the photophysical characterisation

of the β -substituted Au (III) corrole compounds (Figure 1.15), as well as the related oxygen sensing behaviour. The phosphorescence emission of gold corroles at ambient temperature was suppressed by air, indicating that these corroles are sensitive to molecular oxygen at a range of concentrations relevant for biological uses.



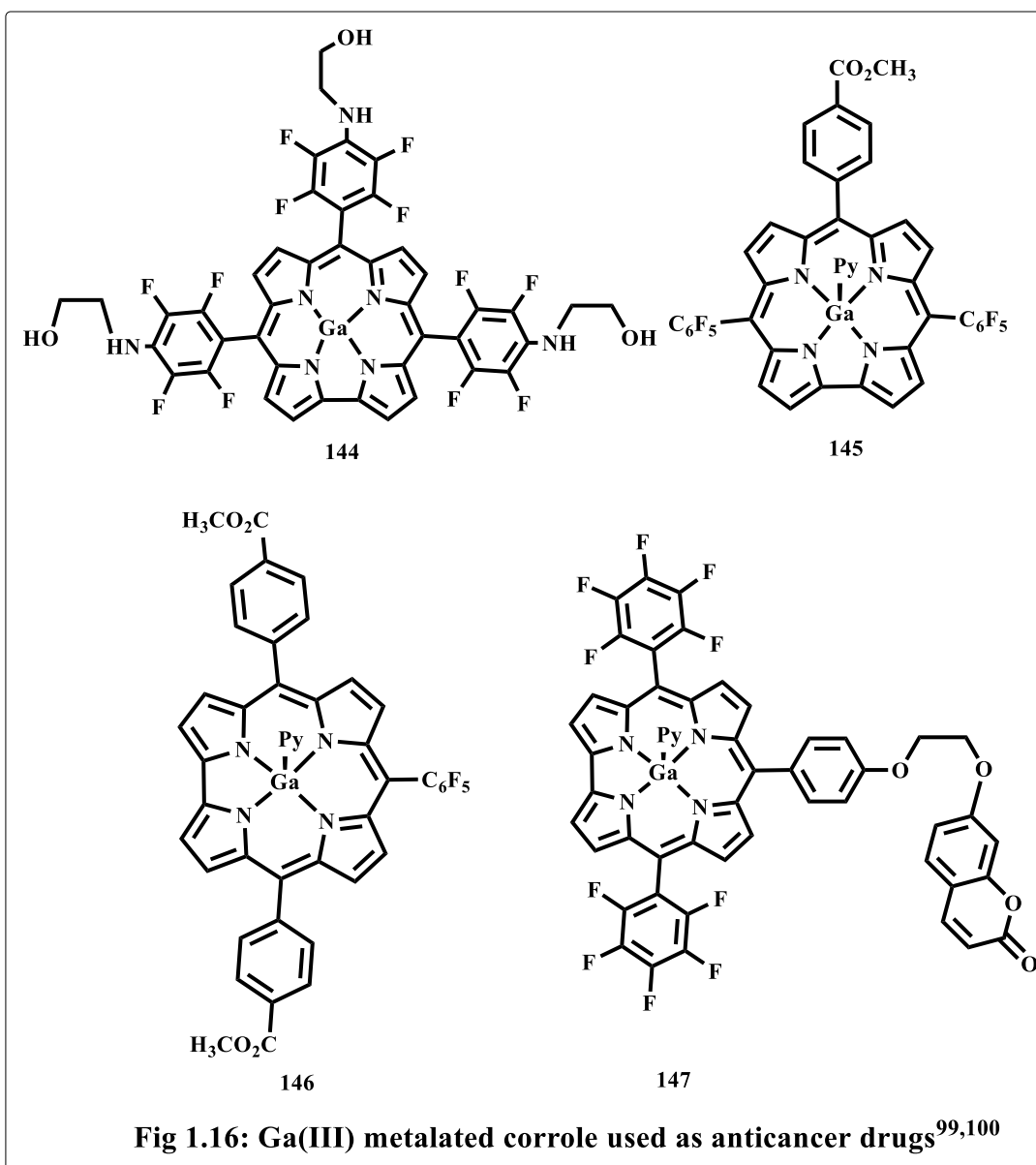
CO detection is critical for both domestic and industrial uses. Although commercial detectors are available, each has its own advantages and disadvantages. Cobalt (III) corroles may bind CO, which is typically exclusively seen in cobalt (II) complexes.^[97,98] The former was also inert to O₂, but the latter was not. As a result, cobalt (III) corroles might be used as CO gas sensors. By examining the absorption properties of all cobalt-corrole complexes, it was determined that CO affinity is directly related to the Lewis

acidity of the cobalt complex and that as the electron density on the cobalt atom increases, the Lewis acidity decreases, resulting in a decrease in CO affinity.



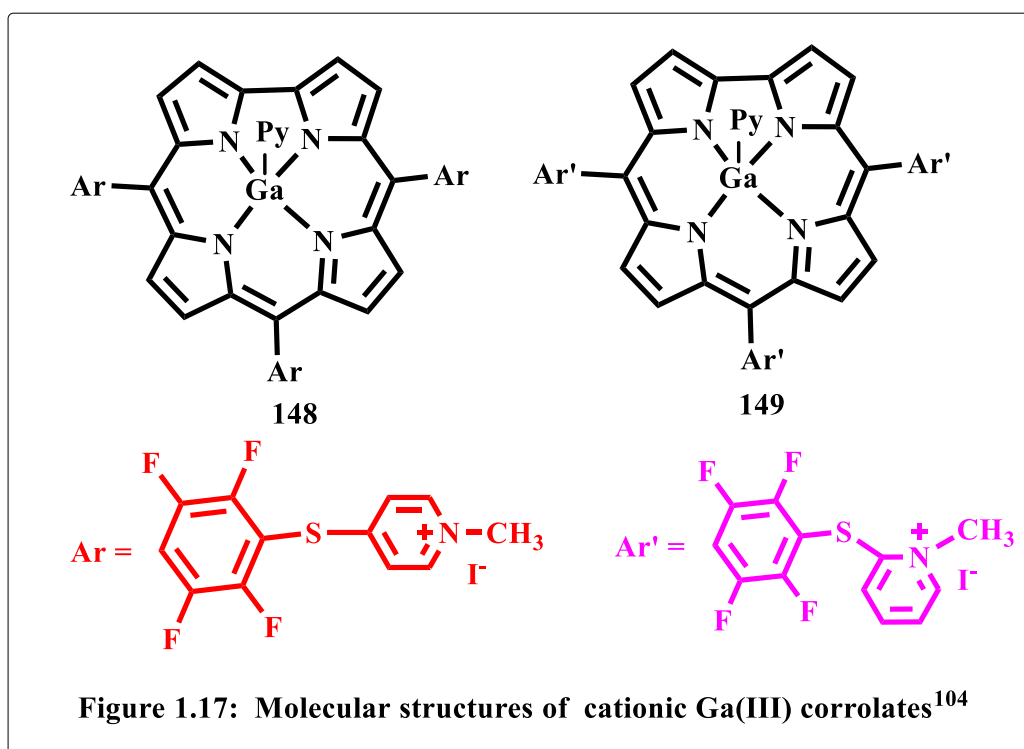
Medical and Biological Applications:

Anti-cancer applications: A recent evaluation of the use of corrole derivatives in cancer therapy was published.^[99] Triarylcorroles operate as photosensitizers in PDT due to their unique optical properties. The corrole, **38**, has been altered with hydroxyl groups, **144**, to increase its accessibility in biological applications (Figure 1.16).^[100] The DNA binding and photosensitizing activities of this hydroxyl corrole and its associated Ga corrole complex against tumour cells were examined. UV-visible spectroscopy revealed red shifts in Soret bands upon DNA binding, implying external binding for both the FB corrole and Ga corrole. This theory is also supported by fluorescence quenching and viscosity measurement.



The Ga-corrole cleaved DNA more efficiently than the FB-corrole following light irradiation, and the photocleavage mechanism was linked to singlet oxygen generation.

The DNA binding interaction of Ga-corrole, **145**, **146**, was later evaluated. The interaction of these complexes with DNA was determined by detecting the fluorescence quenching of **145**, **146** in the presence of CT-DNA. A Ga-corrole - DNA complex is not luminous. The absorption spectra indicate the presence of a groove binding mode, which was validated by viscosity measurements using the Ga-corrole, **145**.

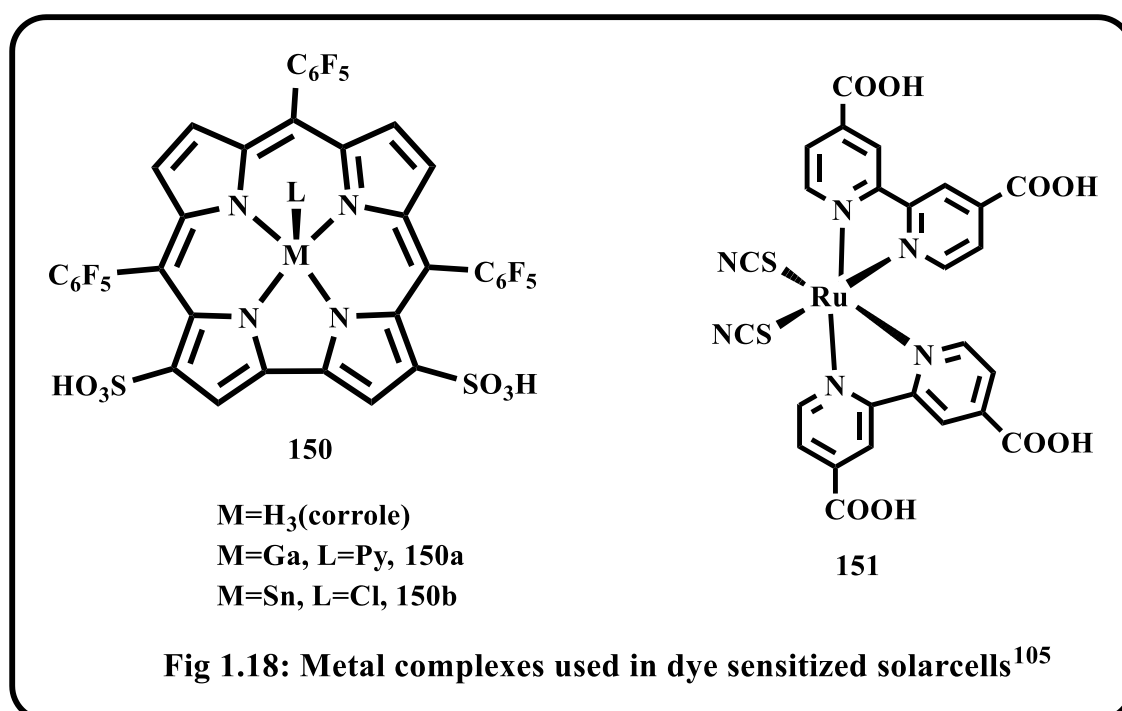


Photodynamic inactivation: Corrole derivatives have lately been investigated for their possible use in the PDI of bacteria and fungus. Cardote *et. al.* investigated the antibacterial effect of Ga metalated cationic corroles (Figure 1.17) against Gram-negative bacteria that produce bioluminescence.^[101] When the photoinactivation activity of Ga corroles was compared to other porphyrin (tPyMePI), it was found that the kinetics of the PDI was similar at higher concentrations of photosensitizers, while the Ga-corroles, **148**, **149**, was able to achieve complete photoinactivation of pathogens in a lesser duration than the corresponding porphyrin.

Dye-sensitized solar cell:

Alternative energy sources have the potential to decrease reliance on costly fossil fuels and improve economic stability, which drives researchers to create renewable energy resources. As the corroles frontier orbitals are more energetic than those of porphyrins; their use as sensitizers in DSSCs was investigated. The bis-sulfonated

tris(pentafluorophenyl) corrole and their Ga and Sn complexes were investigated for this purpose (Figure 1.18). Solar cells with dye sensitization are the most promising and cost-effective methods of converting solar energy to electrical energy. The most often employed dyes in this application are Ru (II) bipyridine derivatives, **151**, and porphyrinoids. The FB corrole, **150**, its gallium, **150a**, and tin, **150b**, complexes were selected due to their structural resemblance to the most effective dyes, **151**.^[102] It was found that all these complexes were bonded to mesoporous material TiO₂, but the efficiency of the Sn complex was much less regardless of FB-corrole. However, the Ga-corrole complex have comparable efficiency. The different measurements showed that suitably substituted corroles were superior as a sensitizer compared with other tetrapyrrolic derivatives.



References

- [1] A. R. Battersby, C. J. R. Fookes, G. W. J. Matcham, E. McDonald, *Nature* **1980**, 285, 17–21.
- [2] J. M. Vanderkooi, M. Erecińska, *Eur. J. Biochem.* **1975**, 60, 199–207.
- [3] J. L. R. Anderson, C. T. Armstrong, G. Kodali, B. R. Lichtenstein, D. W. Watkins, J. A. Mancini, A. L. Boyle, T. A. Farid, M. P. Crump, C. C. Moser, P. L. Dutton, *Chem. Sci.* **2014**, 5, 507–514.
- [4] L. J. A., H. D. L., S. Igor, S. Magdalene, *Infect. Immun.* **2002**, 70, 1461–1467.
- [5] C. J. Weschler, B. M. Hoffman, F. Basolo, *J. Am. Chem. Soc.* **1975**, 97, 5278–5280.
- [6] A. Osuka, K. Maruyama, *Chem. Lett.* **1987**, 16, 825–828.
- [7] A. Kaplan, E. Korin, A. Bettelheim, *Eur. J. Inorg. Chem.* **2014**, 2014, 2288–2295.
- [8] T. Wang, D. Zhu, G. Liu, W. Tao, W. Cao, L. Zhang, L. Wang, H. Chen, L. Mei, L. Huang, X. Zeng, *RSC Adv.* **2015**, 5, 50617–50627.
- [9] A. W. Johnson, A. Todd, in *Vitam. Horm.*, Elsevier, **1957**, pp. 1–30.
- [10] S. J. Sessler, J. L.; Weghorn, *Expanded, Contracted & Isomeric Porphyrins*, Elsevier, **1997**.
- [11] R. . Kadish, K. M.; Smith, K. M.; Guillard, *The Porphyrin Handbook*, Elsevier, **n.d.**
- [12] A. W. Johnson, R. Price, *J. Chem. Soc.* **1960**, 1649–1653.
- [13] A. W. Johnson, I. T. Kay, *J. Chem. Soc.* **1965**, 1620–1629.
- [14] H. R. Harrison, O. J. R. Hodder, D. C. Hodgkin, *J. Chem. Soc. B Phys. Org.* **1971**, 640–645.
- [15] J. F. B. Barata, M. G. P. M. S. Neves, M. A. F. Faustino, A. C. Tomé, J. A. S. Cavaleiro, *Chem. Rev.* **2017**, 117, 3192–3253.
- [16] J. M. Dyke, N. S. Hush, M. L. Williams, I. S. Woolsey, *Mol. Phys.* **1971**, 20, 1149–1152.

-
- [17] M. J. Broadhurst, R. Grigg, G. Shelton, A. W. Johnson, *J. Chem. Soc. Perkin Trans. 1* **1972**, 143–151.
- [18] Z. Gross, N. Galili, L. Simkhovich, I. Saltsman, M. Botoshansky, D. Bläser, R. Boese, I. Goldberg, *Org. Lett.* **1999**, *1*, 599–602.
- [19] R. PAOLESSE, F. SAGONE, A. MACAGNANO, T. BOSCHI, L. PRODI, M. MONTALTI, N. ZACCHERONI, F. BOLLETTA, K. M. SMITH, *J. Porphyr. Phthalocyanines* **1999**, *03*, 364–370.
- [20] Y. S. Balazs, I. Saltsman, A. Mahammed, E. Tkachenko, G. Golubkov, J. Levine, Z. Gross, *Magn. Reson. Chem.* **2004**, *42*, 624–635.
- [21] R. Paolesse, E. Tassoni, S. Licocchia, M. Paci, T. Boschi, *Inorganica Chim. Acta* **1996**, *241*, 55–60.
- [22] M. Conlon, A. W. Johnson, W. R. Overend, D. Rajapaksa, C. M. Elson, *J. Chem. Soc. Perkin Trans. 1* **1973**, 2281–2288.
- [23] M. J. Broadhurst, R. Grigg, A. W. Johnson, *J. Chem. Soc. {,} Perkin Trans. 1* **1972**, 1124–1135.
- [24] M. Kin Tse, Z. Zhang, K. Shing Chan, *Chem. Commun.* **1998**, 1199–1200.
- [25] R. Orłowski, D. Gryko, D. T. Gryko, *Chem. Rev.* **2017**, *117*, 3102–3137.
- [26] R. Paolesse, S. Mini, F. Sagone, T. Boschi, L. Jaquinod, D. J. Nurco, K. M. Smith, *Chem. Commun.* **1999**, 1307–1308.
- [27] B. Koszarna, D. T. Gryko, *J. Org. Chem.* **2006**, *71*, 3707–3717.
- [28] V. Kral, P. Vašek, B. Dolensky, *Collect. Czechoslov. Chem. Commun.* **2004**, *69*, 1126–1136.
- [29] D. T. Gryko, J. P. Fox, D. P. Goldberg, *J. Porphyr. Phthalocyanines* **2004**, *8*, 1091–1105.
- [30] T. Chatterjee, V. S. Shetti, R. Sharma, M. Ravikanth, *Chem. Rev.* **2017**, *117*, 3254–3328.

-
- [31] M. Bröring, F. Brégier, E. Cónsul Tejero, C. Hell, M. C. Holthausen, *Angew. Chemie Int. Ed.* **2007**, *46*, 445–448.
- [32] D. Sakow, B. Böker, K. Brandhorst, O. Burghaus, M. Bröring, *Angew. Chemie* **2013**, *125*, 5012–5015.
- [33] H. Kamiya, T. Kondo, T. Sakida, S. Yamaguchi, H. Shinokubo, *Chem. Eur. J.* **2012**, *18*, 16129–16135.
- [34] N. Wachi, T. Kondo, S. Ito, S. Hiroto, J.-Y. Shin, H. Shinokubo, *J. Porphyr. Phthalocyanines* **2014**, *18*, 675–678.
- [35] R. He, H. Yue, J. Kong, *Molecules* **2017**, *22*, 1400.
- [36] D. Sakow, D. Baabe, B. Böker, O. Burghaus, M. Funk, C. Kleeberg, D. Menzel, C. Pietzonka, M. Bröring, *Chem. Eur. J.* **2014**, *20*, 2913–2924.
- [37] M. Bröring, S. Köhler, C. Pietzonka, *J. Porphyr. Phthalocyanines* **2012**, *16*, 641–650.
- [38] Y. Xie, P. Wei, X. Li, T. Hong, K. Zhang, H. Furuta, *J. Am. Chem. Soc.* **2013**, *135*, 19119–19122.
- [39] J. Rösner, B. Cordes, S. Bahn Müller, G. Homolya, D. Sakow, P. Schweyen, R. Wicht, M. Bröring, *Angew. Chemie* **2017**, *129*, 10099–10102.
- [40] B. Sridevi, S. Jeyaprakash Narayanan, T. K. Chandrashekar, U. Englich, K. Ruhlandt-Senge, *Chem. Eur. J.* **2000**, *6*, 2554–2563.
- [41] J. Sankar, H. Rath, V. Prabhuraja, S. Gokulnath, T. K. Chandrashekar, C. S. Purohit, S. Verma, *Chem. Eur. J.* **2007**, *13*, 105–114.
- [42] M. J. Broadhurst, R. Grigg, A. W. Johnson, *J. Chem. Soc. D Chem. Commun.* **1969**, 23–24.
- [43] M. Pawlicki, L. Latos-Grażyński, L. Szterenberga, *J. Org. Chem.* **2002**, *67*, 5644–5653.
- [44] M. Pawlicki, D. Bykowski, L. Szterenberga, L. Latos-Grażyński, *Angew. Chemie Int. Ed.* **2012**, *51*, 2500–2504.
-

-
- [45] A. W. Johnson, I. T. Kay, R. Rodrigo, *J. Chem. Soc. Perkin Trans* **1963**, *1*, 1124–1135.
- [46] M. Horie, Y. Hayashi, S. Yamaguchi, H. Shinokubo, *Chem. Eur. J.* **2012**, *18*, 5919–5923.
- [47] B. Umasekhar, V. S. Shetti, M. Ravikanth, *RSC Adv.* **2018**, *8*, 21100–21132.
- [48] A. Ghosh, T. Chatterjee, W.-Z. Lee, M. Ravikanth, *Org. Lett.* **2013**, *15*, 1040–1043.
- [49] I. Gupta, M. Ravikanth, *J. Org. Chem.* **2004**, *69*, 6796–6811.
- [50] S. J. Narayanan, B. Sridevi, T. K. Chandrashekar, U. Englich, K. Ruhlandt-Senge, *Org. Lett.* **1999**, *1*, 587–590.
- [51] J. Sankar, H. Rath, V. PrabhuRaja, T. K. Chandrashekar, J. J. Vittal, *J. Org. Chem.* **2004**, *69*, 5135–5138.
- [52] H. Kalita, D. Kalita, W. Lee, J. Bellare, M. Ravikanth, *Chem. Eur. J.* **2014**, *20*, 10404–10413.
- [53] H. Kalita, M. Ravikanth, *Chem. Eur. J.* **2015**, *21*, 7399–7402.
- [54] S. Venkatraman, R. Kumar, J. Sankar, T. K. Chandrashekar, K. Sendhil, C. Vijayan, A. Kelling, M. O. Senge, *Chem. Eur. J.* **2004**, *10*, 1423–1432.
- [55] K. Fujino, Y. Hirata, Y. Kawabe, T. Morimoto, A. Srinivasan, M. Toganoh, Y. Miseki, A. Kudo, H. Furuta, *Angew. Chemie* **2011**, *123*, 6987–6991.
- [56] M. Li, P. Wei, M. Ishida, X. Li, M. Savage, R. Guo, Z. Ou, S. Yang, H. Furuta, Y. Xie, *Angew. Chemie Int. Ed.* **2016**, *55*, 3063–3067.
- [57] B. C.-H. C. Lee, W.-S. Cho, J.-W. Ka, H.-J. Kim and P. H. Lee, *Korean Chem. Soc.* **2000**, *21*, 429–433.
- [58] J.-Y. Shin, *J. Porphyr. Phthalocyanines* **2020**, *24*, 191–199.
- [59] T. Ito, Y. Hayashi, S. Shimizu, J. Shin, N. Kobayashi, H. Shinokubo, *Angew. Chemie* **2012**, *124*, 8670–8673.
- [60] G. Hohlneicher, D. Bremm, J. Wytko, J. Bley-Esrich, J. Gisselbrecht, M. Gross, M. Michels, J. Lex, E. Vogel, *Chem. Eur. J.* **2003**, *9*, 5636–5642.
-

-
- [61] A. Mahammed, M. Botoshansky, Z. Gross, *Dalt. Trans.* **2012**, *41*, 10938–10940.
- [62] K. Sudhakar, V. Velkannan, L. Giribabu, *Tetrahedron Lett.* **2012**, *53*, 991–993.
- [63] R. Paolesse, L. Jaquinod, M. O. Senge, K. M. Smith, *J. Org. Chem.* **1997**, *62*, 6193–6198.
- [64] M. Stefanelli, M. Mastroianni, S. Nardis, S. Licocchia, F. R. Fronczek, K. M. Smith, W. Zhu, Z. Ou, K. M. Kadish, R. Paolesse, *Inorg. Chem.* **2007**, *46*, 10791–10799.
- [65] Z. Gross, A. Mahammed, *J. Porphyr. Phthalocyanines* **2002**, *6*, 553–555.
- [66] Z. Gross, N. Galili, I. Saltsman, *Angew. Chemie Int. Ed.* **1999**, *38*, 1427–1429.
- [67] C. I. M. Santos, E. Oliveira, J. F. B. Barata, M. A. F. Faustino, J. A. S. Cavaleiro, M. G. P. M. S. Neves, C. Lodeiro, *J. Mater. Chem.* **2012**, *22*, 13811–13819.
- [68] C. Li, M. Fechtel, Y. Feng, B. Kräutler, *J. Porphyr. Phthalocyanines* **2012**, *16*, 556–563.
- [69] T. H. Ngo, F. Puntoriero, F. Nastasi, K. Robeyns, L. Van Meervelt, S. Campagna, W. Dehaen, W. Maes, *Chem. Eur. J.* **2010**, *16*, 5691–5705.
- [70] W. Maes, T. H. Ngo, J. Vanderhaeghen, W. Dehaen, *Org. Lett.* **2007**, *9*, 3165–3168.
- [71] T. H. Ngo, F. Nastasi, F. Puntoriero, S. Campagna, W. Dehaen, W. Maes, *J. Org. Chem.* **2010**, *75*, 2127–2130.
- [72] M. J. Broadhurst, R. Grigg, G. Shelton, A. W. Johnson, *J. Chem. Soc. D Chem. Commun.* **1970**, 231–233.
- [73] I. Saltsman, I. Goldberg, Z. Gross, *Tetrahedron Lett.* **2003**, *44*, 5669–5673.
- [74] C. Brückner, C. A. Barta, R. P. Brinas, J. A. Krause Bauer, *Inorg. Chem.* **2003**, *42*, 1673–1680.
- [75] W. Sinha, M. G. Sommer, N. Deibel, F. Ehret, B. Sarkar, S. Kar, *Chem. Eur. J.* **2014**, *20*, 15920–15932.
- [76] A. B. Alemayehu, A. Ghosh, *J. Porphyr. Phthalocyanines* **2011**, *15*, 106–110.

-
- [77] K. E. Thomas, A. B. Alemayehu, J. Conradie, C. Beavers, A. Ghosh, *Inorg. Chem.* **2011**, *50*, 12844–12851.
- [78] W. Sinha, M. G. Sommer, M. van der Meer, S. Plebst, B. Sarkar, S. Kar, *Dalt. Trans.* **2016**, *45*, 2914–2923.
- [79] F. Jérôme, B. Billier, J. Barbe, E. Espinosa, S. Dahaoui, C. Lecomte, R. Guillard, *Angew. Chemie Int. Ed.* **2000**, *39*, 4051–4053.
- [80] K. M. Kadish, F. Burdet, F. Jérôme, J.-M. Barbe, Z. Ou, J. Shao, R. Guillard, *J. Organomet. Chem.* **2002**, *652*, 69–76.
- [81] L. Simkhovich, I. Luobeznova, I. Goldberg, Z. Gross, *Chem. Eur. J.* **2003**, *9*, 201–208.
- [82] R. Zhan, *Electrochemical and Spectroelectrochemical Studies of Porphyrins, Corrolazines, and Related Macrocycles*, University Of Houston, **2006**.
- [83] B. Ramdhanie, J. Telsler, A. Caneschi, L. N. Zakharov, A. L. Rheingold, D. P. Goldberg, *J. Am. Chem. Soc.* **2004**, *126*, 2515–2525.
- [84] S. Will, J. Lex, E. Vogel, V. A. Adamian, E. Van Caemelbecke, K. M. Kadish, *Inorg. Chem.* **1996**, *35*, 5577–5583.
- [85] L. Simkhovich, Z. Gross, *Inorg. Chem.* **2004**, *43*, 6136–6138.
- [86] O. Yadav, A. Varshney, A. Kumar, *Inorg. Chem. Commun.* **2017**, *86*, 168–171.
- [87] I. Saltsman, Y. Balazs, I. Goldberg, Z. Gross, *J. Mol. Catal. A Chem.* **2006**, *251*, 263–269.
- [88] S. Licoccia, R. Paolesse, E. Tassoni, F. Polizio, T. Boschi, *J. Chem. Soc. Dalt. Trans.* **1995**, 3617–3621.
- [89] G. Lu, S. Yan, M. Shi, W. Yu, J. Li, W. Zhu, Z. Ou, K. M. Kadish, *Chem. Commun.* **2015**, *51*, 2411–2413.
- [90] A. L. Ward, H. L. Buckley, W. W. Lukens, J. Arnold, *J. Am. Chem. Soc.* **2013**, *135*, 13965–13971.
- [91] Z. Gross, L. Simkhovich, N. Galili, *Chem. Commun.* **1999**, 599–600.
-

-
- [92] I. Luobeznova, M. Raizman, I. Goldberg, Z. Gross, *Inorg. Chem.* **2006**, *45*, 386–394.
- [93] M. Wiedau-Pazos, J. J. Goto, S. Rabizadeh, E. B. Gralla, J. A. Roe, M. K. Lee, J. S. Valentine, D. E. Bredesen, *Science (80-.)*. **1996**, *271*, 515–518.
- [94] A. Mahammed, Z. Gross, *Angew. Chemie* **2006**, *118*, 6694–6697.
- [95] R. Paolesse, S. Nardis, D. Monti, M. Stefanelli, C. Di Natale, *Chem. Rev.* **2017**, *117*, 2517–2583.
- [96] C. M. Lemon, D. C. Powers, P. J. Brothers, D. G. Nocera, *Inorg. Chem.* **2017**, *56*, 10991–10997.
- [97] K. M. Kadish, L. Frémond, Z. Ou, J. Shao, C. Shi, F. C. Anson, F. Burdet, C. P. Gros, J.-M. Barbe, R. Guillard, *J. Am. Chem. Soc.* **2005**, *127*, 5625–5631.
- [98] K. M. Kadish, Z. Ou, J. Shao, C. P. Gros, J.-M. Barbe, F. Jérôme, F. Bolze, F. Burdet, R. Guillard, *Inorg. Chem.* **2002**, *41*, 3990–4005.
- [99] R. D. Teo, J. Y. Hwang, J. Termini, Z. Gross, H. B. Gray, *Chem. Rev.* **2017**, *117*, 2711–2729.
- [100] Z. Liang, H. Liu, G. Jiang, J. Wen, Y. Liu, X. Xiao, *Chinese J. Chem.* **2016**, *34*, 997–1005.
- [101] T. A. F. Cardote, J. F. B. Barata, C. Amador, E. Alves, M. G. P. M. S. Neves, J. A. S. Cavaleiro, A. Cunha, A. Almeida, M. A. F. Faustino, *An. Acad. Bras. Cienc.* **2018**, *90*, 1175–1185.
- [102] D. Walker, S. Chappel, A. Mahammed, B. S. Brunshwig, J. R. Winkler, H. B. Gray, A. Zaban, Z. Gross, *J. Porphyr. Phthalocyanines* **2006**, *10*, 1259–1262.

Regioselective thiocyanation of corroles and the synthesis of gold nanoparticle–corrole assemblies

2.1 Introduction

2.2 Result and Discussion

2.2.1 Generalization of Synthetic Procedure

2.3 Spectral Characterisation

2.3.1 NMR Spectroscopy

2.3.2 Mass Spectrometry

2.3.3 IR spectroscopy

2.3.4 Single crystal XRD Analysis

2.3.5 Electronic Absorption Spectroscopy

2.4 Application of 1 in synthesis of gold Nano particle

2.4.1 Generalized Synthetic protocol

2.4.2 Time Evolution UV-Spectra for characterization of gold nano particle

2.4.3 Time Evolution emission spectra and fluorescence for characterization of gold nano particles

2.4.4 Transmission electron microscopy characterization

2.4.5 Electronic Absorption Spectrum

2.4.6 X-ray photoelectron spectroscopy

2.5 Conclusion

2.6 Experimental Section

2.6.1 Materials

2.6.2 Physical measurements

2.6.3 Crystal Structure Determination

2.6.4 Syntheses

2.1 Introduction:

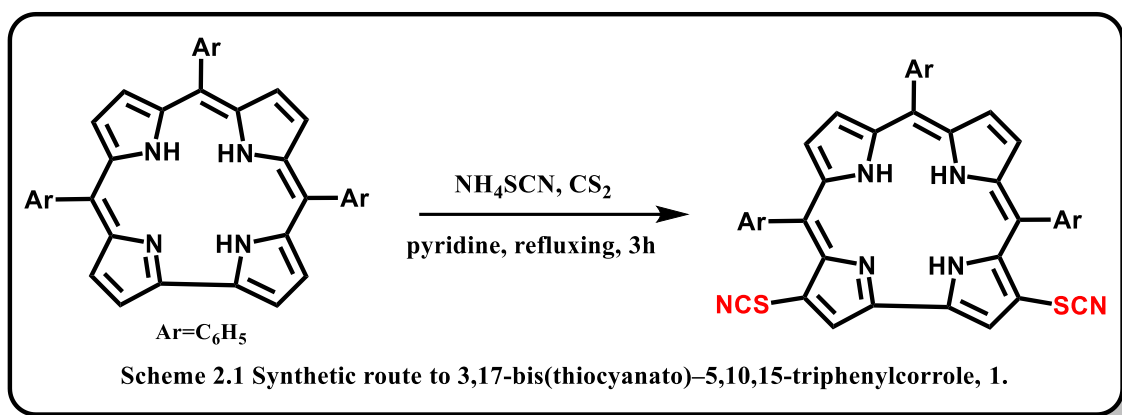
Gold nanoparticles (Au NPs) are extensively used in various areas like catalysis,^[1-3] medicine,^[4-6] sensors,^[7,8] fuel cells,^[9-11] surface enhanced Raman spectroscopy,^[12-14] probes for transmission electron microscopy,^[15-17] and antibiotics.^[18] One can easily coat the surface of Au NPs with various molecules, either small or big, and thus can fine tune their physical and chemical properties.^[19-22] In this context, Au NPs bearing π -conjugated molecules are ideal platforms for various nanoelectronic devices.^[23-26] Thus there is widespread research interest in studying porphyrinoid coated gold nanoparticles.^[27-30] Feringa *et al.* demonstrated that porphyrins having π -conjugation can coordinate with the Au (111) surface via intramolecular interactions (*via* linker groups) and also *via* interfacial interactions (*via* inner nitrogens).^[31] Corrole, a ring contracted version of porphyrin, has interesting and different photo physical properties in comparison to porphyrin.^[32-59] Thus, it is expected that corrole coated Au NPs will show great promise in designing newer varieties of functional materials having diverse applications. The importance of the multi-dentate ligand in binding the surface of the Au NPs in a specific orientation was demonstrated independently by Ohyama *et al.*^[60] and Teranishi *et al.*^[61] Very few research papers indeed highlight the importance of polydentate ligands as binders of gold nanoparticles.^[62] Tour *et al.* reported that organic thiocyanates can easily form assemblies on gold surfaces without the help of any external agent and have several advantages over free thiols or other thiol based precursors.^[63] Their observations have prompted us to choose the thiocyanato appended corrole as a possible precursor for the synthesis of gold nanoparticle–corrole assemblies. The existing literature reports that *meso*-substituted porphyrinoids are used exclusively as binders for gold nanoparticles, and the related β -substituted derivatives are rarely used for this purpose. As β -substitution has a more pronounced effect on the electronic structure, we have chosen β -

substitution at the corrole periphery. In order to obtain the thiocyanato appended corrole derivative, we have developed a simple and novel protocol for the regio-selective thiocyanation of corrole. To the best of our knowledge, the thiocyanato group has never been inserted at the corrole periphery. We have synthesized corrole coated gold nanoparticles by using a one-phase strategy.^[60] Corrole and H₂AuCl₄ solutions were mixed together, and then a NaBH₄ solution was added and stirred for 3 hours. No co-stabilizers (citrate, TOAB, etc.) were used for this purpose. The thiocyanato appended corrole, 3,17-bis(thiocyanato)-5,10,15-triphenylcorrole (**1**), was prepared by following a strategy developed by our group (Scheme 2.1).

2.2 Result and Discussion

2.2.1 Generalization of Synthetic Procedure

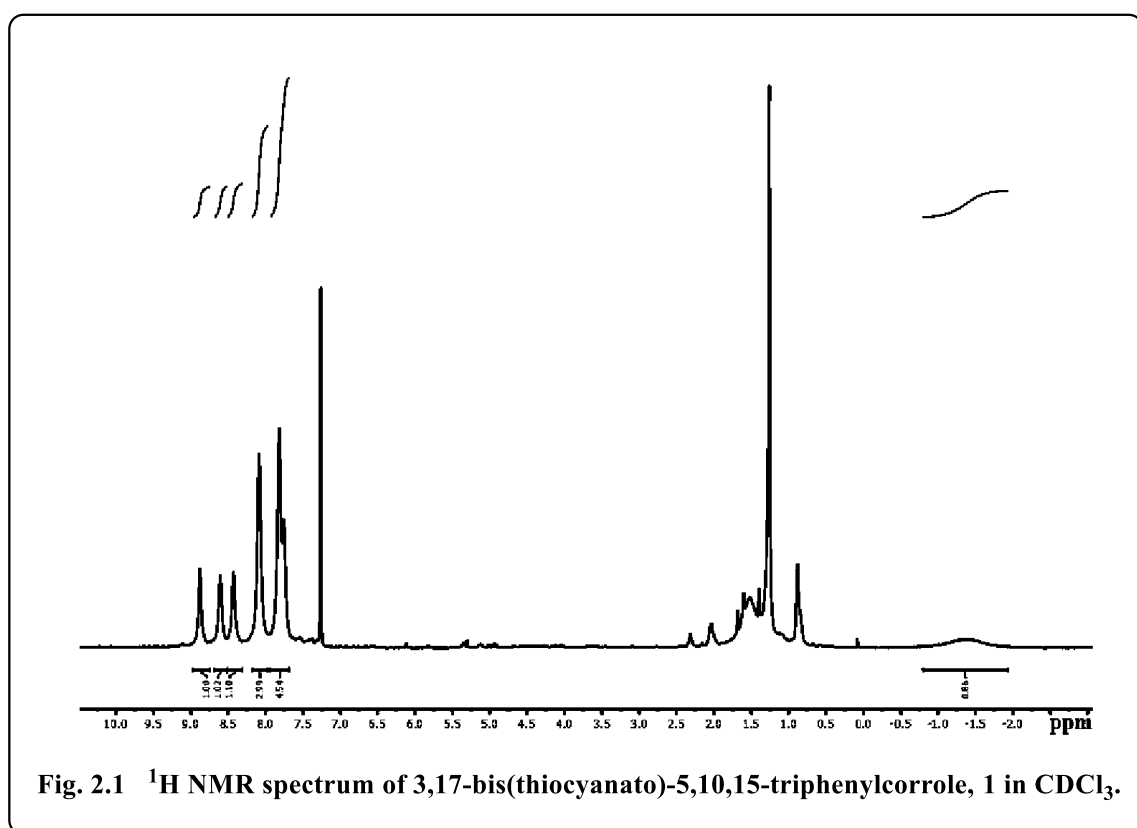
5,10,15-triphenylcorrole (TPC) in a carbon disulfide solution was treated with an excess amount of NH₄SCN and excess pyridine. Refluxing for 3 hours resulted in the formation of **1** in good yields (Scheme 2.1). The newly synthesized thiocyanato appended corrole (**1**) has been fully characterized using several spectroscopic techniques like CHN analysis, FT-IR analysis, ¹H NMR, ESI-mass spectrometry, XPS and single crystal XRD (Fig. 2.1–2.6 and Table 2.1, 2.2). Considering thiocyanate to be a potent nucleophile, this reaction should be considered a unique class of the nucleophilic aromatic substitution reaction in corrole.^[64] Paolesse *et al.* described this class of reactions as nucleophilic aromatic substitution of hydrogens, occurring *via* two steps. The first step is the formation of a α -adduct by simple addition of the nucleophile to the corrole ring and the second step is the elimination of hydride. Pyridine is suspected to be a hydride ion abstractor here.



2.3 Spectral Characterisation:

2.3.1 NMR Spectroscopy

The ¹H NMR spectrum of **1** exhibits normal chemical shifts in accordance with the ‘twenty one’ aromatic protons in the region δ , ~ 8.91–7.78 ppm. Negligible shielding is observed in **1** in comparison with 5,10,15-triphenylcorrole (Figure. 2.1).



2.3.2 Mass Spectrometry:

The electrospray mass spectrum in methanol showed peaks centred at $m/z = 641.145$ corresponding to $[1+H]^+$ (641.15 calcd for $C_{39}H_{25}N_6S_2$)(Figure 2.2).

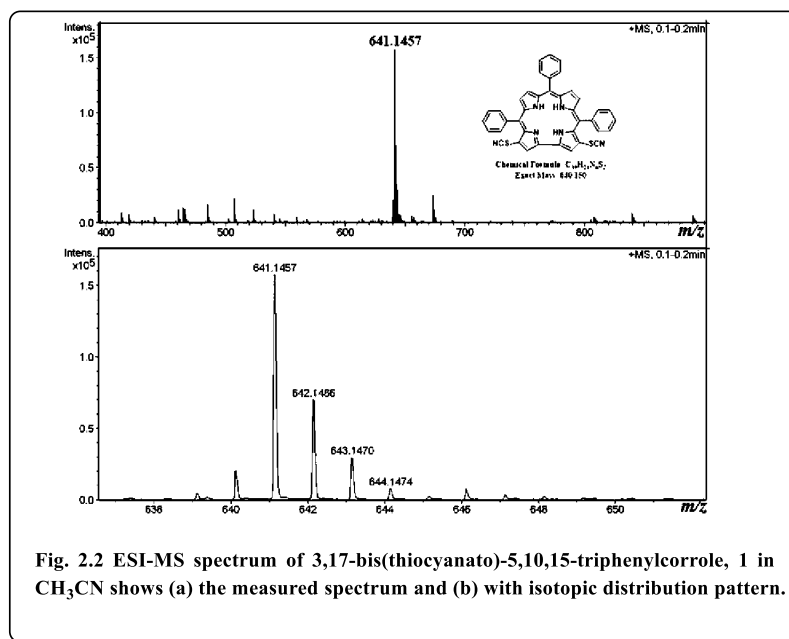


Fig. 2.2 ESI-MS spectrum of 3,17-bis(thiocyanato)-5,10,15-triphenylcorrole, 1 in CH_3CN shows (a) the measured spectrum and (b) with isotopic distribution pattern.

2.3.3 IR Spectroscopy:

The FT-IR spectrum of 1 as a KBr pellet shows a peak at 2154 cm^{-1} due to CN group stretching. The spectrum of Gold nanoparticle–Corrole assemblies shows the absence of CN group stretching at 2154 cm^{-1} (Figure 2.3).

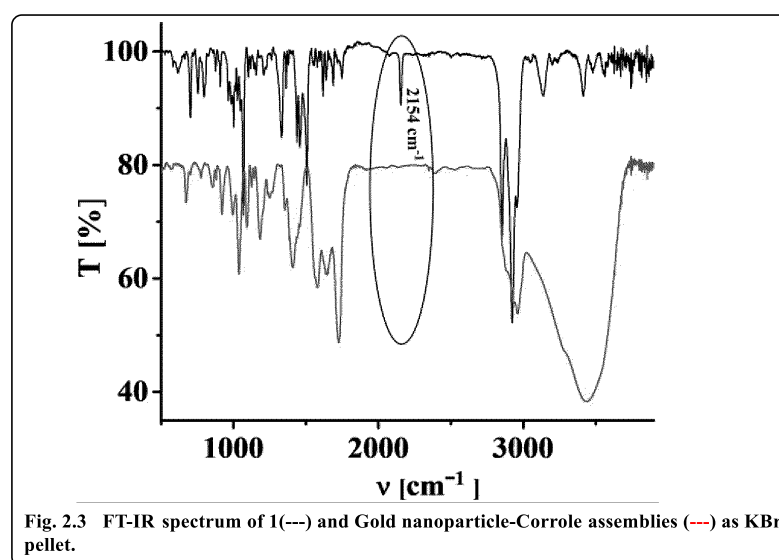


Fig. 2.3 FT-IR spectrum of 1(---) and Gold nanoparticle-Corrole assemblies (—) as KBr pellet.

2.3.4 Crystal Structure

The crystal system is triclinic, and the unit cell contains two molecules of 1. Important crystallographic parameters for compound 1 are shown in (Table 2.1). Bond distances and angles of 1 are in agreement with those of other FB corrole derivatives. Pyrrolic nitrogen atoms have shown deviations from the mean corrole plane (considering the 19-carbon atom plane to be the mean corrole plane) by distances varying from 0.488 to -0.052 Å in 1. The corresponding deviations in 5,10,15-triphenylcorrole (TPC) are 0.128 to -0.195 Å. The dihedral angles between the planes of the phenyl rings (meso-substituted phenyl group) and the 19-carbon mean corrole plane vary significantly and are 43.74 - 78.37° . The corresponding dihedral angles in TPC are 41.74 - 50.33° . [54] Thus, it appears that the insertion of two thiocyanate groups at the β -pyrrolic position induced significant saddling of the corrole framework. The two $C\equiv N$ (for N (5)-C (38) and N (6)-C (39)) bond distances of 1 are 1.13 Å and 1.14 Å and the two $S-C\equiv N$ bond angles (for S (1)-C (38)-N (5) and S (2)-C (39)-N (6)) are 177.66° and 178.85° .

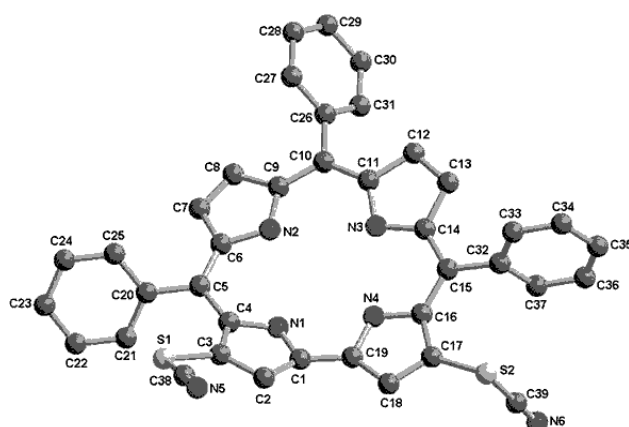


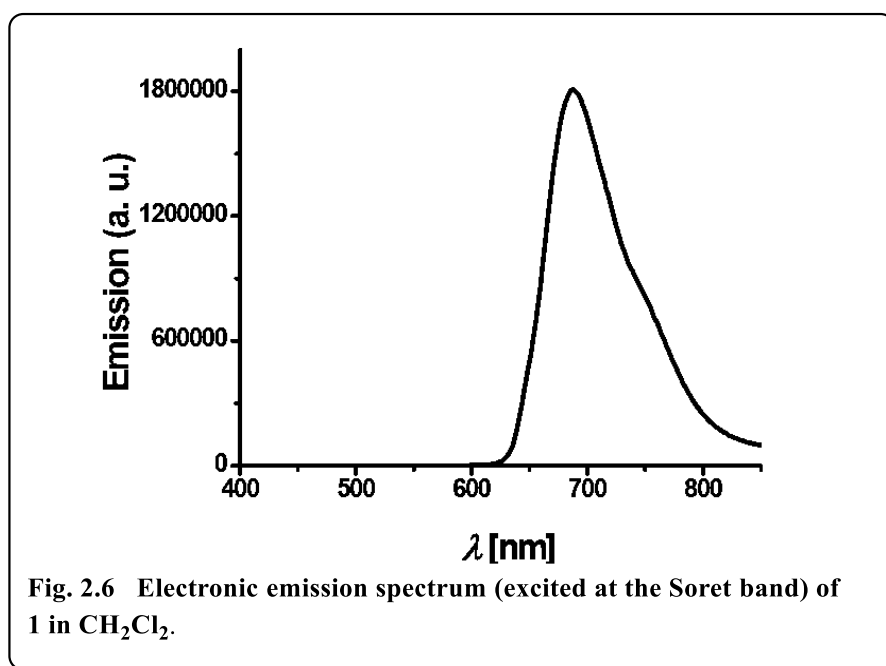
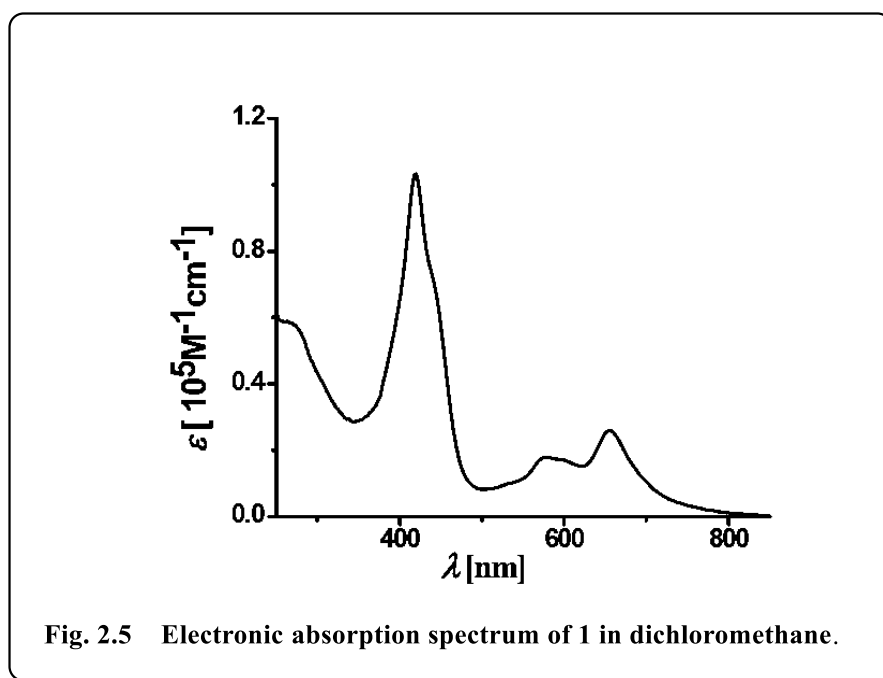
Fig. 2.4 Perspective view of 1. Hydrogen atoms are omitted for clarity.

Table 2.1 Crystallographic Data for **1**.

compound code	1
molecular formula	C ₃₉ H ₂₄ N ₆ S ₂
Fw	641.47
Radiation	Cu K α
crystal symmetry	Triclinic
space group	P-1
<i>a</i> (Å)	8.6895 (2)
<i>b</i> (Å)	13.6651 (4)
<i>c</i> (Å)	13.7221(3)
α (deg)	97.560
β (deg)	104.489
γ (deg)	96.725
<i>V</i> (Å ³)	1544.64(7)
<i>Z</i>	2
μ (mm ⁻¹)	1.878
<i>T</i> (K)	298
<i>D</i> _{calcd} (g cm ⁻³)	1.380
2 θ range (deg)	3.303 to 66.997
<i>e</i> data (<i>R</i> _{int})	4275 (0.0639)
<i>R</i> ₁ (<i>I</i> > 2 σ (<i>I</i>))	0.0647
<i>WR</i> ₂ (all data)	0.1813
GOF	1.077
$\Delta\rho_{\max}$, $\Delta\rho_{\min}$ (e Å ⁻³)	0.33, -0.41

2.3.5 Photophysical properties:

The UV-Vis spectra of **1** is similar to the other corroles and soret band appears at 419 nm and other Q-bands in the region 570-660 nm in CH₂Cl₂ (Figure 2.5). **1** displayed strong fluorescence at 688 nm in DCM (Figure 2.6).

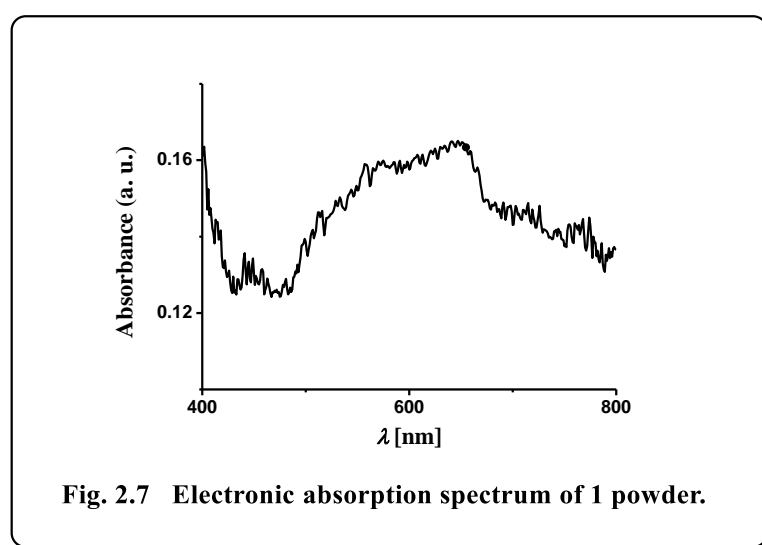


2.4 Application of **1** in synthesis of gold Nano particles:

2.4.1 Generalized Synthetic protocol

Gold nanoparticles coated with **1** were prepared by addition of NaBH_4 to a premixed mixture of **1** and HAuCl_4 . The newly synthesized **1**-Au NPs were characterized by CHN, EDS and FT-IR analysis (Figure 2.14 and 2.3). The EDS spectrum of **1**-Au NPs shows

the presence of all the constituent elements (Au, N, and S). From CHN analysis, we can roughly estimate that there are 200 corrole ligands on a single Au NP surface. This implies that there are many physisorbed corrole molecules at the surface which do not have direct contact with the gold surface. The UV-Vis spectra of the solid samples of **1** (very broad and red shifted) clearly indicate extensive aggregate formation (Figure. 2.7). The FT-IR spectrum of Au NP–corrole assemblies obtained using a KBr pellet shows the absence of C≡N group stretching at 2154 cm^{-1} (Figure. 2.3). This confirms that the ligand moiety loses the C≡N group while binding with the Au surface.



2.4.2 Time Evolution UV-Spectra for characterization of gold nano particles

The time evolution of the UV-Vis spectra for mixtures of **1** ($\sim 10^{-6}\text{ M}$), NaBH_4 ($\sim 10^{-4}\text{ M}$), and HAuCl_4 ($\sim 10^{-5}\text{ M}$) in DMF was shown in Figure 2.8. The initial spectrum (black colour, colour online) was for pure **1** in the DMF solution. It was observed that the positions of the Soret and Q bands in **1** are negligibly changed upon addition of NaBH_4 . However, both bands are drastically different in intensity upon gradual addition of the HAuCl_4 solution. The red coloured final spectrum (colour online) was obtained after the addition of optimal concentration of the HAuCl_4 ($\sim 2 \times 10^{-5}\text{ M}$) solution. The final

spectrum obtained after 2.5 hours shows a clear signature of the combination of the characteristic Soret band of corrole **1** (as a weak shoulder) and the strong plasmon band of gold nanoparticles. The surface plasmon resonance (SPR) band appears at 525 nm.^{[60],[61]} The intensity of the Q bands of **1** is drastically reduced but it still remains as a shoulder at around 655 nm. However, the Soret bands are broadened but the shifts of the bands are negligible. A direct comparison of these UV-Vis spectra with that of the FB corrole **1** (prior to Au–thiol contact formation) is not possible because after the interaction of FB corrole **1** with the gold nanoparticles, the thiocyanate group loses the cyanide fragment (after Au–thiol contact formation) and thus the ligand electronic structure is perturbed.

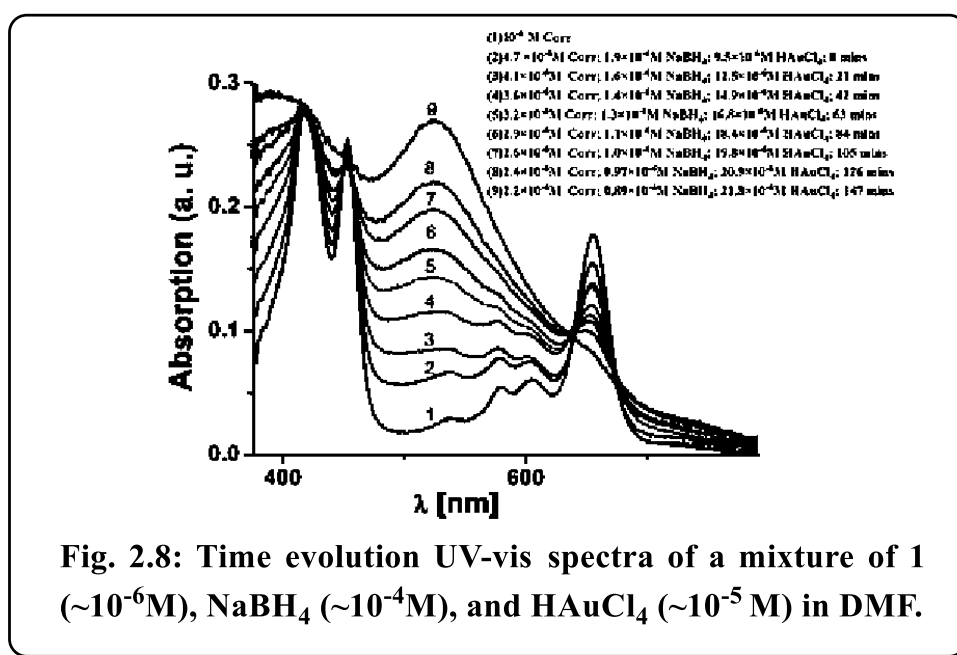


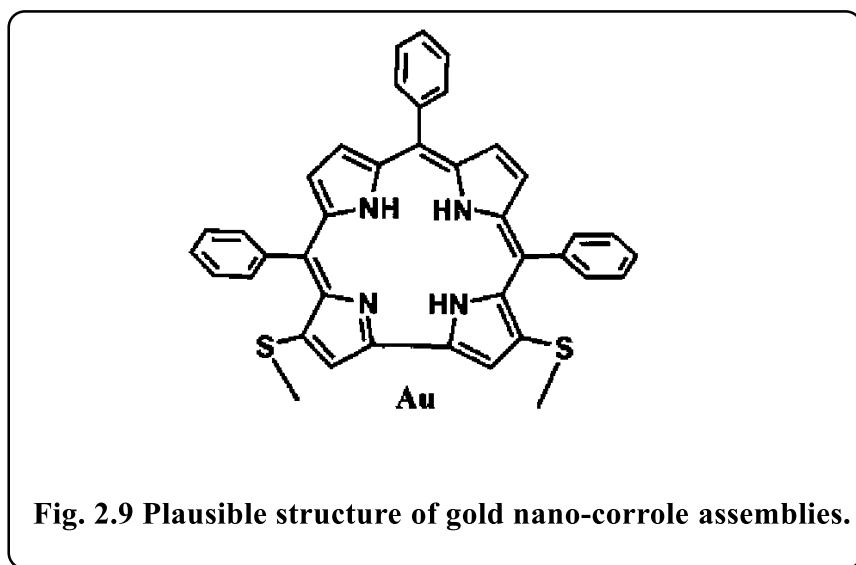
Fig. 2.8: Time evolution UV-vis spectra of a mixture of **1** ($\sim 10^{-6}$ M), NaBH₄ ($\sim 10^{-4}$ M), and HAuCl₄ ($\sim 10^{-5}$ M) in DMF.

These results are in complete agreement with those for previously reported porphyrin thioester protected gold nanoparticles.^[61] In line with the previous report by Teranishi *et al.*, our absorption spectra also suggest that a strong electronic interaction exists between the corrole and the gold surface (Figure. 2.8).^[61] However, in contrast to them, we believe that in our case the parallel binding mode of corrole to the gold surface is not feasible

due to the steric hindrance of the *meso*-aryl groups. Thus a face-off binding mode of corrole (due to the lack of one *meso*-carbon) is proposed here (Figure 2.9).

2.4.3 Time Evolution emission spectra and fluorescence for characterization of gold nano particles

The time evolution fluorescence spectra of a mixture of **1** ($\sim 10^{-6}$ M), NaBH_4 ($\sim 10^{-4}$ M), and HAuCl_4 ($\sim 10^{-5}$ M) in DMF was shown in figure 2.10. The initial spectrum (black colour, colouronline) was for pure **1** in the DMF solution. The position of the emission bands is negligibly changed upon addition of NaBH_4 . However, a drastic change of the corrole fluorescence intensity is observed upon gradual addition of the HAuCl_4 solution.(Figure 2.10) The fluorescence quenching is obvious as the corrole molecules transfer their excitation energy to the gold nanoparticles.^[65,66]



The excited state lifetimes of **1** and 1- Au NPs were found to be 3.69 ns and 1.19 ns, respectively (Figure 2.11). Considering that only static quenching is viable,^[65] the change in the lifetime of corrole **1** on binding with the Au surface is attributed to the change of the ligand structure in 1-Au NPs (the two thiocyanate groups are converted to thiol groups on binding with Au).

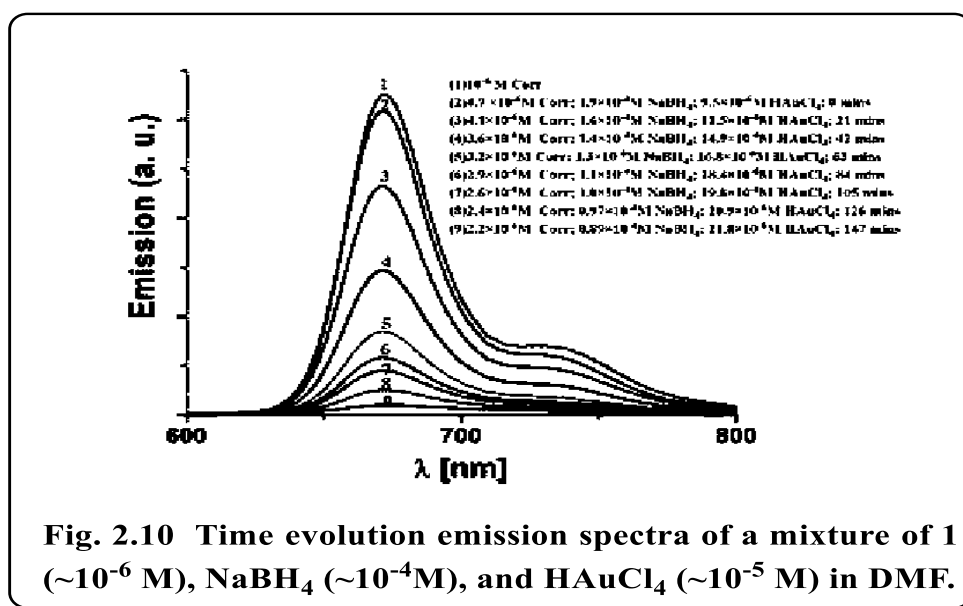


Fig. 2.10 Time evolution emission spectra of a mixture of **1** ($\sim 10^{-6} \text{M}$), NaBH_4 ($\sim 10^{-4} \text{M}$), and HAuCl_4 ($\sim 10^{-5} \text{M}$) in DMF.

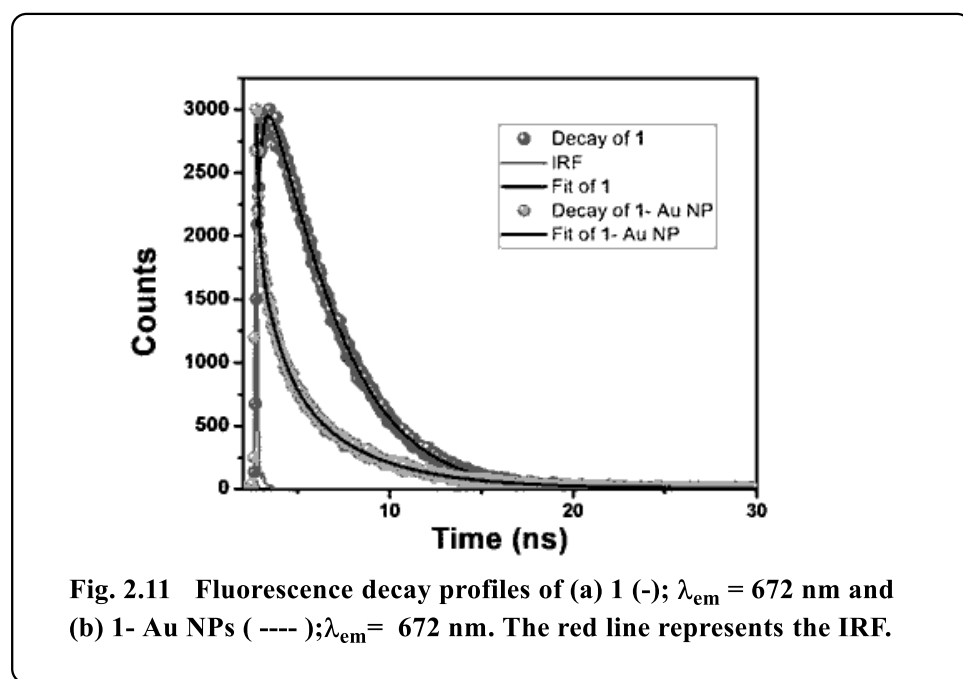


Fig. 2.11 Fluorescence decay profiles of (a) **1** (-); $\lambda_{\text{em}} = 672 \text{ nm}$ and (b) **1**- Au NPs (----); $\lambda_{\text{em}} = 672 \text{ nm}$. The red line represents the IRF.

2.4.4 Transmission electron microscopy characterization

A representative TEM image is shown in Figure 2.13. One can easily visualize the diffraction contrast fringes and thus it can confirm the crystalline nature of the **1** coated gold nanoparticles.^[60] Particle size analysis indicates that the mean diameter of the **1** coated gold nanoparticles is $\sim 6.5 \text{ nm}$. (Figure 2.12)

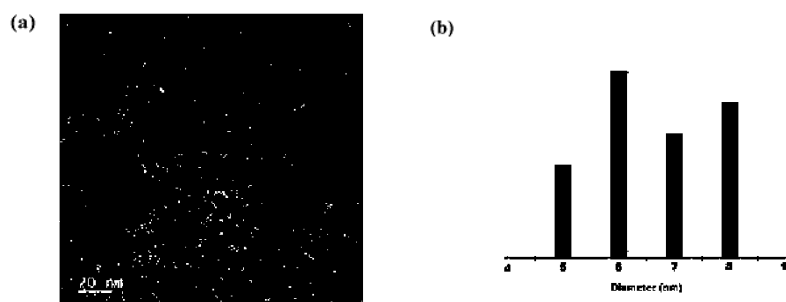


Fig. 2.12 (a) TEM image of the nanoparticles (the inset shows the diffraction contrast fringes) and (b) histograms of the particle size.

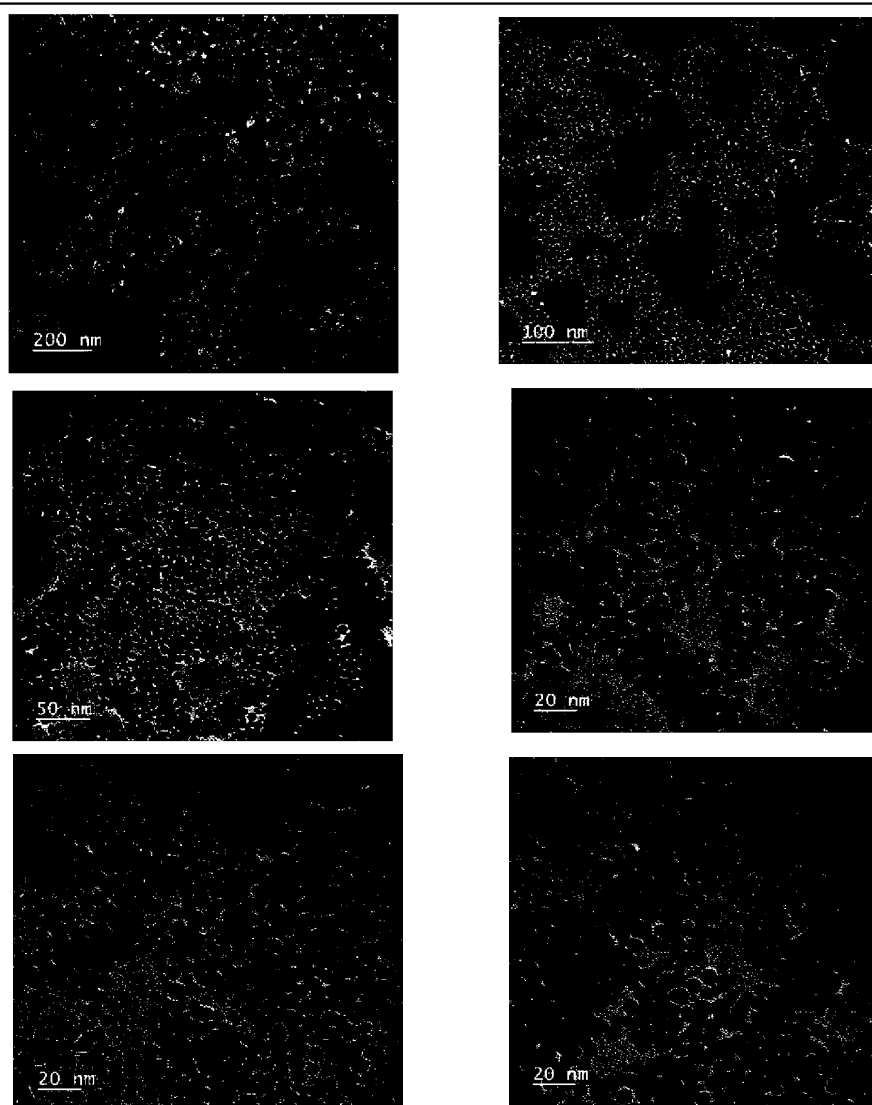
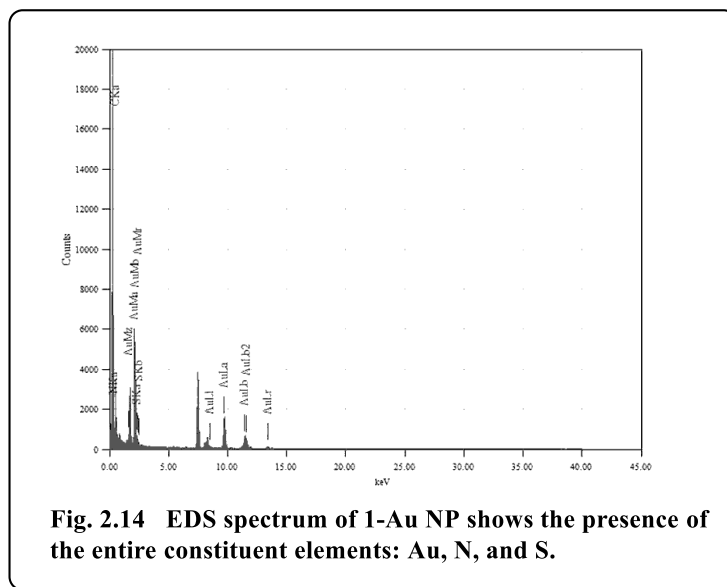
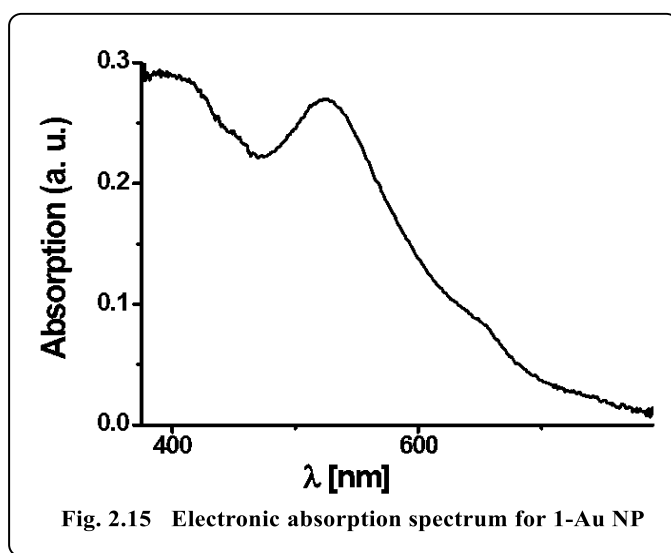


Fig. 2.13 TEM image of nanoparticle



2.4.5 Electronic Absorption Spectrum:

Gold nanoparticles coated with **1** are stable under ambient conditions for a few weeks as concluded from the characteristic surface plasmon resonance (SPR) band at 525 nm (Figure 2.15). This is in contrast with the stability of gold nanoparticles alone obtained through NaBH_4 reduction without the use of the stabilizing corrole molecule, **1**.^[60]

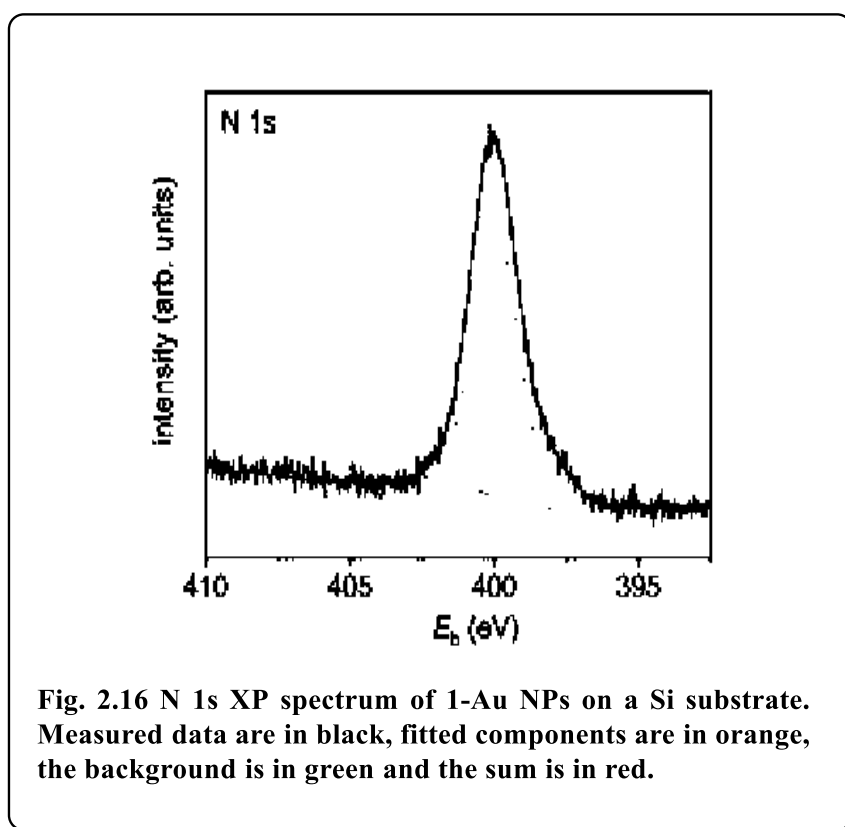


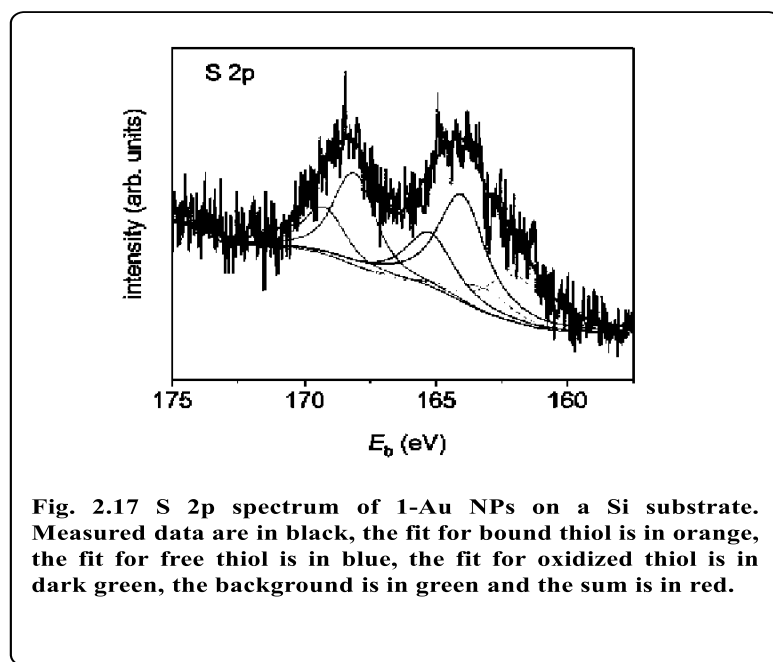
2.4.6 X-ray photoelectron spectroscopy :

1-Au NPs were also studied by X-ray photoelectron spectroscopy (XPS). The composition of the organic contributions is 85 at% carbon, 11 at% nitrogen and 4 at%

sulphur, approximately matching the expected ratio of 87 : 9 : 4 for **1** with cleaved CN groups. The N 1s signal (Figure 2.16) consists of three components which can be assigned to imine nitrogen (398.2 eV, 1.3 at%), amine nitrogen (399.9 eV, 9.6 at%) and amide nitrogen (400.3 eV). The latter is most probably due to the residual DMF which is left after synthesis and was therefore removed from the calculation of at% for the organic components. The imine and amine nitrogen contributions can be assigned to the four nitrogen atoms in the corrole framework.^[67,68] However, the ratio between amine and imine nitrogen is much higher than expected for pure corrole and might be an indication of extensive π - π stacking.

The S 2p signal (Figure 2.17) is also composed of three signals, which can be assigned to thiol bound to the gold surface (162.0 eV, 0.8 at%), free thiol (164.0 eV, 1.7 at%) and oxidized thiol (168.1 eV, 1.2 at%).^[69] As the ratio of corrole ligands per Au NP has been estimated from CHN analysis to be 200 : 1, it is obvious that only a minor number of corrole ligands can bind directly to the gold surface. Thus, many ligands are only adsorbed by π - π stacking and thus have free thiol groups which can easily be oxidized.





2.5 Conclusion

In conclusion, we have developed a simple and novel protocol for the regio-selective thiocyanation of corrole. The thiocyanato appended corrole **1** acts as a stabilizer for gold nano particles. A unique face-off binding mode in corrole (due to lack of one *meso*-carbon) is proposed here which is not at all feasible in porphyrins. The corrole **1** and the Au nanoparticle hybrid exhibits interesting photophysical properties. The change of absorption and emission spectra are remarkable and these also clearly indicates that a strong electronic interaction exists between the corrole and the Au nanoparticles. These studies will certainly be helpful in designing various multi-dentate corrole based ligand in order to stabilize Au nanoparticles with specific size and functions depending on the choice of corrole framework.

2.6 Experimental Section

2.6.1 Materials

The precursor's pyrrole, HAuCl_4 , *p*-chloranil, and aldehydes were purchased from Aldrich, USA. NH_4SCN (>98.5% purity), Carbon disulphide was purchased from Merck

pvt. ltd chemicals. Other chemicals were of reagent grade. Hexane and CH_2Cl_2 were distilled from KOH and CaH_2 respectively. For spectroscopy studies, HPLC grade solvents were used. 5,10,15-triphenylcorrole was prepared by following the previous literatures.^[43]

2.6.2 Physical Measurements

UV–Vis spectral studies were performed on a Perkin–Elmer LAMBDA-750 spectrophotometer. Emission spectral studies were performed on a Perkin Elmer, LS 55 spectrophotometer using optical cell of 1 cm path length. Time resolved fluorescence measurements were carried out using a time-correlated single photon counting (TCSPC) spectrometer (Edinburgh Instruments, Life Spec II). The elemental analyses were carried out with a Perkin–Elmer 240C elemental analyzer. FT–IR spectra were recorded on a Perkin–Elmer spectrophotometer with samples prepared as KBr pellets. The NMR measurements were carried out using a Bruker 400 MHz NMR spectrometer. Chemical shifts are expressed in parts per million (ppm) relative to residual chloroform ($\delta = 7.26$). Electrospray mass spectra were recorded on a Bruker Micro TOF–QII mass spectrometer. Transmission electron microscope (TEM) images for size and size distribution were obtained by using a JEOL JEM-F200 (operating at 200 kV) equipped with an energy dispersive spectrometer (EDS). TEM images for the samples were obtained by using a One View camera (Gatan, Pleasanton, CA). XPS spectra were measured using an Escalab 250 Xi spectrometer (Thermo Fisher, East Grinstead, UK) equipped with a monochromatized Al K_α source (1486.6 eV) and external charge compensation. Survey spectra were measured with a band pass of 100 eV, detail spectra for N 1s, C 1s, O 1s, S 2p and Au 4f with a band pass of 10 eV. Data acquisition and evaluation were done using the software Avantage (Version 5.982, Thermo Fisher).

2.6.3 Crystal Structure Determination

Single crystals of **1** were grown by slow diffusion of a solution of the **1** in dichloromethane into hexane, followed by slow evaporation under atmospheric conditions. The crystal data of **1** were collected on a Rigaku Oxford diffractometer at 293 K. Selected data collection parameters and other crystallographic results are summarized in Table 2.1. All data were corrected for Lorentz polarization and absorption effects. The program package SHELXTL^[70] was used for structure solution and full matrix least squares refinement on F^2 . Hydrogen atoms were included in the refinement using the riding model. Contributions of H atoms for the water molecules were included but were not fixed. Disordered solvent molecules were taken out using SQUEEZE command in PLATON.^[71]

CCDC 1901425 contain the supplementary crystallographic data for **1**. These data can be obtained free of charge via www.ccdc.cam.ac.uk/data_request/cif.

2.6.4 Syntheses

Synthesis of 3,17-bis(thiocyanato)–5,10,15-triphenylcorrole, 1:

25 mg (0.0475mmol) of 5,10,15-triphenylcorrole was dissolved in 20ml of carbon disulfide, and then excess amount of NH_4SCN (approx. 2gm) was added to it. The reaction mixture was stirred for 5 mins at RT and then 20ml of pyridine was added to it and the resulting solution was refluxed for 3 hours. The residual solvent was evaporated to dryness and the crude product was dissolved in dichloromethane, white color precipitated was separated through filtration and the green color solution was kept under dark for 24 hours. The crude product was purified by using a column chromatography through silica gel (100-200 mesh). The desired fraction was eluted by using a mixture of 40% DCM and 60% hexane.

For 3,17-bis(thiocyanato)–5,10,15-triphenylcorrole, 1:

Yield: 40% (12 mg). Anal. Calcd (found) for $C_{39}H_{24}N_6S_2$ (**1**): C, 73.10 (73.26); H, 3.78 (3.87); N, 13.12 (13.23); λ_{\max}/nm ($\epsilon/M^{-1}cm^{-1}$) in CH_2Cl_2 : 419 (103000), 574 (18000), 595 (17500), 656 (26000). 1H NMR (400 MHz, $CDCl_3$) δ 8.88 (s, 2H, H- β), 8.61 (s, 2H, H- β), 8.43 (s, 2H, H- β), 8.08 (s, 6H, Ar-H), 7.78 (m, 9H, Ar-H), -1.38 (s, 3H). **1** displayed strong fluorescence at 688 nm in DCM. The electrospray mass spectrum in methanol showed peaks centred at $m/z = 641.145$ corresponding to $[1+H]^+$ (641.15 calcd for $C_{39}H_{25}N_6S_2$).

Preparation of 1 coated gold nanoparticles (1-Au NPs):

10^{-3} M $HAuCl_4$ stock solution was prepared by dissolving 3.39 mg of $HAuCl_4 \cdot 3H_2O$ in 10ml of DMF. Equimolar concentration of 3,17-bis(thiocyanato)–5,10,15-triphenylcorrole solution was prepared by dissolving 6.40 mg of corrole in 10 ml of DMF. 10^{-2} M $NaBH_4$ stock solution was prepared in DMF. Initially a mixture of 0.5 ml corrole solution (10^{-3} M) and 4.475 ml of $HAuCl_4$ (10^{-3} M) solution was mixed together and stirred for 30 seconds. After that 2 ml $NaBH_4$ (10^{-2} M) solution was added to the mixture and then stirred for another 2 hour 45 minutes. The color of the solution gradually changes from green to brown to red. After that the solution was centrifuged (10,000 rpm, RT for 20 minutes) and the obtained **1** coated Au-Nano-particles was washed with water for two times and then it was dispersed in water. For TEM measurements, copper grids pre-coated with carbon film, 300 mesh was used. The samples were prepared by using drop casting method.

For 1-Au NP:

Anal. Calcd (found) for $\{Au_{2997}(C_{37}H_{24}N_4S_2)_{200}\}$ (**1-Au NP**): C, 12.54 (24.333); H, 0.68 (4.70); N, 1.58 (5.889), S, 1.81 (0.983). It is assumed that there are 2650 ± 1450 Au atoms

for each nanoparticle (Au nanoparticle having size of $\sim 4.4 \pm 0.8$ nm).⁴ Thus the number 2997 (Au atoms) is purely an approximation to fit the data.

Sample Preparation for FT-IR measurement:

10^{-3} M HAuCl_4 stock solution was prepared by dissolving 3.39 mg of $\text{HAuCl}_4 \cdot 3\text{H}_2\text{O}$ in 10 ml of DMF. Equimolar concentration of 3,17-bis(thiocyanato)-5,10,15-triphenylcorrole solution was prepared by dissolving 6.40 mg of corrole in 10 ml of DMF. 10^{-2} M NaBH_4 stock solution was prepared in DMF. Initially a mixture of 10 ml corrole solution and 30 ml of NaBH_4 solution was mixed together and sonicated for 30 mins. After that 10 ml HAuCl_4 solution was added to the prefixed mixture and the sonication was continued for another one hour. The color of the solution gradually changes from green to brown to red. After red color appears it was sonicated for another 2 hours. Then the mixture was stirred for another 12 hours. After that the solution was centrifuged (10,000 rpm, RT for 10 minutes) and the obtained **1** coated Au-Nanoparticles were washed with water for two times and then it was dispersed in ethanol. The solution was evaporated to dryness and the FTIR spectra was recorded on a KBr pellet.

References

- [1] M.-C. Daniel, D. Astruc, *Chem. Rev.* **2004**, *104*, 293–346.
- [2] A. Corma, H. Garcia, *Chem. Soc. Rev.* **2008**, *37*, 2096–2126.
- [3] C. T. Campbell, *Science (80-.)*. **2004**, *306*, 234–235.
- [4] D. A. Giljohann, D. S. Seferos, W. L. Daniel, M. D. Massich, P. C. Patel, C. A. Mirkin, *Spherical Nucleic Acids* **2020**, 55–90.
- [5] E. C. Dreaden, A. M. Alkilany, X. Huang, C. J. Murphy, M. A. El-Sayed, *Chem. Soc. Rev.* **2012**, *41*, 2740–2779.
- [6] J. J. Li, L. I. Zou, D. Hartono, C. Ong, B. Bay, L. Lanry Yung, *Adv. Mater.* **2008**, *20*, 138–142.
- [7] S. Chah, M. R. Hammond, R. N. Zare, *Chem. Biol.* **2005**, *12*, 323–328.
- [8] G. Peng, U. Tisch, O. Adams, M. Hakim, N. Shehada, Y. Y. Broza, S. Billan, R. Abdah-Bortnyak, A. Kuten, H. Haick, *Nat. Nanotechnol.* **2009**, *4*, 669–673.
- [9] Y.-C. Lu, Z. Xu, H. A. Gasteiger, S. Chen, K. Hamad-Schifferli, Y. Shao-Horn, *J. Am. Chem. Soc.* **2010**, *132*, 12170–12171.
- [10] R. Muszynski, B. Seger, P. V Kamat, *J. Phys. Chem. C* **2008**, *112*, 5263–5266.
- [11] J. Luo, L. Wang, D. Mott, P. N. Njoki, Y. Lin, T. He, Z. Xu, B. N. Wanjana, I. S. Lim, C. Zhong, *Adv. Mater.* **2008**, *20*, 4342–4347.
- [12] C. E. Talley, J. B. Jackson, C. Oubre, N. K. Grady, C. W. Hollars, S. M. Lane, T. R. Huser, P. Nordlander, N. J. Halas, *Nano Lett.* **2005**, *5*, 1569–1574.
- [13] K. L. Wustholz, A.-I. Henry, J. M. McMahon, R. G. Freeman, N. Valley, M. E. Piotti, M. J. Natan, G. C. Schatz, R. P. Van Duyne, *J. Am. Chem. Soc.* **2010**, *132*, 10903–10910.

-
- [14] A. L. and F. R. A. N. Félidj, J. Aubard, G. Lévi, J. R. Krenn, A. Hohenau, G. Schider, *Appl. Phys. Lett* **2003**, 82, 3095–3097.
- [15] T. A. Taton, C. A. Mirkin, R. L. Letsinger, *Science (80-.)*. **2000**, 289, 1757–1760.
- [16] J. J. Storhoff, R. Elghanian, R. C. Mucic, C. A. Mirkin, R. L. Letsinger, *J. Am. Chem. Soc.* **1998**, 120, 1959–1964.
- [17] S. G. Penn, L. He, M. J. Natan, *Curr. Opin. Chem. Biol.* **2003**, 7, 609–615.
- [18] I. Yacoby, I. Benhar, *Infect. Disord. Targets (Formerly Curr. Drug Targets-Infectious Disord.* **2007**, 7, 221–229.
- [19] J. Lee, M. S. Han, C. A. Mirkin, *Angew. Chemie* **2007**, 46, 4093–4096.
- [20] G. H. Woehrle, L. O. Brown, J. E. Hutchison, *J. Am. Chem. Soc.* **2005**, 127, 2172–2183.
- [21] S.-Y. Lin, S.-W. Liu, C.-M. Lin, C. Chen, *Anal. Chem.* **2002**, 74, 330–335.
- [22] K.-S. Kim, D. Dembereinyamba, H. Lee, *Langmuir* **2004**, 20, 556–560.
- [23] B. C. Sih, M. O. Wolf, *Chem. Commun.* **2005**, 3375–3384.
- [24] M. Ikeda, N. Tanifuji, H. Yamaguchi, M. Irie, K. Matsuda, *Chem. Commun.* **2007**, 1355–1357.
- [25] J. van Herrikhuyzen, S. J. George, M. R. J. Vos, N. A. J. M. Sommerdijk, A. Ajayaghosh, S. C. J. Meskers, A. P. H. J. Schenning, *Angew. Chemie* **2007**, 119, 1857–1860.
- [26] K. Matsuda, H. Yamaguchi, T. Sakano, M. Ikeda, N. Tanifuji, M. Irie, *J. Phys. Chem. C* **2008**, 112, 17005–17010.
- [27] T. Hasobe, H. Imahori, P. V Kamat, T. K. Ahn, S. K. Kim, D. Kim, A. Fujimoto, T. Hirakawa, S. Fukuzumi, *J. Am. Chem. Soc.* **2005**, 127, 1216–1228.
- [28] T. Akiyama, M. Nakada, N. Terasaki, S. Yamada, *Chem. Commun.* **2006**, 395–397.

-
- [29] D. Conklin, S. Nanayakkara, T.-H. Park, M. F. Lagadec, J. T. Stecher, M. J. Therien, D. A. Bonnell, *Nano Lett.* **2012**, *12*, 2414–2419.
- [30] A. Satake, M. Fujita, Y. Kurimoto, Y. Kobuke, *Chem. Commun.* **2009**, 1231–1233.
- [31] N. Katsonis, J. Vicario, T. Kudernac, J. Visser, M. M. Pollard, B. L. Feringa, *J. Am. Chem. Soc.* **2006**, *128*, 15537–15541.
- [32] E. Vogel, S. Will, A. S. Tilling, L. Neumann, J. Lex, E. Bill, A. X. Trautwein, K. Wieghardt, *Angew. Chemie* **1994**, *33*, 731–735.
- [33] Z. Gross, *JBIC J. Biol. Inorg. Chem.* **2001**, *6*, 733–738.
- [34] M. Bröring, F. Brégier, E. Cónsul Tejero, C. Hell, M. C. Holthausen, *Angew. Chemie Int. Ed.* **2007**, *46*, 445–448.
- [35] A. Ghosh, *Chem. Rev.* **2017**, *117*, 3798–3881.
- [36] R. Orłowski, D. Gryko, D. T. Gryko, *Chem. Rev.* **2017**, *117*, 3102–3137.
- [37] Y. Fang, Z. Ou, K. M. Kadish, *Chem. Rev.* **2017**, *117*, 3377–3419.
- [38] K. Fujino, Y. Hirata, Y. Kawabe, T. Morimoto, A. Srinivasan, M. Toganoh, Y. Miseki, A. Kudo, H. Furuta, *Angew. Chemie* **2011**, *123*, 6987–6991.
- [39] S. Hiroto, K. Furukawa, H. Shinokubo, A. Osuka, *J. Am. Chem. Soc.* **2006**, *128*, 12380–12381.
- [40] A. Mahammed, I. Giladi, I. Goldberg, Z. Gross, *Chem. Eur. J.* **2001**, *7*, 4259–4265.
- [41] S. Hirabayashi, M. Omote, N. Aratani, A. Osuka, *Bull. Chem. Soc. Jpn.* **2012**, *85*, 558–562.
- [42] B. Koszarna, D. T. Gryko, *Chem. Commun.* **2007**, 2994–2996.
- [43] B. Koszarna, D. T. Gryko, *J. Org. Chem.* **2006**, *71*, 3707–3717.
- [44] R. Paollesse, S. Nardis, M. Stefanelli, F. R. Fronczek, M. G. H. Vicente, *Angew. Chemie Int. Ed.* **2005**, *44*, 3047–3050.

-
- [45] H. L. Buckley, W. A. Chomitz, B. Koszarna, M. Tasior, D. T. Gryko, P. J. Brothers, J. Arnold, *Chem. Commun.* **2012**, *48*, 10766–10768.
- [46] C. F. Zipp, J. P. Michael, M. A. Fernandes, H. M. Marques, *South African J. Chem.* **2013**, *66*, 158–166.
- [47] W. Sinha, M. G. Sommer, N. Deibel, F. Ehret, M. Bauer, B. Sarkar, S. Kar, *Angew. Chemie* **2015**, *54*, 13769–13774.
- [48] W. Sinha, M. G. Sommer, N. Deibel, F. Ehret, B. Sarkar, S. Kar, *Chem. Eur. J.* **2014**, *20*, 15920–15932.
- [49] W. Sinha, M. G. Sommer, L. Hettmanczyk, B. Patra, V. Filippou, B. Sarkar, S. Kar, *Chem. Eur. J.* **2017**, *23*, 2396–2404.
- [50] B. Patra, S. Sobottka, W. Sinha, B. Sarkar, S. Kar, *Chem. Eur. J.* **2017**, *23*, 13858–13863.
- [51] A. Garai, S. Sobottka, R. Schepper, W. Sinha, M. Bauer, B. Sarkar, S. Kar, *Chem. Eur. J.* **2018**, *24*, 12613–12622.
- [52] X.-S. Ke, Y. Hong, V. M. Lynch, D. Kim, J. L. Sessler, *J. Am. Chem. Soc.* **2018**, *140*, 7579–7586.
- [53] R. S. Czernuszewicz, V. Mody, A. Czader, M. Gałęzowski, D. T. Gryko, *J. Am. Chem. Soc.* **2009**, *131*, 14214–14215.
- [54] M. Autret, S. Will, E. Van Caemelbecke, J. Lex, J.-P. Gisselbrecht, M. Gross, E. Vogel, K. M. Kadish, *J. Am. Chem. Soc.* **1994**, *116*, 9141–9149.
- [55] J. H. Palmer, A. C. Durrell, Z. Gross, J. R. Winkler, H. B. Gray, *J. Am. Chem. Soc.* **2010**, *132*, 9230–9231.
- [56] H.-Y. Liu, F. Yam, Y.-T. Xie, X.-Y. Li, C. K. Chang, *J. Am. Chem. Soc.* **2009**, *131*, 12890–12891.
- [57] B. Brizet, N. Desbois, A. Bonnot, A. Langlois, A. Dubois, J.-M. Barbe, C. P. Gros,

-
- C. Goze, F. Denat, P. D. Harvey, *Inorg. Chem.* **2014**, *53*, 3392–3403.
- [58] S. Kuck, G. Hoffmann, M. Bröring, M. Fechtel, M. Funk, R. Wiesendanger, *J. Am. Chem. Soc.* **2008**, *130*, 14072–14073.
- [59] K. E. Thomas, H. Vazquez-Lima, Y. Fang, Y. Song, K. J. Gagnon, C. M. Beavers, K. M. Kadish, A. Ghosh, *Chem. Eur. J.* **2015**, *21*, 16839–16847.
- [60] J. Ohyama, Y. Hitomi, Y. Higuchi, M. Shinagawa, H. Mukai, M. Kodera, K. Teramura, T. Shishido, T. Tanaka, *Chem. Commun.* **2008**, 6300–6302.
- [61] M. Kanehara, H. Takahashi, T. Teranishi, *Angew. Chemie* **2008**, *120*, 313–316.
- [62] B. C. Mei, K. Susumu, I. L. Medintz, H. Mattoussi, *Nat. Protoc.* **2009**, *4*, 412–423.
- [63] J. W. Ciszek, M. P. Stewart, J. M. Tour, *J. Am. Chem. Soc.* **2004**, *126*, 13172–13173.
- [64] M. Stefanelli, F. Mandoj, S. Nardis, M. Raggio, F. R. Fronczek, G. T. McCandless, K. M. Smith, R. Paolesse, *Org. Biomol. Chem.* **2015**, *13*, 6611–6618.
- [65] A. J. Shaikh, F. Rabbani, T. A. Sherazi, Z. Iqbal, S. Mir, S. A. Shahzad, *J. Phys. Chem. A* **2015**, *119*, 1108–1116.
- [66] A. Ishida, Y. Sakata, *Chem. Commun.* **1998**, 57–58.
- [67] H. Aldahhak, M. Paszkiewicz, F. Allegretti, D. A. Duncan, S. Tebi, P. S. Deimel, P. Casado Aguilar, Y.-Q. Zhang, A. C. Papageorgiou, R. Koch, *J. Phys. Chem. C* **2017**, *121*, 2192–2200.
- [68] E. Steene, A. Dey, A. Ghosh, *J. Am. Chem. Soc.* **2003**, *125*, 16300–16309.
- [69] M. S. Boeckl, A. L. Bramblett, K. D. Hauch, T. Sasaki, B. D. Ratner, J. W. Rogers, *Langmuir* **2000**, *16*, 5644–5653.
- [70] G. M. Sheldrick, *Acta Crystallogr. Sect. A Found. Crystallogr.* **2008**, *64*, 112–122.
- [71] P. V Van der Sluis, A. L. Spek, *Acta Crystallogr. Sect. A Found. Crystallogr.* **1990**, *46*, 194–201
-

Photocatalytic C–H Thiocyanation of Corroles: Development of Near- Infrared (NIR)-Emissive Dyes

3.1 Introduction

3.2 Generalization of Synthetic Procedure

3.3 Result and Discussion

3.3.1 Synthesis and characterization

3.4 Spectral Characterisation

3.4.1 NMR Spectroscopy

3.4.2 IR spectroscopy

3.4.3 Mass Spectrometry

3.4.4 UV-Vis and emission Spectroscopy

3.4.5 Single crystal XRD Analysis

3.5 Analysis of Reaction Mechanism

3.6 Mechanistic Studies

3.6.1 The radical trapping experiments

3.6.2 Characterization of (SCN)₂ by Mass spectra

3.7 Conclusion

3.8 Experimental Section

3.8.1 Materials

3.8.2 Physical measurements

3.8.3 Crystal Structure Determination

3.8.4 Syntheses

3.1 Introduction

Porphyrinoids are traditionally used as photosensitizers in singlet oxygen generation reactions.^[1-4] However, the applications of porphyrinoids in photo-redox reactions are rather limited.^[5,6] Depending on the reaction conditions, the photo-excited triplet states of porphyrinoids can behave as either oxidant or reductant. A close comparison with the values of both ground state and excited state redox potentials of tetraphenylporphyrin, it is evident that in the excited state, the porphyrinoids are more efficient electron donors and more efficient electron acceptors than in the ground state. Thus porphyrinoids have great potential to replace the traditional photo-redox catalysts like $[\text{Ru}(\text{bpy})_3]^{2+}$ and $[\text{Ir}(\text{ppy})_3]$ {bpy=bipyridine and ppy = 2-phenylpyridine}.^[7,8] Advantageously, the electronic and physicochemical properties of porphyrinoids can be fine-tuned by suitable functionalization at the periphery.^[9] Porphyrinoids, which will absorb the whole UV-vis region of the spectrum will have great potential in this regard. Corrole, a contracted version of porphyrin having 18π -electron has many similarities with porphyrins.^[10] The spectroscopic properties of corroles are similar to that of porphyrin in many aspects.^[10-33] The triplet state lifetime of corroles is in the range of 10^{-4} to 10^{-5} s.^[10] Similar to porphyrin, corroles also act as a photosensitizer.^[34,35] Although there are few examples of porphyrin as in photo-redox catalysis, similar studies in corroles are still rare. Herein we have reported the application of corroles in photo-catalysis reaction. A unique reaction has been designed, in which corrole acts as a self-catalyst and introduces four thiocyanato groups in the β -pyrrolic positions and thus resulted in the formation of tetrathiocyanato corroles. It is worthwhile to mention that the thiocyanate motif is a potential building block in organic chemistry as it is the precursor of a host of sulfur-containing functional groups (e.g., sulfides, thioesters, and thiophenols) and also acts as a starting material of various heterocyclic compounds (e.g., thiazoles).^[36,37] Visible light-induced thiocyanation has

recently gained grounds to synthesize various thiocyanato appended arenes and heterocycles.^[38–40] Thus these thiocyanato appended corroles will act as possible precursors for the synthesis of several sulfur-containing corrole derivatives and which will have potential implication in dyes and drugs. It was also observed that the β -substitutions at the corrole ring has a pronounced effect on its electronic structure.^[41–45] We have observed previously that through ordinary chemical means up to two thiocyanato groups can be inserted in the corrole periphery. The insertion of two thiocyanato groups in corrole periphery was achieved in very drastic conditions and with low yields.^[46] Although numerically it may not be a very big deal to inset four thiocyanato groups instead of two thiocyanato groups. However, to our ultimate surprise, we have observed that the photophysical properties are drastically altered in the case of tetrathiocyanatocorroles in comparison to dithiocyanatocorroles. In general, 18π -electron systems like porphyrins and corroles has strong absorption in the 400–450nm region, and also, they have much weaker absorption at around 500–650nm (Q-peaks).^[9,10] However, in the case of tetrathiocyanatocorroles, we have observed strong absorption in the whole visible region of the spectrum with a high molar absorption coefficient.

3.2 Generalization of Synthetic Procedure:

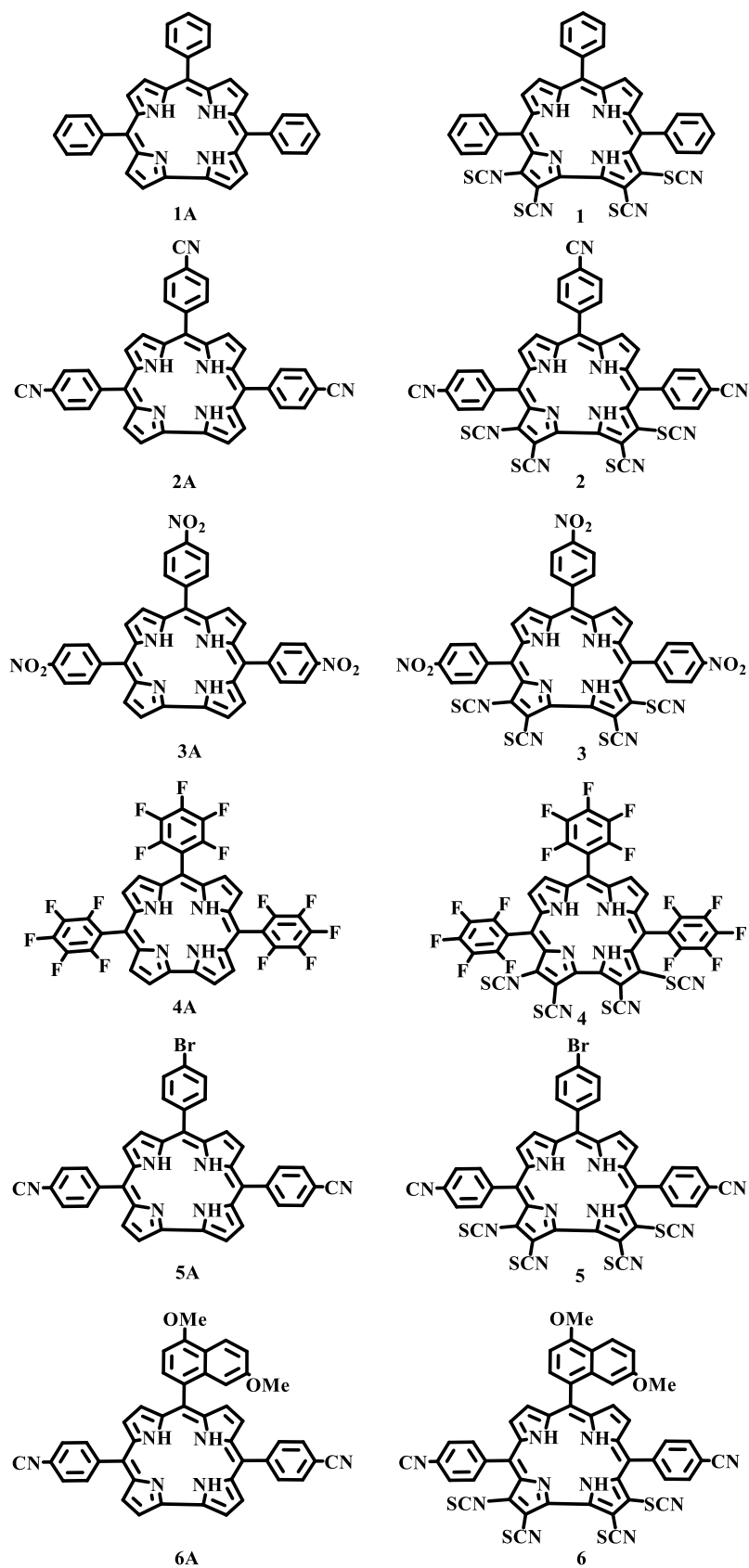
In order to generalize this photochemical thiocyanation reaction, the substituents at the meso-phenyl rings of corroles were varied from electron withdrawing groups (-CN [**2A**], -NO₂ [**3A**], -F [**4A**], and -Br [**5A**]) to electron donating groups (-OMe [**6A**]) including the unsubstituted phenyl ring (-H [**1A**]). All the tetrathiocyanatocorroles were thoroughly characterized by several spectroscopic techniques. A representative example was also characterized by single-crystal XRD analysis. The present work thus describes the synthesis and characterization of six new tetrathiocyanatocorroles, namely 2,3,17,18-tetrathiocyanato-5, 10, 15-triphenylcorrole, **1**, 2, 3, 17, 18-tetrathiocyanato-5, 10,

15-tris(4-cyanophenyl) corrole, **2**, 2, 3, 17, 18 - tetrathiocyanato-5, 10, 15-tris (4-nitrophenyl) corrole, **3**, 2, 3, 17, 18 - tetrathiocyanato - 5, 10, 15 - tris (pentafluorophenyl) corrole, **4**, 2, 3, 17, 18 tetrathiocyanato - 10 - (4 - bromophenyl) - 5, 15 - bis (4 - cyanophenyl) corrole, **5**, and 2, 3, 17, 18 - tetrathiocyanato - 10 - (4, 7 - dimethoxynaphthalen-1-yl) - 5, 15 - bis(4 - cyanophenyl) corrole, **6** (Scheme 3.1). Four A₃-corrole and two trans-A₂B corrole have been chosen here as substrates to have the difference in energies of their molecular orbitals and thus having a difference in their photophysical properties. To explore the ability of these newly synthesized FB corroles {FB= free base} as potential ligand scaffolds, we have synthesized a new gold corrole complex namely, {2,3,17,18 - tetrathiocyanato-5,10,15 - tris(4-cyanophenyl) corrolato-Au(III)}, **2-Au**. The corrolato-Au (III) complex, **2-Au** was thoroughly characterized by several spectroscopic techniques including single-crystal XRD analysis.

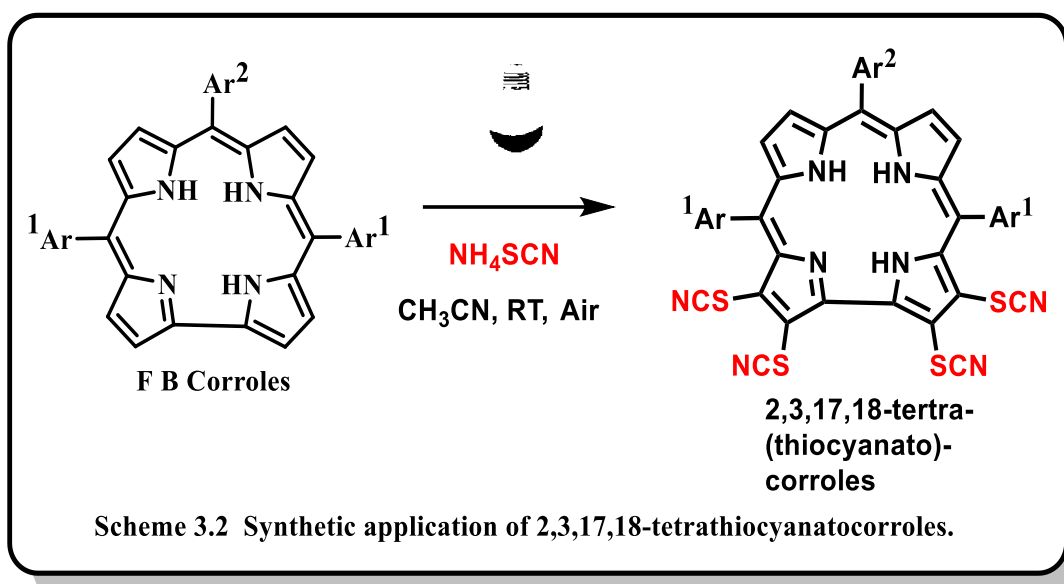
3.3 Result and Discussion

3.3.1 Synthesis and characterization

Tetrathiocyanatocorrole derivatives (**1-6**) were synthesized by following a photocatalytic synthetic process developed by us. The corresponding free-base corroles (**1A-6A**) were dissolved in acetonitrile, and then excess NH₄SCN was added to it. The reaction mixture was stirred at room temperature under irradiation with a CFL lamp {CFL = compact fluorescent lamps} (20 watts) for 5 hours in the air and resulted in the formation of tetrathiocyanatocorrole derivatives (**1-6**) in good yields (Scheme 3.2). Au (III) was inserted in the corrole cavity using gold acetate as a metal precursor in an acetonitrile and pyridine mixture at RT {RT= room temperature). Purity and composition of the tetrathiocyanatocorrole derivatives (**1-6**) and the corrolato-Au (III) complex, **2-Au** were established by their satisfactory elemental analyses, UV-Vis, emission, IR, NMR, ESI-MS data, and single-crystal XRD data (Figures 3.1-3.32 and Tables 3.1-3.5).



Scheme 3.1. Structures of the corroles 1A-6A and the corresponding 2,3,17,18-tetrathiocyanatocorrole derivatives 1-6.



A series of different solvents were screened to search for the most effective reaction media for these catalytic reactions. Polar solvents (as NH_4SCN is soluble in polar solvents) such as acetone, ethanol, THF {THF=Tetrahydrofuran}, CH_3OH , DCE {DCE=1,2-Dichloroethane}, and 1, 4-dioxane were screened for this purpose (Table 3.1). Alcohols, acetone, THF, 1,4-dioxane, and DCE are well known free radical scavenger and thus leads to the destruction of in situ generated SCN radical and as a result they dictate the formation of 2,3,17,18-tetrathiocyanatocorroles (**1-6**). It is worthwhile to mention here that CH_3CN turns out to be the most effective solvent and the reaction yield is consistently high with a value of ~50.0%. (Table 3.1 & Table 3.2) We have observed that there are no traces of mono/di/tri-substituted corroles are formed as side products in the optimized reaction conditions. It was also observed that in the absence of a CFL lamp, the reaction failed to deliver the desired product even after performing this reaction at room temperature and keeping all reactants, reaction conditions, and reaction time unchanged. This confirms that the light energy from a CFL lamp is necessary for this reaction and it is a pure light-driven reaction.

Table 3.1 Yield in Different Solvents

Solvent	YIELD
THF	< 1%
DCE	< 1%
CH ₃ OH	< 5%
1,4-Dioxane	< 5%
Acetone	~ 10%
Ethanol	< 15%
CH ₃ CN	~ 50%

This reaction also failed to deliver the product without the absence of a thiocyanate source. NH₄SCN has turned out to be the best source of thiocyanate group here.^[47] It is possible to use KSCN as an alternate thiocyanate source, however in comparison to NH₄SCN, a 50% lowering of reaction yield was observed.

Table 3.2 1-6 yield

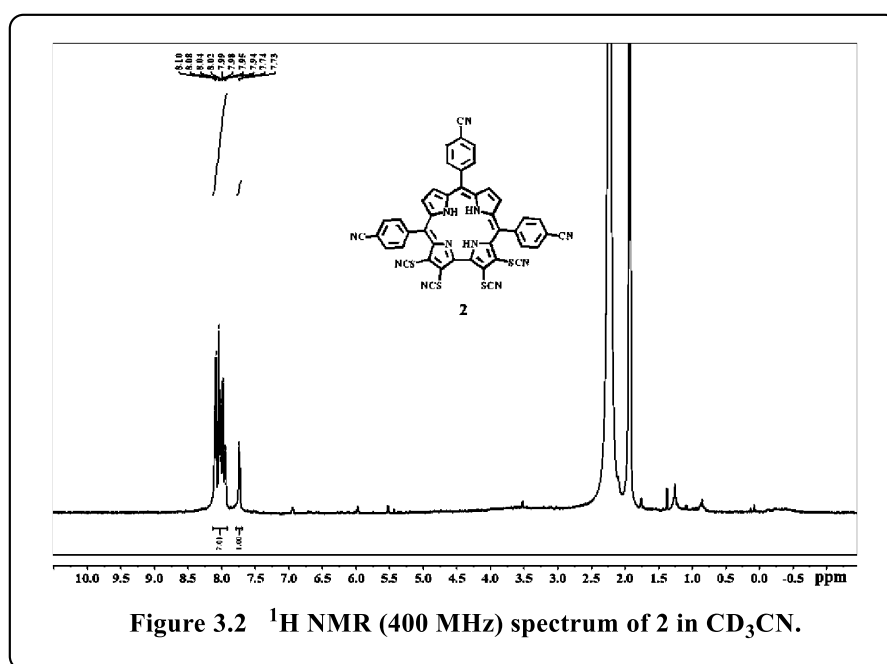
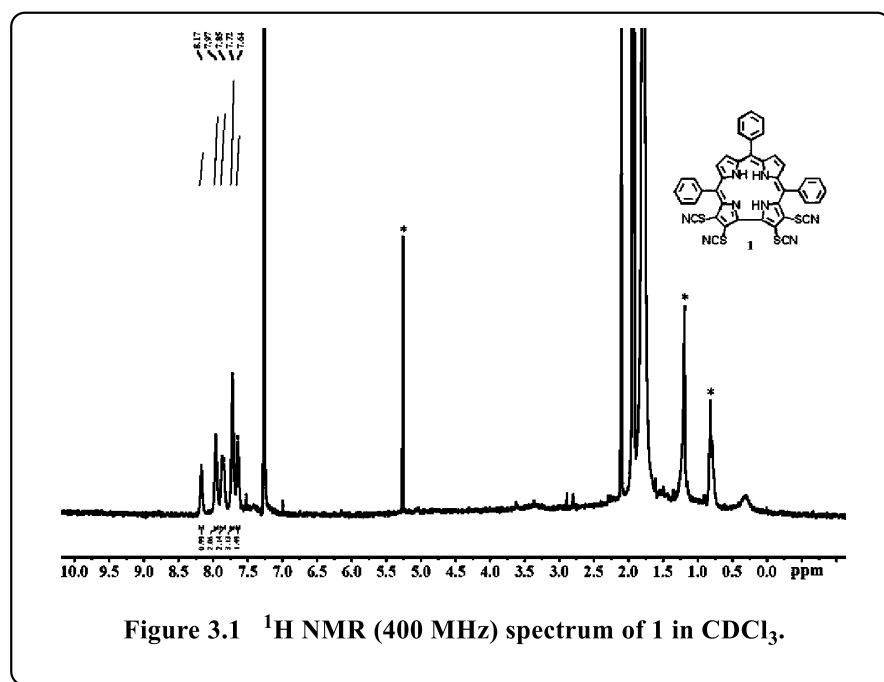
Reactant	Product	Yield%
1A	1	30
2A	2	32
3A	3	12
4A	4	35
5A	5	48
6A	6	46

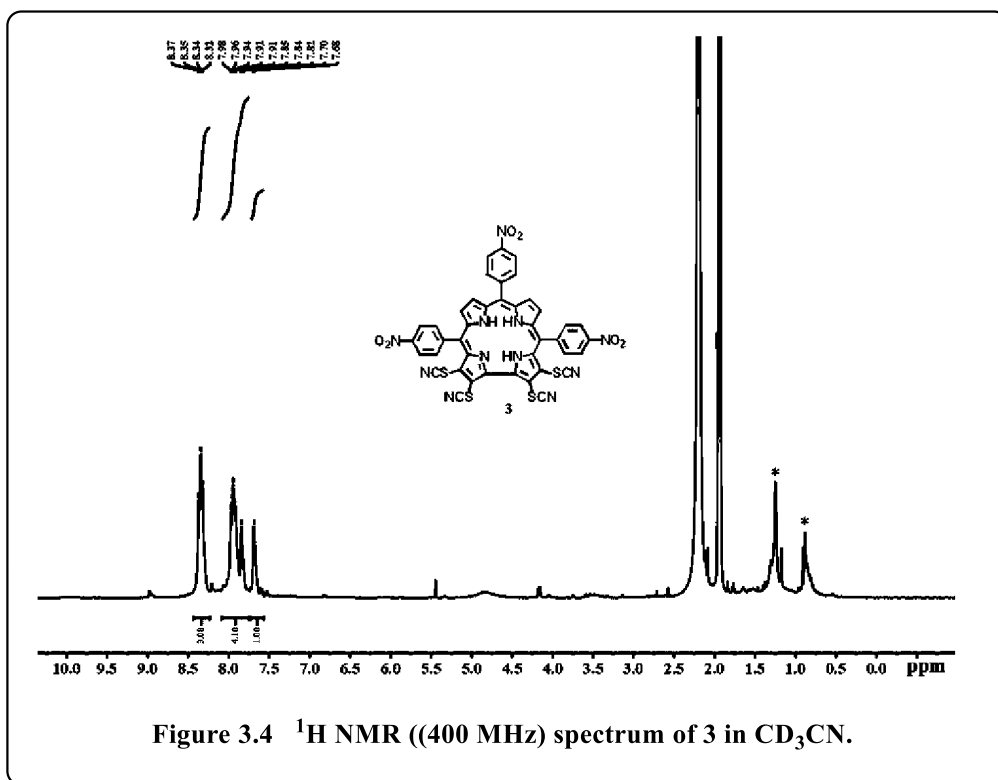
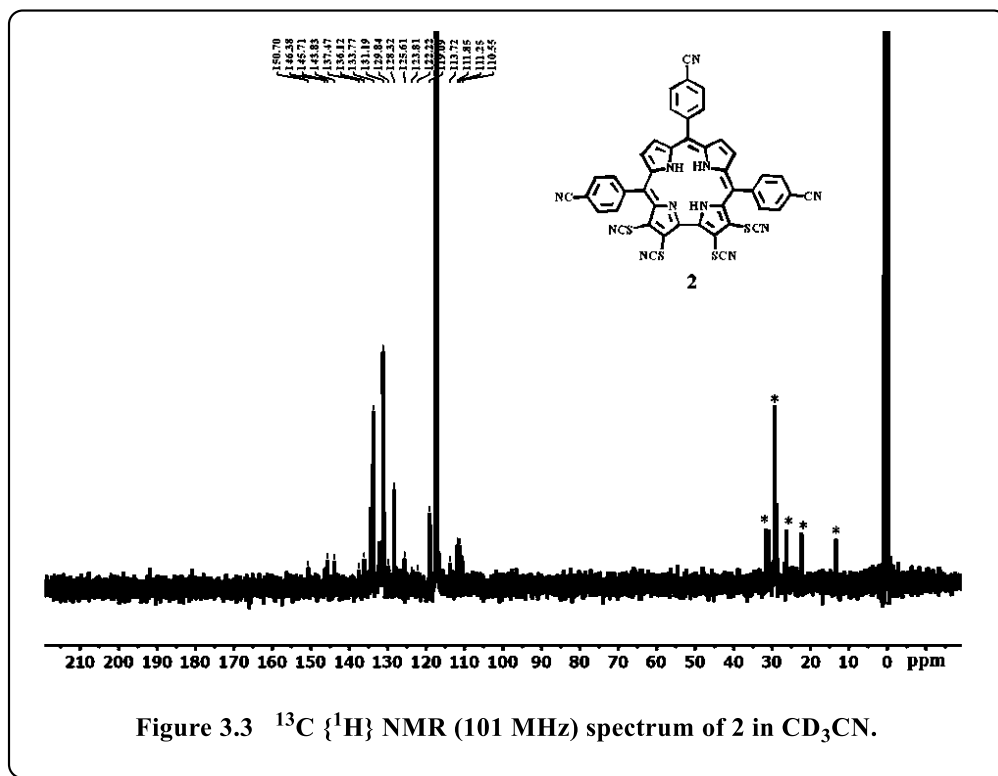
3.4 Spectral Characterization:

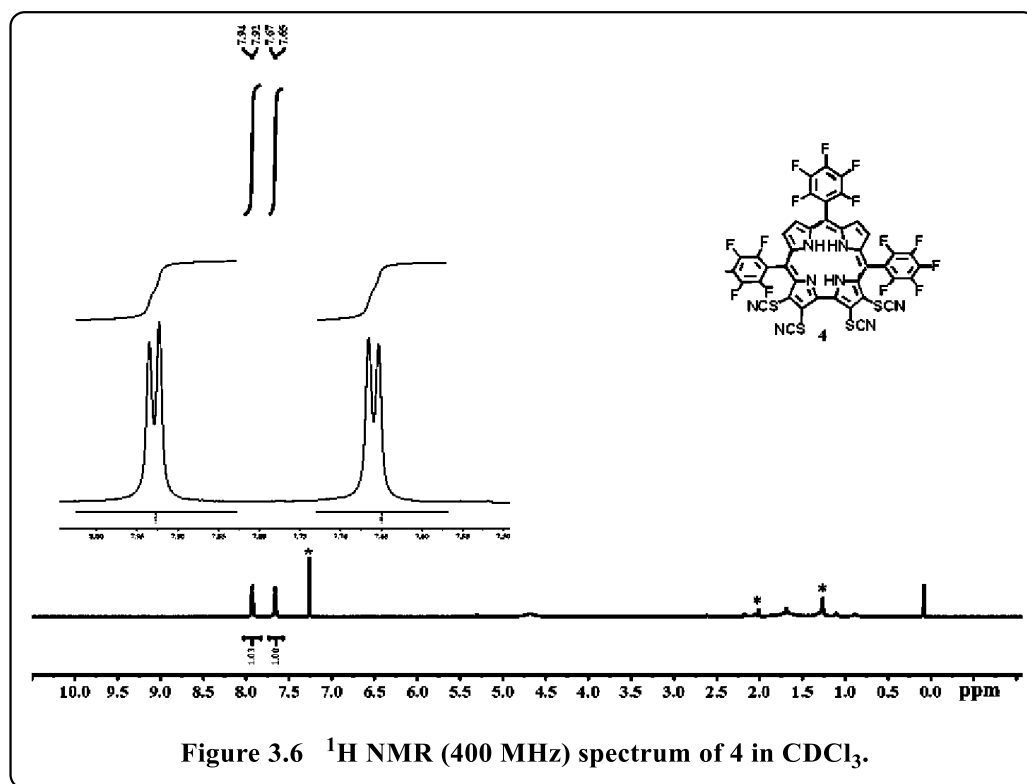
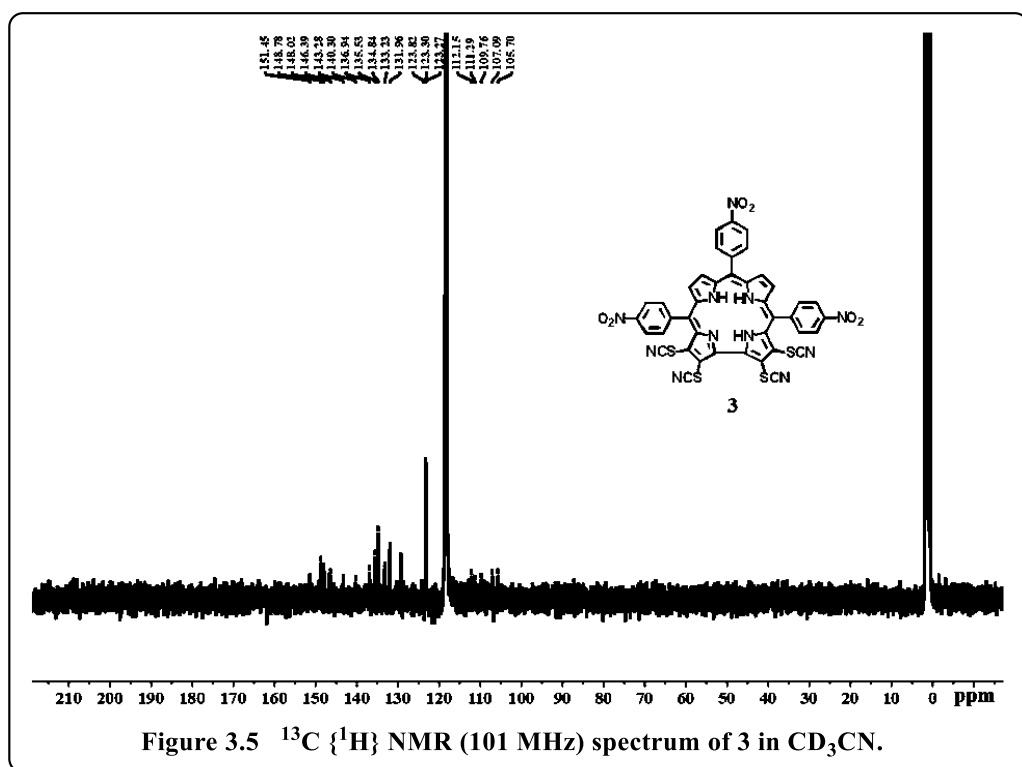
3.4.1 NMR Spectroscopy:

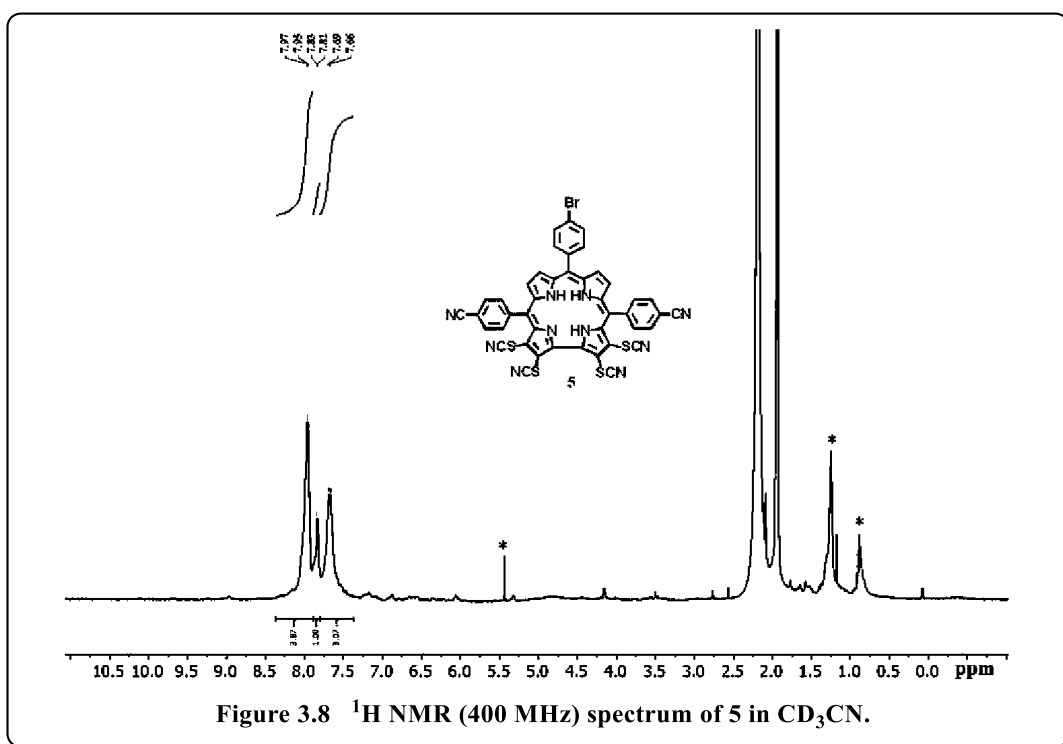
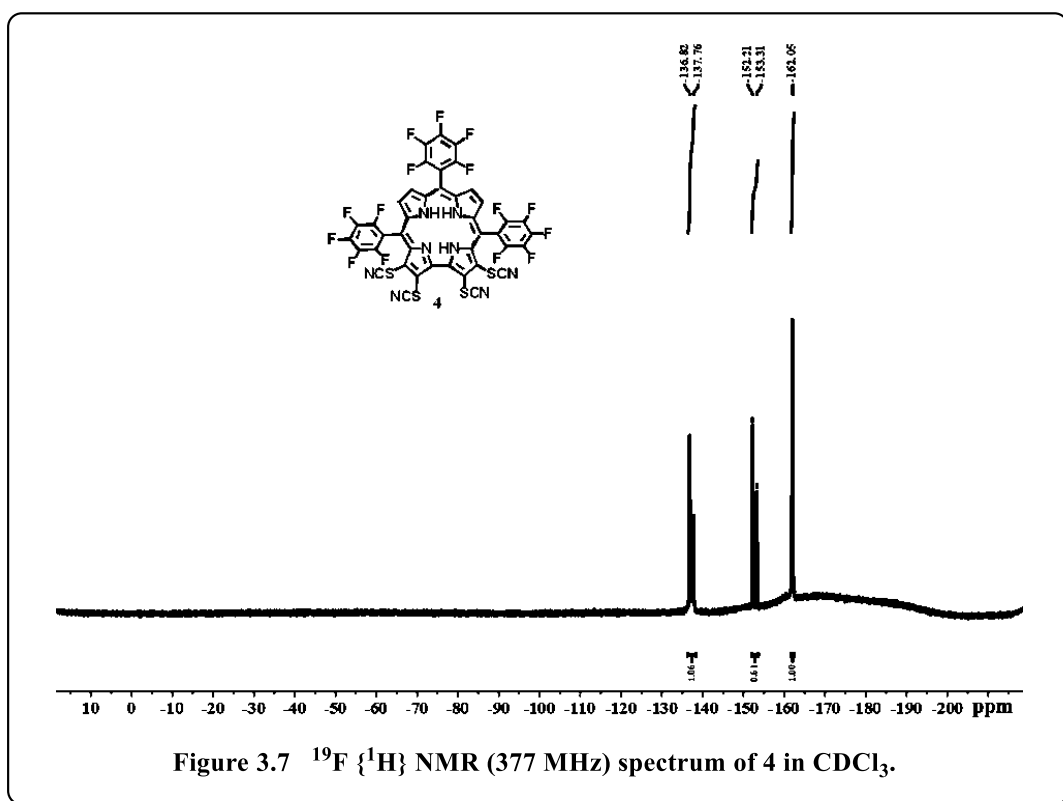
The ¹H NMR spectrum of **1** exhibit sharp peaks in the region δ , ~ 8.17–7.64 ppm, **2** exhibits sharp peaks in the region δ , ~ 8.09–7.74 ppm, **3** exhibits sharp peaks in the region δ , ~ 8.41–7.68 ppm, **4** exhibits sharp peaks in the region δ , ~ 7.93–7.66 ppm, **5** exhibits sharp peaks in the region δ , ~ 7.97–7.69 ppm, and **6** exhibits sharp peaks in the region δ , ~ 8.27–6.52 ppm. The peaks are shielded by ~0.8 ppm in the 2,3,17,18-tetrathiocyanatocorroles (**1-6**) corresponding

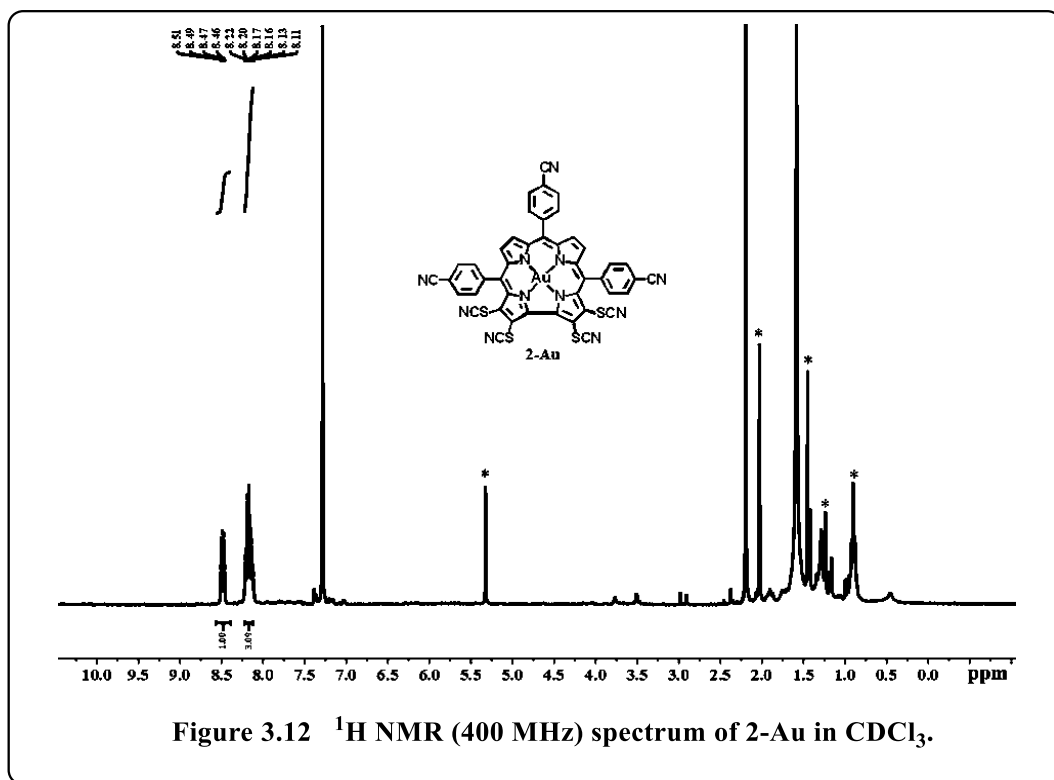
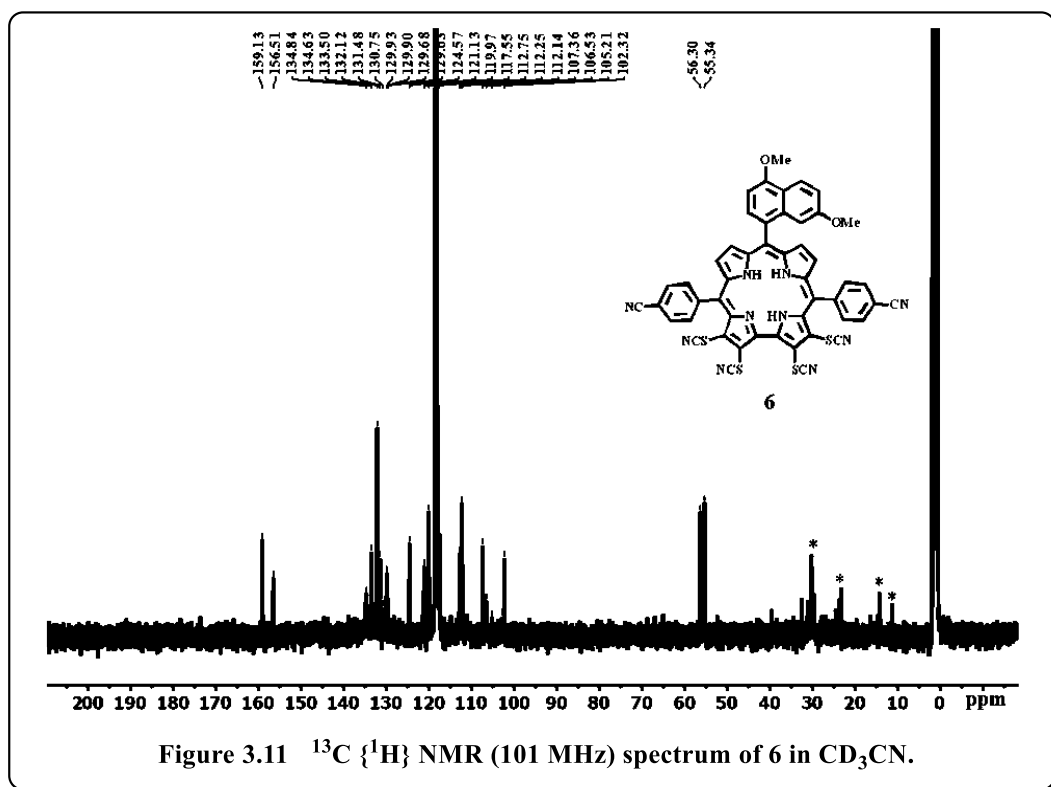
to their starting FB corrole (**1A-6A**) analogues. ^{13}C NMR spectrum of all these tetrathiocyanacorrole derivatives shows their characteristic signals due to the presence of SCN moiety at δ values of around ~ 111.0 - 112.0 ppm (Figures 3.1-3.11). The diamagnetic nature of the corrolato-Au (III) complex, **2-Au** is evident from its sharp resonances and having normal chemical shifts (Figures 3.12-3.13).

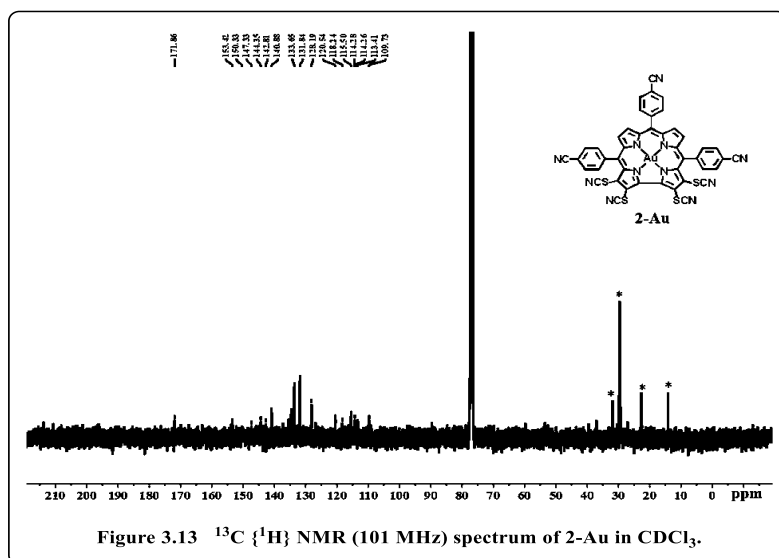






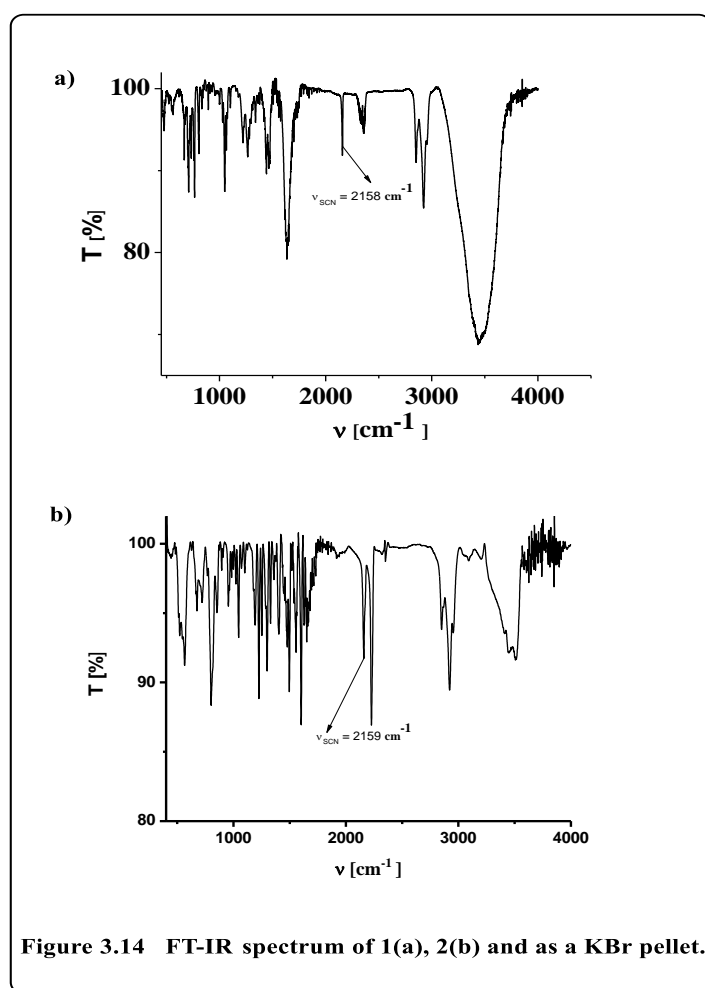






3.4.2 IR Spectroscopy:

The FT-IR spectra of **1-6** as KBr pellets show peaks at 2158, 2159, 2157, 2162, 2155, and 2156 cm^{-1} respectively due to strong S-CN stretching vibration (Figure 3.14 - 3.16).



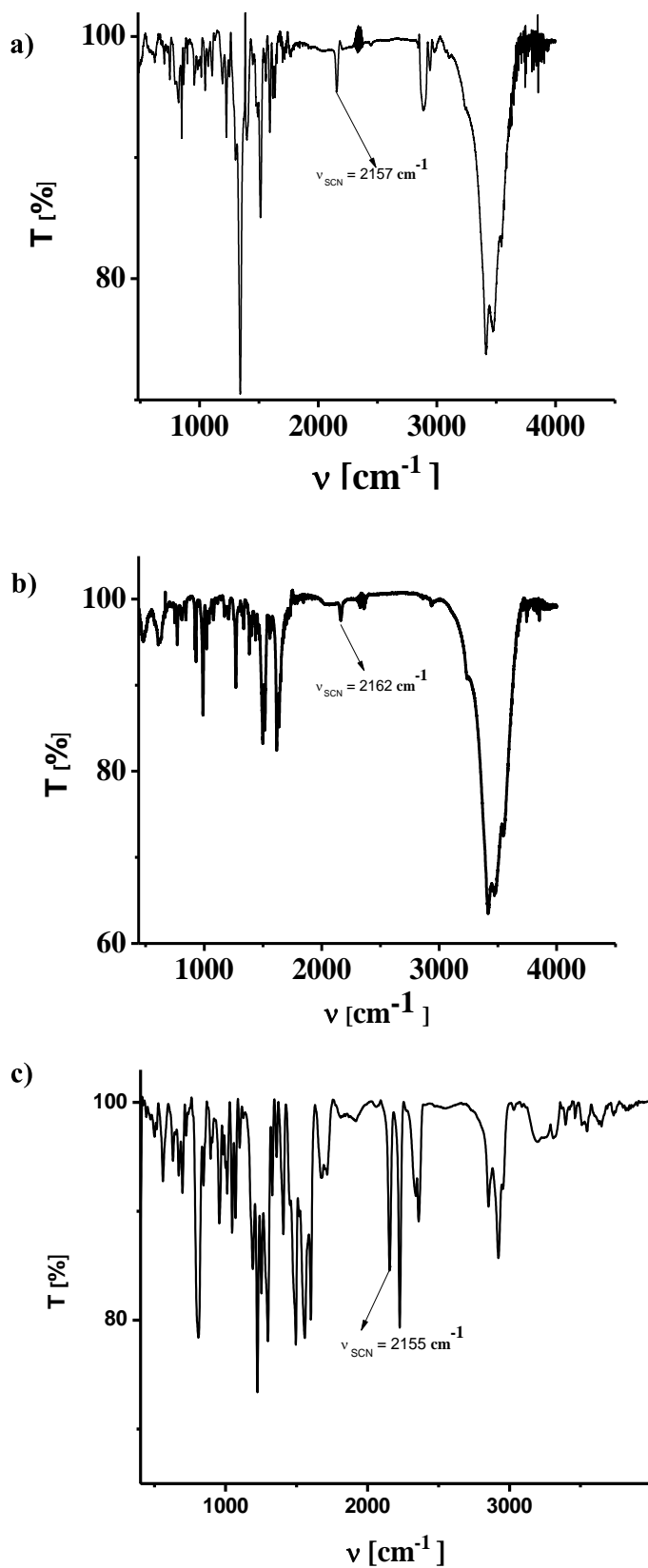
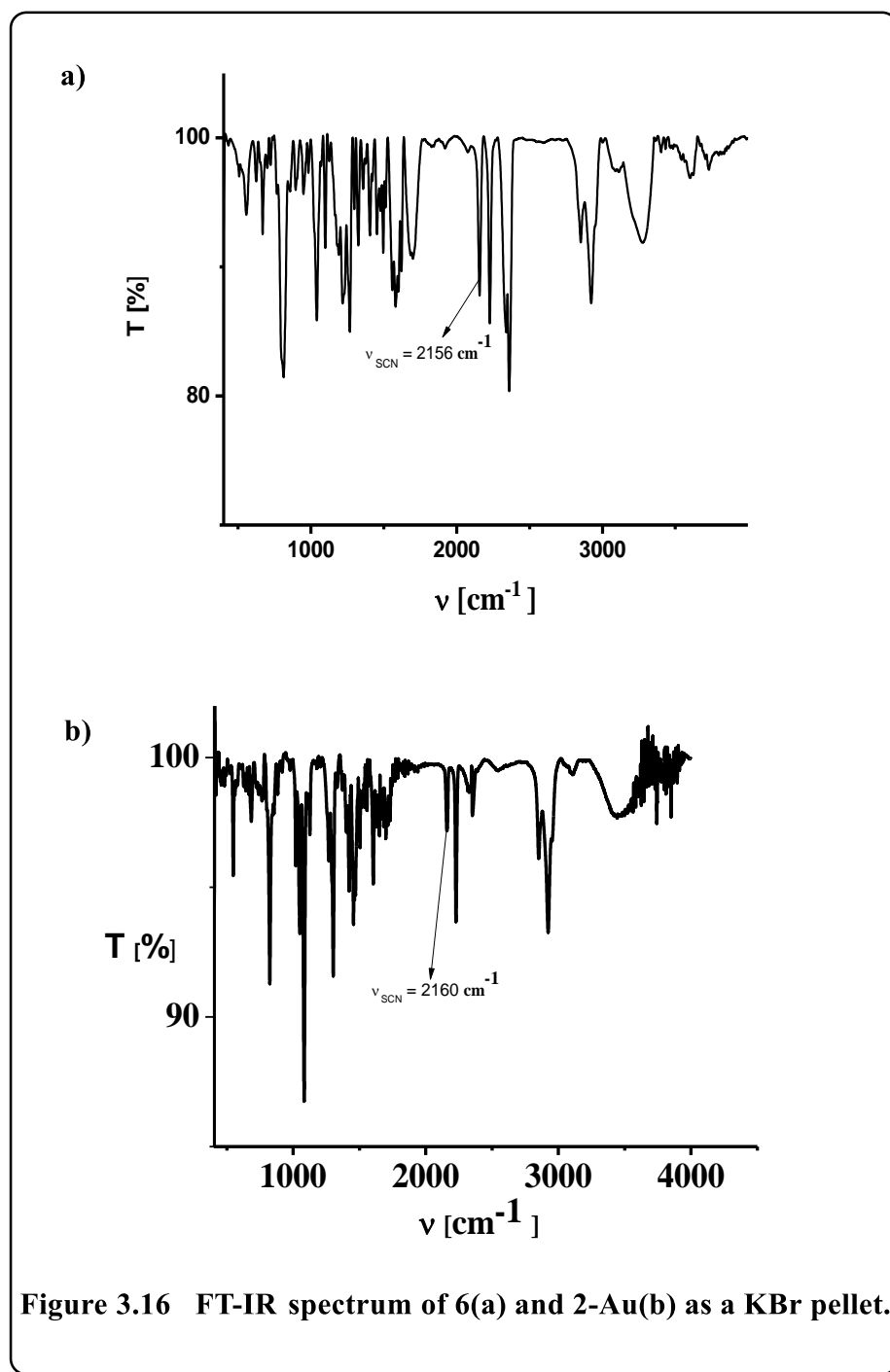


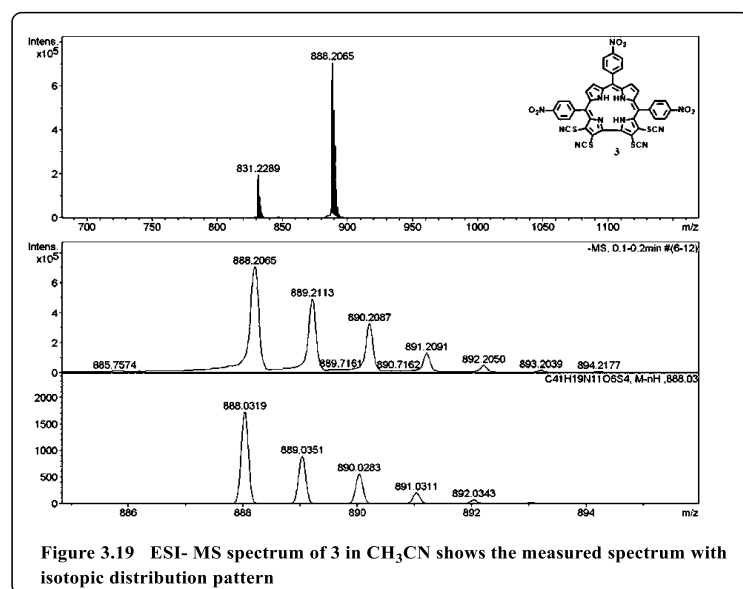
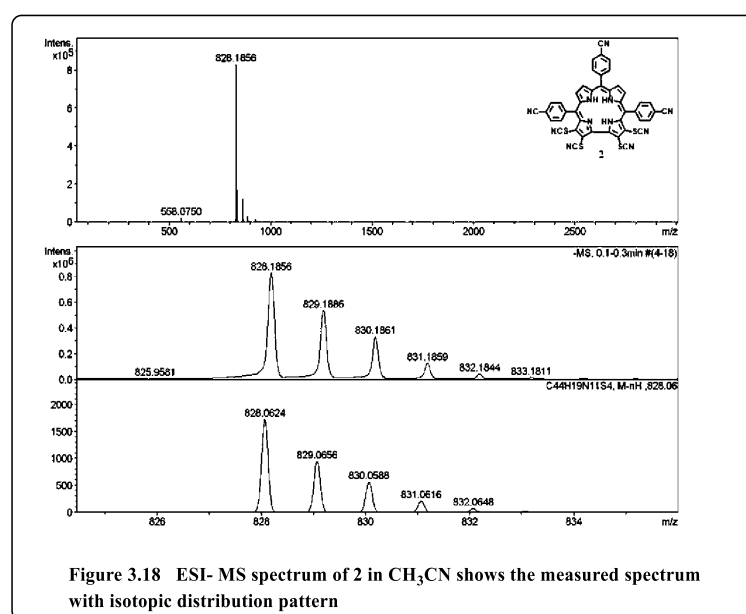
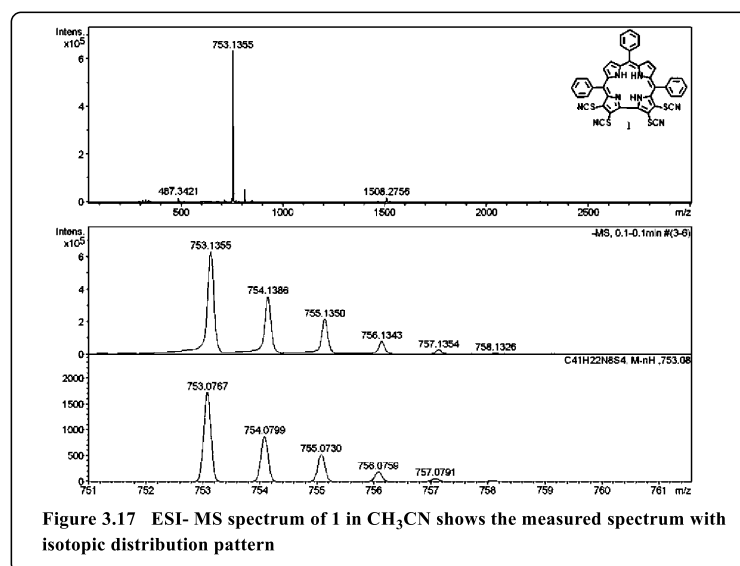
Figure 3.15 FT-IR spectrum of 3(a), 5(b) and 5(c) as a KBr pellet.



3.4.3 Mass Spectrometry:

The electrospray mass spectrum in methanol showed peaks centred HRMS (ESI) m/z : [1-**H**]⁻ Calculated for $\text{C}_{41}\text{H}_{21}\text{N}_8\text{S}_4$ 753.0767; Found 753.1355 (Figure 3.17)

The electrospray mass spectrum in methanol showed peaks centred HRMS (ESI) m/z : [2-**H**]⁻ Calculated for $\text{C}_{44}\text{H}_{18}\text{N}_{11}\text{S}_4$ 828.0624; Found 828.1856 (Figure 3.18).



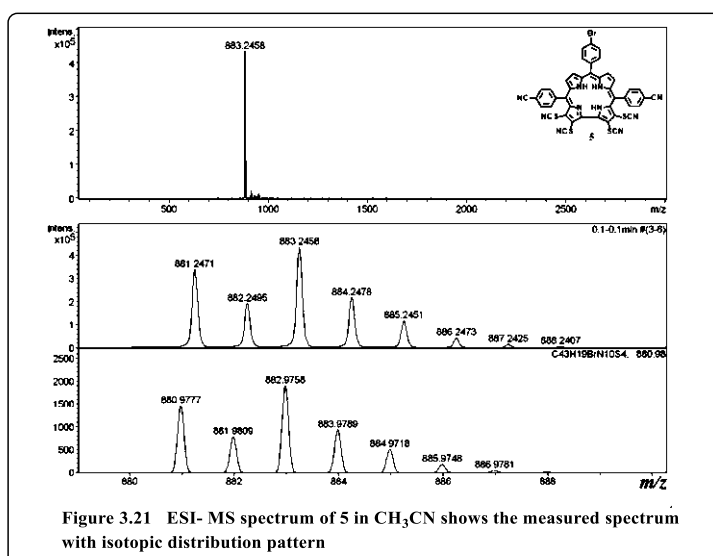
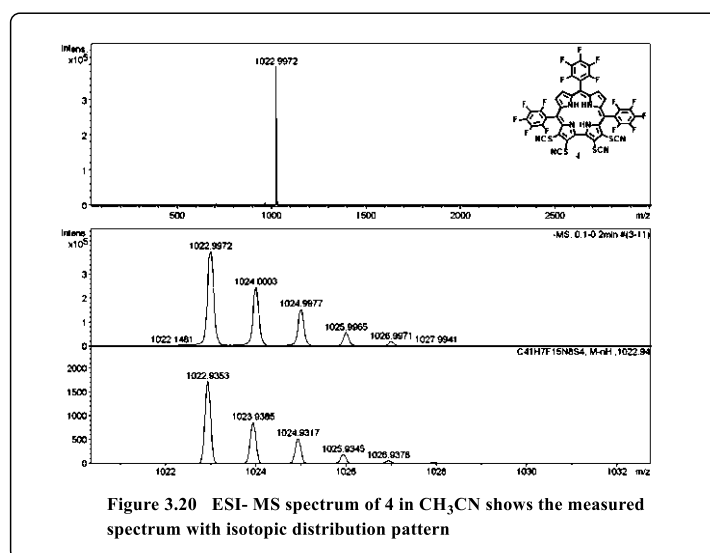
The electrospray mass spectrum in methanol showed peaks centred HRMS (ESI) m/z : [**3-H**]⁻ Calculated for C₄₁H₁₈N₁₁O₆S₄ 888.0319; Found 888.2065 (Figure 3.19).

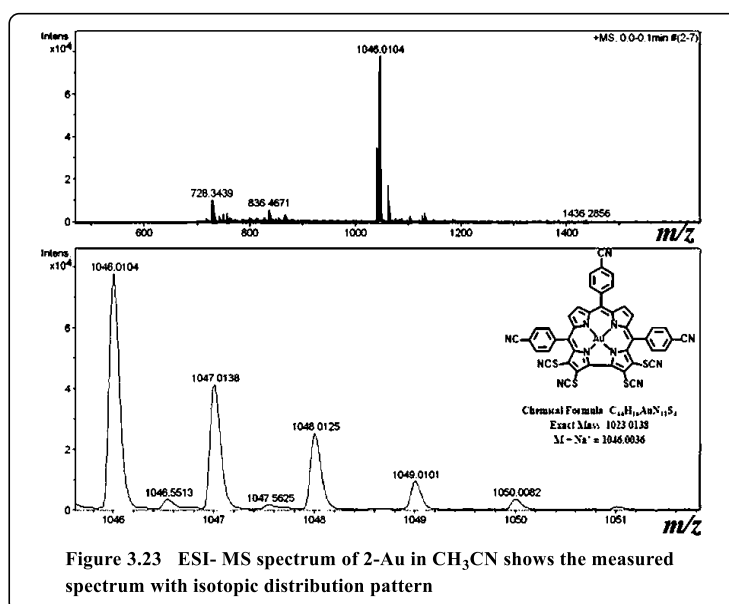
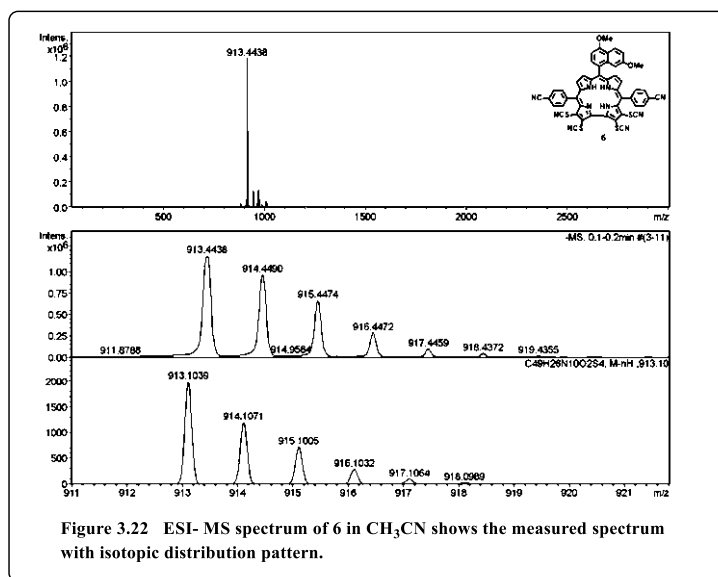
The electrospray mass spectrum in methanol showed peaks centred HRMS (ESI) m/z : [**4-H**]⁻ Calculated for C₄₁H₆F₁₅N₈S₄ 1022.9353; Found 1022.9972 (Figure 3.20).

The electrospray mass spectrum in methanol showed peaks centred HRMS (ESI) m/z : [**5+H**]⁺ Calculated for C₄₃H₂₀N₁₀S₄Br 882.9758; Found 883.2458 (Figure 3.21).

The electrospray mass spectrum in methanol showed peaks centred HRMS (ESI) m/z : [**6-H**]⁻ Calculated for C₄₉H₂₅N₁₀O₂S₄ 913.1039; Found 913.4438 (Figure 3.22).

The electrospray mass spectrum in methanol showed peaks centred HRMS (ESI) m/z : [**2-Au+Na**]⁺ Calculated for C₄₄H₁₆AuN₁₁S₄Na 1046.0036; Found 1046.0104 (Figure 3.23)

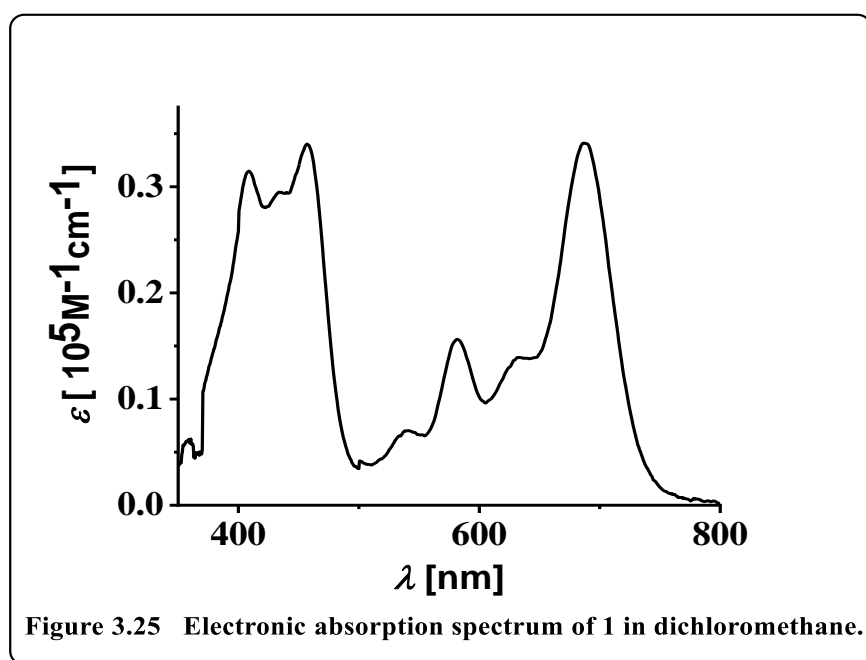
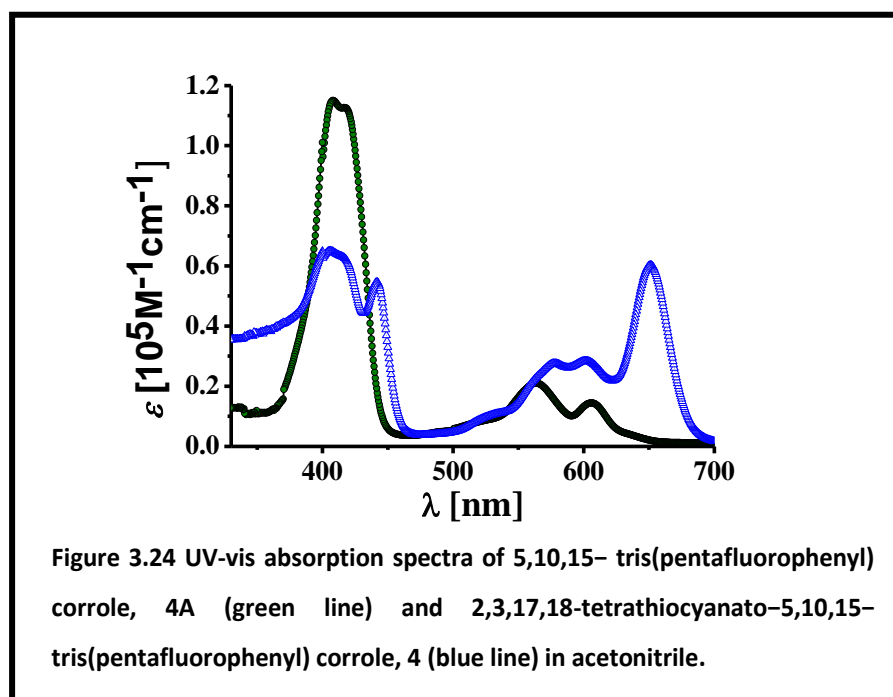




3.4.4 Electronic absorption spectroscopy:

The electronic absorption spectra of tetrathiocyanatocorroles, **1-6**, are shown in Figures 3.24-3.27. The Soret band here is further splitted into at least three distinct bands and thus indicates a lower symmetry compared to the FB corroles (Table 3.3, Figure 3.24). The most interesting phenomena are the appearance of at least four Q-bands, out of them, the lowest energy band is as intense as the Soret bands. The Q bands in porphyrinoids are in general pseudoparity-forbidden and thus very weak.^[48] Thus suitable external substitution

can break this pairing property and Q bands can be intensified. Unlike porphyrin and corroles, these absorption features of Q bands are fairly similar to the Q-type bands in the chlorophyll-*a* molecule. It was observed that the absorption feature of these modified corrole derivatives (both position and intensity) bears a nice similarity with the chlorophyll-*a* macrocycle.^[49]



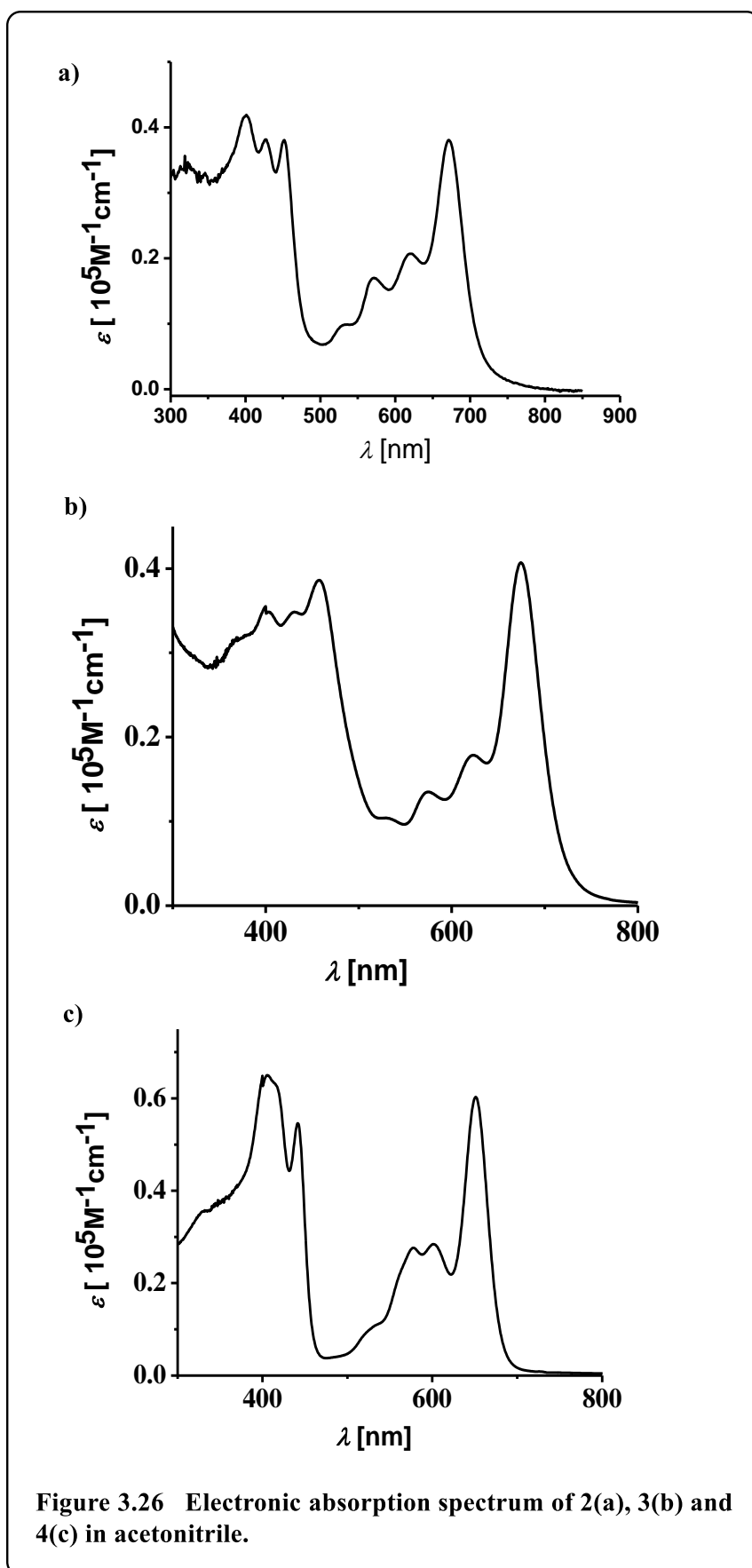


Figure 3.26 Electronic absorption spectrum of 2(a), 3(b) and 4(c) in acetonitrile.

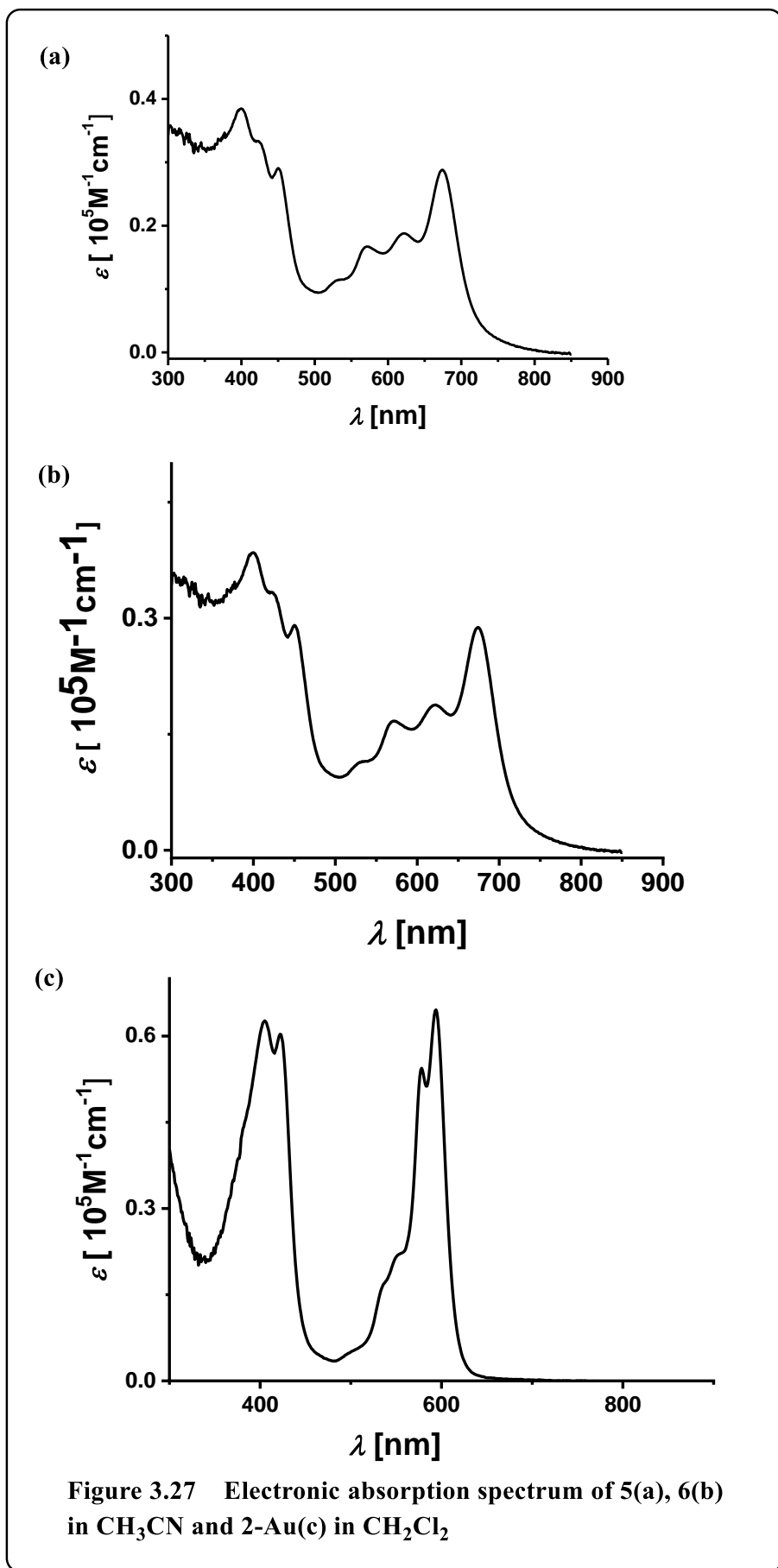


Figure 3.27 Electronic absorption spectrum of 5(a), 6(b) in CH_3CN and 2-Au(c) in CH_2Cl_2

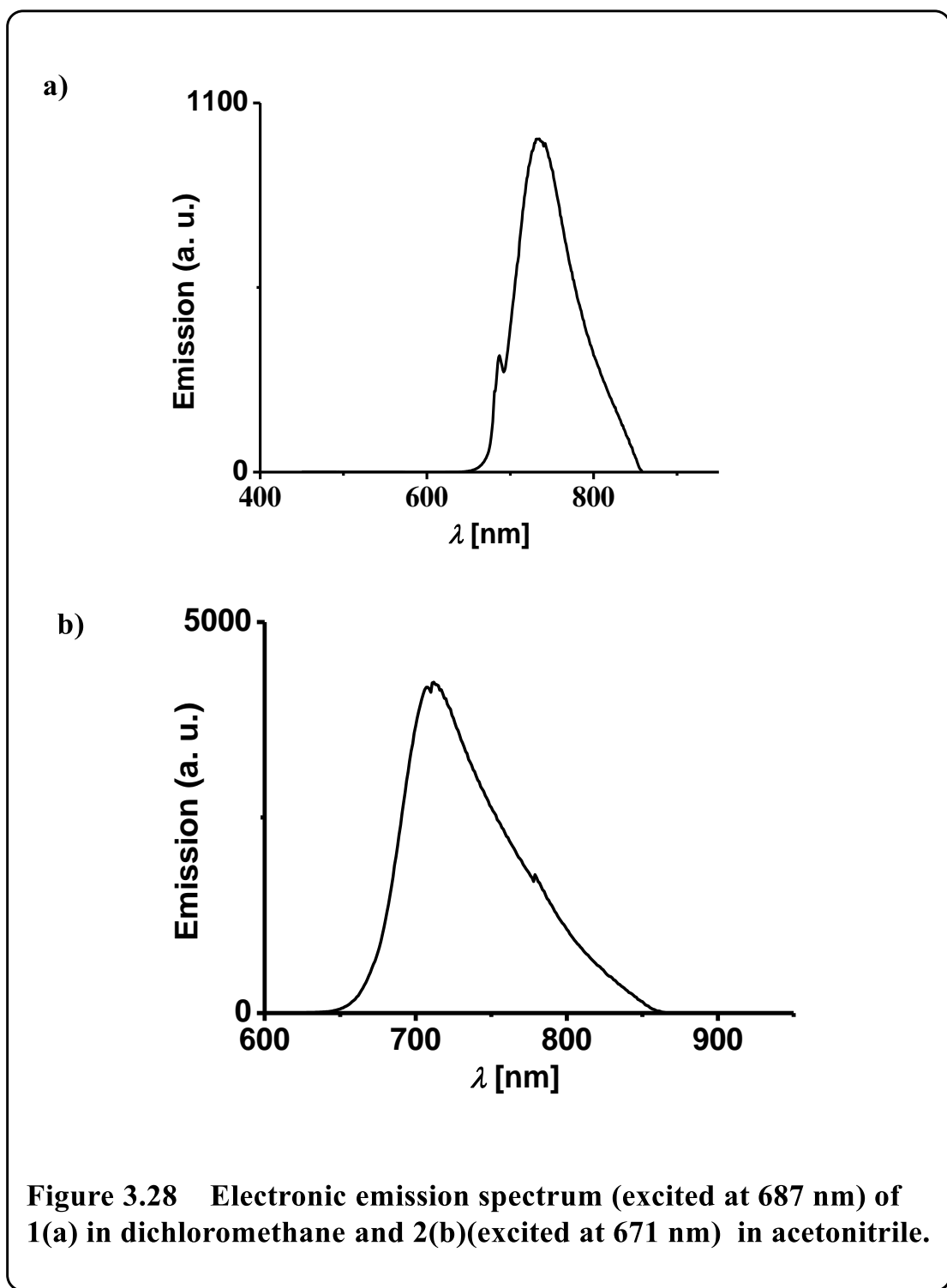
Table 3.3 UV–Vis data ^a in acetonitrile^b and dichloromethane^c

Compound	UV–vis. Data ^{a,b} λ_{\max} / nm (ϵ / M ⁻¹ cm ⁻¹)
1^c	408 (32000), 433 (30000), 456 (34000), 539 (7000), 581 (15700), 632 (14000), 686 (34000)
2^b	400 (41671), 426 (38104), 451 (37821), 528 (9656), 570 (17030), 619 (20716), 671 (37985)
3^b	403 (35 000), 430 (35200), 457 (38 600), 532 (10400), 573 (13500), 621 (18000), 674 (41,000)
4^b	407 (65000), 441 (55000), 528 (10300), 577 (28000), 601(28500), 651 (60500)
5^b	399 (38567), 423 (33328), 450 (29059), 530 (11358), 568 (16597), 619 (18791), 673 (28850)
6^b	399 (38537), 422 (33403), 449 (28940), 529 (11477), 569 (16716), 621(18764), 673 (28806)
2-Au^c	404 (62628), 422 (60304), 536 (16883), 551 (21900), 577 (54309), 593 (64535)

^a Error limits: λ_{\max} , ± 1 nm and ϵ , $\pm 10\%$

3.4.4 Emission Properties:

These tetrathiocyanatocorroles, **1-6** showed a significant red-shifted emission band compared to their parent corroles (**1A-6A**). The tail of the emission band reaches up to 850 nm (Figures 3.28-3.29). These tetrathiocyanatocorrole derivatives (**1-6**) thus has the strong potential to become near-infrared (NIR)-emissive dyes. The obtained fluorescence quantum yields of **1-6** were estimated to be 0.07 for **1**, 0.08 for **2**, 0.11 for **4**, 0.10 for **5**, and 0.15 for **6** respectively. The low-lying singlet excited states of **1-6** are responsible for the origin of these kinds of emissive properties.^[10]



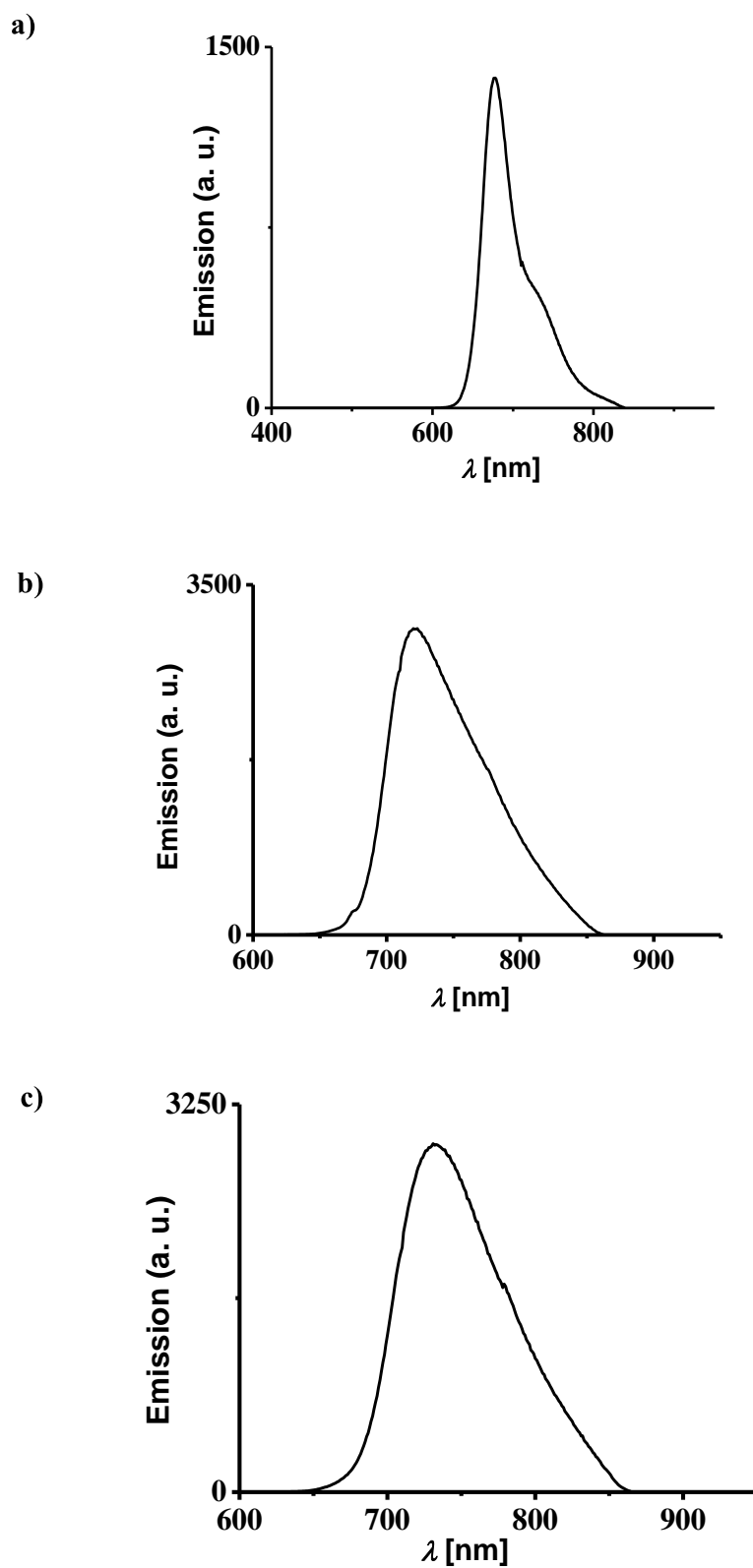


Figure 3.29 Electronic emission spectrum of 4(a) (excited at 651 nm), 5(b) (excited at 673 nm) and 6(c) (excited at 670 nm) in acetonitrile.

3.4.5 Single crystal XRD Analysis:

The crystal system of 2,3,17,18-tetrathiocyanatocorrole, **2** is triclinic in nature and the unit cell has two molecules of **2**. Although statistically four possible atropisomers can be obtained (based on the orientation of the SCN moieties at above (b) or below (a) the plane of the corrole ring), we have obtained only one atropisomer^[50] (a_2b_2 isomers) here (Figure 3.30 and Table 3.4). Important crystallographic parameters for **2** are summarized in Table 3.4. Bond angles and distances of **2** tallies well with the previously reported other FB corrole derivatives.^[10] The pyrrolic nitrogen atoms deviate from the 19-carbon atom mean corrole plane by distances ranging from 0.189–(−0.149) Å in **2**. The deviations observed in **2** are very much similar to that of the 5,10,15-triphenylcorrole (TPC). The corresponding deviations in TPC are 0.128–(−0.195) Å.^[49] However, the dihedral angles (between the planes of the *meso*-substituted phenyl rings and the 19-carbon mean corrole plane) in **2** differs significantly in comparison to the TPC. The dihedral angles in **2** are in the range of 63.64–85.46° and the corresponding values in TPC are in the range of 41.74–50.33°.^[51] Thus the insertion of four thiocyanate moieties at the four β -pyrrolic positions (2, 3, 17, and 18) has imparted significant distortion to the corrole molecule, **2**.

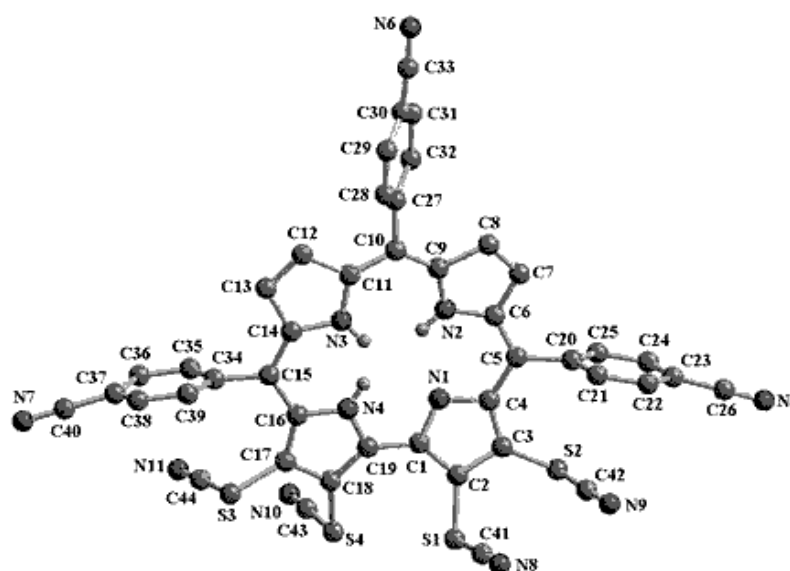


Figure 3.30 Single-crystal X-ray structure of **2**. Hydrogen atoms are omitted for clarity.

Table 3.4 Crystallographic Data for **2**.

compound code	2
molecular formula	C ₄₄ H ₁₉ N ₁₁ S ₄ , S, 2(H ₂ O)
Fw	898.03
Radiation	Mo K α
crystal symmetry	Triclinic
space group	P -1
<i>a</i> (Å)	6.5412(3)
<i>b</i> (Å)	15.3321(15)
<i>c</i> (Å)	25.553(3)
α (deg)	101.921(9)
β (deg)	95.256(7)
γ (deg)	96.892(6)
<i>V</i> (Å ³)	2471.4(4)
<i>Z</i>	2
μ (mm ⁻¹)	0.28
<i>T</i> (K)	298
<i>D</i> _{calcd} (g cm ⁻³)	1.207
2 θ range (deg)	6.72-52.74
<i>e</i> data (<i>R</i> _{int})	6178 (0.1390)
R1 (<i>I</i> > 2 σ (<i>I</i>))	0.1390
WR2 (all data)	0.3721
GOF	1.024
$\Delta\rho_{\max}$, $\Delta\rho_{\min}$ (e Å ⁻³)	0.95, -0.63

The two thiocyanate groups are attached to each pyrrolic rings in *cis* fashion, but they are in *trans* orientation with respect to the thiocyanate group attached with the neighbouring pyrrole ring. The four C \equiv N (derived from SCN unit) bond distances of **2** are in the range of 1.11-1.16 Å and the four \angle S-C \equiv N bond angles are in the range of 176.47–179.07°.

The crystal system of {2,3,17,18-tetrathiocyanato-5,10,15-tris(4-cyanophenyl)corrolato-Au(III)}, **2-Au**, is monoclinic in nature and the unit cell has four molecules of **2-Au**. In contrast to the free base 2,3,17,18-tetrathiocyanatocorrole, for **2-Au** we have

obtained only a₄ atropisomer. Important crystallographic parameters for **2-Au** are summarized in Table 3.5. Bond angles and distances of **2-Au** are tallies well with the previously reported other Au (III)-corroles.^[52] Gold atom deviates from the mean N₄ corrole plane by 0.0083 Å (Figure 3.31). The geometry around the gold center is not perfectly square planar.

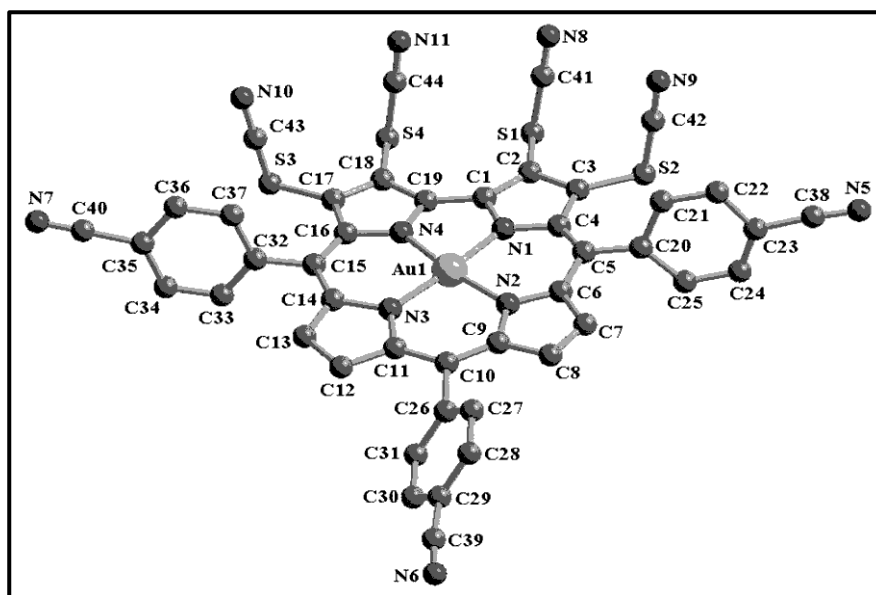


Figure 3.31 Single-crystal X-ray structure of 2-Au. Hydrogen atoms are omitted for clarity.

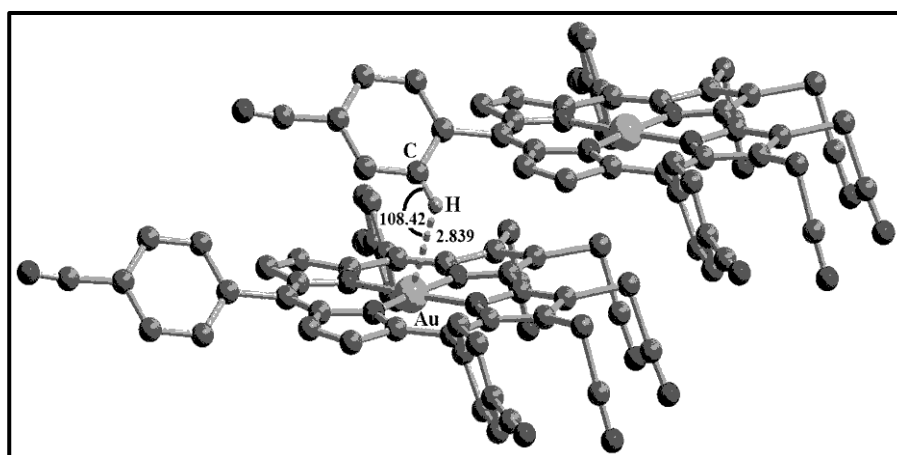


Figure 3.32 X-ray single-crystal structure analysis of 2-Au, showing C-H...Au interactions [$\angle\text{C-H}\dots\text{Au} = 108.42^\circ$ and $\text{C-H}\dots\text{Au} = 2.838\text{\AA}$] between neighbouring molecules. The entry in square brackets is the angle and distance.

The bite angles of N1-Au-N2, N2-Au-N3, N3-Au-N4, and N4-Au-N1 are 90.81°, 94.23°, 93.69°, and 81.27° respectively. The Au-N bond distances are in the range from 1.98 Å for Au-N2 to 1.91 Å for Au-N1 bonds and are slightly longer than related Au(III) corrole.^[50] The pyrrolic nitrogen atoms deviate from the 19-carbon atom mean corrole plane by distances ranging from 0.0196 Å – (–0.0584) Å. The dihedral angles in **2-Au** are in the range of 48.82–75.56°. X-ray single-crystal structure analysis of **2-Au**, showing C-H...Au interactions between neighbouring **2-Au** molecules and thus constitute a rare example of C-H...Au interaction driven supramolecular assembly formation in the gold chemistry (Figure 3.32). Earlier researchers have concluded that a significant strong C-H... Au interaction exists if the H...Au separation falls in the range of 2.3–3.0 Å, C-H...Au angle falls in the range of 120–180°, and also an observable change noticed in the confirmation analysis.^[53–56] Herein we have observed H...Au distance of 2.838Å and C-H...Au angle of 108.42°. The orientation of thiocyanate group also changes and resulted in the transformation of $\alpha_2\beta_2$ atropisomer in corrole (**2**) to α_4 atropisomer in the gold corrole (**2-Au**).

Table 3.5 Crystallographic Data for **2-Au**.

compound code	2-Au
molecular formula	C ₄₄ H ₁₆ Au N ₁₁ S ₄
Fw	1023.88
Radiation	Cu <i>K</i> α
crystal symmetry	monoclinic
space group	<i>P</i> 2 ₁ / <i>n</i>
<i>a</i> (Å)	18.1706(7)
<i>b</i> (Å)	6.73850(1)
<i>c</i> (Å)	33.9461(8)
α (deg)	90
β (deg)	90.330(3)
γ (deg)	90
<i>V</i> (Å ³)	4156.4(2)

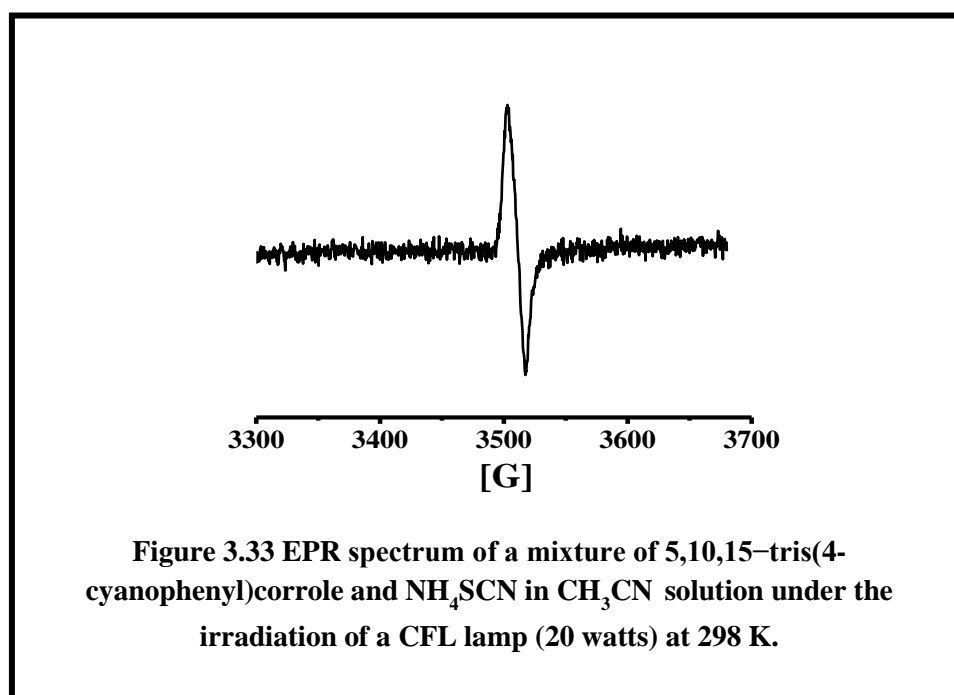
Z	4
μ (mm ⁻¹)	8.916
T(K)	100
D_{calcd} (g cm ⁻³)	1.636
2 θ range (deg)	4.592-68.244
<i>e</i> data (R_{int})	5804 (0.072)
R1 ($I > 2\sigma(I)$)	0.119
WR2 (all data)	0.2979
GOF	1.04
$\Delta\rho_{\text{max}}, \Delta\rho_{\text{min}}$ (e Å ⁻³)	6.29, -2.35

3.5 Analysis of the reaction mechanism:

To understand the reaction mechanism, several control reactions were performed (Figures 3.33-3.38). To clarify if the reaction proceeds via a radical pathway, we have used radical inhibitors (Scheme 3.5 & 3.6). When 2.5 equivalents of a commonly used radical inhibitor, like TEMPO {TEMPO=2,2,6,6-tetramethyl-1-piperidinyloxy}, was used in the reaction mixture, we have not observed the formation of the desired 2,3,17,18-tetrathiocyanatocorrole derivatives (**1-6**). Besides that, while treating the reaction mixture with another radical inhibitor, like BHT {BHT = Butylated hydroxytoluene}, we have observed the formation of an adduct of BHT with thiocyanate radical. The adduct was characterized by ESI-MS spectra (Figure 3.34). While performing the reaction of 5,10,15-tris(4-cyanophenyl)corrole with NH₄SCN under irradiation with a CFL lamp, we have observed the presence of (SCN)₂ in the reaction mixture by ESI-MS spectra (Figure 3.35). The origin of (SCN)₂ can be demonstrated via the coupling of two thiocyanates radical. All this evidence supports the formation of thiocyanate radical via the photoexcitation of a mixture of free base corrole and NH₄SCN. It has been observed that the excited state of porphyrinoids is more potent oxidants and reductants in comparison to their ground state. The oxidation and reduction potential in the excited state of corroles can be estimated from the Gibbs energy of the PET processes.^[57] For example, the reduction

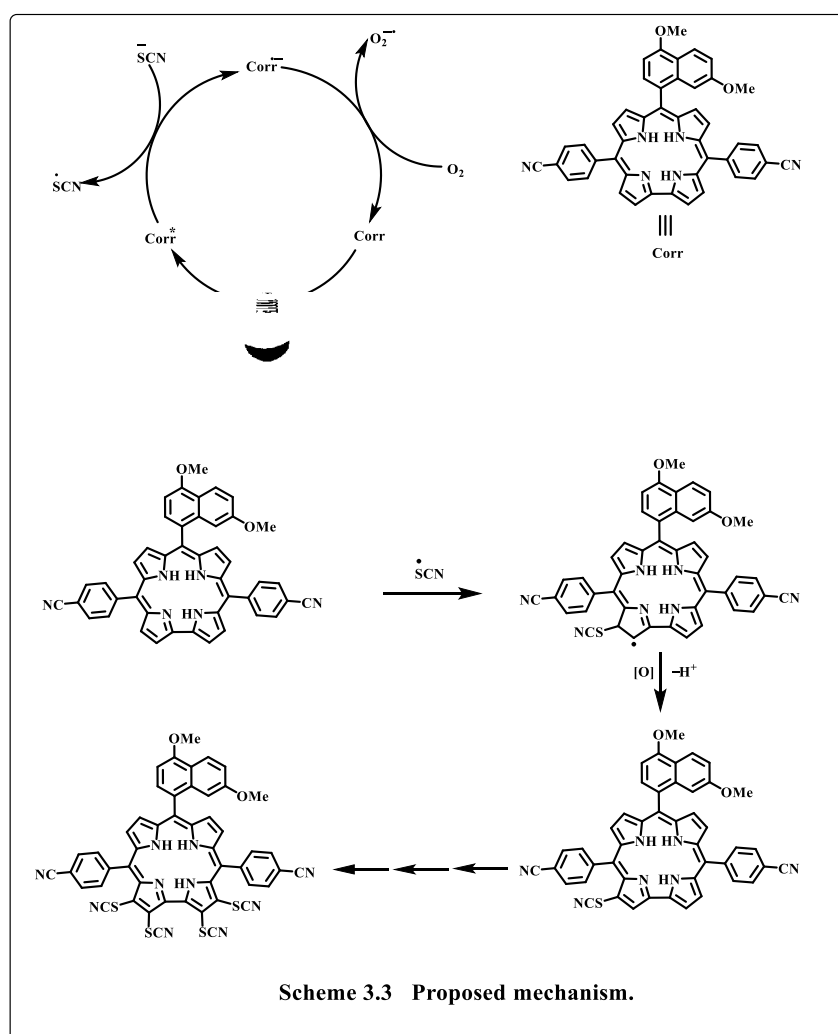
potential of the 5,10,15-tris(4-cyanophenyl)corrole in the excited state was found out to be +1.03 V vs. SCE (Figures 3.36-3.38). This value is higher than the oxidation potential of NH_4SCN ($E_{\text{ox}} = 0.65$ V vs SCE). Thus, the oxidation of NH_4SCN is thermodynamically favorable. In addition to that, we have also recorded the EPR spectrum of a mixture of 5,10,15-tris(4-cyanophenyl)corrole and NH_4SCN in CH_3CN solution under the irradiation of a CFL lamp (20 watts) at 298 K. An isotropic EPR signal is observed with a g value of 2.003 (Figure 3.33). A peak-to-peak separation of 15 G is also observed.

However, the hyperfine coupling due to nitrogen nuclei is not resolved. The isotropic EPR signal having a narrow linewidth and a g value close to the free radical value indicates a corrole based radical.^[58]



Which in conjunction with the favorable reduction potential of the FB corrole, clearly indicates the generation of a corrole based radical anion ($\text{corrole}^{\cdot-}$). Based on the above observations, and also from the previous literatures,^[39] we have proposed a plausible mechanism for the formation of tetrathiocyanatocorrole derivatives (**1-6**) (Scheme 3.3). FB corroles and NH_4SCN in CH_3CN solution under the irradiation of a CFL lamp resulted in

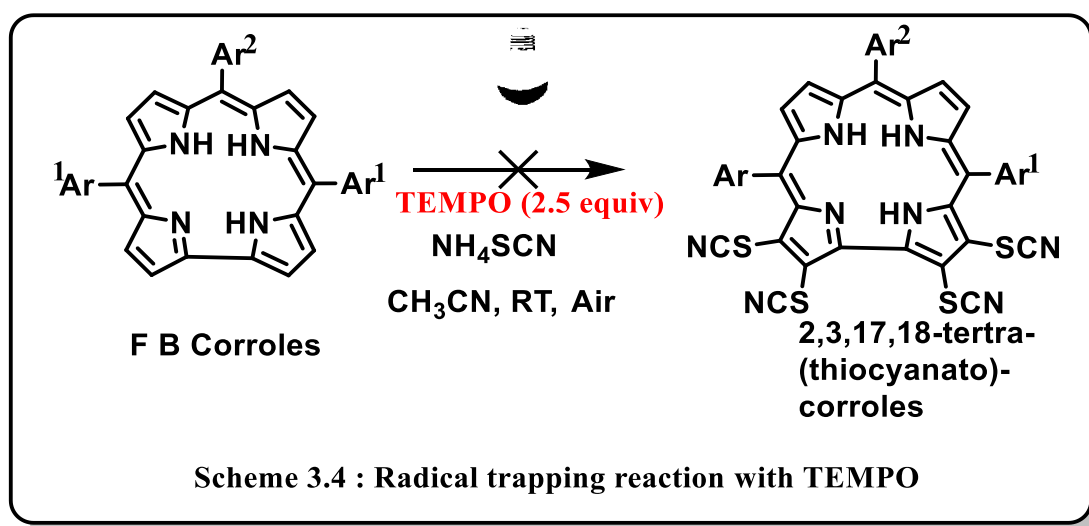
the formation of excited corroles (corrole*). In the next step, a single electron is transferred from SCN^- anion to the excited corroles (corrole*) and resulted in the generation of SCN^\bullet radical and corrole radical anion (corrole $^{\bullet-}$) respectively. This corrole radical anion can be quenched *via* the transfer of an extra electron to atmospheric O_2 and thus resulted the formation of $\text{O}_2^{\bullet-}$. In the succeeding step, the generated SCN^\bullet radical can directly couple with the corrole macrocycle and produce the monothiocyanatocorrole radical intermediate. Subsequent oxidation followed by deprotonation resulted the formation of monothiocyanatocorrole derivatives. The process can work cyclically and generates the tetrathiocyanatocorrole derivatives (**1-6**). We have used the NH_4SCN in excess quantities and thus is responsible for the insertion of four thiocyanato groups in the corrole periphery.



3.6 Mechanistic Studies

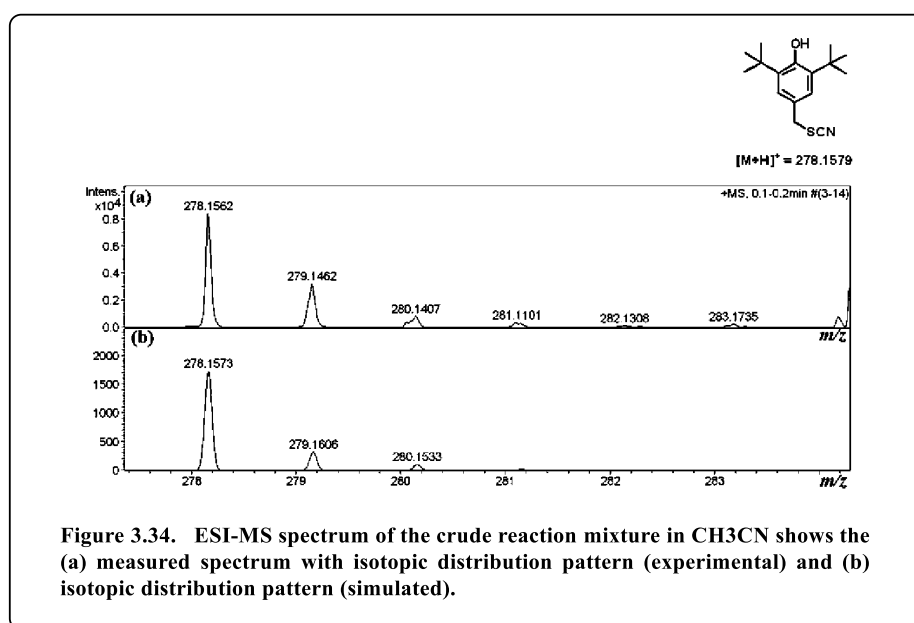
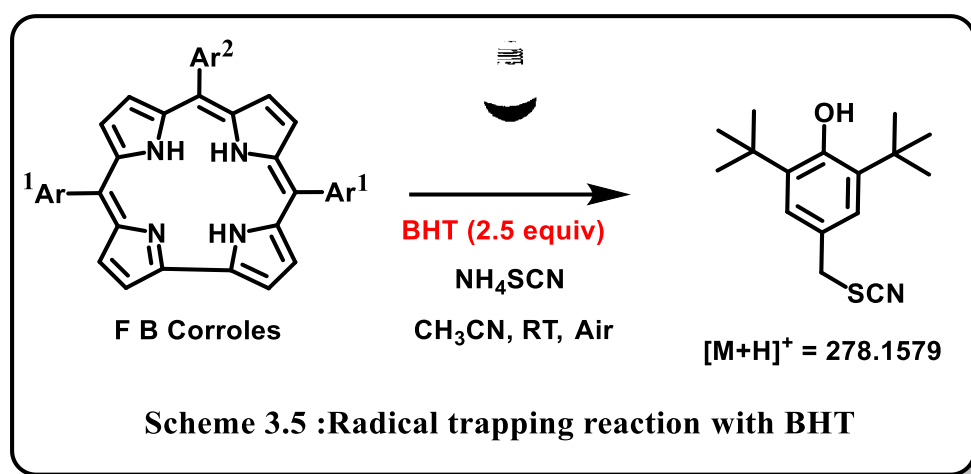
3.6.1 The radical trapping experiments:

50 mg (0.083 mmol) of 5,10,15-tris(4-cyanophenyl)corrole was dissolved in 15ml of acetonitrile, and then 500mg NH_4SCN (6.6 mmol) followed by TEMPO (2.5 equiv, 0.2 mmol) was added to it.^[59,60] The reaction mixture was stirred at room temperature under irradiation with a CFL lamp (20 watt) for 2.5 hours in air. At this point, a second batch of reagents, NH_4SCN (500mg) and acetonitrile (15ml) were added in the reaction mixture. The solution was stirred for another 2.5 hours. The residual solvent was evaporated to dryness and the reaction mixture was dissolved in dichloromethane. The reaction mixture was separated by using column chromatography through silica gel (100-200 mesh). No desired product was obtained (Scheme 3.4).



50 mg (0.083 mmol) of 5,10,15-tris(4-cyanophenyl)corrole was dissolved in 15ml of acetonitrile, and then 500mg NH_4SCN (6.6 mmol) followed by BHT (2.5 equiv) was added to it.^[61] The reaction mixture was stirred at room temperature under irradiation with a CFL lamp (20 watt) for 2.5 hours in air. At this point, a second batch of reagents, NH_4SCN (500mg) and acetonitrile (15ml) were added in the reaction mixture. The solution was stirred for another 2.5 hours. The residual solvent was evaporated to dryness and the

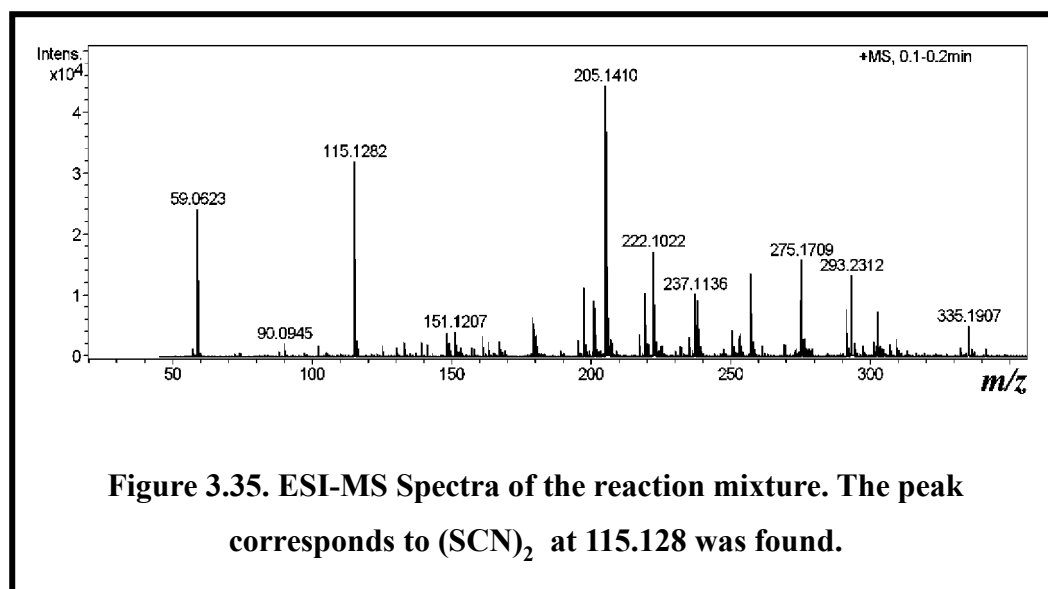
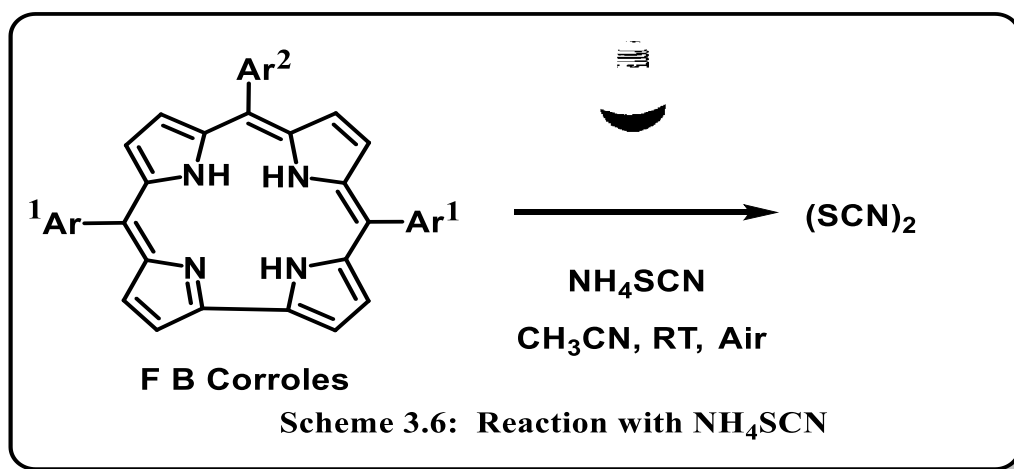
reaction mixture was dissolved in dichloromethane (scheme 3.5). The reaction mixture was monitored by ESI MS spectra. (Figure 3.34)



3.6.2 Characterization of (SCN)₂ by Mass spectra:

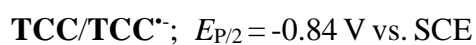
50 mg (0.083 mmol) of 5,10,15-tris(4-cyanophenyl)corrole was dissolved in 15ml of acetonitrile, and then 500mg NH₄SCN (6.6 mmol) was added to it.(Scheme 3.6) The reaction mixture was stirred at room temperature under irradiation with a CFL lamp (20 watt) for 2.5 hours in air. At this point, a second batch of reagents, NH₄SCN (500mg) and acetonitrile (15ml) were added in the reaction mixture. The solution was stirred for another

2.5 hours. The residual solvent was evaporated to dryness and the reaction mixture was analyzed by ESI-MS. (Figure 3.35).



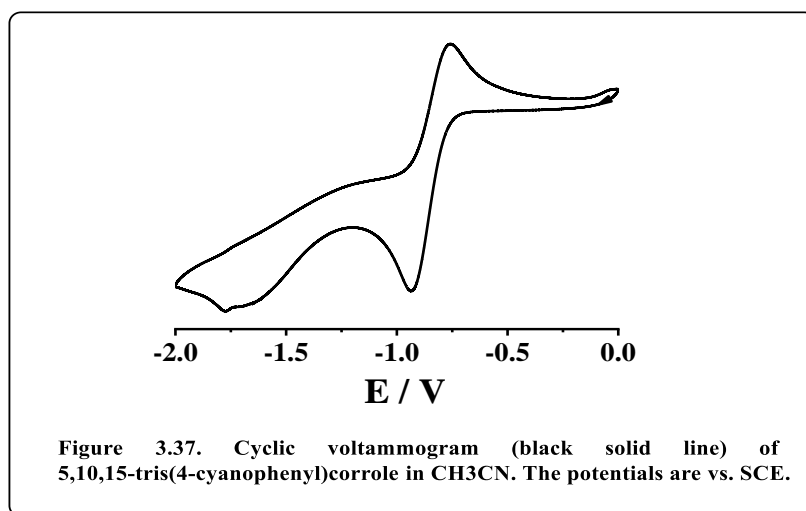
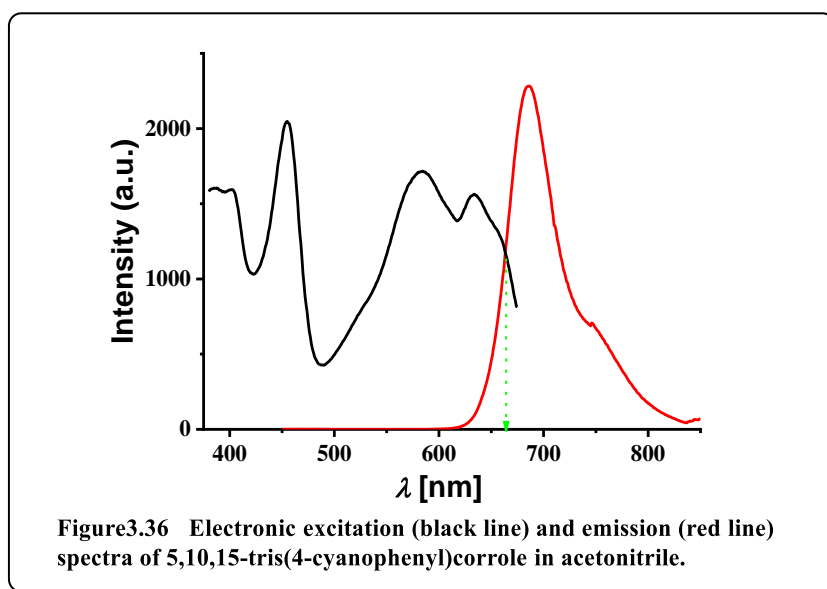
Cyclic voltammogram experiment:

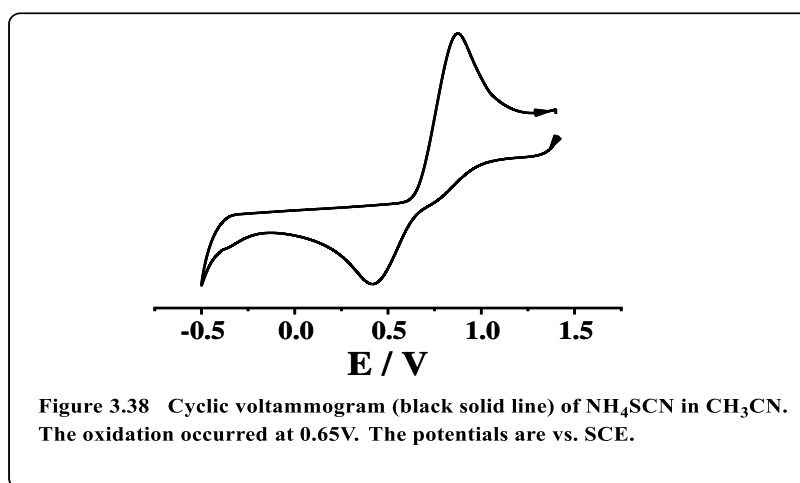
The ground state reduction potential of 5,10,15-tris(4-cyanophenyl)corrole [TCC] was measured by using the cyclic voltammogram experiment (Figure 3.37). The first reduction potential was estimated as -0.84 V vs. SCE.



The reduction potential of excited 5,10,15-tris(4-cyanophenyl)corrole [TCC] is estimated by using the Gibbs energy of photoinduced electron transfer processes.^[47,57] This can be calculated by summing the ground state reduction potential and $E_{0,0}$. $E_{0,0}$ is the energy separation between the zero vibrational levels of the ground state and zero vibrational levels of the excited state. The approximate value can be estimated from the intersection point of excitation wavelength and emission wavelength. (Figure 3.36)

$$\begin{aligned}
 E(\text{TCC}^*/\text{TCC}^{\bullet-}) &= E(\text{TCC}/\text{TCC}^{\bullet-}) + E_{0,0} \\
 &= -0.84 \text{ V} + 1.873 \text{ V} \\
 &= +1.03 \text{ V vs. SCE}
 \end{aligned}$$





3.7 Conclusions

In conclusion, we have developed a new synthetic methodology for the facile synthesis of a new class of corrole ligands bearing four thiocyanate groups at the four neighboring β -positions (2,3,17,18) in the corrole periphery. To date, there is no synthetic protocol available in the literature that describes the synthesis of tetrathiocyanatocorroles in general. A photocatalytic synthetic pathway was developed for the first time to establish the synthesis of these new classes of tetra-substituted corroles (**1-6**). Single-crystal XRD analysis reveals that these tetrathiocyanatocorrole macrocycles (**1-6**) are significantly distorted and exists as $\alpha_2\beta_2$ atropisomers. The mechanism of this reaction has been thoroughly investigated and it indicates that a radical pathway is involved. The absorption and emission spectra of these tetrathiocyanatocorrole macrocycles (**1-6**) vary significantly in comparison to the starting free base corroles (**1A-6A**). In the absorption spectra, the Soret region is split into three bands of equal intensity and the intensity of the Q bands is significantly strengthened. This can be considered as a rare occasion in which the intensity of Soret and Q-bands equalizes. The absorption feature of these modified corrole derivatives (both position and intensity) bears a nice similarity with the naturally-occurring chromophore, chlorophyll-*a*. Thus, these newly synthesized molecules can be considered

as a spectroscopic model for chlorophyll-*a* pigments. The emission region is significantly red-shifted and falls in the NIR region. In a representative corrolato Au(III) complex (**2-Au**), the observed Au...H-C interactions certainly points that these Au(III)-corrole complexes are capable of activating the unfunctionalized C-H groups via weak interactions and thus will have potential implications in C-H activation reactions.^[61] Thus the present synthetic protocol will pave the way for the future development of a new series of FB corroles and their possible metal complexes for a wide range of applications.

3.8 Experimental Section

3.8.1 Materials:

The precursor's pyrrole, *p*-chloranil, and aldehydes were purchased from Aldrich, USA. NH₄SCN (>98.5% purity), acetonitrile (HPLC) was purchased from Merck pvt. ltd chemicals. Other chemicals were of reagent grade. Hexane, CH₂Cl₂, CH₃CN were distilled from KOH and CaH₂ respectively. For spectroscopy studies, HPLC grade solvents were used. For the synthesis of FB corroles, a protocol developed by Gryko et al. was used. The synthetic methodologies and full spectroscopic characterization of free base corroles corrole are provided in the previous literatures.^[27, 32-33]

3.8.2 Physical Measurements:

The elemental analyses were carried out with a Euro EA elemental analyser. UV-Vis spectral studies were performed on a Perkin-Elmer LAMBDA-750 spectrophotometer. Emission spectral studies were performed on a Shimadzu RF-6000 Spectro fluorophotometer using optical cell of 1 cm path length. FT-IR spectra were recorded on a Perkin-Elmer spectrophotometer with samples prepared as KBr pellets. The NMR measurements were carried out using a Bruker 400 MHz NMR spectrometer. Chemical

shifts are expressed in parts per million (ppm) relative to residual acetonitrile ($\delta = 1.93$). Electrospray mass spectra were recorded on a Bruker Micro TOF—QII mass spectrometer. Cyclic voltammetry measurements were carried out using a CS350 electrochemical test system (China). A glassy carbon working electrode, a platinum wire as an auxiliary electrode, and an Ag-AgCl reference electrode were used in a three-electrode configuration. Tetrabutylammonium perchlorate (TBAP) was the supporting electrolyte (0.1 M), and the concentration of the solution was 10^{-3} M with respect to the complex. The half-wave potential E_{298}^0 was set equal to $0.5 (E_{pa} + E_{pc})$, where E_{pa} and E_{pc} are anodic and cathodic cyclic voltammetric peak potentials, respectively. The scan rate used was 100 mV s^{-1} . EPR spectra at X-band frequency (ca. 9.5 GHz) were obtained with a Bruker EMX (ER 073) System. The measurements were carried out in synthetic quartz glass tubes. For light promoted reactions, a Philips energy saver CFL/LED lamp 20W B22 (200 V- 240 V ~50 Hz; Luminous Flux: 2000 Lumens; Photometric Code: 865/15157; crystal white/ 6500k) was placed in front of the borosilicate reaction vessel at a distance of 20 cm without any filter.

3.8.3 Crystal Structure Determination:

Single crystals of **2** were grown from the solution of **2** in dichloromethane layered over methanol, followed by slow evaporation under atmospheric conditions. ORTEP diagram of **2** is shown in Figure S1 (hydrogen atoms are omitted for clarity). Ellipsoids are drawn at 50% probability. The compound **2** crystallizes in triclinic P -1 space group with two **2** in per unit cell. The crystal data of **2** were collected on a Rigaku Oxford diffractometer (MoK α radiation; $\lambda = 0.7107 \text{ \AA}$) at 298 K. Selected data collection parameters and other crystallographic results are summarized in Table 3.4. All data were corrected for Lorentz polarization and absorption effects. The program package SHELXTL was used for

structure solution and full matrix least squares refinement on F^2 .^[62] Hydrogen atoms were included in the refinement using the riding model. Contributions of H atoms for the water molecules were included but were not fixed. Disordered solvent molecules were taken out using SQUEEZE command in PLATON.^[63] CCDC 2043450 contains the supporting crystallographic data for **2**.

Single crystals of **2-Au** were grown from the solution of **2-Au** in dichloromethane layered over hexane, followed by slow evaporation under atmospheric conditions. The compound **2-Au** crystallizes in monoclinic $P2_1/n$ space group with four **2-Au** in per unit cell. The crystal data of **2-Au** were collected on a Rigaku Oxford diffractometer (Cu $K\alpha$ radiation) at 100 K. Selected data collection parameters and other crystallographic results are summarized in Table 3.5. All data were corrected for Lorentz polarization and absorption effects. The program package SHELXTL^[62] was used for structure solution and full matrix least squares refinement on F^2 . Hydrogen atoms were included in the refinement using the riding model. Contributions of H atoms for the water molecules were included but were not fixed. Disordered solvent molecules were taken out using SQUEEZE command in PLATON.^[63] CCDC 2043451 contains the supporting crystallographic data for **2-Au**.

3.8.4 Syntheses:

Synthesis of 2,3,17,18-tetrathiocyanato–5,10,15–triphenylcorrole, **1**:

50 mg (0.095 mmol) of 5,10,15–triphenylcorrole was dissolved in 15ml of acetonitrile, and then 500mg NH_4SCN (6.6 mmol) was added to it. The reaction mixture was stirred at room temperature under irradiation with a CFL/LED lamp (20 watt) for 2.5 hours in air. At this point, a second batch of reagents, NH_4SCN (500mg) and acetonitrile (15ml) were added in the reaction mixture. The solution was stirred for another 2.5 hours. The residual solvent was evaporated to dryness and the crude product was dissolved in dichloromethane. The

crude product was purified by using column chromatography through silica gel (100-200 mesh). The desired product was eluted by using a mixture of 97% DCM and 3% acetonitrile. The final form of the compound was obtained as green crystalline materials.

For 2,3,17,18-tetrathiocyanato-5,10,15-triphenylcorrole, 1:

Yield: 30% (21 mg). Anal. Calcd for $C_{41}H_{22}N_8S_4$ (**1**): C, 65.23; H, 2.94; N, 14.84. Found: C, 65.34; H, 2.99; N, 14.71. λ_{max}/nm ($\epsilon/M^{-1}cm^{-1}$) in CH_2Cl_2 : 408 (32000), 433 (30000), 456 (34000), 539 (7000), 581 (15700), 632 (14000), 686 (34000) (Figure 3.25). 1H NMR (400 MHz, Chloroform-*d*) δ 8.17 (m, 2H), 7.96 (m, 4H), 7.86 (m, 4H), 7.72 (m, 6H), 7.64 (m, 3H). **1** displayed strong fluorescence at 734 nm in CH_2Cl_2 (Figure 3.28). HRMS (ESI) m/z : [**1-H**]⁻ Calcd for $C_{41}H_{21}N_8S_4$ 753.0767; Found 753.1355 (Figure 3.17).

Synthesis of 2,3,17,18-tetrathiocyanato-5,10,15-tris(4-cyanophenyl)corrole, 2:

50 mg (0.083 mmol) of 5,10,15-tris(4-cyanophenyl)corrole was dissolved in 15ml of acetonitrile, and then 500mg NH_4SCN (6.6 mmol) was added to it. The reaction mixture was stirred at room temperature under irradiation with a CFL/LED lamp (20 watt) for 2.5 hours in air. At this point, a second batch of reagents, NH_4SCN (500mg) and acetonitrile (15ml) were added in the reaction mixture. The solution was stirred for another 2.5 hours. The residual solvent was evaporated to dryness and the crude product was dissolved in dichloromethane. The crude product was purified by using column chromatography through silica gel (100-200 mesh). The desired product was eluted by using a mixture of 85% DCM and 15% acetonitrile. The final form of the compound was obtained as green crystalline materials.

For 2,3,17,18-tetrathiocyanato-5,10,15-tris(4-cyanophenyl)corrole, 2:

Yield: 32% (22 mg). Anal. Calcd for $C_{44}H_{19}N_{11}S_4$ (**2**): C, 63.67; H, 2.31; N, 18.56. Found: C, 63.54; H, 2.20; N, 18.43. λ_{max}/nm ($\epsilon/M^{-1}cm^{-1}$) in CH_3CN : 400 (41671), 426 (38104), 451

(37821), 528 (9656), 570 (17030), 619 (20716), 671 (37985) (Figure 3.26). ^1H NMR (400 MHz, Acetonitrile- d_3) δ 8.09 (d, $J = 7.8$ Hz, 4H), 8.03 (d, $J = 7.9$ Hz, 4H), 7.99 (d, $J = 3.5$ Hz, 4H), 7.95 (d, $J = 4.8$ Hz, 2H), 7.74 (d, $J = 5.0$ Hz, 2H). ^{13}C $\{^1\text{H}\}$ NMR (101 MHz, CD_3CN) δ 150.7, 145.7, 143.83, 137.5, 136.1, 133.8, 131.2, 129.8, 128.3, 125.6, 123.5, 122.2, 119.1, 117.3, 113.7, 111.8, 111.3, 110.6. **2** displayed strong fluorescence at 712 nm in CH_3CN (Figure 3.28). HRMS (ESI) m/z : [**2-H**] $^-$ Calcd for $\text{C}_{44}\text{H}_{18}\text{N}_{11}\text{S}_4$ 828.0624; Found 828.1856 (Figure 3.18).

Synthesis of 2,3,17,18-tetrathiocyanato-5,10,15-tris(4-nitrophenyl)corrole, 3:

50 mg (0.076 mmol) of 5,10,15-tris(4-nitrophenyl)corrole was dissolved in 15ml of acetonitrile, and then 500mg NH_4SCN (6.6 mmol) was added to it. The reaction mixture was stirred at room temperature under irradiation with a CFL/LED lamp (20 watt) for 2.5 hours in air. At this point, a second batch of reagents, NH_4SCN (500mg) and acetonitrile (15ml) were added in the reaction mixture. The solution was stirred for another 2.5 hours. The residual solvent was evaporated to dryness and the crude product was dissolved in dichloromethane. The crude product was purified by using column chromatography through silica gel (100-200 mesh). The desired product was eluted by using a mixture of 85% DCM and 15% acetonitrile. The final form of the compound was obtained as green crystalline materials.

For 2,3,17,18-tetrathiocyanato-5,10,15-tris(4-nitrophenyl)corrole, 3:

Yield: 12% (8 mg). Anal. Calcd for $\text{C}_{41}\text{H}_{19}\text{N}_{11}\text{O}_6\text{S}_4$ (**3**): C, 55.34; H, 2.15; N, 17.31. Found: C, 55.45; H, 2.23; N, 17.24. $\lambda_{\text{max}}/\text{nm}$ ($\epsilon/\text{M}^{-1}\text{cm}^{-1}$) in CH_3CN : 403 (35 000), 430 (35200), 457 (38 600), 532 (10400), 573 (13500), 621 (18000), 674 (41,000) (Figure 3.26). ^1H NMR (400 MHz, Acetonitrile- d_3) δ 8.41 – 8.27 (m, 6H), 7.96 (d, $J = 13.0$ Hz, 6H), 7.84 (s, 2H), 7.68 (m, 2H). ^{13}C $\{^1\text{H}\}$ NMR (101 MHz, CD_3CN) δ 151.1, 148.8, 146.4, 143.3, 140.3,

136.9, 135.5, 133.2, 131.9, 129.3, 123.3, 112.8, 112.1, 109.1, 107.1, 105.7. HRMS (ESI) m/z : [**3-H**]⁻ Calcd for C₄₁H₁₈N₁₁O₆S₄ 888.0319; Found 888.2065 (Figure 3.19).

Synthesis of 2,3,17,18-tetrathiocyanato-5,10,15- tris(pentafluorophenyl) corrole, 4:

50 mg (0.063 mmol) of 5,10,15- tris(pentafluorophenyl) corrole was dissolved in 15ml of acetonitrile, and then 500mg NH₄SCN (6.6 mmol) was added to it. The reaction mixture was stirred at room temperature under irradiation with a CFL/LED lamp (20 watt) for 2.5 hours in air. At this point, a second batch of reagents, NH₄SCN (500mg) and acetonitrile (15ml) were added in the reaction mixture. The solution was stirred for another 2.5 hours. The residual solvent was evaporated to dryness and the crude product was dissolved in dichloromethane. The crude product was purified by using column chromatography through silica gel (100-200 mesh). The desired product was eluted by using a mixture of 88% DCM and 12% acetonitrile. The final form of the compound was obtained as sea green crystalline materials.

For 2,3,17,18-tetrathiocyanato-5,10,15- tris(pentafluorophenyl) corrole, 4:

Yield: 35% (22 mg). Anal. Calcd for C₄₁H₇F₁₅N₈S₄(**4**): C, 48.05; H, 0.69; N, 10.93. Found: C, 48.13; H, 0.77; N, 10.86. λ_{\max}/nm ($\epsilon/\text{M}^{-1}\text{cm}^{-1}$) in CH₃CN: 407 (65000), 441 (55000), 528 (10300), 577 (28000), 601(28500), 651 (60 500) (Figure 3.26). ¹H NMR (400 MHz, Chloroform-*d*) δ 7.93 (d, $J=4.9$ Hz, 2H), 7.66 (d, $J=4.8$ Hz, 2H). ¹⁹F {¹H} NMR (377 MHz, Chloroform-*d*) δ -137.3 (m, 6F), -152.8 (m, 3F), -161.9 (m, 6F). **4** displayed strong fluorescence at 677 nm in CH₃CN (Figure 3.29). HRMS (ESI) m/z : [**4-H**]⁻ Calcd for C₄₁H₆F₁₅N₈S₄ 1022.9353; Found 1022.9972 (Figure 3.20).

2,3,17,18tetrathiocyanato-10-(4-bromophenyl)-5,15-bis(4-cyanophenyl)corrole, 5:

50 mg (0.076 mmol) of 10-(4-bromophenyl)-5,15-bis(4-cyanophenyl)corrole was dissolved in 15ml of acetonitrile, and then 500mg NH₄SCN (6.6 mmol) was added to it.

The reaction mixture was stirred at room temperature under irradiation with a CFL/LED lamp (20 watt) for 2.5 hours in air. At this point, a second batch of reagents, NH_4SCN (500mg) and acetonitrile (15ml) were added in the reaction mixture. The solution was stirred for another 2.5 hours. The residual solvent was evaporated to dryness and the crude product was dissolved in dichloromethane. The crude product was purified by using column chromatography through silica gel (100-200 mesh). The desired product was eluted by using a mixture of 90% DCM and 10% acetonitrile. The final form of the compound was obtained as green crystalline materials.

2, 3, 17, 18 tetrathiocyanato – 10 – (4 – bromophenyl) – 5,15 – bis (4 – cyanophenyl) corrole, 5:

Yield: 48% (32 mg). Anal. Calcd for $\text{C}_{43}\text{H}_{19}\text{N}_{10}\text{S}_4\text{Br}$ (**5**): C, 58.43; H, 2.17; N, 15.85. Found: C, 58.57; H, 2.28; N, 15.71. $\lambda_{\text{max}}/\text{nm}$ ($\epsilon/\text{M}^{-1}\text{cm}^{-1}$) in CH_3CN : 399 (38567), 423 (33328), 450 (29059), 530 (11358), 568 (16597), 619 (18791), 673 (28850) (Figure 3.27). ^1H NMR (400 MHz, Acetonitrile- d_3) δ 7.97 (m, 8H), 7.84 (d, $J = 4.7$ Hz, 2H), 7.69 (m, 6H). ^{13}C { ^1H } NMR (101 MHz, CD_3CN) δ 163.4, 152.0, 146.8, 144.9, 141.4, 137.1, 136.3, 134.7, 133.1, 132.1, 131.6, 131.2, 129.6, 122.0, 120.0, 117.2, 112.7, 112.3, 111.1, 109.2, 106.5. **5** displayed strong fluorescence at 722 nm and a shoulder at 775 nm in acetonitrile (Figure 3.29). HRMS (ESI) m/z : [**5+H**] $^+$ Calcd for $\text{C}_{43}\text{H}_{20}\text{N}_{10}\text{S}_4\text{Br}$ 882.9758; Found 883.2458 (Figure 3.21).

Synthesis of 2,3,17,18-tetrathiocyanato-10-(4,7-dimethoxynaphthalen-1-yl)-5,15-bis(4-cyanophenyl)corrole, 6:

50 mg (0.073 mmol) of 10-(4, 7-dimethoxynaphthalen-1-yl)-5, 15-bis(4-cyanophenyl) corrole was dissolved in 15ml of acetonitrile, and then 500mg NH_4SCN (6.6 mmol) was added to it. The reaction mixture was stirred at room temperature under irradiation with a

CFL/LED lamp (20 watt) for 2.5 hours in air. At this point, a second batch of reagents, NH_4SCN (500mg) and acetonitrile (15ml) were added in the reaction mixture. The solution was stirred for another 2.5 hours. The residual solvent was evaporated to dryness and the crude product was dissolved in dichloromethane. The crude product was purified by using column chromatography through silica gel (100-200 mesh). The desired product was eluted by using a mixture of 80% DCM and 20% acetonitrile. The final form of the compound was obtained as green crystalline materials.

For 2, 3, 17, 18 – tetrathiocyanato – 10 – (4, 7 – dimethoxynaphthalen - 1 - yl) - 5, 15-bis(4 - cyanophenyl) corrole, 6:

Yield: 45% (30 mg). Anal. Calcd for $\text{C}_{49}\text{H}_{26}\text{N}_{10}\text{O}_2\text{S}_4$ (**6**): C, 64.32; H, 2.86; N, 15.31. Found: C, 64.23; H, 2.73; N, 15.44. $\lambda_{\text{max}}/\text{nm}$ ($\epsilon/\text{M}^{-1}\text{cm}^{-1}$) in CH_3CN : 399 (38537), 422 (33403), 449 (28940), 529 (11477), 569 (16716), 621(18764), 673 (28806) (Figure 3.27). ^1H NMR (400 MHz, Acetonitrile- d_3) δ 8.27 (d, $J = 9.4$ Hz, 1H), 8.04 – 7.84 (m, 8H), 7.68 (m, 3H), 7.41 (s, 2H), 7.06 (d, $J = 9.7$ Hz, 1H), 6.89 (d, $J = 7.9$ Hz, 1H), 6.52 (s, 1H), 4.05 (s, 3H), 3.09 (s, 3H). ^{13}C { ^1H } NMR (101 MHz, CD_3CN) δ 159.1, 156.5, 134.8, 134.6, 133.5, 132.1, 131.5, 130.7, 129.9, 129.9, 129.7, 129.6, 124.6, 121.1, 120.0, 117.6, 112.8, 112.3, 112.1, 107.4, 106.5, 105.2, 102.3, 56.3, 55.3. **6** displayed strong fluorescence at 733 nm and a shoulder at 780 nm in acetonitrile (Figure 3.29). HRMS (ESI) m/z : [**6-H**] $^-$ Calcd for $\text{C}_{49}\text{H}_{25}\text{N}_{10}\text{O}_2\text{S}_4$ 913.1039; Found 913.4438 (Figure 3.22).

Synthesis of {2,3,17,18-tetrathiocyanato–5,10,15–tris(4-cyanophenyl) corrolato-Au(III)}, 2-Au

For the insertion of Au(III) in corrole cavity, a previously reported protocol was followed.^[50] 32 mg (0.04 mmol) of 2,3,17,18-tetrathiocyanato–5,10,15–tris(4-cyanophenyl)corrole was dissolved in 10 ml of acetonitrile, and then excess of gold acetate

(112 mg; 0.30 mmol) was added to it followed by pyridine (10 ml). The reaction mixture was stirred for 45 mins under room temperature. After that, the solvent was evaporated and the brown color crude product was subjected to column chromatography using a silica gel (100–200 mesh) column. The desired product (reddish blue) was eluted by using a mixture of 96% DCM and 4% acetonitrile. The final form of the compound was obtained as reddish pink crystalline materials.

For {2,3,17,18-tetrathiocyanato-5,10,15-tris(4-cyanophenyl) corrolato-Au(III)}, 2-Au

Yield: 46% (18 mg). Anal. Calcd for $C_{44}H_{16}AuN_{11}S_4$ (**2-Au**): C, 51.61; H, 1.58; N, 15.05. Found: C, 51.74; H, 1.69; N, 14.97. λ_{\max}/nm ($\epsilon/M^{-1}cm^{-1}$) in CH_2Cl_2 : 404 (62628), 422 (60304), 536 (16883), 551 (21900), 577 (54309), 593 (64535) (Figure 3.27). 1H NMR (400 MHz, $CDCl_3$) δ 8.50–8.42 (m, 4H), 8.23–8.06 (m, 12H) (Figure 3.12). ^{13}C { 1H } NMR (101 MHz, $CDCl_3$) δ 171.9, 153.2, 150.3, 147.3, 144.4, 142.8, 140.9, 133.6, 131.8, 128.2, 120.5, 118.0, 115.5, 114.3, 113.2, 109.6. HRMS (ESI) m/z : [**2-Au+Na**] $^+$ Calcd for $C_{44}H_{16}AuN_{11}S_4Na$ 1046.0036; Found 1046.0104 (Figure 3.23).

References

- [1] R. Bonnett, M. Berenbaum, *Photosensit. Compd. their Chem. Biol. Clin. use* **1989**, *146*, 40–53.
- [2] R. K. Pandey, T. J. Dougherty, D. Kessel, *Handbook of Photodynamic Therapy: Updates on Recent Applications of Porphyrin-Based Compounds*, World Scientific, **2016**.
- [3] R. Pereira, P.M., Tomé, J.P. and Fernandes, *Molecular Targeted Photodynamic Therapy for Cancer*, Handbook Of Porphyrin Science, **2016**.
- [4] K. Rybicka-Jasińska, W. Shan, K. Zawada, K. M. Kadish, D. Gryko, *J. Am. Chem. Soc.* **2016**, *138*, 15451–15458.
- [5] K. Rybicka-Jasińska, B. Koenig, D. Gryko, *European J. Org. Chem.* **2017**, *2017*, 2104–2107.
- [6] R. C. e Silva, L. O. da Silva, A. de Andrade Bartolomeu, T. J. Brocksom, K. T. de Oliveira, *Beilstein J. Org. Chem.* **2020**, *16*, 917–955.
- [7] C. K. Prier, D. A. Rankic, D. W. C. MacMillan, *Chem. Rev.* **2013**, *113*, 5322–5363.
- [8] K. Zeitler, *Visible Light Photocatal. Org. Chem.* **2018**, 159–232.
- [9] R. Guilard, K. M. Kadish, K. M. Smith, R. Guilard, *The Porphyrin Handbook*, Academic Press New York, **2003**.
- [10] T. Patra, B.; Mondal, S.; Kar, S. Corroles, in: Scott, R. A.; Storr, *Encycl. Inorg. Bioinorg. Chem.* **2020**, DOI <https://doi.org/10.1002/9781119951438.eibc2729>.
- [11] R. Paolesse, S. Nardis, M. Stefanelli, F. R. Fronczek, M. G. H. Vicente, *Angew. Chemie Int. Ed.* **2005**, *44*, 3047–3050.

-
- [12] I. Aviv-Harel, Z. Gross, *Chem. Eur. J.* **2009**, *15*, 8382–8394.
- [13] A. Ghosh, *Chem. Rev.* **2017**, *117*, 3798–3881.
- [14] R. Orłowski, D. Gryko, D. T. Gryko, *Chem. Rev.* **2017**, *117*, 3102–3137.
- [15] Y. Fang, Z. Ou, K. M. Kadish, *Chem. Rev.* **2017**, *117*, 3377–3419.
- [16] K. Fujino, Y. Hirata, Y. Kawabe, T. Morimoto, A. Srinivasan, M. Toganoh, Y. Miseki, A. Kudo, H. Furuta, *Angew. Chemie* **2011**, *123*, 6987–6991.
- [17] S. Hiroto, K. Furukawa, H. Shinokubo, A. Osuka, *J. Am. Chem. Soc.* **2006**, *128*, 12380–12381.
- [18] W. Sinha, M. G. Sommer, N. Deibel, F. Ehret, M. Bauer, B. Sarkar, S. Kar, *Angew. Chemie Int. Ed.* **2015**, *54*, 13769–13774.
- [19] W. Sinha, M. G. Sommer, N. Deibel, F. Ehret, B. Sarkar, S. Kar, *Chem. Eur. J.* **2014**, *20*, 15920–15932.
- [20] W. Sinha, M. G. Sommer, M. van der Meer, S. Plebst, B. Sarkar, S. Kar, *Dalt. Trans.* **2016**, *45*, 2914–2923.
- [21] B. Patra, S. Sobottka, W. Sinha, B. Sarkar, S. Kar, *Chem. Eur. J.* **2017**, *23*, 13858–13863.
- [22] D. K. Dogutan, R. McGuire Jr, D. G. Nocera, *J. Am. Chem. Soc.* **2011**, *133*, 9178–9180.
- [23] W. Sinha, M. G. Sommer, L. Hettmanczyk, B. Patra, V. Filippou, B. Sarkar, S. Kar, *Chem. Eur. J.* **2017**, *23*, 2396–2404.
- [24] B. Patra, S. Sobottka, S. Mondal, B. Sarkar, S. Kar, *Chem. Commun.* **2018**, *54*, 9945–9948.

-
- [25] B. Koszarna, D. T. Gryko, *J. Org. Chem.* **2006**, *71*, 3707–3717.
- [26] Z. Gross, N. Galili, L. Simkhovich, I. Saltsman, M. Botoshansky, D. Bläser, R. Boese, I. Goldberg, *Org. Lett.* **1999**, *1*, 599–602.
- [27] M. Autret, S. Will, E. Van Caemelbecke, J. Lex, J.-P. Gisselbrecht, M. Gross, E. Vogel, K. M. Kadish, *J. Am. Chem. Soc.* **1994**, *116*, 9141–9149.
- [28] H.-Y. Liu, F. Yam, Y.-T. Xie, X.-Y. Li, C. K. Chang, *J. Am. Chem. Soc.* **2009**, *131*, 12890–12891.
- [29] B. Brizet, N. Desbois, A. Bonnot, A. Langlois, A. Dubois, J.-M. Barbe, C. P. Gros, C. Goze, F. Denat, P. D. Harvey, *Inorg. Chem.* **2014**, *53*, 3392–3403.
- [30] I. Aviv, Z. Gross, *Chem. Commun.* **2007**, 1987–1999.
- [31] K. E. Thomas, H. Vazquez-Lima, Y. Fang, Y. Song, K. J. Gagnon, C. M. Beavers, K. M. Kadish, A. Ghosh, *Chem. Eur. J.* **2015**, *21*, 16839–16847.
- [32] S. Mondal, P. K. Naik, J. K. Adha, S. Kar, *Coord. Chem. Rev.* **2019**, *400*, 213043.
- [33] S. Nardis, F. Mandoj, M. Stefanelli, R. Paolesse, *Coord. Chem. Rev.* **2019**, *388*, 360–405.
- [34] A. Mahammed, Z. Gross, *Coord. Chem. Rev.* **2019**, *379*, 121–132.
- [35] C. M. Lemon, *Pure Appl. Chem.* **2020**, *92*, 1901–1919.
- [36] S. Patai, *Chemistry of Cyanates and Their Thio Derivatives*, J. Wiley, **1977**.
- [37] A. A. Newman, *Chemistry and Biochemistry of Thiocyanic Acid and Its Derivatives*, Academic Press, **1975**.
- [38] W. Fan, Q. Yang, F. Xu, P. Li, *J. Org. Chem.* **2014**, *79*, 10588–10592.
- [39] S. Mitra, M. Ghosh, S. Mishra, A. Hajra, *J. Org. Chem.* **2015**, *80*, 8275–8281.

-
- [40] K. Nikoofar, *Chem. Sci. Trans.* **2013**, 691–700.
- [41] J. F. B. Barata, M. G. P. M. S. Neves, M. A. F. Faustino, A. C. Tomé, J. A. S. Cavaleiro, *Chem. Rev.* **2017**, *117*, 3192–3253.
- [42] J. A. S. Barata, J. F. B.; Santos, C. I. M.; Neves, M. G. P. M. S.; Faustino, M. A. F.; Cavaleiro, *Springer-Verlag: Berlin* **2014**, *10*, 79–141.
- [43] C. M. Lemon, P. J. Brothers, *J. Porphyr. Phthalocyanines* **2011**, *15*, 809–834.
- [44] S. Nardis, G. Pomarico, M. Stefanelli, S. Lentini, D. O. Cicero, F. R. Fronczek, K. M. Smith, R. Paolesse, *J. Porphyr. Phthalocyanines* **2016**, *20*, 465–474.
- [45] C. M. Lemon, R. L. Halbach, M. Huynh, D. G. Nocera, *Inorg. Chem.* **2015**, *54*, 2713–2725.
- [46] K. Sahu, S. Mondal, B. Patra, T. Pain, S. K. Patra, C. Dosche, S. Kar, *Nanoscale Adv.* **2020**, *2*, 166–170.
- [47] Y.-L. Ban, J.-L. Dai, X.-L. Jin, Q.-B. Zhang, Q. Liu, *Chem. Commun.* **2019**, *55*, 9701–9704.
- [48] T. Hashimoto, Y.-K. Choe, H. Nakano, K. Hirao, *J. Phys. Chem. A* **1999**, *103*, 1894–1904.
- [49] L. L. Shipman, T. M. Cotton, J. R. Norris, J. J. Katz, *J. Am. Chem. Soc.* **1976**, *98*, 8222–8230.
- [50] D. C. Barber, R. A. Freitag-Beeston, D. G. Whitten, *J. Phys. Chem.* **1991**, *95*, 4074–4086.
- [51] C. F. Zipp, J. P. Michael, M. A. Fernandes, H. M. Marques, *South African J. Chem.* **2013**, *66*, 158–166.
- [52] K. E. Thomas, A. B. Alemayehu, J. Conradie, C. Beavers, A. Ghosh, *Inorg. Chem.* **2011**, *50*, 12844–12851.
-

-
- [53] H. Schmidbaur, H. G. Raubenheimer, L. Dobrzańska, *Chem. Soc. Rev.* **2014**, *43*, 345–380.
- [54] M. Rigoulet, S. Massou, E. D. S. Carrizo, S. Mallet-Ladeira, A. Amgoune, K. Miqueu, D. Bourissou, *Proc. Natl. Acad. Sci.* **2019**, *116*, 46–51.
- [55] M. Kumar, J. S. Francisco, *J. Am. Chem. Soc.* **2020**, *142*, 6001–6006.
- [56] H. Schmidbaur, *Angew. Chemie Int. Ed.* **2019**, *58*, 5806–5809.
- [57] N. A. Romero, D. A. Nicewicz, *Chem. Rev.* **2016**, *116*, 10075–10166.
- [58] M. Schweyen, P.; Brandhorst, K.; Wicht, R.; Wolfram, B.; Bröring, *Angew. Chem.* **2015**, *127*, 8331–8334.
- [59] K. Tong, X. Liu, Y. Zhang, S. Yu, *Chem. Eur. J.* **2016**, *22*, 15669–15673.
- [60] H. Egami, T. Ide, Y. Kawato, Y. Hamashima, *Chem. Commun.* **2015**, *51*, 16675–16678.
- [61] M. Bakar, M. Sugiuchi, M. Iwasaki, Y. Shichibu, K. Konishi, *Nat. Commun.* **2017**, *8*, 1–7.
- [62] G. M. Sheldrick, *Acta Crystallogr. Sect. A Found. Crystallogr.* **2008**, *64*, 112–122.
- [63] P. V Van der Sluis, A. L. Spek, *Acta Crystallogr. Sect. A Found. Crystallogr.* **1990**, *46*, 194

Investigation of the Nature of Intermolecular Interactions in Tetra (thiocyanato)corrolato-Ag(III) Complexes: Agostic or Hydrogen bonded?

4.1 Introduction

4.2 Result and Discussion

2.3.1 Generalization of Synthetic Procedure

4.3 Spectral Characterisation

4.3.1 NMR Spectroscopy

4.3.2 Mass Spectrometry

4.3.3 IR spectroscopy

4.3.4 Photophysical properties

4.3.5 Single crystal XRD Analysis

4.4 Theoretical Investigation

4.4.1 Computational Methodologies

4.4.2 Details of Topology Analysis

4.5 Conclusion

4.6 Experimental Section

4.6.1 Materials

4.6.2 Physical measurements

4.6.3 Crystal Structure Determination

4.6.4 Synthesis

4.1 Introduction

The different noncovalent interactions are often being the driving force for the designing principle of various supramolecular architectures having pre-defined functionalities.^[1-4] These noncovalent interactions dictate the intermolecular separation between the molecules and also their arrangements in the three-dimension crystal lattice.^[5,6] Thus the supramolecular interactions (the collection of several intermolecular interactions including the hydrogen bonding interactions) in the coordination compounds resulted in a diverse range of solid-state structures. It has to be kept in mind that the nature of hydrogen bonding interactions is not alike in the traditional organic compounds and also in the typical coordination/organometallic compounds.^[7-10] Earlier reports have demonstrated that metal-hydrogen interactions are extremely soft in nature and also are polarizable.^[11] The nature of metal-hydrogen interactions is also depending on the electronic nature of the metal ion and also on the electronic and steric nature of the coordinated ligands. Herein, we have investigated the intermolecular interactions between an Ag(III) ion stabilized in a corrole coordination core and a C-H group appended to the peripheral phenyl ring of the corrole based ligand. Corrole, a trianionic ligand, is analogous to the well-known porphyrin macrocycle in many aspects. Both the macrocycle is an 18π electron aromatic system. However, corrole is a contracted version of porphyrin in the sense that it contains one *meso* carbon less than that of porphyrin. Owing to its electronic richness and also due to the contracted inner core, it often stabilizes metals in higher oxidation states.^[12-21] The stabilization of Ag in the +III oxidation state in corrole, as opposed to the +II oxidation state in porphyrin, has been well documented in the literature.^[22] In the present case, we have used a β -substituted corrole system which is modified at the four consecutive β -positions. The 2,3,17,18-tetra (thiocyanato) corrole based system is thus used as a ligand scaffold here.^[23,24] silver

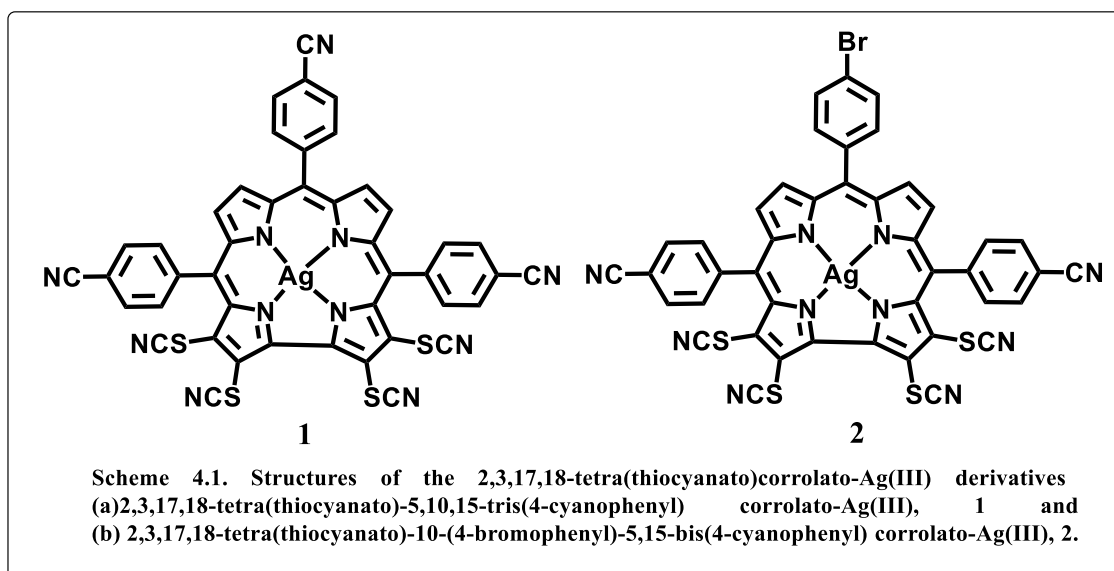
complexes of this class of chelating ligand were never described earlier in the literature. The said modification in the corrole periphery thus generated a newer variety of corrole based systems.

4.2 Results and Discussion

4.2.1 Generalization of synthetic protocol

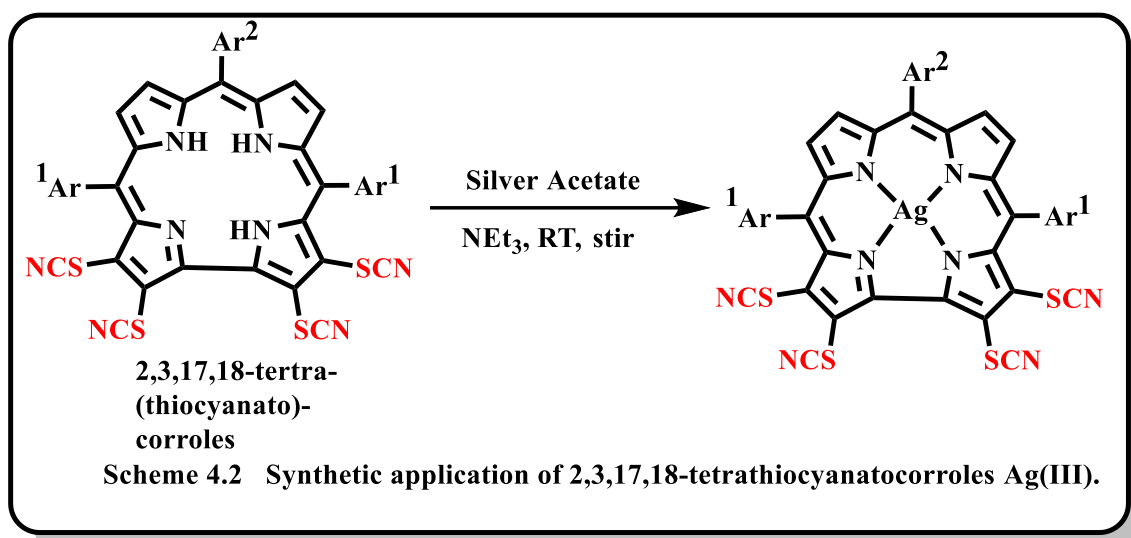
The present work describes the synthesis and spectroscopic characterization of two new silver corrole complexes, namely, 2, 3, 17, 18 – tetra (thiocyanato) – 5, 10, 15 – tris (4-cyanophenyl) corrolato – Ag (III), **1**, and 2, 3, 17, 18- tetra (thiocyanato) – 10 – (4 – bromophenyl) – 5, 15 – bis (4 – cyanophenyl) corrolato - Ag(III), **2** (Scheme 4.1). The corrolato - Ag(III) complexes were thoroughly characterized by several spectroscopic techniques, including single - crystal XRD analysis of a representative derivative. A combined structural and theoretical study will decipher here a rare example of intermolecular hydrogen bond formation between an electron-deficient metal center [Ag(III)] and a C-H covalent bond. The electron donation from this C-H covalent bond will eventually satisfy the electronic requirement of the electron-deficient Ag(III) center. Among the coinage group metals, silver is an ordinary transition metal compared to the other members like copper and gold. Gold has significant relativistic effects and thus is significantly different from silver. The routineness of the silver in the triad is obvious due to its relatively less relativistic effects than gold.^[25-35] Although the conventional hydrogen bonding interactions in transition metal complexes are well explored in general, however, the C-H \cdots M interactions are much less explored in the coinage metal group in particulars. Although there are few examples of C-H \cdots Au and C-H \cdots Cu interactions in the literature^[36-51] but the examples related to C-H \cdots Ag are almost nonexistent.^[36,46,47,50] The present study offers a rare example of intermolecular C-H \cdots Ag interactions between neighboring tetra (thiocyanato) corrolato-Ag(III)

molecules in the crystal lattice. We have performed detailed theoretical investigations to support the experimentally obtained X-ray diffraction analysis. Theoretical investigations like electron density topology based on atoms in molecules (AIM) theory and Natural Bond Orbital (NBO) analysis provide greater insight into the nature of weak C–H⋯Ag interactions. This work is thus destined as a directive for future research also provides information about the orbital interactions ($\sigma_{\text{C-H}}/\sigma^*_{\text{C-H}}$ with vacant/filled silver d-orbitals) and their interaction energies. This understanding will pave the way for the construction of newer classes of supramolecular architectures incorporating C–H⋯Ag interactions.



Synthesis and characterization

Silver was inserted into the corrole cavity by using silver acetate as a metal precursor in an acetonitrile and triethylamine mixture at RT {RT= room temperature) in the air (Scheme 4.2).^[52] Air is responsible for the generation of Ag(III) oxidation state and which is consequently stabilized in the corrole cavity. Purity and composition of the 2,3,17,18-tetra(thiocyanato)corrolato-Ag(III) derivatives (**1–2**) were established by their satisfactory elemental analyses, ESI-MS data, UV-Vis, FT-IR, NMR, and single-crystal XRD data (Figures 4.1-4.8 and Tables 4.1-4.2).



4.3 Spectral Characterisation:

4.3.1 NMR Spectroscopy

The ^1H NMR spectrum of **1** exhibits intense peaks in the region, $\sim 8.35\text{--}8.07$ ppm. The ^1H NMR spectrum of **2** exhibits sharp peaks in the region, $\sim 8.39\text{--}7.92$ ppm. The aromatic protons are deshielded by $0.25\text{--}0.35$ ppm in the corrolato-Ag(III) complexes corresponding to their starting FB corrole analogs (Figures 4.1 and 4.2). The corrolato-Ag(III) complexes are diamagnetic, evident from their sharp peaks and chemical shifts in the expected regions.

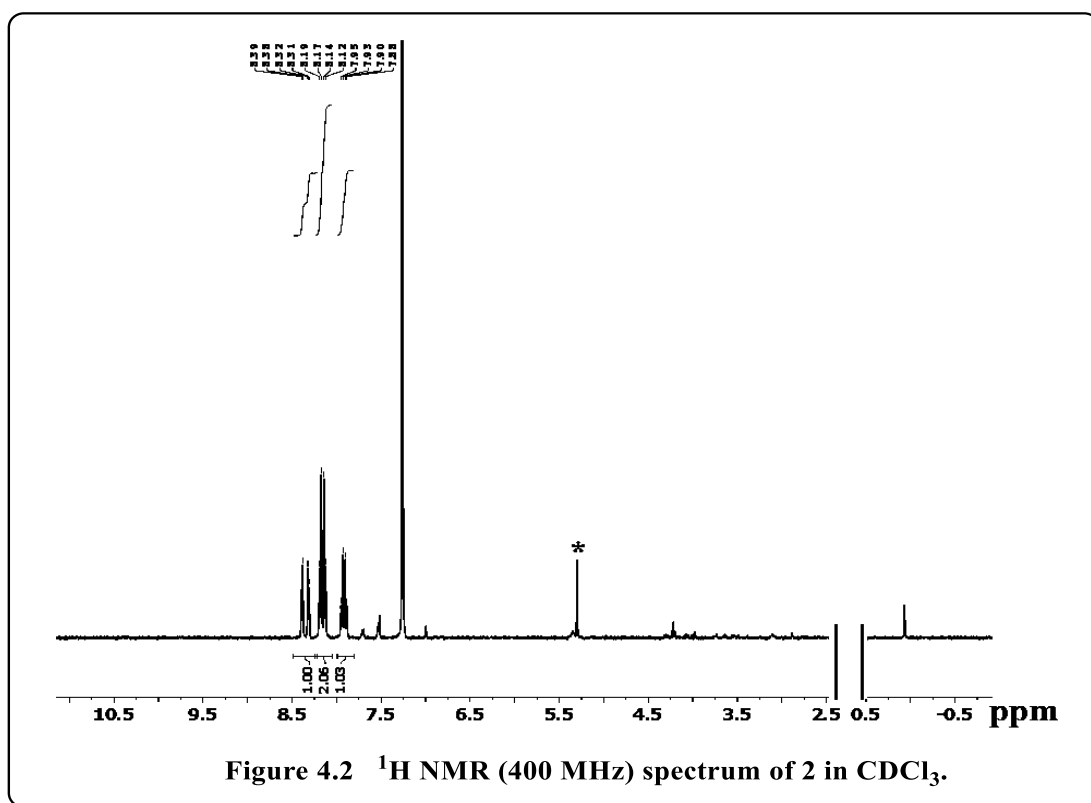
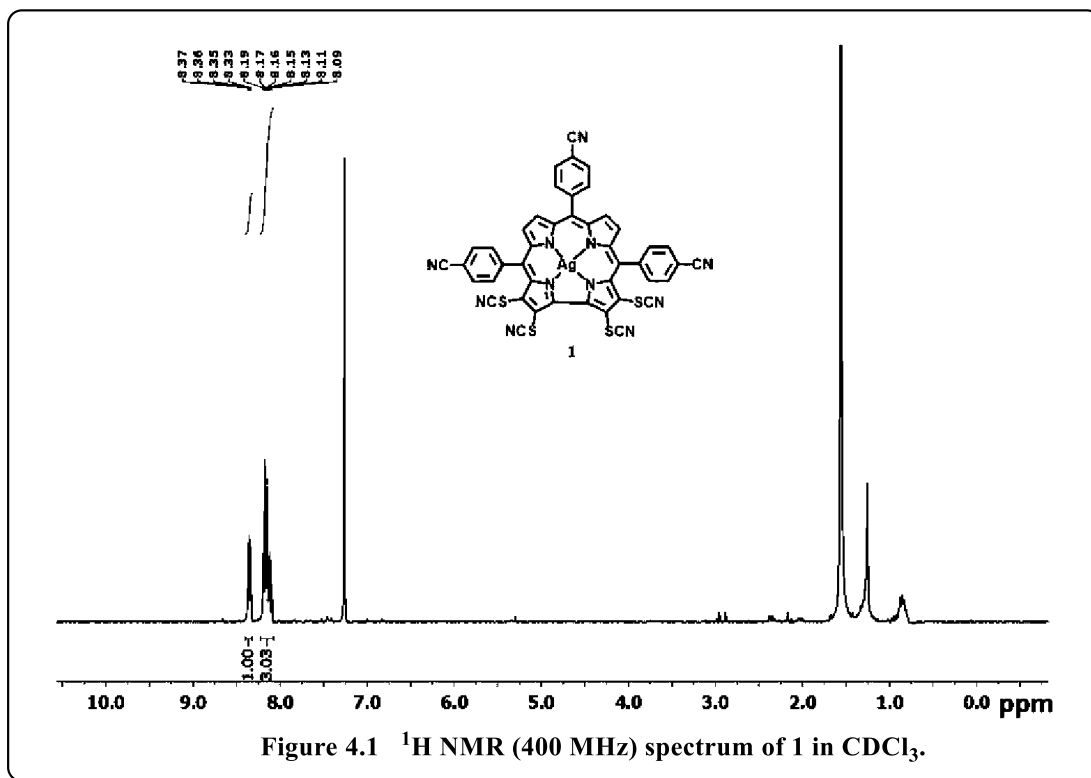
4.3.2 Mass Spectrometry:

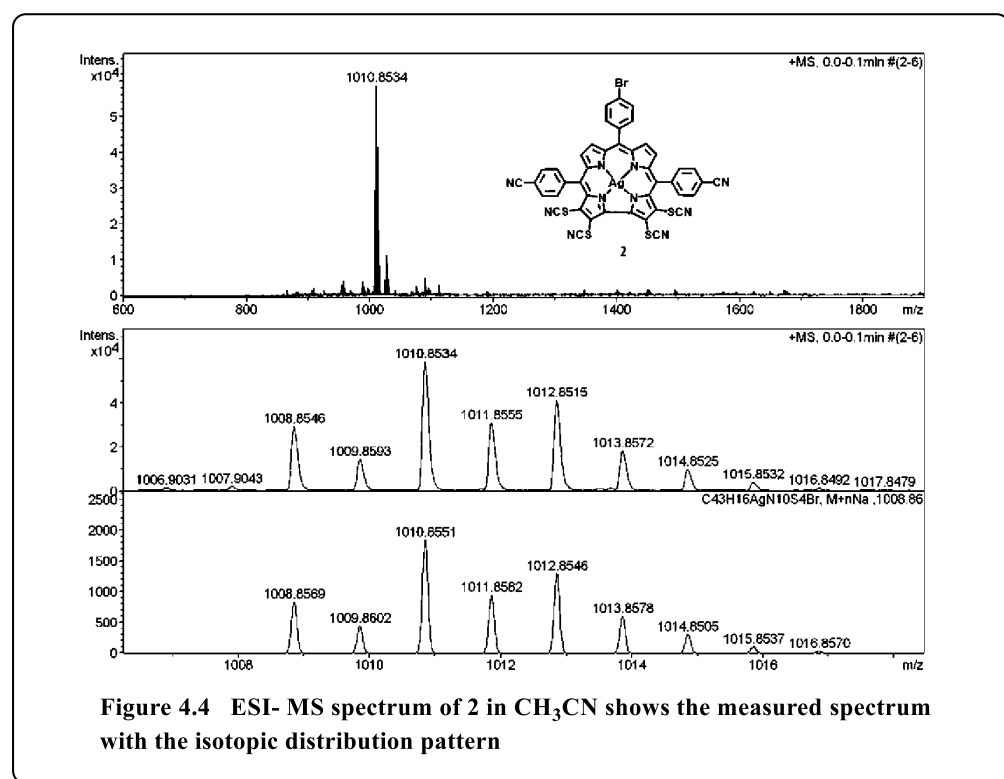
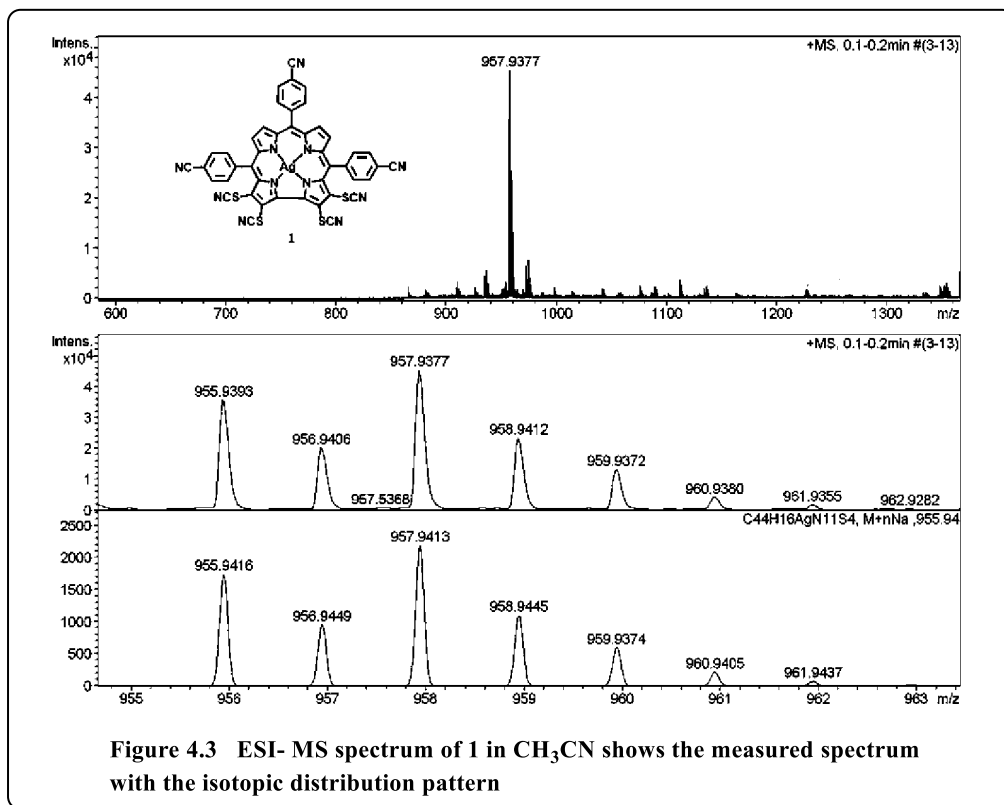
The electrospray mass spectrum showed the peaks centered HRMS (ESI) m/z : $[\mathbf{2}+\text{Na}]^+$
 Calcd for $\text{C}_{43}\text{H}_{16}\text{AuBrN}_{10}\text{S}_4\text{Na}$ 1098.9183; Found 1098.7538 (Figure 4.3).

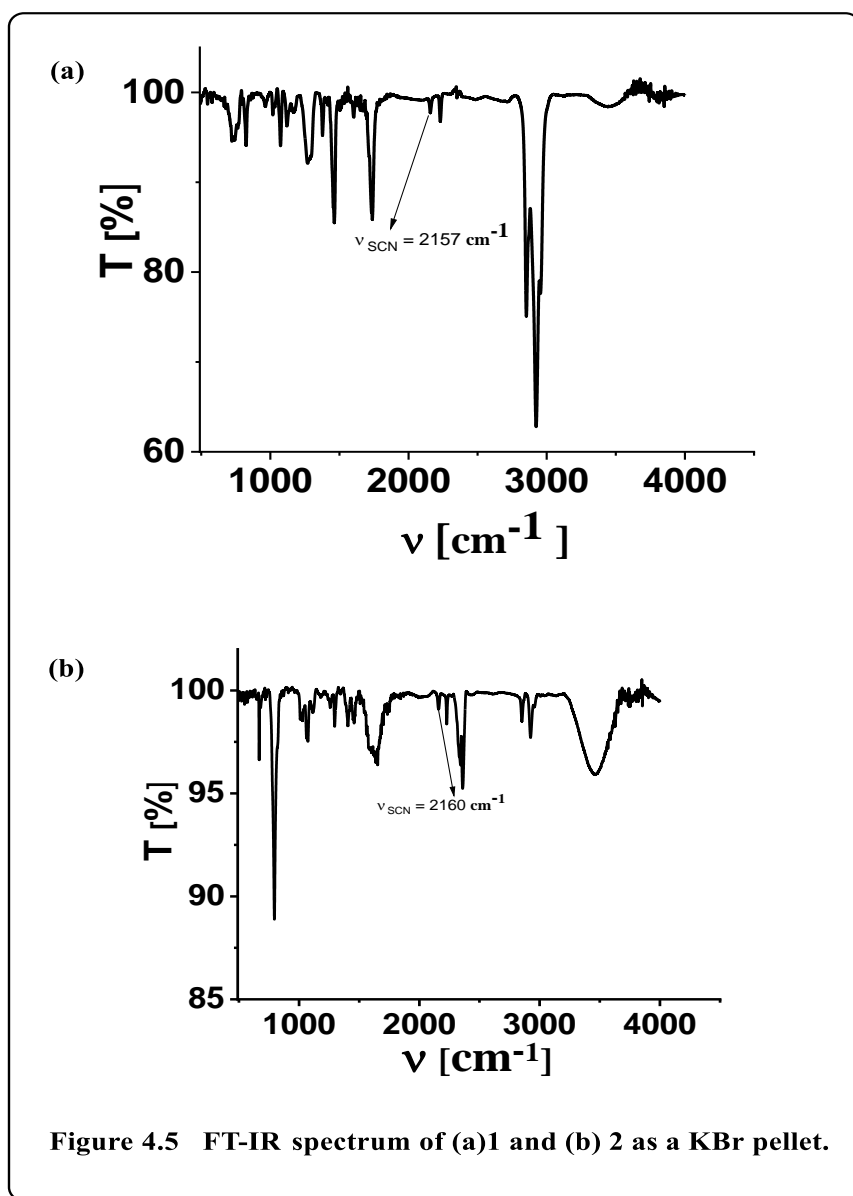
The electrospray mass spectrum showed the peaks centered HRMS (ESI) m/z : $[\mathbf{1}+\text{Na}]^+$
 Calcd for $\text{C}_{49}\text{H}_{23}\text{AuN}_{10}\text{O}_2\text{S}_4\text{Na}$ 1131.0446; Found 1131.0570 (Figure 4.4).

4.3.3 IR Spectroscopy:

The FT-IR spectra (as KBr pellets) of **1** and **2** exhibited strong S-CN stretching vibration at 2164 , and 2157 cm^{-1} , respectively (Figures 4.5)







4.3.4 Photophysical properties:

The electronic absorption spectra of tetra(thiocyanato)corrolato-Ag(III) derivatives, **1-2**, are shown in figures 4.6-4.7. It is interesting to note that the absorption spectra of tetra(thiocyanato)corrolato-Ag(III) derivatives are drastically different than the β -unsubstituted corrolato-Ag(III) derivatives.^[52] In comparison to the related β -unsubstituted corrolato-Ag(III) derivatives, in tetra(thiocyanato)corrolato-Ag(III) derivatives, the Soret band is splitted and thus it indicates lower symmetry in the case of tetra(thiocyanato)corrolato-Ag(III) derivatives, **1** and **2**. In addition to that, the Q bands

are also split into at least two distinct bands. It was also observed that the intensity of the Soret and Q bands are almost equalized. These phenomena are quite unique in nature in the tetra(thiocyanato)corrolato-Ag(III) derivatives. Thus, the four thiocyanate groups at the β positions in tetra(thiocyanato)corrolato derivative are responsible for breaking the pairing property and increasing the intensity Q bands.^[23]

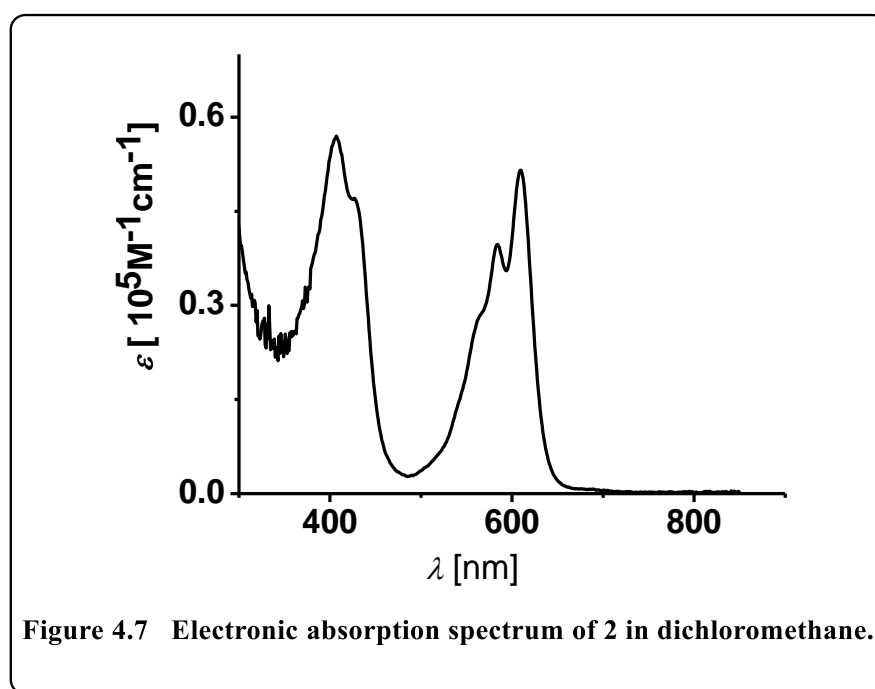
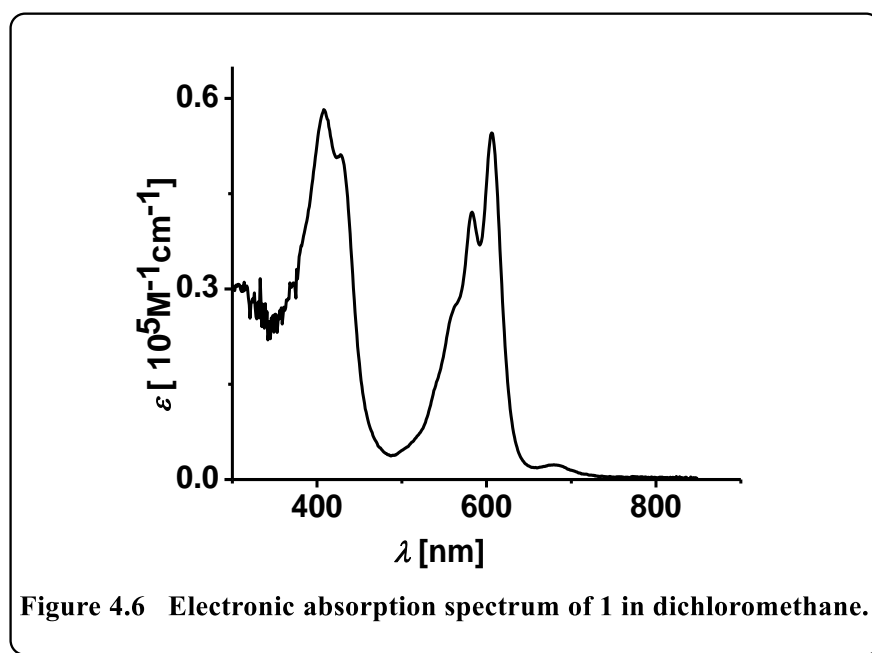


Table 4.1 UV–Vis data in dichloromethane^a

Compound	UV–vis. Data λ_{\max} / nm (ϵ / M ⁻¹ cm ⁻¹)
1	408 (57992), 428 (51003), 562 (27423), 582 (41990), 606 (54368)
2	407 (56788), 427 (47062), 564 (28225), 583 (39555), 609 (51301)

^a Error limits : λ_{\max} , ± 1 nm and ϵ , $\pm 10\%$.

4.3.5 Crystal Structure:

The compound {2,3,17,18-tetra(thiocyanato)–5,10,15–tris(4-cyanophenyl)corrolato-Ag(III)}, **1** crystallizes in the monoclinic space group $P2_1/n$. Important crystallographic parameters for **1** are summarized in Table 4.2.

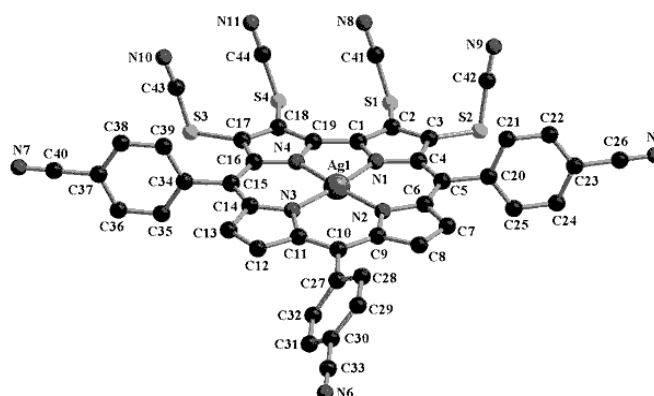


Figure 4.8. Single-crystal X-ray structure of **1**. Hydrogen atoms are omitted for clarity.

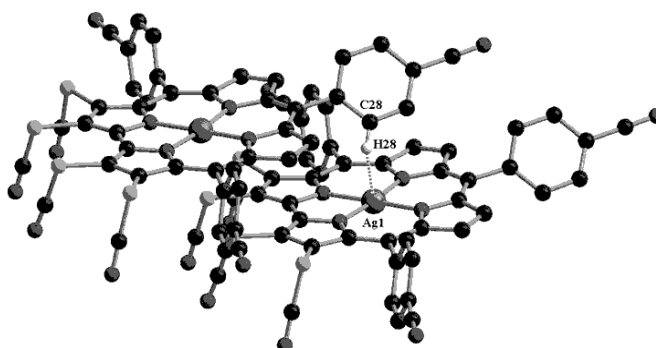


Figure 4.9 Two adjacent molecules in the molecular stack of complex **1** (highlighting the C-H \cdots Ag interactions). Selected bond distance (Å) and angle ($^\circ$): C28-H28 \cdots Ag1 = 2.608 Å and \angle C28-H28 \cdots Ag1 = 108.1 $^\circ$. All hydrogen atoms, except the one in close contact with the Ag(III), have been omitted for clarity.

Bond distances and angles of **1** agree with those of the previously reported Ag(III)-corroles.^[52] Silver atom deviates from the mean N4-corrolato plane by 0.030 Å (Figure 4.8). Four pyrrolic nitrogen atoms of the corrole ring form the N4-corrolato plane. A close comparison of the values related to the deviation of the silver ion from the mean N4-corrolato plane in the β -unsubstituted corrolato-Ag(III) derivatives (~ 0.003 Å)^[52] and the tetra(thiocyanato)corrolato-Ag(III) derivatives (0.030 Å), it is clearly evident that the deviation is significantly larger in the latter case. The geometry around the silver center is slightly distorted from the perfect square planar. The bite angles of N1-Ag-N2, N2-Ag-N3, N3-Ag-N4, and N4-Ag-N1 are 92.7(2)°, 94.2(2)°, 92.4(2)°, and 80.7(2)° respectively. The Ag-N bond distances are in the range from 1.948(5) Å to 1.966(5) Å are close comparable within their e.s.d.'s with those previously reported for a β -unsubstituted Ag(III) corrole.^[52] The dihedral angle formed between the 23-atom mean corrolato plane and the mean plane of an individual pyrrole ring ranges from the highest 4.88° (for pyrrole ring containing N3 atom) to the lowest 2.19° (for pyrrole ring containing N2 atom). The dihedral angle formed between the 23-atom mean corrolato plane and the mean plane of an individual *meso*-phenyl ring at 5-, 10- and 15- positions are 74.76(4)°, 49.56(4)°, and 81.44(4)° respectively. X-ray single-crystal structure analysis of **1** reveals C-H...Ag interactions, the length of the C28-H28 bond of 1.1 Å implies the Ag1-H28 distance of 2.608 Å and the C28-H28-Ag1 angle of 108.1° (Figure 4.9). The difference Fourier map clearly shows a disorder over two positions of the phenyl ring [C27-C32]. It appears that intermolecular C-H...Ag interaction is responsible for the crystal disorder (Figure 4.10) and is manifested by the rotation of the 4-cyanophenyl ring at the corrole periphery. Thus the interaction at the atomic level i.e., C-H groups and Ag(III) sites creates both attractive and repulsive forces and in order to balance these two opposite forces, these disorders are observed at the crystal lattice. Geometry optimization of the conformer (both monomer and dimer) shown in figure 4.11 has been carried out.

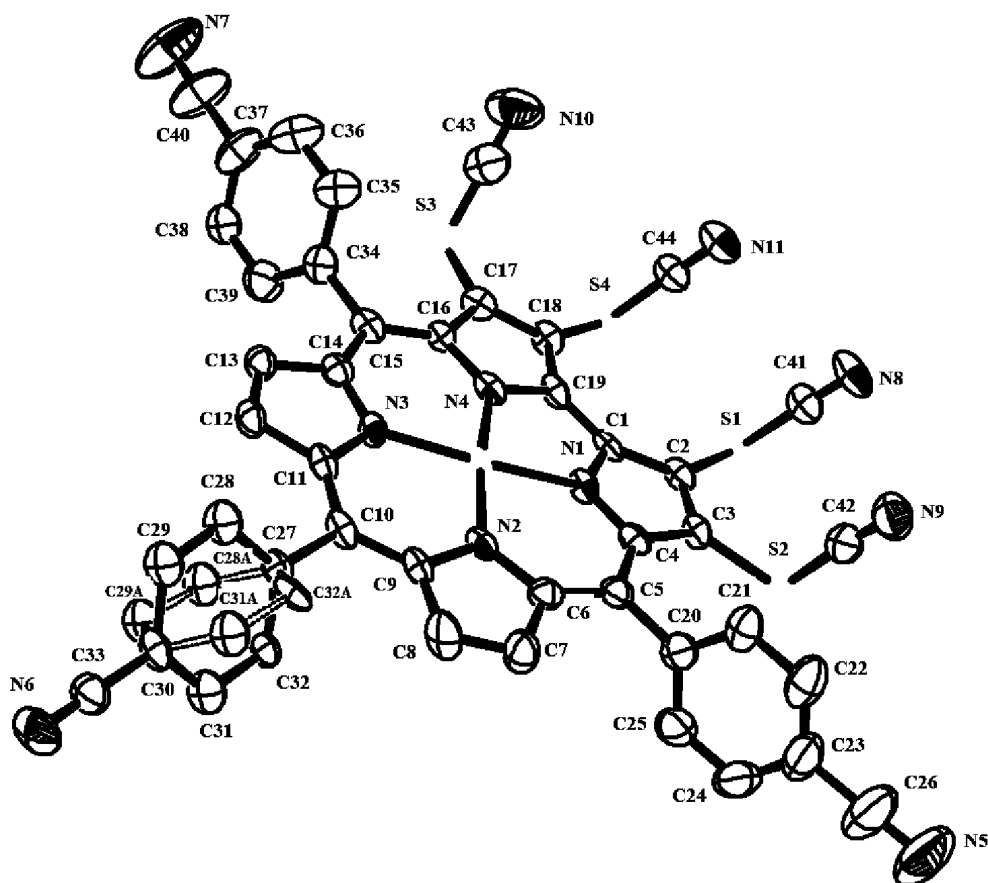


Figure 4.10 ORTEP diagram of **1**. Hydrogen atoms are omitted for clarity. Ellipsoids are drawn at 50% probability.

Table 4.2 Crystallographic Data for **1**.

compound code	1
molecular formula	$C_{44} H_{16} Ag N_{11} S_4$
Fw	934.79
Radiation	Cu $K\alpha$
crystal symmetry	Monoclinic
space group	$P2_1/n$
$a(\text{\AA})$	20.8439 (4)
$b(\text{\AA})$	6.7072 (1)
$c(\text{\AA})$	31.9882 (5)
$\alpha(\text{deg})$	90
$\beta(\text{deg})$	90.341(1)
$\gamma(\text{deg})$	90

$V(\text{\AA}^3)$	4472.01(13)
Z	4
$\mu (\text{mm}^{-1})$	5.72
$T(\text{K})$	100
$D_{\text{calcd}} (\text{g cm}^{-3})$	1.388
2θ range (deg)	4.16-74.78
e data (R_{int})	8138 (0.058)
$R1 (I > 2\sigma(I))$	0.0729
WR2 (all data)	0.1771
GOF	1.083
$\Delta\rho_{\text{max}}, \Delta\rho_{\text{min}} (e \text{\AA}^{-3})$	2.42, -1.39

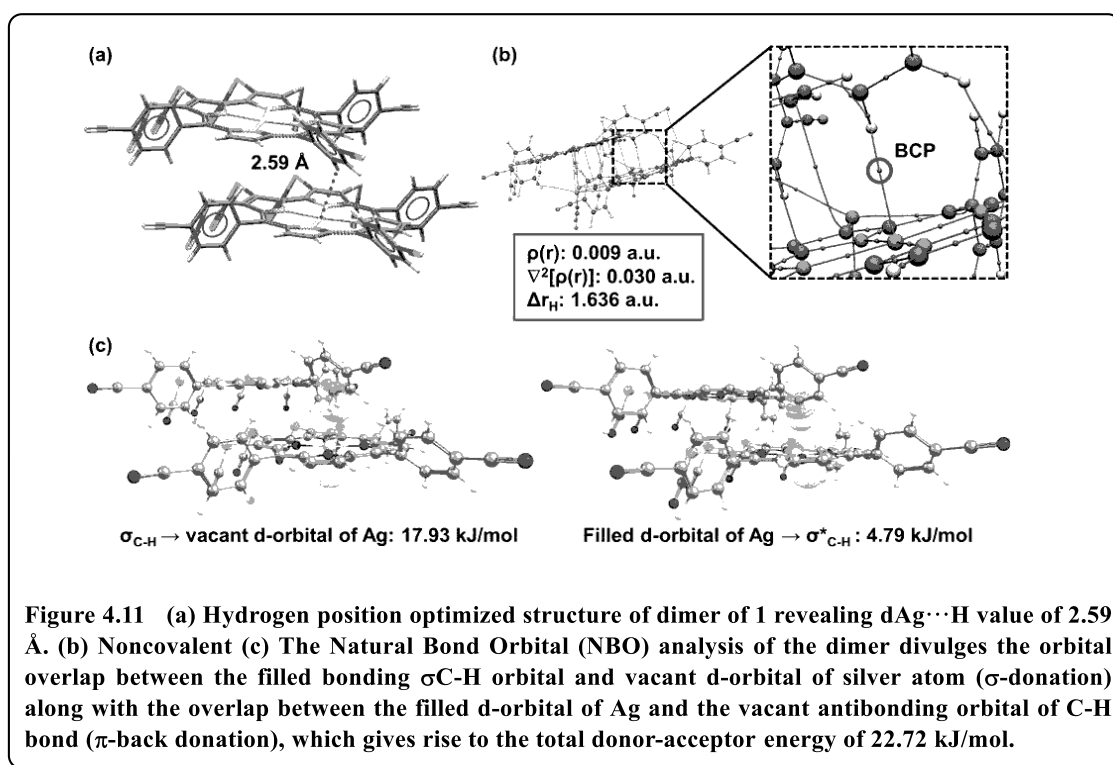
4.4. Theoretical Investigation:

The C-H \cdots Ag interaction in the crystal lattice of compound **1** has been investigated in detail with quantum chemical calculations. We incepted the process by optimizing the positions of hydrogen atoms in the monomer and the dimer by using the RI-B97-D3 functional with cc-pVDZ basis set for C, N, H, O, and def2-TZVP basis set for Ag.^[53-59] For both cases, the molecular charge was considered zero, and the optimizations were performed in the closed-shell electronic configurations. As all the electrons are paired in the square planar d^8 Ag(III) complexes, these molecules are singlet in the ground state. The optimization of the dimer resulted in the Ag \cdots H distance ($d_{\text{Ag}\cdots\text{H}}$) of 2.597 Å and an angle, $\angle\text{C-H}\cdots\text{Ag}$ of 109.62°. Figure 4a shows the hydrogen position optimized structure of the dimer of **1**. The observed distance, $d_{\text{Ag}\cdots\text{H}}$ (2.59 Å), is within the sum of the van der Waals' radii of the interacting atoms (Ag: 1.72 Å; H: 1.20 Å), and it provoked us to look into the interaction further with different methodologies viz. topology analysis and Natural Bond Orbital (NBO) analysis.^[60,61] The wavefunctions for the monomer and dimers obtained at the level of the theory mentioned above were used for the AIM analysis. A brief description of the basic concepts of Bader's theory is provided in the

supporting information.^[62,63] The presence of a bond path between the two nuclei infers that the nuclei are bonded to each other (either covalently or non-covalently). This bond path is usually characterized by the bond critical point (BCP) present at the minimum charge density along the bond vector.

The analysis of this BCP gives us two important parameters: (i) electron density [$\rho(r)$] and (ii) Laplacian of electron density [$\nabla^2\rho(r)$]. Koch and Popelier suggested $0.002 \text{ a.u.} < \rho(r) < 0.034 \text{ a.u.}$ and $0.024 \text{ a.u.} < \nabla^2\rho(r) < 0.139 \text{ a.u.}$ are the typical range for the for C-H \cdots O interaction.^[64] We checked $\rho(r)$ and $\nabla^2\rho(r)$ values at the BCP along the C-H \cdots Ag interaction and found of 0.009 a.u. and 0.030 a.u. respectively for the parameters mentioned above. Apart from these two criteria, another criterion is used to establish hydrogen bonding is mutual penetration of H-atom (Δr_H).^[60,65] The Δr_H value should be positive to have an H-bond between Ag and H atoms. The calculated value for Δr_H is 1.636 a.u., proving the formation of a H-bond. Figure 4.11b shows the molecular graph with BCP between Ag and H-atoms along with the parameters mentioned above. The magnitude of the ratio of kinetic electron energy density (G_c) to potential electron energy density (V_c) [$|G_c/V_c|$] is another parameter to estimate the non-covalency or covalency of an interaction. If the value is greater than or equals 1, then the interaction is purely noncovalent in nature, $0.5 \leq |G_c/V_c| < 1$ indicates slight covalent nature, and lower than 0.5 indicates the presence of a purely covalent bond.^[66] In this case, this value is greater than 1 (1.124), which indicates the presence of a H-bond between silver and hydrogen atoms. However, the dimer of **1** possesses several interactions apart from this H-bond such as π - π stacking, C-H $\cdots\pi$ interactions. Therefore, it is not easy to elucidate the interaction energy of that C-H \cdots Ag interaction particularly. Thus, we took Espinosa's empirical formula to calculate the interaction energy of a particular interaction from the

V_c at BCP, which states: $E_{\text{int}} = V_c/2$.^[67] This formulation gives us the C-H \cdots Ag interaction energy of -13 kJ/mol.



We have performed the Natural Bond Orbital (NBO) analysis to garner further support. The NBO analysis provides information about the orbital interactions and their interaction energies. After careful analysis, we have found that the $\sigma_{\text{C-H}}$ orbital overlaps with the vacant d-orbital of Ag with significant interaction energy of 17.93 kJ/mol (Figure 4.11c, left panel). The filled d-orbital of Ag overlaps with the $\sigma_{\text{C-H}}^*$ orbital with interaction energy of 4.79 kJ/mol (Figure 4.11c, right panel). If the C-H \cdots Ag interaction were a H-bond, then the latter orbital interaction would be the only interaction present in the dimer. However, in this case, both the interactions are present, and the former dominates. This kind of orbital overlap indicates the presence of an agostic interaction between Ag and H atoms. Therefore, it is not unambiguous to assign the said interaction as either a H-bond or an agostic interaction. The AIM analysis suggests the presence of a weak H-bond, whereas the NBO analysis suggests it to be an agostic interaction. Thus

the C-H...Ag (d^8) interaction in these complexes is a point of great debate. Sometimes, it is difficult to differentiate between intermolecular interactions such as agostic, anagostic, pseudo-agostic, or hydrogen bonding. It can be inferred that these kinds of intermolecular interactions in square-planar d^8 Ag(III) complexes are intermediate in nature, and thus they cannot be considered as typical hydrogen bonds nor a pure agostic interaction.

4.4.1 Computational Methodologies:

All structures were optimized using Turbomole-6.5 software package.^[68] The wavefunction calculation was performed using Gaussian-09 software package.^[69] AIM analyses were performed in Multiwfn software.^[70] The NBO calculations were performed using NBO-3.0 program using Gaussian-09 software.

4.4.2 Details of Topology Analysis:

The bond path is the maximal gradient path linking bond critical point (BCP) and associated two local maxima of charge density. This bond path is characterized by the BCP, which indicates the minimum charge density along the bond but maximum along the perpendicular direction of the bond (the bond refers to the bond where the BCP is present). The BCP is characterized by the number of zero eigenvalues of the associated Hessian matrix and the algebraic sum of their signs. (3, -1) is the notation of a bond critical point. This has one positive curvature associated with the charge density along the bond path and two negative curvatures associated with the charge density in the perpendicular direction of the bond path. The characteristics of this BCP is discussed in the main manuscript in the form of the $\rho(r)$ and $\nabla^2\rho(r)$. Now, there are other types of non-degenerate critical points: (3, -3), (3, +1), and (3, +3). (3, -3) denotes the nuclei positions (local maxima of the charge density), (3,+1) denotes the ring critical point, and (3, +3) denotes the cage critical point.

Another criteria mentioned in the main manuscript is mutual penetration. This parameter is calculated from the non-bonded radius (NBR) of each atom interacting, i.e., the NBR of H and Ag-atoms and the distance between the interacting atoms. NBR is the shortest distance between the nucleus and the $\rho(r) = 0.001$ a.u. isosurface. The mutual penetration is the difference between the summation of NBR of the atoms and the intermolecular distance (source: Multiwfn software manual). Here the mutual penetration is $\Delta r_H = [(\text{NBR of Ag} + \text{NBR of H}) - d_{\text{Ag}\cdots\text{H}}] / 0.529$ a.u., where all the distances are in Å.

Optimized Cartesian Co-ordinates of 1

{ Cartesian coordinates of the optimized structures (in Å) }

Ag	7.249520000	3.579700000	11.975850000
N	5.853910000	4.924430000	11.749060000
N	6.147640000	2.502460000	13.178580000
N	8.171250000	4.815770000	10.783030000
N	8.815630000	2.396480000	12.132910000
C	6.194220000	6.013680000	10.955760000
C	7.495860000	5.951300000	10.440760000
C	4.604490000	4.990830000	12.244870000
C	4.855110000	2.876050000	13.562760000
C	6.581170000	1.410520000	13.882630000
C	9.433340000	4.748030000	10.258430000
C	8.886140000	1.277720000	12.894220000
C	9.987090000	2.578920000	11.425980000
C	5.039290000	6.812500000	10.984550000
C	8.390860000	6.682380000	9.605890000
C	4.105160000	3.959260000	13.140520000
C	4.073750000	6.198790000	11.765050000
C	4.461730000	1.891430000	14.519190000
C	7.844820000	0.846450000	13.796270000
C	5.450590000	1.012120000	14.723910000
C	9.567120000	5.937880000	9.493930000
C	10.290340000	3.652070000	10.555920000
C	10.167260000	0.713650000	12.673500000
C	10.835410000	1.497050000	11.781040000
S	4.845210000	8.406130000	10.219410000
S	8.159500000	8.283390000	8.939580000
C	2.716000000	4.116880000	13.652320000
S	2.515990000	6.960730000	12.165540000
H	3.472901800	1.876451300	14.982753900

C	8.104170000	-0.319930000	14.698320000
H	5.420613900	0.132513500	15.364320400
S	11.010040000	6.525430000	8.671530000
C	11.611920000	3.586340000	9.842600000
H	10.563169700	-0.169400800	13.173028900
H	11.844230500	1.348110800	11.394322700
C	3.760960000	7.957420000	8.985330000
C	7.108070000	7.901750000	7.654640000
C	1.645380000	3.735240000	12.823840000
C	2.479290000	4.687660000	14.899840000
C	1.497950000	6.321540000	10.978160000
C	7.819330000	-0.160970000	15.977820000
C	8.646620000	-1.502410000	14.263290000
C	10.611280000	6.180690000	7.062870000
C	11.663610000	3.271770000	8.511910000
C	12.789690000	3.923710000	10.527130000
N	3.013250000	7.654930000	8.185630000
N	6.358470000	7.685110000	6.822960000
H	1.839408900	3.302563400	11.837867100
C	0.373440000	3.972000000	13.252480000
H	3.325553900	4.980653700	15.531395400
C	1.184510000	4.889550000	15.312480000
N	0.720860000	5.941910000	10.213650000
H	7.481243200	0.794580200	16.386251600
C	8.032770000	-1.240830000	16.889470000
H	8.883081500	-1.671805800	13.209866300
C	8.851600000	-2.542030000	15.194130000
N	10.359420000	5.949290000	5.952900000
H	10.742181800	3.043447600	7.965215900
C	12.861830000	3.262380000	7.862560000
H	12.739413700	4.197860500	11.586773900
C	13.971350000	3.930420000	9.858590000
H	-0.475091400	3.725738200	12.604217500
C	0.138970000	4.547480000	14.474400000
H	0.975200000	5.347239400	16.285532100
C	8.489810000	-2.464900000	16.444840000
H	7.800126400	-1.093117800	17.950131400
H	9.275276300	-3.477675900	14.804996400
H	12.888940800	3.018635900	6.793722100
C	14.019030000	3.574270000	8.502310000
H	14.899278600	4.210907000	10.370354100
N	16.256940000	3.655420000	7.222810000
C	15.292690000	3.648720000	7.785790000
C	-1.187290000	4.876130000	14.922230000

N	-2.264490000	5.151130000	15.200520000
C	8.676070000	-3.537380000	17.369280000
N	8.836320000	-4.407970000	18.111400000

Optimized Cartesian Co-ordinates of Dimer of 1

Ag	7.249520000	3.579700000	11.975850000
N	5.853910000	4.924430000	11.749060000
N	6.147640000	2.502460000	13.178580000
N	8.171250000	4.815770000	10.783030000
N	8.815630000	2.396480000	12.132910000
C	6.194220000	6.013680000	10.955760000
C	7.495860000	5.951300000	10.440760000
H	8.964680300	5.071571500	13.230887400
C	4.604490000	4.990830000	12.244870000
C	4.855110000	2.876050000	13.562760000
C	6.581170000	1.410520000	13.882630000
C	9.433340000	4.748030000	10.258430000
C	8.886140000	1.277720000	12.894220000
C	9.987090000	2.578920000	11.425980000
C	5.039290000	6.812500000	10.984550000
C	8.390860000	6.682380000	9.605890000
C	8.646620000	5.204790000	14.263290000
C	4.105160000	3.959260000	13.140520000
C	4.073750000	6.198790000	11.765050000
C	4.461730000	1.891430000	14.519190000
C	7.844820000	0.846450000	13.796270000
C	5.450590000	1.012120000	14.723910000
C	9.567120000	5.937880000	9.493930000
C	10.290340000	3.652070000	10.555920000
C	10.167260000	0.713650000	12.673500000
C	10.835410000	1.497050000	11.781040000
S	4.845210000	8.406130000	10.219410000
S	8.159500000	8.283390000	8.939580000
C	8.104170000	6.387270000	14.698320000
C	8.851600000	4.165170000	15.194130000
C	2.716000000	4.116880000	13.652320000
S	2.515990000	6.960730000	12.165540000
H	3.473211000	1.875235100	14.983359300
C	8.104170000	-0.319930000	14.698320000
H	5.422786900	0.133122400	15.365103800
S	11.010040000	6.525430000	8.671530000
C	11.611920000	3.586340000	9.842600000
H	10.561600200	-0.169752000	13.173433900

H	11.844000300	1.346970400	11.394234600
C	3.760960000	7.957420000	8.985330000
C	7.108070000	7.901750000	7.654640000
C	7.844820000	7.553650000	13.796270000
C	7.819330000	6.546230000	15.977820000
C	8.489810000	4.242300000	16.444840000
H	9.281798600	3.234423100	14.802883700
C	1.645380000	3.735240000	12.823840000
C	2.479290000	4.687660000	14.899840000
C	1.497950000	6.321540000	10.978160000
C	7.819330000	-0.160970000	15.977820000
C	8.646620000	-1.502410000	14.263290000
C	10.611280000	6.180690000	7.062870000
C	11.663610000	3.271770000	8.511910000
C	12.789690000	3.923710000	10.527130000
N	3.013250000	7.654930000	8.185630000
N	6.358470000	7.685110000	6.822960000
C	6.581170000	8.117720000	13.882630000
C	8.886140000	7.984920000	12.894220000
H	7.478125300	7.500528600	16.386974000
C	8.032770000	5.466370000	16.889470000
C	8.676070000	3.169820000	17.369280000
H	1.839601600	3.301920400	11.838169300
C	0.373440000	3.972000000	13.252480000
H	3.326486100	4.977528900	15.531885700
C	1.184510000	4.889550000	15.312480000
N	0.720860000	5.941910000	10.213650000
H	7.485419000	0.789890000	16.395916600
C	8.032770000	-1.240830000	16.889470000
H	8.882970000	-1.673708200	13.210051200
C	8.851600000	-2.542030000	15.194130000
N	10.359420000	5.949290000	5.952900000
H	10.742116600	3.042943900	7.965533300
C	12.861830000	3.262380000	7.862560000
H	12.739929800	4.196315000	11.587443300
C	13.971350000	3.930420000	9.858590000
N	6.147640000	9.209660000	13.178580000
C	5.450590000	7.719320000	14.723910000
N	8.815630000	9.103680000	12.132910000
C	10.167260000	7.420850000	12.673500000
H	7.796676300	5.614868800	17.949386100
N	8.836320000	2.299230000	18.111400000
H	-0.475256700	3.725213500	12.604656100
C	0.138970000	4.547480000	14.474400000

H	0.973794400	5.345901100	16.285957000
C	8.489810000	-2.464900000	16.444840000
H	7.806060400	-1.082572600	17.949462500
H	9.275029600	-3.477272600	14.803952300
H	12.889200400	3.018375000	6.793823300
C	14.019030000	3.574270000	8.502310000
H	14.899873200	4.209942800	10.369822100
Ag	7.249520000	10.286900000	11.975850000
C	4.855110000	9.583250000	13.562760000
C	4.461730000	8.598630000	14.519190000
H	5.419098600	6.837199000	15.360767800
C	9.987090000	9.286120000	11.425980000
H	10.565698500	6.537199800	13.169287400
C	10.835410000	8.204250000	11.781040000
N	16.256940000	3.655420000	7.222810000
C	15.292690000	3.648720000	7.785790000
C	-1.187290000	4.876130000	14.922230000
N	-2.264490000	5.151130000	15.200520000
C	8.676070000	-3.537380000	17.369280000
N	8.836320000	-4.407970000	18.111400000
N	5.853910000	11.631630000	11.749060000
N	8.171250000	11.522970000	10.783030000
C	6.194220000	12.720880000	10.955760000
C	7.495860000	12.658500000	10.440760000
C	4.604490000	11.698030000	12.244870000
C	9.433340000	11.455230000	10.258430000
C	5.039290000	13.519700000	10.984550000
C	8.390860000	13.389580000	9.605890000
C	4.105160000	10.666460000	13.140520000
C	4.073750000	12.905990000	11.765050000
C	9.567120000	12.645080000	9.493930000
C	10.290340000	10.359270000	10.555920000
S	4.845210000	15.113330000	10.219410000
S	8.159500000	14.990590000	8.939580000
C	2.716000000	10.824080000	13.652320000
S	2.515990000	13.667930000	12.165540000
S	11.010040000	13.232630000	8.671530000
C	11.611920000	10.293540000	9.842600000
C	3.760960000	14.664620000	8.985330000
C	7.108070000	14.608950000	7.654640000
C	1.645380000	10.442440000	12.823840000
C	2.479290000	11.394860000	14.899840000
C	1.497950000	13.028740000	10.978160000
C	10.611280000	12.887890000	7.062870000

C	11.663610000	9.978970000	8.511910000
C	12.789690000	10.630910000	10.527130000
N	3.013250000	14.362130000	8.185630000
N	6.358470000	14.392310000	6.822960000
H	3.472233700	8.583566400	14.981275300
H	1.840352800	10.010233600	11.838229000
C	0.373440000	10.679200000	13.252480000
H	3.325298000	11.691059800	15.530542300
C	1.184510000	11.596750000	15.312480000
N	0.720860000	12.649110000	10.213650000
N	10.359420000	12.656490000	5.952900000
H	10.743736800	9.745360100	7.966949000
C	12.861830000	9.969580000	7.862560000
H	12.739728300	10.907619400	11.586230300
C	13.971350000	10.637620000	9.858590000
H	11.845008800	8.058310900	11.395458400
H	-0.474302900	10.431884000	12.603530700
C	0.138970000	11.254680000	14.474400000
H	0.975131800	12.056562100	16.284474700
H	12.887381700	9.724200300	6.793981600
C	14.019030000	10.281470000	8.502310000
H	14.898977100	10.919996300	10.369785600
C	-1.187290000	11.583330000	14.922230000
N	-2.264490000	11.858330000	15.200520000
C	15.292690000	10.355920000	7.785790000
N	16.256940000	10.362620000	7.222810000

4.5 Conclusions

In conclusion, we have synthesized two new Ag(III)-corroles bearing four thiocyanato groups appended at the neighboring β -positions. The absorption spectra of these tetra(thiocyanato)corrolato-Ag(III) derivatives are drastically altered than the previously reported β -unsubstituted corrolato-Ag(III) derivatives. In comparison to the parent β -unsubstituted corrolato-Ag(III) derivatives, in tetra(thiocyanato)corrolato-Ag(III) derivatives, the Soret band is split into two distinct bands and thus it indicates lower symmetry. In addition to that, the Q bands are also split into at least two distinct bands. It was also observed that the intensity of the Soret band and Q bands are almost

equalized and this phenomenon is quite unique in nature. X-ray single-crystal structure analysis of **1**, reveals C-H \cdots Ag interactions, having Ag \cdots H distance of 2.611 Å and C-H \cdots Ag angle of 115.11°. The C-H \cdots Ag interactions are rarely demonstrated in discrete coordination/organometallic compounds. This essentially prompted us to perform a detailed theoretical calculation on these systems to understand the nature of weak interactions. The critical study of the exclusive formation of the C-H \cdots Ag interaction in the crystal packing of the structure of **1** has been carried out by performing benchmark quantum chemical calculations. Crystal structure optimization discloses the Ag \cdots H distance of 2.597 Å and \angle C-H \cdots Ag of 109.62°. The NBO analysis provides us with information about the orbital interactions and their interaction energies. After careful analysis, we found that the $\sigma_{\text{C-H}}$ orbital overlaps with the vacant d-orbital of Ag with significant interaction energy of 17.93 kJ/mol. The filled d-orbital of Ag overlaps with the $\sigma^*_{\text{C-H}}$ orbital with an interaction energy of 4.79 kJ/mol. \angle C-H \cdots Ag angle fits with the typical agostic interaction. Whereas, H \cdots Ag distance is contrary to the agostic interaction. H \cdots Ag distance fitted nicely with the weak H-bonded interactions. Thus, a clear-cut distinction of agostic interaction vs. H-bonded interaction is rather difficult. In fact, our analysis indicates an intermediate mixed situation.

4.6 Experimental Section

4.6.1 Materials:

The precursor's pyrrole, *p*-chloranil, silver acetate (99.99%), and aldehydes were purchased from Aldrich, USA. NH₄SCN (>98.5% purity), triethylamine, acetonitrile (HPLC) was purchased from Merck chemicals. Other chemicals were of reagent grade. Hexane, CH₂Cl₂, CH₃CN were distilled from KOH and CaH₂ respectively. For spectroscopy studies, HPLC-grade solvents were used. For the synthesis of FB corroles, a protocol developed by Gryko et al. was used.^[71] The synthetic methodologies and full spectroscopic characterization of free

base corroles: 2,3,17,18-tetra (thiocyanato) – 5, 10, 15 – tris (4-cyanophenyl) corrole, and 2, 3, 17, 18-tetra (thiocyanato) – 10 – (4-bromophenyl) – 5,15 – bis(4 – cyanophenyl) corrole were reported earlier by us.

4.6.2 Physical Measurements:

The elemental analyses were carried out with a Euro EA elemental analyzer. UV-Vis spectral studies were performed on a Perkin–Elmer LAMBDA-750 spectrophotometer. Emission spectral studies were performed on a Perkin Elmer, LS 55 spectrophotometer using an optical cell of 1 cm path length. FT–IR spectra were recorded on a Perkin–Elmer spectrophotometer with samples prepared as KBr pellets. The NMR measurements were carried out using a Bruker 400 MHz NMR spectrometer. Chemical shifts are expressed in parts per million (ppm) relative to residual chloroform ($\delta = 7.26$). Electrospray mass spectra were recorded on a Bruker Micro TOF–QII mass spectrometer.

4.6.3 Crystal Structure Determination:

Single crystals of **1** were grown from the solution of **1** in the dichloromethane-hexane mixture (1:1), followed by slow evaporation under atmospheric conditions. ORTEP diagram of **1** is shown in Figure 4.10 (hydrogen atoms are omitted for clarity). Ellipsoids are drawn at 50% probability. The crystal data of **1** were collected on a Rigaku Oxford diffractometer (Cu $K\alpha$ radiation) at 100 K. Selected data collection parameters and other crystallographic results are summarized in Table 4.1. All data were corrected for Lorentz polarization and absorption effects. The program package SHELXTL^[72] was used for structure solution and full-matrix least-squares refinement on F^2 . Hydrogen atoms were included in the refinement using the riding model. The difference Fourier map clearly shows a disorder over two positions of the phenyl ring C27/32. The data are successfully refined by splitting this phenyl ring over two positions, each at about half (refined) occupancy. And no restraint is applied to these C27/32 atoms. Disordered solvent

molecules were taken out using SQUEEZE command in PLATON.^[73] CCDC 2132565 contains the supporting crystallographic data for **1**. These data can be obtained free of charge via www.ccdc.cam.ac.uk/data_request/cif.

4.6.4 Syntheses:

Synthesis of 2,3,17,18-tetra(thiocyanato)-5,10,15-tris(4-cyanophenyl) corrolato-Ag(III), 1

25mg (0.030 mmol) of 2,3,17,18-tetra(thiocyanato)-5,10,15-tris(4-cyanophenyl) corrole was dissolved in 5ml of acetonitrile, and then 44 mg of silver acetate was added to it (0.26 mmol) followed by 10ml of triethylamine. The reaction mixture was stirred at room temperature for 1 h in the air. After that, the solvent was evaporated, and the bluish color crude product was subjected to column chromatography using a silica gel (100–200 mesh) column. The desired product (reddish blue) was eluted using a mixture of 93% dichloromethane and 7% acetonitrile. The final form of the compound was obtained as bluish crystalline materials.

For 2,3,17,18-tetra(thiocyanato)-5,10,15-tris(4-cyanophenyl) corrolato-Ag(III), 1

Yield: 32% (9 mg). Anal. Calcd for $C_{44}H_{16}AgN_{11}S_4$ (**1**): C, 56.53; H, 1.73; N, 16.48. Found: C, 56.75; H, 1.61; N, 16.67. $\lambda_{Max/nm}$ ($\epsilon / M^{-1}cm^{-1}$) in CH_2Cl_2 : 408 (57992), 428 (51003), 562 (27423), 582 (41990), 606 (54368). 1H NMR (400 MHz, Chloroform-*d*) δ 8.35 (m, 4H), 8.21 – 8.07 (m, 12H) (Figure 4.1). ^{13}C { 1H } NMR (101 MHz, $CDCl_3$) δ 157.5, 156.9, 156.2, 141.2, 139.7, 139.3, 138.0, 134.5, 134.4, 133.9, 132.3, 132.2, 131.2, 129.4, 127.9, 118.3, 118.3, 114.5, 114.1, 109.7, 109.6. HRMS (ESI) m/z : [**1**+Na] $^+$ Calcd for $C_{44}H_{16}AgN_{11}S_4Na$ 957.9413; Found 957.9377 (Figure 4.3).

Synthesis of 2, 3, 17, 18 – tetra - (thiocyanato) – 10 – (4 – bromophenyl) – 5, 15 – bis (4 – cyanophenyl) corrolato - Ag(III), 2

26mg (0.029mmol) of 2,3,17,18- tetra (thiocyanato) – 10 – (4–bromophenyl)– 5,15 – bis(4– cyanophenyl) corrole was dissolved in 5ml of acetonitrile, and then 44mg (0.26mmol) of silver acetate was added to it followed by 10ml of triethyl amine .The reaction mixture was stirred at room temperature for 1 h in air. After that, the solvent was evaporated and the bluish color crude product was subjected to column chromatography using a silica gel (100–200 mesh) column. The desired product (reddish blue) was eluted by using a mixture of 96% DCM and 4% acetonitrile. The final form of the compound was obtained as bluish crystalline materials.

For 2, 3, 17, 18-tetra (thiocyanato)–10–(4–bromophenyl)–5,15–bis(4–cyanophenyl) corrolato-Ag(III)}, 2

Yield: 25% (7 mg). Anal. Calcd for $C_{43}H_{16}AgBrN_{10}S_4$ (**2**): C, 52.24; H, 1.63; N, 14.17. Found: C, 52.43; H, 1.77; N, 14.36. $\lambda_{\max/nm}$ ($\epsilon/M^{-1}cm^{-1}$) in CH_2Cl_2 : 407 (56778), 427 (47062), 564 (28225), 583 (39555), 609 (51301) (Table 4.2). 1H NMR (400 MHz, Chloroform-*d*) δ 8.39 (d, $J = 5.2$ Hz, 2H), 8.32 (d, $J = 5.2$ Hz, 2H), 8.22 – 8.09 (m, 8H), 7.9 (q, $J = 8.5$ Hz, 4H) (Figure 4.2). HRMS (ESI) m/z : [**2**+Na] $^+$ Calcd for $C_{43}H_{16}AgBrN_{10}S_4Na$ 1010.8551; Found 1010.8534 (Figure 4.4).

References

- [1] E. R. Johnson, S. Keinan, P. Mori-Sánchez, J. Contreras-García, A. J. Cohen, W. Yang, *J. Am. Chem. Soc.* **2010**, *132*, 6498–6506.
- [2] G. R. Desiraju, *Nature* **2001**, *412*, 397–400.
- [3] K. Müller-Dethlefs, P. Hobza, *Chem. Rev.* **2000**, *100*, 143–168.
- [4] K. E. Riley, P. Hobza, *Wiley Interdiscip. Rev. Comput. Mol. Sci.* **2011**, *1*, 3–17.
- [5] J. G. Brandenburg, S. Grimme, *Acta Crystallogr. Sect. B Struct. Sci. Cryst. Eng. Mater.* **2016**, *72*, 502–513.
- [6] K. S. Mali, K. Lava, K. Binnemans, S. De Feyter, *Chem. Eur. J.* **2010**, *16*, 14447–14458.
- [7] D. C. Sherrington, K. A. Taskinen, *Chem. Soc. Rev.* **2001**, *30*, 83–93.
- [8] D. Braga, F. Grepioni, K. Biradha, V. R. Pedireddi, G. R. Desiraju, *J. Am. Chem. Soc.* **1995**, *117*, 3156–3166.
- [9] G.-J. Zhao, K.-L. Han, *Acc. Chem. Res.* **2012**, *45*, 404–413.
- [10] G. S. Nichol, W. Clegg, *Cryst. Growth Des.* **2009**, *9*, 1844–1850.
- [11] R. G. Pearson, *Chem. Rev.* **1985**, *85*, 41–49.
- [12] S. Patra, B.; Mondal, S.; *Encyclopedia of Inorganic and Bioinorganic Chemistry* Kar, 1–24.
- [13] I. Aviv, Z. Gross, *Chem. Commun.* **2007**, 1987–1999.
- [14] S. Nardis, F. Mandoj, M. Stefanelli, R. Paolesse, *Coord. Chem. Rev.* **2019**, *388*, 360–405.
- [15] I. Aviv-Harel, Z. Gross, *Chem. Eur. J.* **2009**, *15*, 8382–8394.

-
- [16] Y. Fang, Z. Ou, K. M. Kadish, *Chem. Rev.* **2017**, *117*, 3377–3419.
- [17] R. Orłowski, D. Gryko, D. T. Gryko, *Chem. Rev.* **2017**, *117*, 3102–3137.
- [18] S. Hiroto, K. Furukawa, H. Shinokubo, A. Osuka, *J. Am. Chem. Soc.* **2006**, *128*, 12380–12381.
- [19] K. Fujino, Y. Hirata, Y. Kawabe, T. Morimoto, A. Srinivasan, M. Toganoh, Y. Miseki, A. Kudo, H. Furuta, *Angew. Chemie* **2011**, *123*, 6987–6991.
- [20] J. F. B. Barata, M. G. P. M. S. Neves, M. A. F. Faustino, A. C. Tomé, J. A. S. Cavaleiro, *Chem. Rev.* **2017**, *117*, 3192–3253.
- [21] A. Ghosh, *Chem. Rev.* **2017**, *117*, 3798–3881.
- [22] C. Brückner, *J. Chem. Educ.* **2004**, *81*, 1665.
- [23] T. Hashimoto, Y.-K. Choe, H. Nakano, K. Hirao, *J. Phys. Chem. A* **1999**, *103*, 1894–1904.
- [24] K. Sahu, S. Mondal, S. M. Mobin, S. Kar, *J. Org. Chem.* **2021**, *86*, 3324–3333.
- [25] P. Pyykko, *Chem. Rev.* **1988**, *88*, 563–594.
- [26] L. Brammer, J. M. Charnock, P. L. Goggin, R. J. Goodfellow, T. F. Koetzle, A. G. Orpen, *J. Chem. Soc. Chem. Commun.* **1987**, 443–445.
- [27] M. Brookhart, M. L. H. Green, *J. Organomet. Chem.* **1983**, *250*, 395–408.
- [28] J. M. Casas, L. R. Falvello, J. Forniés, A. Martín, A. J. Welch, *Inorg. Chem.* **1996**, *35*, 6009–6014.
- [29] D. Braga, F. Grepioni, E. Tedesco, K. Biradha, G. R. Desiraju, *Organometallics* **1997**, *16*, 1846–1856.
- [30] L. R. Falvello, *Angew. Chemie Int. Ed.* **2010**, *49*, 10045–10047.
- [31] S. Chatterjee, J. A. Krause, A. G. Oliver, W. B. Connick, *Inorg. Chem.* **2010**, *49*, 9798–9808.

-
- [32] W. Yao, O. Eisenstein, R. H. Crabtree, *Inorganica Chim. Acta* **1997**, *254*, 105–111.
- [33] L. Brammer, *Dalt. Trans.* **2003**, 3145–3157.
- [34] G. Brookhart, M.; Green, M. L. H.; Parkin, *Proc. Natl. Acad. Sci.* **2007**, *104*, 6908.
- [35] J. Saßmannshausen, *Dalt. Trans.* **2012**, *41*, 1919–1923.
- [36] R. R. Annapureddy, F. Burg, J. Gramüller, T. P. Golub, C. Merten, S. M. Huber, T. Bach, *Angew. Chemie* **2021**, *133*, 7999–8005.
- [37] F. Kraus, H. Schmidbaur, S. S. Al-juaid, *Inorg. Chem.* **2013**, *52*, 9669–9674.
- [38] G. dos Passos Gomes, G. Xu, X. Zhu, L. Chamoreau, Y. Zhang, O. Bistri-Aslanoff, S. Roland, I. V Alabugin, M. Sollogoub, *Chem. Eur. J.* **2021**, *27*, 8127–8142.
- [39] C.-S. Liu, P.-Q. Chen, E.-C. Yang, J.-L. Tian, X.-H. Bu, Z.-M. Li, H.-W. Sun, Z. Lin, *Inorg. Chem.* **2006**, *45*, 5812–5821.
- [40] T. S. Thakur, G. R. Desiraju, *Chem. Commun.* **2006**, 552–554.
- [41] T. S. Thakur, G. R. Desiraju, *J. Mol. Struct. THEOCHEM* **2007**, *810*, 143–154.
- [42] C.-S. Liu, P.-Q. Chen, Z. Chang, J.-J. Wang, L.-F. Yan, H.-W. Sun, X.-H. Bu, Z. Lin, Z.-M. Li, S. R. Batten, *Inorg. Chem. Commun.* **2008**, *11*, 159–163.
- [43] A. Colombo, R. Ossola, M. Magni, D. Roberto, D. Jacquemin, C. Castellano, F. Demartin, C. Dragonetti, *Dalt. Trans.* **2018**, *47*, 1018–1022.
- [44] L. M. Scherf, S. A. Baer, F. Kraus, S. M. Bawaked, H. Schmidbaur, *Inorg. Chem.* **2013**, *52*, 2157–2161.
- [45] E. S. Kryachko, *J. Mol. Struct.* **2008**, *880*, 23–30.
- [46] F. Groenewald, J. Dillen, H. G. Raubenheimer, C. Esterhuysen, *Angew. Chemie Int. Ed.* **2016**, *55*, 1694–1698.
-

-
- [47] H. Schmidbaur, H. G. Raubenheimer, L. Dobrzańska, *Chem. Soc. Rev.* **2014**, *43*, 345–380.
- [48] M. Straka, E. Andris, J. Vícha, A. Růžička, J. Roithová, L. Rulíšek, *Angew. Chemie Int. Ed.* **2019**, *58*, 2011–2016.
- [49] M. Vaddamanu, A. Sathyanarayana, Y. Masaya, S. Sugiyama, O. Kazuhisa, K. Velappan, K. Subramaniyam, K. Hisano, O. Tsutsumi, G. Prabusankar, *Organometallics* **2020**, *39*, 2202–2206.
- [50] H. Darmandeh, J. Löffler, N. V Tzouras, B. Dereli, T. Scherpf, K. Feichtner, S. Vanden Broeck, K. Van Hecke, M. Saab, C. S. J. Cazin, *Angew. Chemie* **2021**, *133*, 21182–21192.
- [51] R. D. Pike, G. Ayala, A. P. Evans, *J. Chem. Crystallogr.* **2014**, *44*, 520–526.
- [52] C. Brückner, C. A. Barta, R. P. Brinas, J. A. Krause Bauer, *Inorg. Chem.* **2003**, *42*, 1673–1680.
- [53] J. Calbo, J. C. Sancho-García, E. Ortí, J. Aragó, *Molecules* **2018**, *23*, 118.
- [54] D. K. Sahoo, S. Jena, J. Dutta, A. Rana, H. S. Biswal, *J. Phys. Chem. A* **2019**, *123*, 2227–2236.
- [55] Y. Minenkov, Å. Singstad, G. Occhipinti, V. R. Jensen, *Dalt. Trans.* **2012**, *41*, 5526–5541.
- [56] J. G. Brandenburg, C. Bannwarth, A. Hansen, S. Grimme, *J. Chem. Phys.* **2018**, *148*, 64104.
- [57] F. Weigend, R. Ahlrichs, *Phys. Chem. Chem. Phys.* **2005**, *7*, 3297–3305.
- [58] T. H. Dunning Jr, *J. Chem. Phys.* **1989**, *90*, 1007–1023.
- [59] D. E. Woon, T. H. Dunning Jr, *J. Chem. Phys.* **1993**, *98*, 1358–1371.

-
- [60] J. Dutta, D. K. Sahoo, S. Jena, K. D. Tulsian, H. S. Biswal, *Phys. Chem. Chem. Phys.* **2020**, *22*, 8988–8997.
- [61] S. J. Grabowski, *J. Mol. Model.* **2013**, *19*, 4713–4721.
- [62] R. F. W. Bader, *Acc. Chem. Res.* **1985**, *18*, 9–15.
- [63] H. S. Biswal, A. Kumar Sahu, A. Frontera, A. Bauzá, *J. Chem. Inf. Model.* **2021**, *61*, 3945–3954.
- [64] U. Koch, P. L. A. Popelier, *J. Phys. Chem.* **1995**, *99*, 9747–9754.
- [65] D. Mani, E. Arunan, *Phys. Chem. Chem. Phys.* **2013**, *15*, 14377–14383.
- [66] M. Ziólkowski, S. J. Grabowski, J. Leszczynski, *J. Phys. Chem. A* **2006**, *110*, 6514–6521.
- [67] E. Espinosa, I. Alkorta, J. Elguero, E. Molins, *J. Chem. Phys.* **2002**, *117*, 5529–5542.
- [68] *Univ. Karlsruhe Forschungszentrum Karlsruhe GmbH* **2013**, 1989–2007.
- [69] J. R. Cheeseman, G. Scalmani, V. Barone, B. Mennucci, G. A. Petersson, H. Nakatsuji, M. Caricato, X. Li, H. P. Hratchian, A. F. Izmaylov, *Inc. Wallingford* **2009**.
- [70] T. Lu, F. Chen, *J. Comput. Chem.* **2012**, *33*, 580–592.
- [71] B. Koszarna, D. T. Gryko, *J. Org. Chem.* **2006**, *71*, 3707–3717.
- [72] G. M. Sheldrick, *Acta Crystallogr. Sect. A Found. Crystallogr.* **2008**, *64*, 112–122.
- [73] P. V Van der Sluis, A. L. Spek, *Acta Crystallogr. Sect. A Found. Crystallogr.* **1990**, *46*, 194–201.

NIR-Emissive, Singlet-Oxygen–Sensitizing Gold Tetra(thiocyano)corroles

5.1 Introduction

5.2 Result and Discussion

5.2.1 Synthesis of Gold corroles

5.3 Spectral Characterization

5.3.1 NMR Spectroscopy

5.3.2 Mass Spectrometry

5.3.3 IR spectroscopy

5.3.4 Single crystal XRD Analysis

5.3.5 Electrochemistry

5.3.6 Photophysical property

5.4 DFT and TDDFT calculations

5.5 Conclusion

5.6 Experimental Section

5.6.1 Materials

5.6.2 Physical measurements

5.6.3 Crystal Structure Determination

5.6.4 Synthesis

5.6.5 Computational Methodology

5.1 Introduction

Many heavy element porphyrins exhibit distinctive phosphorescence properties relative to non-porphyrinoid complexes and organic phosphorescent materials.^[1-7] Metalloporphyrinoids frequently exhibit phosphorescence at longer wavelengths and relatively shorter triplet lifetimes. They have been widely deployed as oxygen sensors, especially in the biomedical domain.^[8-11] In metalloporphyrinoids, a highly efficient intersystem crossing (ISC) populate the lowest triplet (T_1) excited state, as well as an efficient energy transfer from this T_1 state to the surrounding triplet oxygen (3O_2) generates singlet oxygen (1O_2). The photosensitizers having superior performance have extensive applications in photodynamic therapy (PDT).^[12-15] One of the possible disadvantages of metalloporphyrinoid-based systems is originating from their poor photochemical stability. In this context, the photochemical stability of gold and platinum porphyrinoids is relatively superior.^[14] As the emission energy is heavily dependent on the HOMO and LUMO orbitals, thus the possible way to design the phosphorescent metalloporphyrinoids involves the suitable modifications of the peripheral substituents.^[14] Among the various porphyrinoid derivatives, the molecules like porphyrins and corroles have limited absorption at the longer wavelength.^[14] This essentially hinders their potential applications in various analytical applications. This problem can be addressed by enhancing their absorption profile at the Q-band region. Among the various metalloporphyrinoid derivatives, metallo corroles show distinct photophysical properties.^[16-25] Gold corroles are attracting considerable interest as triplet photosensitizers. They are readily accessible *via* the acetate method, exhibit strong Q bands in the orange region, and NIR phosphorescence under ambient conditions, promising a variety of applications.^[26-41] Like gold porphyrins,^[42-44] gold corroles are also stable under physiological and photochemical conditions. Gold corroles also find

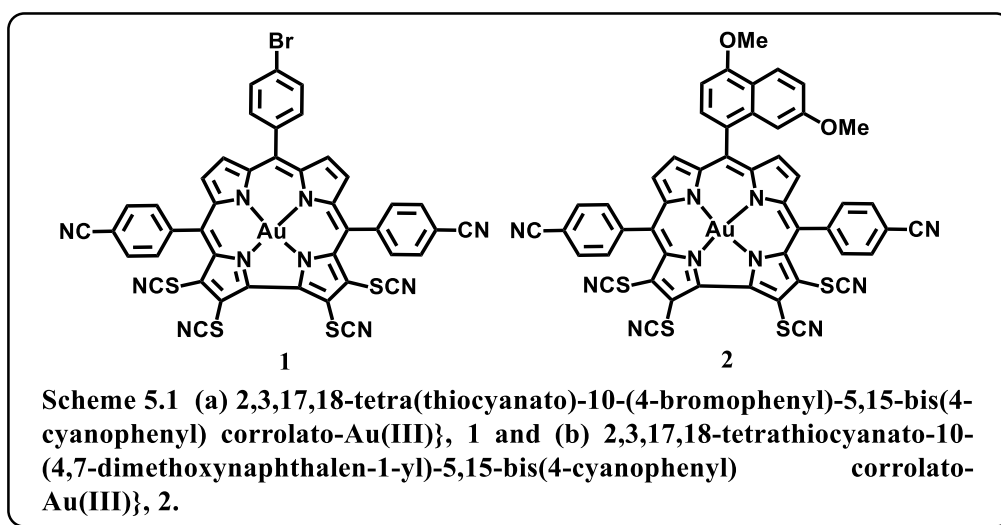
applications in dye-sensitized solar cells.^[38] It is worth mentioning that the photophysical properties of gold corroles bearing various substitutions at the *meso*- and β -positions have been described recently. Gross *et al.* have reported the fascinating variations of photophysical properties in 2,3,17,18-tetra-Br/I/CF₃-substituted gold corroles.^[28] With 2,3,17,18-tetra-SCN-substituted corroles available in our laboratory,^[45] herein we report a study of their corresponding Au complexes. The preliminary photophysical properties of 2,3,17,18-*tetra*-SCN-substituted corroles have demonstrated that their absorption and emission properties are drastically altered while comparing to the unsubstituted parent free-base (FB) corroles. In addition, there will be a great demand for the phosphorescent metalloporphyrinoid having reactive thiocyanate groups (electrophilic in nature) at the β -positions due to ease in using them as labeling reagents for various bio-analytical experiments employing Raman spectroscopy.^[46]

5.2 Results and Discussion

5.2.1 Synthesis of Gold corroles :

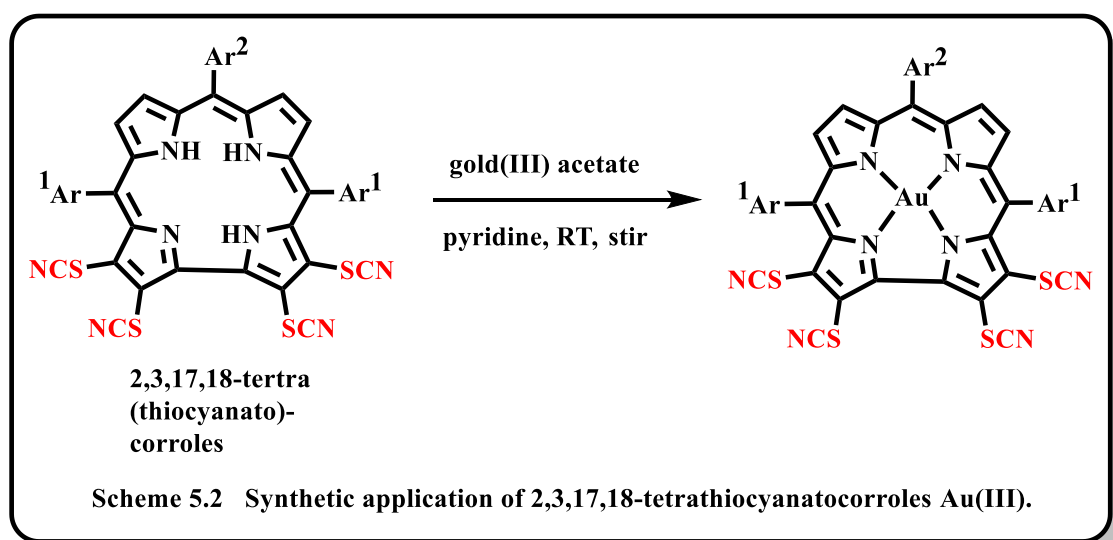
In the present case, we have used a 2,3,17,18-*tetra*-SCN-substituted FB corroles system as a ligand scaffold. Herein, we have described the synthesis and spectroscopic characterization of two new gold corrole complexes, namely, {2,3,17,18-tetra(thiocyanato)-10-(4-bromophenyl)-5,15-bis(4-cyanophenyl) corrolato-Au(III)}, **1**, and {2,3,17,18-tetrathiocyanato-10-(4,7-dimethoxynaphthalen-1-yl)-5,15-bis(4-cyanophenyl) corrolato-Au(III)}, **2** (Scheme 5.1). The full spectroscopic, structural characterization, and DFT calculations of these newly synthesized 2,3,17,18-tetrathiocyanato-corrolato-Au(III) complexes were reported herein. Single-crystal XRD analysis of a representative Au(III) derivative is also presented. The photophysical studies of the newly synthesized 2,3,17,18-tetrathiocyanato-corrolato-Au(III) complexes and their suitability as room temperature near-infrared phosphor is also

described. The potential of these complexes in singlet oxygen sensitization is also highlighted.



Synthesis and characterization:

FB 2,3,17,18-tetrathiocyanato corroles (FB = free base) were prepared by following an earlier literature method developed by us.^[45] Gold metalation was performed into the FB 2,3,17,18-tetrathiocyanato corrole cavity by using gold acetate as a metal precursor in an acetonitrile and pyridine mixture at RT {RT= room temperature) in the aerial condition (Scheme 5.2).^[29]

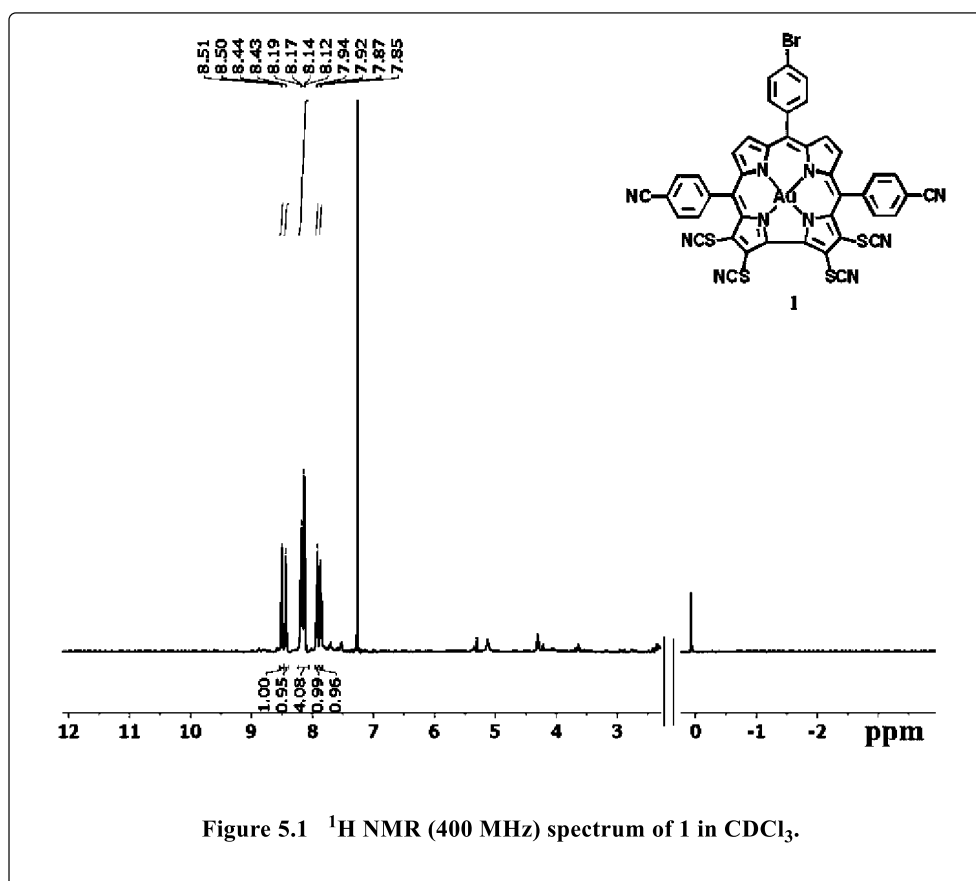


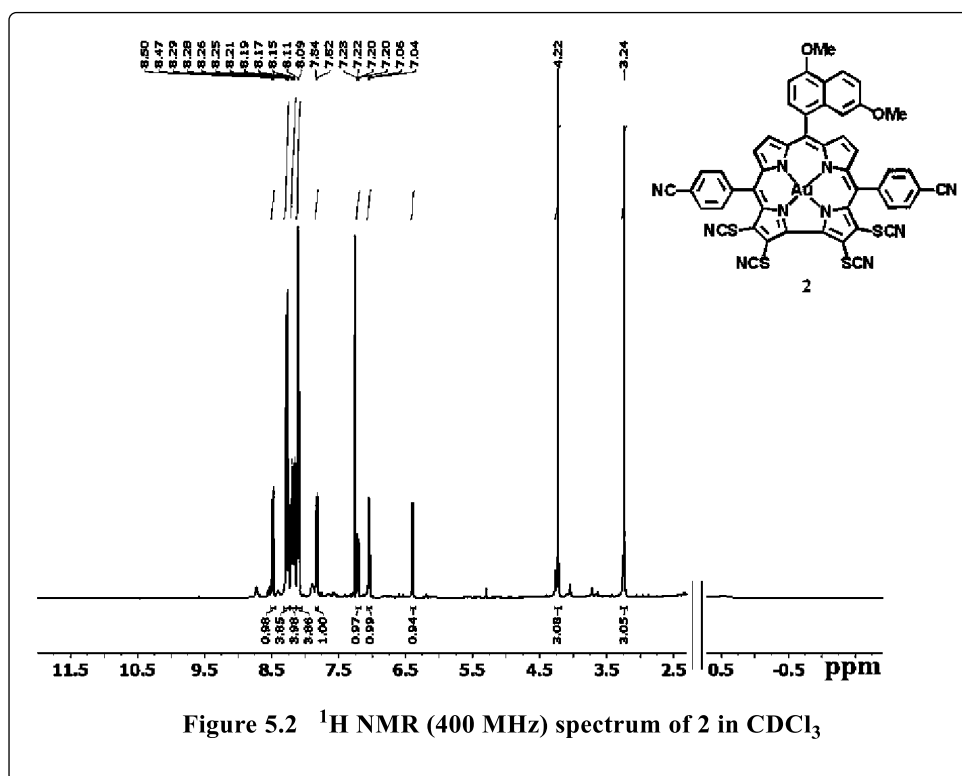
The composition and purity of the 2,3,17,18-tetra(thiocyanato) corrolato-Au (III) complexes (**1–2**) was established by a series of analytical techniques, i.e., CHN analyses, UV/Vis, FT-IR spectroscopy, ESI-HRMS, NMR, and single-crystal XRD analysis (Figures 5.2-5.7, Figure 5.9 & 5.10 ,Tables 5.1-5.2).

5.3 Spectral Characterization:

5.3.1 NMR Spectroscopy

The diamagnetic nature of the 2,3,17,18-tetra(thiocyanato)corrolato-Au(III) complexes (**1** and **2**) is evident from their sharp peaks with normal chemical shifts at the expected regions. The ^1H NMR spectrum of both **1** and **2** exhibits intense peaks in the region $\delta \sim 8.50\text{--}7.86$ ppm and $\delta \sim 8.49\text{--}6.40$ ppm respectively. In case of complex **2**, two sets of sharp singlets appeared at 4.22 and 3.24 ppm corresponds to two sets of methoxy protons (Figures 5.1 and 5.2).





5.3.2 Mass Spectrometry:

The electrospray mass spectrum showed the peaks centred HRMS (ESI) m/z : $[\mathbf{2}+\text{Na}]^+$
 Calcd for $\text{C}_{43}\text{H}_{16}\text{AuBrN}_{10}\text{S}_4\text{Na}$ 1098.9183; Found 1098.7538 (Figure 5.3).

The electrospray mass spectrum showed the peaks centred HRMS (ESI) m/z : $[\mathbf{1}+\text{Na}]^+$
 Calcd for $\text{C}_{49}\text{H}_{23}\text{AuN}_{10}\text{O}_2\text{S}_4\text{Na}$ 1131.0446; Found 1131.0570 (Figure 5.4).

5.3.3 IR Spectroscopy:

The FT-IR spectra (as KBr pellets) of **1** and **2** exhibited strong S-CN stretching vibration at 2164, and 2157 cm^{-1} , respectively (Figures 5.5).

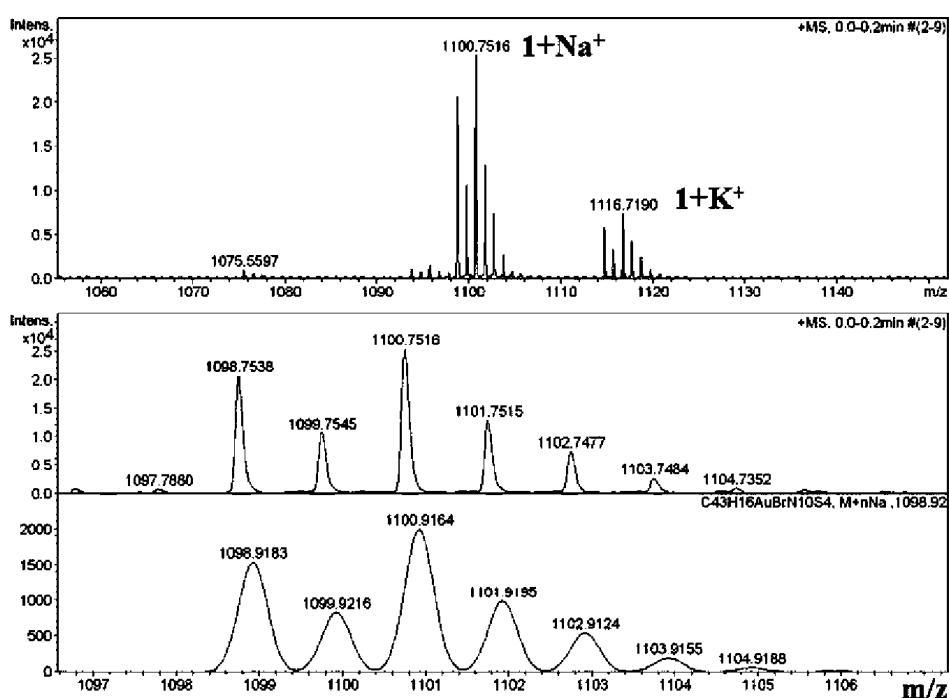


Figure 5.3 ESI- MS spectrum of 1 in CH_3CN shows the measured spectrum with isotopic distribution pattern

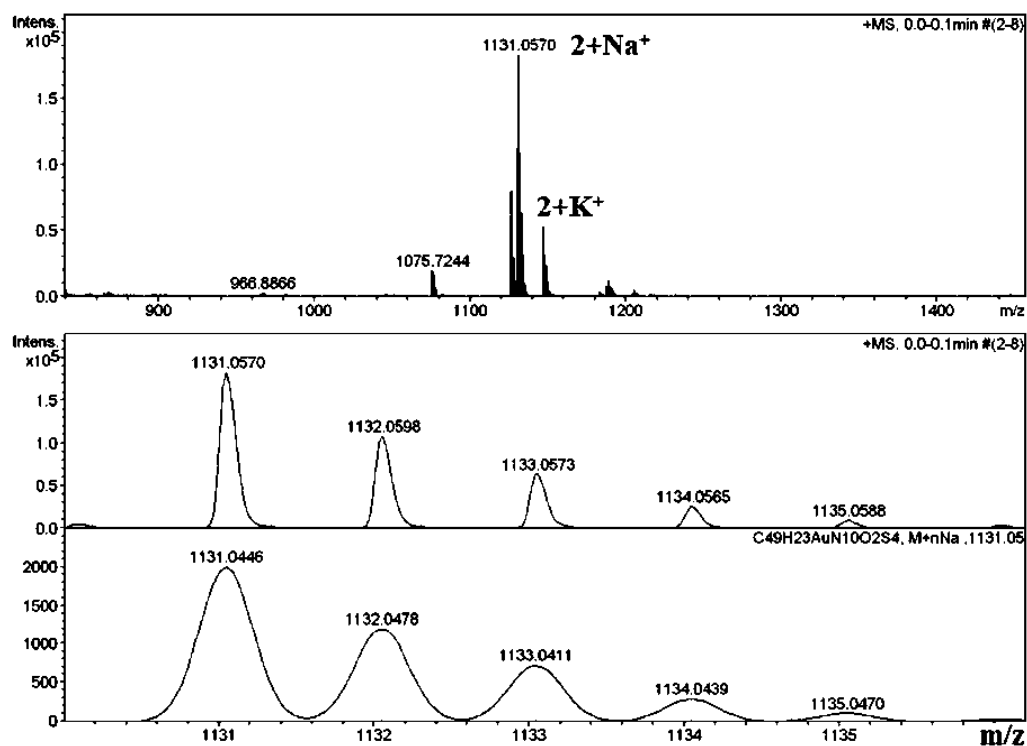
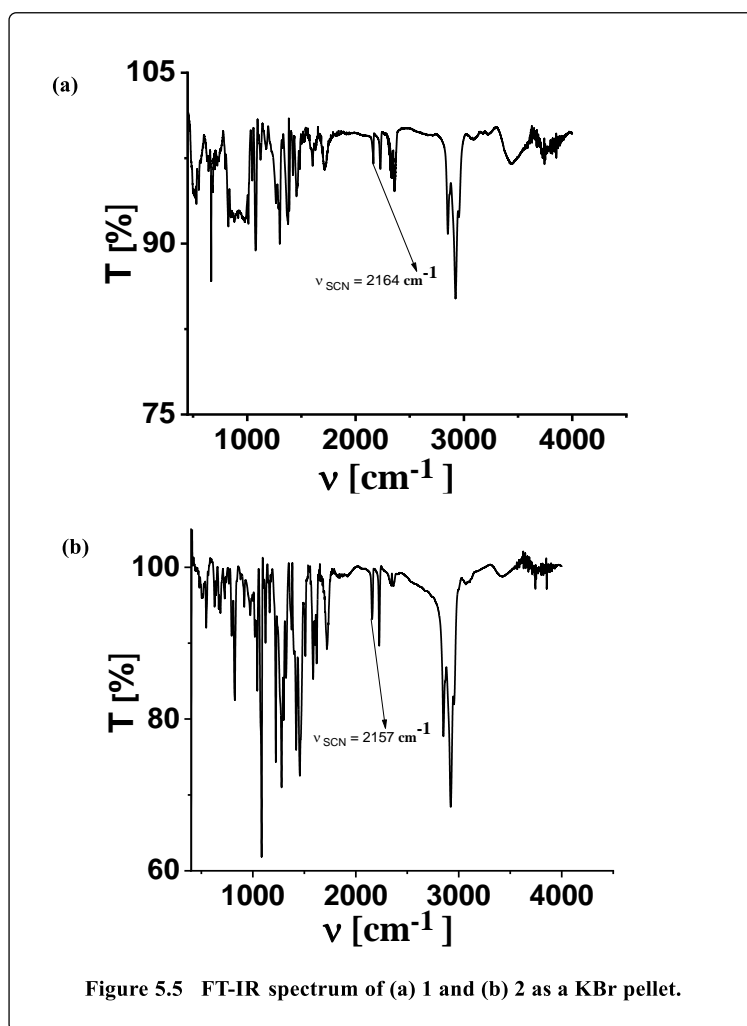


Figure 5.4 ESI- MS spectrum of 2 in CH_3CN shows the measured spectrum with isotopic distribution pattern



5.3.4 Crystal Structure:

The crystal system of *2,3,17,18-tetrathiocyanato-10-(4,7-dimethoxynaphthalen-1-yl)-5,15-bis(4-cyanophenyl) corrolato-Au(III)*, **2** is orthorhombic and the unit cell has sixteen molecules of **2** (Figure 5.6). Important crystallographic parameters for **2** are summarized in Table 5.1. Key features of the structure are similar to those observed in previously obtained structures for Au corroles. Thus, the Au-N bond distances are 1.95 ± 0.01 Å. Unlike Cu corroles,^[47] which are invariably saddled, **2**, like other Au corroles, is essentially planar with C2-C1-C19-C18 and C8-C9-C11-C12 dihedrals around only 6.7° and 14.7° . The saddling of Cu corroles reflects ligand noninnocence, as noted elsewhere, a scenario that does not apply to Au corroles.^{[29],[48]}

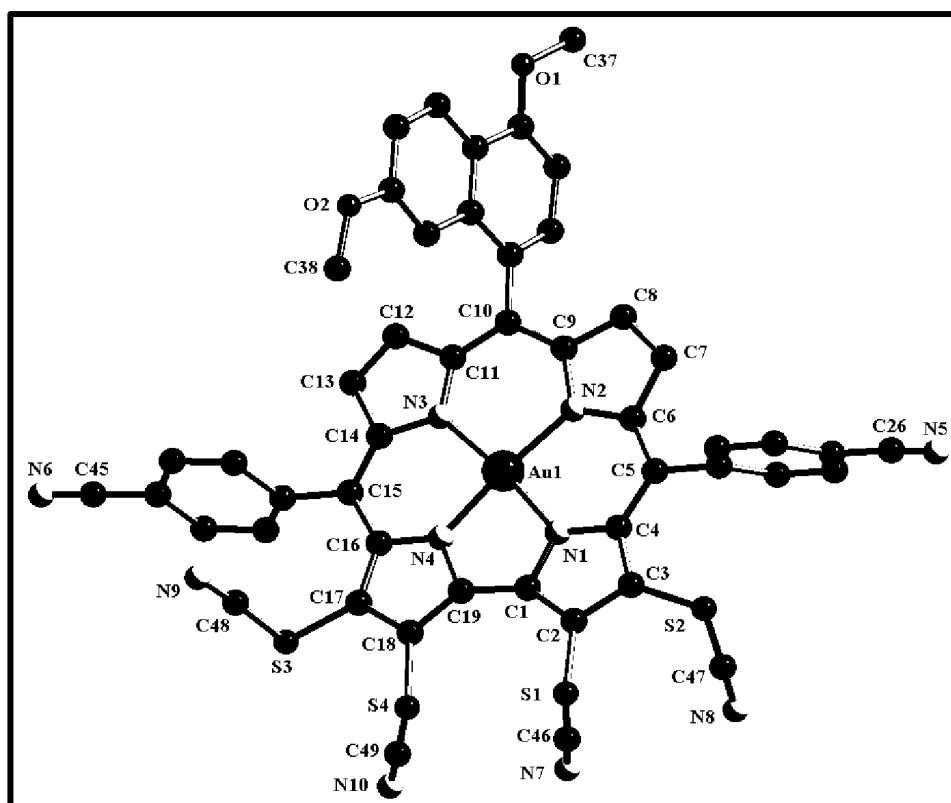


Figure 5.6 Single-crystal X-ray structure of **2**. Hydrogen atoms are omitted for clarity

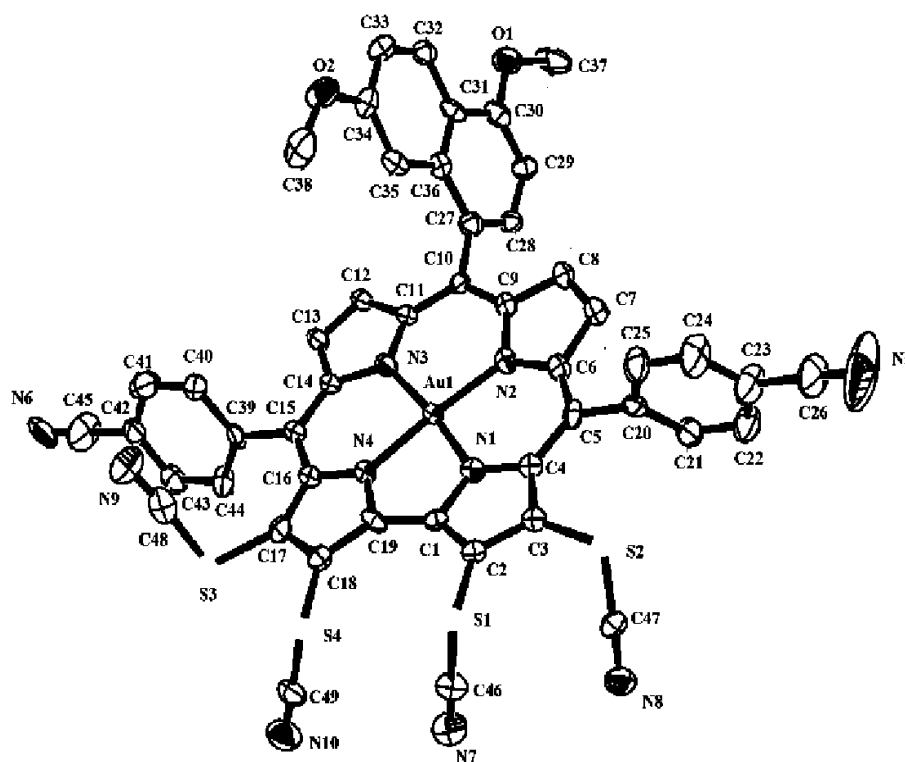


Figure 5.7 ORTEP diagram of **2**. Hydrogen atoms are omitted for clarity. Ellipsoids are drawn at 50% probability

Table 5.1 Crystallographic Data for **2**.

compound code	2
molecular formula	C ₄₉ H ₂₃ Au N ₁₀ O ₂ S ₄
Fw	1108.98
Radiation	Cu K α
crystal symmetry	Orthorhombic
space group	<i>F</i> <i>dd</i> 2
<i>a</i> (Å)	52.0552 (6)
<i>b</i> (Å)	51.4324 (5)
<i>c</i> (Å)	7.14602 (8)
α (deg)	90
β (deg)	90
γ (deg)	90
<i>V</i> (Å ³)	19132.2(4)
<i>Z</i>	16
μ (mm ⁻¹)	7.82
<i>T</i> (K)	100
<i>D</i> _{calcd} (g cm ⁻³)	1.540
2 θ range (deg)	3.78-77.12
<i>e</i> data (<i>R</i> _{int})	7692
R1 (<i>I</i> > 2 σ (<i>I</i>))	0.073
WR2 (all data)	0.168
GOF	1.04
$\Delta\rho_{\max}$, $\Delta\rho_{\min}$ (e Å ⁻³)	1.87, -1.55

5.3.5 Electrochemistry:

To understand the redox properties of **1** and **2**, the cyclic voltammetric and differential pulse voltammetric measurements were performed in dichloromethane (Figure 5.8 and Table 5.2). Tetraethyl ammonium perchlorate (TEAP, 0.1 M) was used as a supporting electrolyte and Ag/AgCl electrode was used as a reference electrode. The tetra(thiocyano)corrolato-Au(III) derivatives, **1** and **2** exhibited one reversible and one irreversible reductive couples. The 1st reversible reductive couple is observed at -0.66 V and the 2nd irreversible reduction couple is observed at -1.13V vs. Ag/AgCl for complex

1. This compound also exhibited one oxidative couple at 1.30 V. The 1st reversible reductive couple is observed at -0.69 V and the 2nd irreversible reduction couple is observed at -1.14V for complex **2**. This compound also exhibited one oxidative couple at 1.28 V. The separation between 1st oxidative couple and the 1st reductive couple is ~2.0 V in both of these complexes. The above redox potentials are dramatically upshifted, by roughly half a volt, relative to those of the non-thiocyanated complexes.^[33] These upshifts are consistent with the Hammett σ_p and σ_m of the SCN groups, which are about the same as those of CN and CF₃ groups. The σ_p and σ_m values for SCN group are 0.52 and 0.51 respectively. The corresponding values for CN group are 0.66 and 0.56 respectively. The values for CF₃ group are 0.54 and 0.43 respectively.^[49] Interestingly, thiocyanato groups have been much less frequently deployed as electron-withdrawing substituents than CN and CF₃, indicating that they may deserve broader exploration. Careful examination of Table 2 shows that tetrathiocyanato-substitution upshifts the reduction potentials somewhat more than the oxidation potentials, resulting in a smaller electrochemical HOMO-LUMO gap for **1** and **2** (about 1.95-2.0 V) than for their non-thiocyanated counterparts.

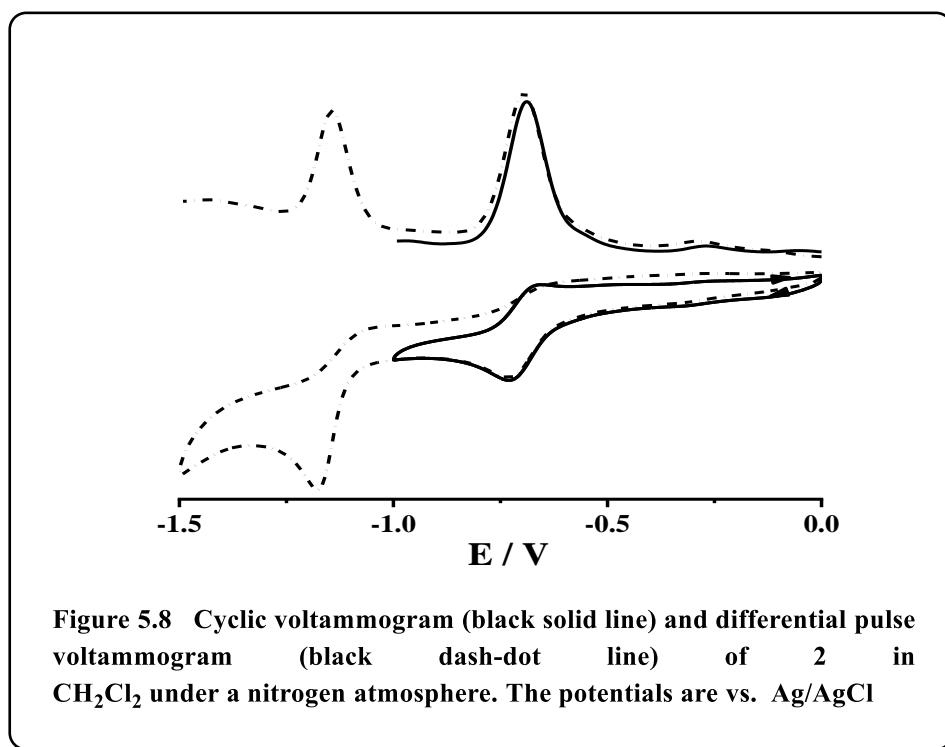


Table 5.2 UV–Vis and electrochemical data of compounds **1**, **2**, **1a** (β -unsubstituted corrolato-Au(III) analogue of compound **1**), and **2a**^[33] (β -unsubstituted corrolato-Au(III) analogue of compound **2**) in dichloromethane.

Compound	UV–vis. Data ^a $\lambda_{\text{max}} / \text{nm} (\epsilon / \text{M}^{-1}\text{cm}^{-1})$	Electrochemical data ^{a,b}	
		Oxidation $E^0, \text{V} (\Delta E_{\text{p}}, \text{mV})$	Reduction $E^0, \text{V} (\Delta E_{\text{p}}, \text{mV})$
1	403 (44000), 421 (40800), 537(12200), 554(17300), 578 (37700), 595 (45000)	+1.30	-0.66 (90), -1.13
2	403 (45800), 422 (41000), 537(13800), 554 (19000), 580 (43000), 596 (42100)	+1.28	-0.69 (90), -1.14
1a ^c	422 (131000), 495 (6400), 533 (15500), 570 (64000)	+0.78(80), +1.15(80)	-1.28(80)
2a ³⁴	423 (142000), 494 (3700), 533 (9300), 572 (37000)	+0.88(70), +1.25(80)	-1.32(80), -1.67(80)

^a In dichloromethane.

^b The potentials are vs. Ag/AgCl, ^c Unpublished data

5.3.6 Photophysical properties:

The UV-Vis spectra of tetra (thiocyanato) corrolato-Au(III) derivatives **1-2** are significantly modified in comparison to the β -unsubstituted corrolato-Au(III) derivatives (see Figure 5.9 & 5.10 for a direct comparison in dichloromethane solution).^[33] The Soret band is splitted into at least two distinct bands and so also the Q bands. The tail of Q bands reached up to 650 nm. This kind of absorption profile is clearly absent in the case of β -unsubstituted corrolato-Au(III) derivatives with similar corrole backbone.^[33]

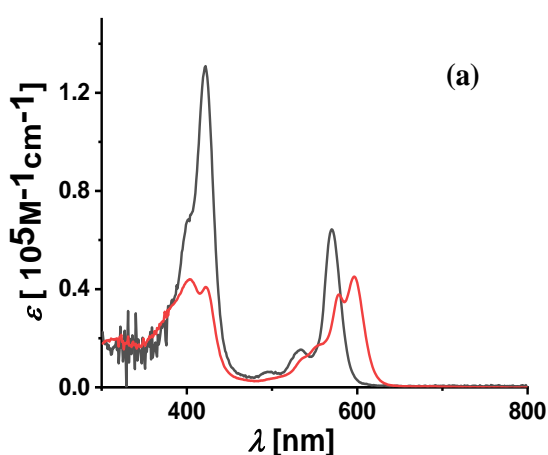


Figure 5.9 (a) Electronic absorption spectra of compounds 1 (red solid line) and 1a (black solid line)(β -unsubstituted corrolato-Au(III) analogue of compound 1).

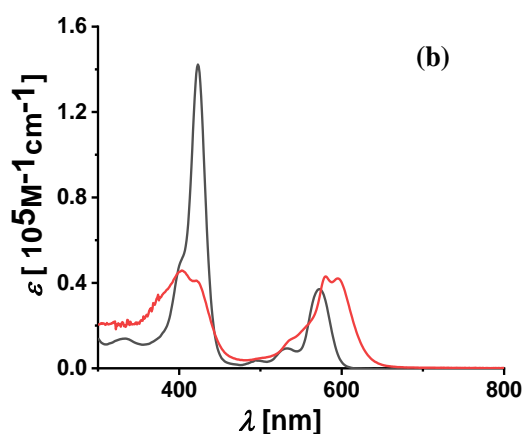
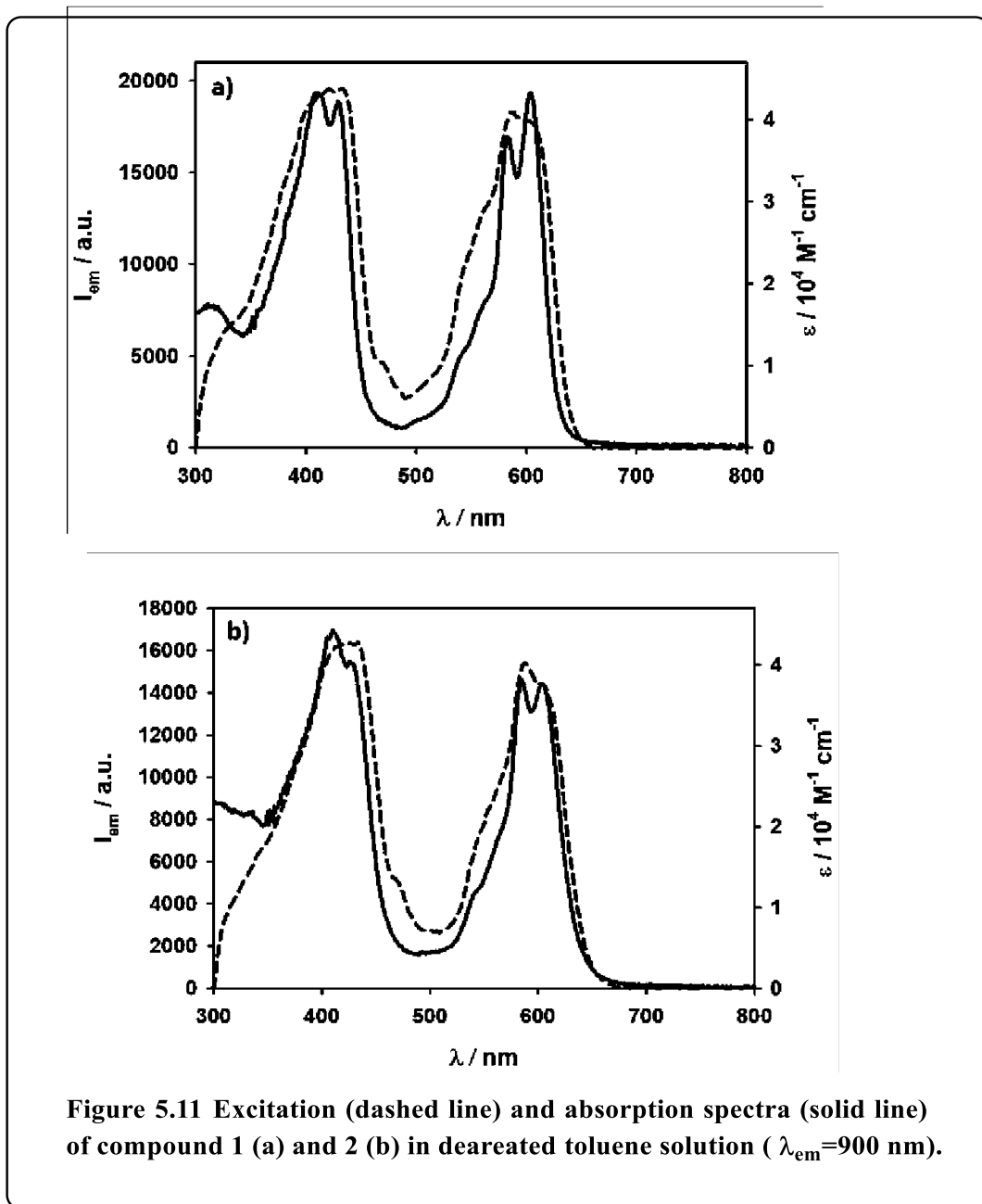


Figure 5.10 (b) Electronic absorption spectra of compounds 2 (red solid line)and 2a (black solid line)(β -unsubstituted corrolato-Au(III) analogue of compound 2) in dichloromethane.

The 2,3,17,18-*tetra*-SCN-substitution in corrole periphery thus can alter the HOMO and LUMO energy spacing and thus can essentially change the transition energies for Q bands. The Q absorption bands of these β -substituted corrolato-Au(III) derivatives are peaked in the red spectral region, a suitable window for PDT and other bioimaging applications, which are not possible in the frequently encountered β -unsubstituted corrolato metal complexes.

Table 5.3 UV–Vis data in dichloromethane^a

Compound	UV–vis. Data
	λ_{max} / nm (ϵ / $M^{-1}cm^{-1}$)
1	403 (44000), 421 (40800), 537(12200), 554(17300), 578 (37700), 595 (45000)
2	403 (45800), 422 (41000), 537(13800), 554 (19000), 580 (43000), 596 (42100)

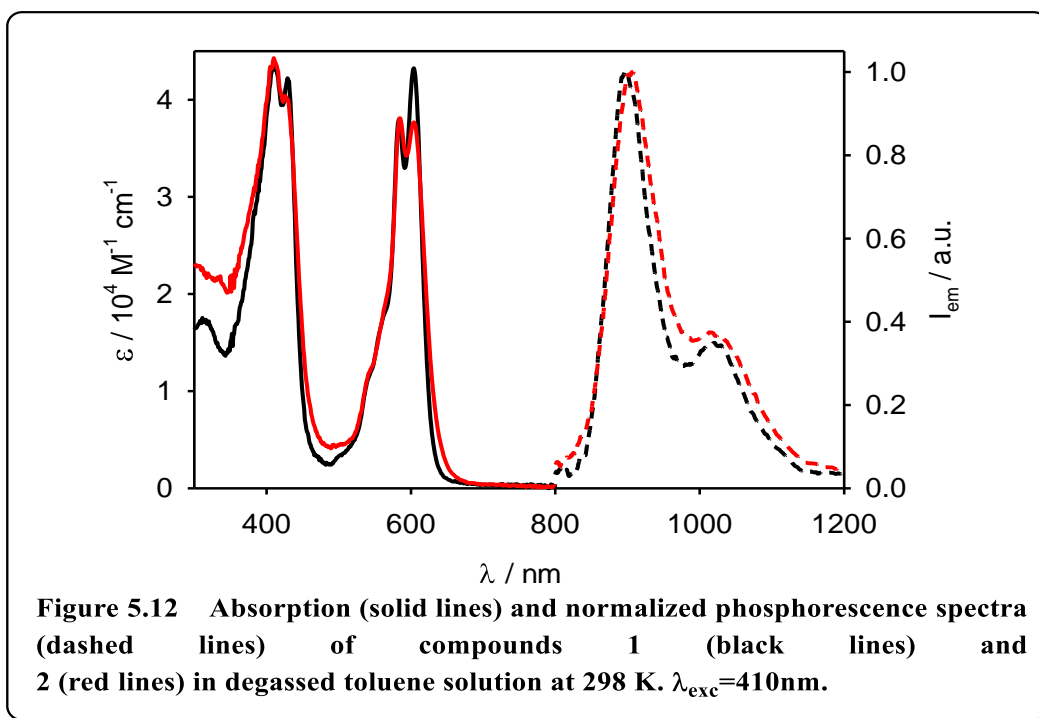
^a Error limits : λ_{max} , ± 1 nm and ϵ , $\pm 10\%$

Compounds **1** and **2** exhibit an emission band peaked at ca. 900 nm (Figure 5.11) in degassed toluene solution ($\lambda_{exc} = 410\text{nm}$). The excitation spectra registered at the emission maximum closely match the corresponding absorption spectra (Figure 5.11), demonstrating that the Au(III) corrolato complexes are responsible for this near infrared emission. The emission intensity decays can be fitted by a mono exponential curve with lifetimes of 10 μs for both complexes, demonstrating that the observed radiative decay is phosphorescence. As previously reported in the literature,^[36] we observe a strong solvent effect on the emission quantum yield: indeed, no emission could be detected for degassed chloroform solutions of **1** and **2**. Compounds **1** and **2** can efficiently sensitize singlet oxygen population (Table 5.3), as demonstrated by the characteristic phosphorescence of singlet oxygen at 1270 nm upon selective excitation of Au (III) corrolato complexes at 615 nm in chloroform solution.

Table 5.4 Most important photophysical data of compounds 1 and 2 in toluene solution at 298 K, unless otherwise noted.

	λ_{abs} /nm	$\epsilon / 10^4 \text{ M}^{-1} \text{ cm}^{-1}$	λ_{em} /nm	Φ_{em}^a	$\tau / \mu\text{s}$	$\Phi(^1\text{O}_2)^b$
1	409, 603	4.33, 4.32	898	0.28%	9.98	57%
2	409, 604	4.42, 3.76	905	0.30%	10.18	46%

^aEmission quantum yields measured in degassed toluene solution. ^bQuantum yield of singlet oxygen ($^1\text{O}_2$) population in chloroform solution upon excitation at 615 nm.



5.4 DFT and TDDFT calculations

Scalar-relativistic (ZORA) DFT and TDDFT calculations provide a coherent rationale for many of the experimental observations outlined above. The experimentally studied compounds were modeled with Au[TPC] and Au[TPC(SCN)₄]. The calculations were carried out with three different exchange-correlation functionals (OLYP, B3LYP, and B3LYP*) and all-electron ZORA STO-TZ2P basis sets. The optimized geometries of Au[TPC] and Au[TPC(SCN)₄] (Figure 5.13) proved nicely consistent with experimental results on simple Au-triaryl-corroles and **2**. Thus, the calculated Au-N distances were in essentially perfect agreement with experiment. The calculations also confirmed the essential planarity or very mild saddling of the corrole macrocycle. Interestingly, examination of the optimized geometries revealed an interesting larger skeletal bond distance alternations for Au[TPC(SCN)₄] than for Au[TPC], which appear to be consistent with experimental crystal structures. Also, Au[TPC(SCN)₄] exhibits a longer pyrrole-pyrrole linkage than Au[TPC], indicating reduced aromatic character after thiocyanation.

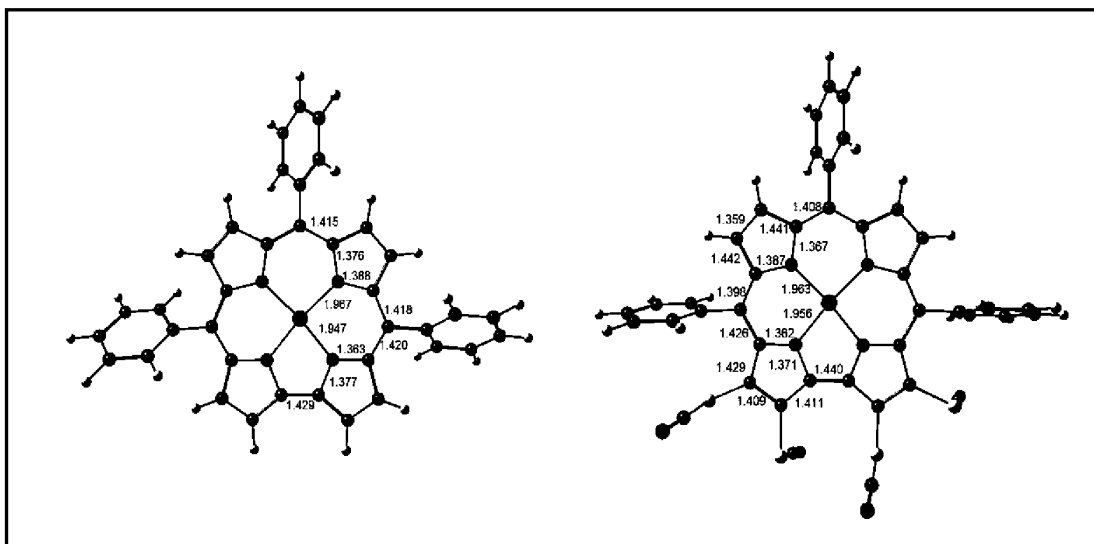


Fig.5.13 Selected distances (Å) in the optimized geometries of Au[TPC] and Au[TPC(SCN)₄].

Table 5.5 presents DFT calculations of the gas-phase IPs and EAs (both vertical and adiabatic) of Au[TPC] and Au[TPC(SCN)₄]. Based on earlier simulations of photoelectron spectra and redox potentials, these values are thought to be semi quantitatively accurate. This conclusion is bolstered by the high level of consistency among the three functionals used, even though we believe the B3LYP* values as the most accurate. The calculations confirm the very strong electron-withdrawing effect of the thiocyno groups. Tetrathiocyanation upshifts the IP and EA of Au[TPC] by 0.9 and 1.3 eV, respectively. The higher substituent effects (relative to what is observed electrochemically) are typical of gas-phase results. The spin density profiles of the ionized states of Au[TPC(SCN)₄], however, are very similar to those of unsubstituted Au(TPC), indicating that the qualitative shapes of the redox-active MOs are not affected by the thiocyno groups.

Table 5.5. Calculated IPs and EAs (eV).

Compound	Functional	Adiabatic		Vertical	
		IP	EA	IP	EA
Au[TPC]	OLYP	5.97	1.32	6.01	1.14
	B3LYP	6.04	1.39	6.11	1.28
	B3LYP*	6.04	1.38	6.11	1.27
Au[TPC(SCN) ₄]	OLYP	6.43	2.46	6.80	2.34
	B3LYP	6.93	2.68	7.11	2.61
	B3LYP*	6.94	2.67	7.14	2.60

Figure 5.14 presents the B3LYP* simulated TDDFT spectra of Au[TPC] and Au[TPC(SCN)₄] in dichloromethane using the COSMO solvation model. The corresponding data are of presented in Table 5.6 and relevant MOs are depicted in Figure 5.15 and Fig. 5.16, respectively. Observe that the calculations qualitatively reproduce the two spectral features emphasized above, namely a sharp reduction in the Soret band intensity and a red shift of the lowest-energy Q band upon thiocyanation. Both these features appear to be related to the reduction of macrocycle aromaticity upon thiocyanation. The Kohn-Sham orbital energies are also qualitatively consistent with the dramatic upshifts in both oxidation and reduction potential upon thiocyanation. Also consistent with experiment is the higher upshift of the LUMO energy, compared to the HOMO, which results in a narrowing of the HOMO-LUMO gap. which results in a narrowing of the HOMO-LUMO gap and a widening of the LUMO/LUMO+1 gap (the so-called Δ LUMO, according to Michl's perimeter model. The latter also provides an alternative explanation of the relative intensity of the Q band. Thiocyanation also significantly upshifts the Au 5d_{x²-y²} orbital, the LUMO +2, but to a lesser degree than the LUMO.

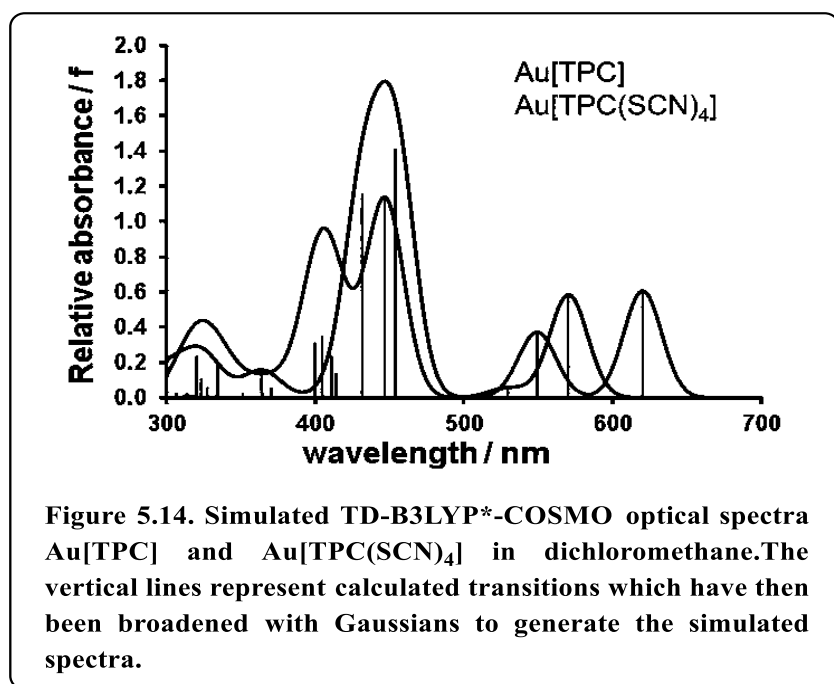


Table 5.6. B3LYP*/ZORA-STO-TZ2P TDDFT results, including transition energies (E) and wavelengths (λ), oscillator strengths (f), MO compositions, and excited state irreps.

Compound	Peak	E (eV)	λ (nm)	f	Weight	From	To	C_2 irrep	
Au[TPC]	Q	2.17	570.3	0.58	92%	HOMO	LUMO	B	
					7%	HOMO-1	LUMO+1	B	
			2.34	529.4	0.05	71%	HOMO-1	LUMO	A
					28%	HOMO	LUMO+1	A	
	Soret	2.73	454.0	1.42	69%	HOMO	LUMO+1	A	
					27%	HOMO-1	LUMO	A	
			2.87	431.8	1.16	91%	HOMO-1	LUMO+1	B
					6%	HOMO	LUMO	B	
	Au[TPC(SCN) ₄]	Q	2.00	620.4	0.61	96%	HOMO	LUMO	B
						3%	HOMO-1	LUMO+1	B
			2.26	549.3	0.37	89%	HOMO-1	LUMO	A
					10%	HOMO	LUMO+1	A	
Soret		2.77	446.9	1.13	83%	HOMO	LUMO+1	A	
					8%	HOMO-1	LUMO	A	
					6%	HOMO-3	LUMO	A	
			2.99	414.0	0.14	78%	HOMO-1	LUMO+2	B
					11%	HOMO-1	LUMO+1	B	
					9%	HOMO-2	LUMO	B	
			3.02	410.9	0.24	58%	HOMO-2	LUMO	B
					21%	HOMO-1	LUMO+1	B	
					19%	HOMO-1	LUMO+2	B	
		3.06	404.7	0.35	60%	HOMO-1	LUMO+1	B	
				30%	HOMO-2	LUMO	B		
		3.10	399.7	0.31	92%	HOMO-3	LUMO	A	

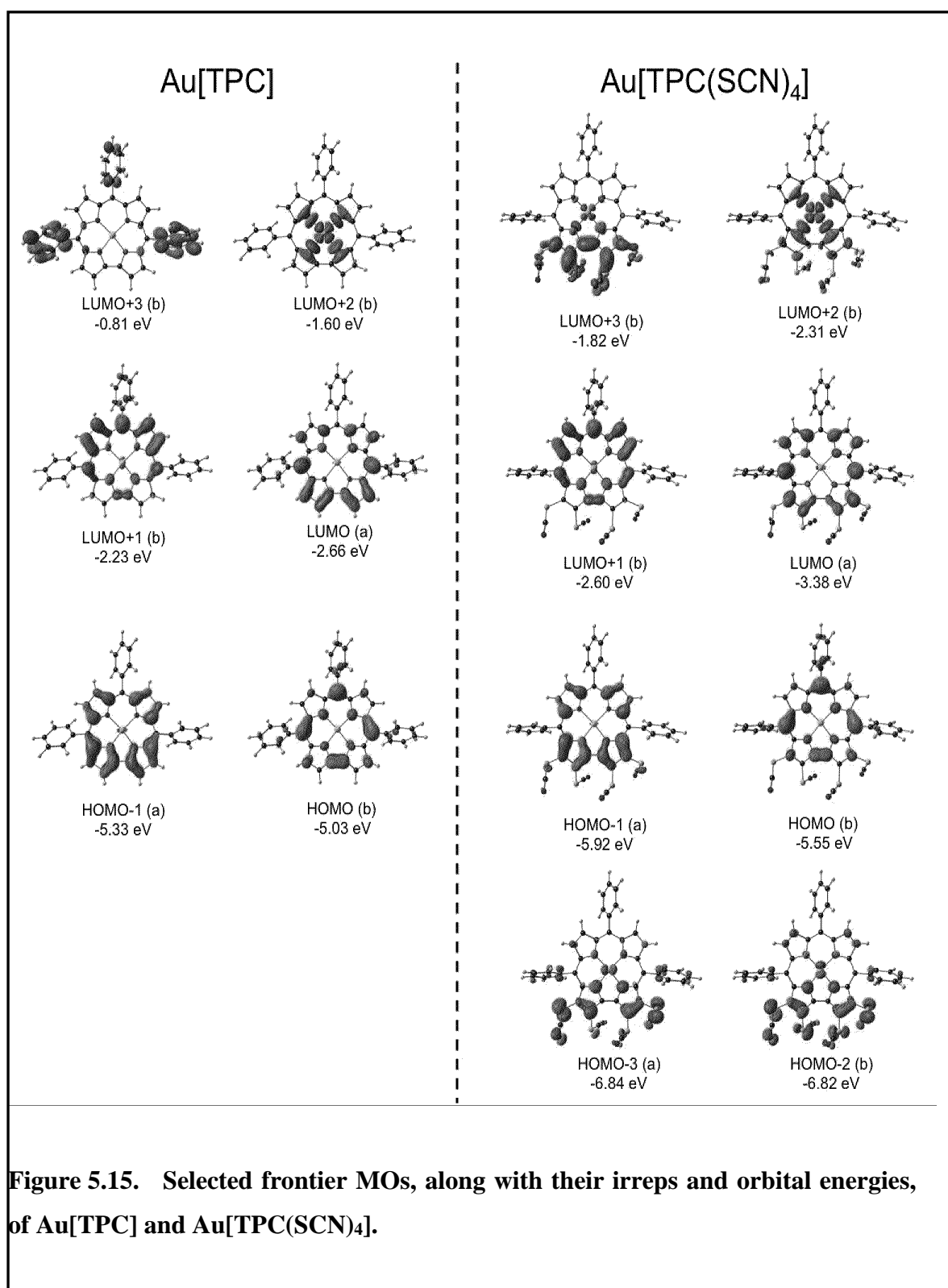
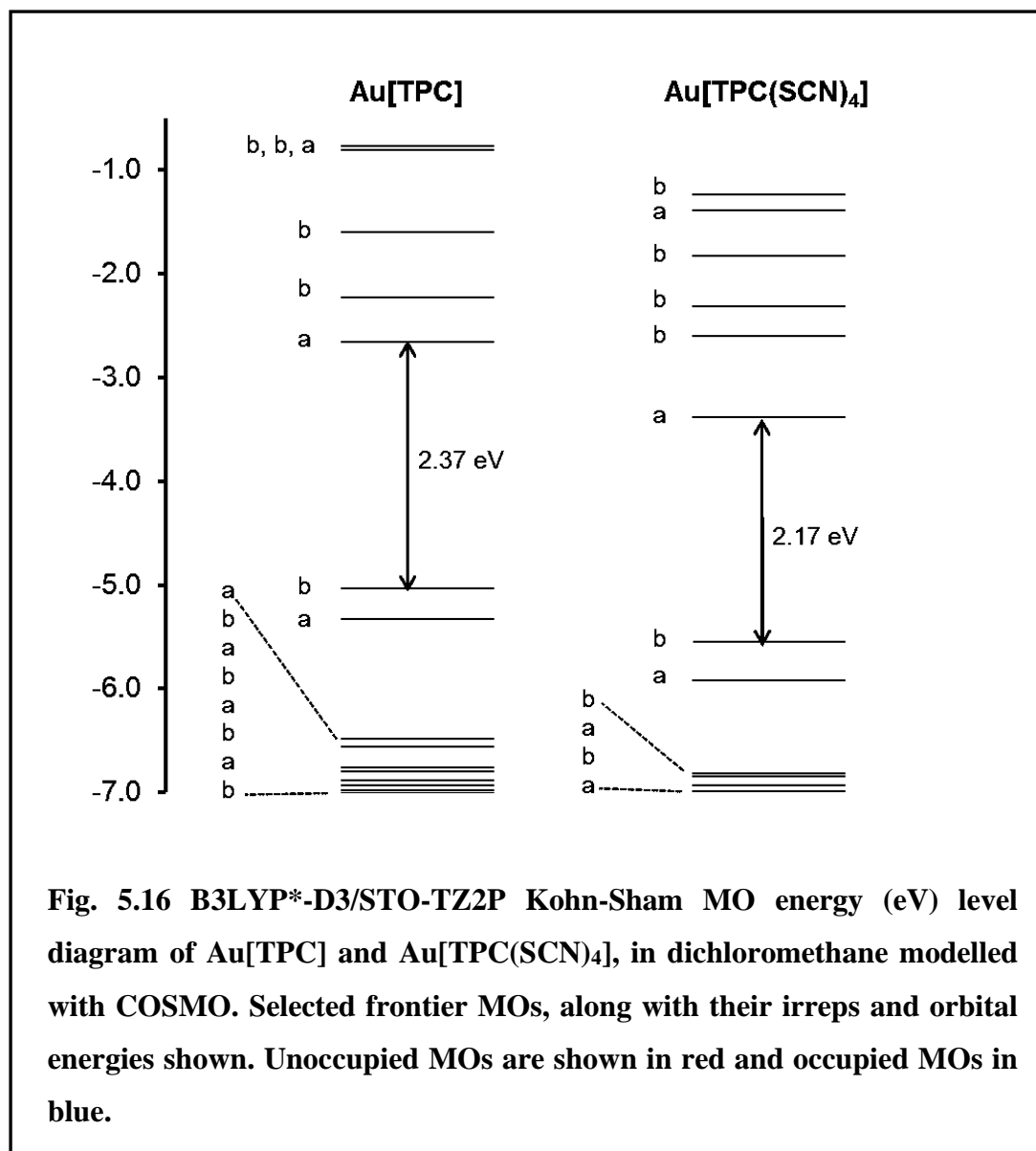


Figure 5.15. Selected frontier MOs, along with their irreps and orbital energies, of Au[TPC] and Au[TPC(SCN)₄].



All compounds were optimized the ZORA Hamiltonian, ZORA/TZ2P basis set, all electron, B3LYP* functional and the Grimme's D3 dispersion correction in the gas phase.

1. Au[TPC] neutral

Au	0.000000000	0.000000000	0.119826000
N	1.387793000	-0.430310000	-1.207558000
N	-1.387793000	0.430310000	-1.207558000
N	-1.183226000	0.419214000	1.610131000
N	1.183226000	-0.419214000	1.610131000
C	2.652323000	-0.898745000	-0.886863000
C	3.276527000	-1.204661000	-2.145453000
C	2.399357000	-0.914718000	-3.153351000
C	1.186841000	-0.415274000	-2.565452000

C	0.000000000	0.000000000	-3.209169000
C	-1.186841000	0.415274000	-2.565452000
C	-2.399357000	0.914718000	-3.153351000
C	-3.276527000	1.204661000	-2.145453000
C	-2.652323000	0.898745000	-0.886863000
C	-3.190925000	1.063587000	0.409652000
C	-2.482544000	0.823232000	1.613371000
C	-2.842876000	0.894181000	2.998862000
C	-1.740030000	0.533910000	3.760570000
C	-0.678175000	0.224102000	2.870466000
C	0.678175000	-0.224102000	2.870466000
C	1.740030000	-0.533910000	3.760570000
C	2.842876000	-0.894181000	2.998862000
C	2.482544000	-0.823232000	1.613371000
C	3.190925000	-1.063587000	0.409652000
C	4.598582000	-1.527350000	0.529434000
C	4.899367000	-2.722774000	1.190874000
C	6.214463000	-3.154043000	1.316415000
C	7.253391000	-2.396600000	0.785189000
C	6.967545000	-1.204283000	0.128136000
C	5.652115000	-0.773992000	0.001181000
C	0.000000000	0.000000000	-4.699407000
C	0.858651000	0.840232000	-5.414522000
C	0.860069000	0.840027000	-6.804448000
C	0.000000000	0.000000000	-7.504495000
C	-0.860069000	-0.840027000	-6.804448000
C	-0.858651000	-0.840232000	-5.414522000
C	-4.598582000	1.527350000	0.529434000
C	-5.652115000	0.773992000	0.001181000
C	-6.967545000	1.204283000	0.128136000
C	-7.253391000	2.396600000	0.785189000
C	-6.214463000	3.154043000	1.316415000
C	-4.899367000	2.722774000	1.190874000
H	4.091511000	-3.319901000	1.596698000
H	6.427156000	-4.087073000	1.825626000
H	8.279131000	-2.732561000	0.883869000
H	7.771106000	-0.602892000	-0.281419000
H	5.433443000	0.161828000	-0.499448000
H	-1.521819000	-1.503405000	-4.871555000
H	1.521819000	1.503405000	-4.871555000
H	1.529558000	1.502344000	-7.341104000
H	0.000000000	0.000000000	-8.588292000
H	-1.529558000	-1.502344000	-7.341104000
H	-4.091511000	3.319901000	1.596698000
H	-6.427156000	4.087073000	1.825626000
H	-8.279131000	2.732561000	0.883869000
H	-7.771106000	0.602892000	-0.281419000
H	-5.433443000	-0.161828000	-0.499448000
H	-4.269021000	1.611509000	-2.252301000
H	-2.561336000	1.046541000	-4.210645000

H	2.561336000	-1.046541000	-4.210645000
H	4.269021000	-1.611509000	-2.252301000
H	3.814373000	-1.174365000	3.373223000
H	1.694186000	-0.488881000	4.837674000
H	-1.694186000	0.488881000	4.837674000
H	-3.814373000	1.174365000	3.373223000

2. Au[TPC] anion

Au	0.000000000	0.000000000	0.132052000
N	1.403401000	-0.416291000	-1.201251000
N	-1.403401000	0.416291000	-1.201251000
N	-1.191845000	0.428995000	1.624300000
N	1.191845000	-0.428995000	1.624300000
C	2.666439000	-0.892577000	-0.886549000
C	3.274163000	-1.215279000	-2.149633000
C	2.386582000	-0.925623000	-3.156746000
C	1.190288000	-0.413711000	-2.569026000
C	0.000000000	0.000000000	-3.205521000
C	-1.190288000	0.413711000	-2.569026000
C	-2.386582000	0.925623000	-3.156746000
C	-3.274163000	1.215279000	-2.149633000
C	-2.666439000	0.892577000	-0.886549000
C	-3.214805000	1.063704000	0.409525000
C	-2.494670000	0.828324000	1.633081000
C	-2.853906000	0.887811000	3.004667000
C	-1.733017000	0.518688000	3.775054000
C	-0.687021000	0.223972000	2.890742000
C	0.687021000	-0.223972000	2.890742000
C	1.733017000	-0.518688000	3.775054000
C	2.853906000	-0.887811000	3.004667000
C	2.494670000	-0.828324000	1.633081000
C	3.805000	-1.063704000	0.409525000
C	4.615298000	-1.522820000	0.525940000
C	4.951824000	-2.630533000	1.321232000
C	6.266096000	-3.062148000	1.442216000
C	7.291742000	-2.400389000	0.771347000
C	6.979510000	-1.297261000	-0.018537000
C	5.664853000	-0.864047000	-0.134662000
C	0.000000000	0.000000000	-4.694530000
C	0.882835000	0.812108000	-5.415521000
C	0.886102000	0.811122000	-6.805939000
C	0.000000000	0.000000000	-7.508300000
C	-0.886102000	-0.811122000	-6.805939000
C	-0.882835000	-0.812108000	-5.415521000
C	-4.615298000	1.522820000	0.525940000
C	-5.664853000	0.864047000	-0.134662000
C	-6.979510000	1.297261000	-0.018537000
C	-7.291742000	2.400389000	0.771347000
C	-6.266096000	3.062148000	1.442216000

C	-4.951824000	2.630533000	1.321232000
H	4.160105000	-3.160715000	1.836532000
H	6.490035000	-3.927793000	2.057258000
H	8.318242000	-2.737604000	0.865052000
H	7.767076000	-0.761641000	-0.538739000
H	5.436001000	0.008334000	-0.734968000
H	-1.567080000	-1.451115000	-4.869982000
H	1.567080000	1.451115000	-4.869982000
H	1.577630000	1.452259000	-7.342155000
H	0.000000000	0.000000000	-8.592901000
H	-1.577630000	-1.452259000	-7.342155000
H	-4.160105000	3.160715000	1.836532000
H	-6.490035000	3.927793000	2.057258000
H	-8.318242000	2.737604000	0.865052000
H	-7.767076000	0.761641000	-0.538739000
H	-5.436001000	-0.008334000	-0.734968000
H	-4.258209000	1.639267000	-2.266560000
H	-2.541888000	1.073064000	-4.213709000
H	2.541888000	-1.073064000	-4.213709000
H	4.258209000	-1.639267000	-2.266560000
H	3.826086000	-1.156956000	3.385587000
H	1.686862000	-0.466727000	4.852528000
H	-1.686862000	0.466727000	4.852528000
H	-3.826086000	1.156956000	3.385587000

3. Au[TPC] cation

Au	0.000000000	0.000000000	0.116982000
N	1.395230000	-0.421615000	-1.210958000
N	-1.395230000	0.421615000	-1.210958000
N	-1.183004000	0.423309000	1.607590000
N	1.183004000	-0.423309000	1.607590000
C	2.645613000	-0.903266000	-0.897974000
C	3.260671000	-1.248633000	-2.141845000
C	2.381141000	-0.960138000	-3.155290000
C	1.191932000	-0.427382000	-2.568325000
C	0.000000000	0.000000000	-3.215172000
C	-1.191932000	0.427382000	-2.568325000
C	-2.381141000	0.960138000	-3.155290000
C	-3.260671000	1.248633000	-2.141845000
C	-2.645613000	0.903266000	-0.897974000
C	-3.196953000	1.063651000	0.420664000
C	-2.488039000	0.822248000	1.615618000
C	-2.848557000	0.877161000	3.004420000
C	-1.743362000	0.521748000	3.760246000
C	-0.686936000	0.226370000	2.858658000
C	0.686936000	-0.226370000	2.858658000
C	1.743362000	-0.521748000	3.760246000
C	2.848557000	-0.877161000	3.004420000
C	2.488039000	-0.822248000	1.615618000

C	3.196953000	-1.063651000	0.420664000
C	4.598338000	-1.517993000	0.531428000
C	4.920269000	-2.646715000	1.297825000
C	6.238317000	-3.067151000	1.411634000
C	7.255326000	-2.359844000	0.778917000
C	6.948353000	-1.231827000	0.023830000
C	5.630791000	-0.817765000	-0.107885000
C	0.000000000	0.000000000	-4.695532000
C	0.949186000	0.745028000	-5.407489000
C	0.940794000	0.751587000	-6.795291000
C	0.000000000	0.000000000	-7.492376000
C	-0.940794000	-0.751587000	-6.795291000
C	-0.949186000	-0.745028000	-5.407489000
C	-4.598338000	1.517993000	0.531428000
C	-5.630791000	0.817765000	-0.107885000
C	-6.948353000	1.231827000	0.023830000
C	-7.255326000	2.359844000	0.778917000
C	-6.238317000	3.067151000	1.411634000
C	-4.920269000	2.646715000	1.297825000
H	4.129242000	-3.210098000	1.777499000
H	6.470887000	-3.952589000	1.990911000
H	8.284068000	-2.686277000	0.873456000
H	7.738184000	-0.669732000	-0.460031000
H	5.398916000	0.070611000	-0.682814000
H	-1.676363000	-1.339754000	-4.867935000
H	1.676363000	1.339754000	-4.867935000
H	1.668083000	1.347486000	-7.333648000
H	0.000000000	0.000000000	-8.575825000
H	-1.668083000	-1.347486000	-7.333648000
H	-4.129242000	3.210098000	1.777499000
H	-6.470887000	3.952589000	1.990911000
H	-8.284068000	2.686277000	0.873456000
H	-7.738184000	0.669732000	-0.460031000
H	-5.398916000	-0.070611000	-0.682814000
H	-4.240419000	1.684214000	-2.245750000
H	-2.534236000	1.123528000	-4.209014000
H	2.534236000	-1.123528000	-4.209014000
H	4.240419000	-1.684214000	-2.245750000
H	3.822814000	-1.140357000	3.382870000
H	1.692734000	-0.466721000	4.836129000
H	-1.692734000	0.466721000	4.836129000
H	-3.822814000	1.140357000	3.382870000

4. Au[TPC(SCN)₄] neutral

Au	0.000000000	0.000000000	0.638463000
C	0.000000000	0.000000000	3.979289000
C	0.000000000	0.000000000	5.472628000
C	0.000000000	0.000000000	8.268736000

C	0.064467000	-1.201358000	7.571324000
C	0.066261000	-1.201437000	6.180809000
C	0.712840000	-0.103893000	-2.114371000
C	1.235360000	-0.179119000	3.331219000
C	1.334725000	-1.698640000	-5.182199000
C	1.803389000	-0.272279000	-2.999061000
C	2.538455000	-0.328243000	3.926260000
C	2.600812000	-0.391226000	-0.842053000
C	2.758753000	-0.398969000	1.658393000
C	2.965593000	-0.460456000	-2.224825000
C	3.329022000	-0.482692000	0.381607000
C	3.450722000	-0.459976000	2.923791000
C	4.812323000	-0.654160000	0.344739000
C	5.235804000	0.637217000	-3.094142000
C	5.384147000	-1.914353000	0.524984000
C	5.641568000	0.454085000	0.173402000
C	6.765760000	-2.064321000	0.520530000
C	7.022943000	0.303007000	0.169301000
C	7.587345000	-0.955745000	0.342052000
C	-0.064467000	1.201358000	7.571324000
C	-0.066261000	1.201437000	6.180809000
C	-0.712840000	0.103893000	-2.114371000
C	-1.235360000	0.179119000	3.331219000
C	-1.334725000	1.698640000	-5.182199000
C	-1.803389000	0.272279000	-2.999061000
C	-2.538455000	0.328243000	3.926260000
C	-2.600812000	0.391226000	-0.842053000
C	-2.758753000	0.398969000	1.658393000
C	-2.965593000	0.460456000	-2.224825000
C	-3.329022000	0.482692000	0.381607000
C	-3.450722000	0.459976000	2.923791000
C	-4.812323000	0.654160000	0.344739000
C	-5.235804000	-0.637217000	-3.094142000
C	-5.384147000	1.914353000	0.524984000
C	-5.641568000	-0.454085000	0.173402000
C	-6.765760000	2.064321000	0.520530000
C	-7.022943000	-0.303007000	0.169301000
C	-7.587345000	0.955745000	0.342052000
H	0.000000000	0.000000000	9.352488000
H	0.111684000	-2.140822000	8.109708000
H	0.115112000	-2.137702000	5.636664000
H	2.728448000	-0.325459000	4.987472000
H	4.516726000	-0.582658000	3.025775000
H	4.742640000	-2.777316000	0.661102000
H	5.204248000	1.435143000	0.031342000
H	7.200874000	-3.047519000	0.656553000
H	7.655124000	1.170444000	0.022110000
H	8.664801000	-1.073101000	0.337058000
H	-0.111684000	2.140822000	8.109708000
H	-0.115112000	2.137702000	5.636664000

H	-2.728448000	0.325459000	4.987472000
H	-4.516726000	0.582658000	3.025775000
H	-4.742640000	2.777316000	0.661102000
H	-5.204248000	-1.435143000	0.031342000
H	-7.200874000	3.047519000	0.656553000
H	-7.655124000	-1.170444000	0.022110000
H	-8.664801000	1.073101000	0.337058000
N	1.015018000	-2.761619000	-5.510142000
N	1.252523000	-0.184677000	-0.854916000
N	1.419702000	-0.230173000	1.975736000
N	5.752270000	1.664581000	-3.225799000
N	-1.015018000	2.761619000	-5.510142000
N	-1.252523000	0.184677000	-0.854916000
N	-1.419702000	0.230173000	1.975736000
N	-5.752270000	-1.664581000	-3.225799000
S	1.798217000	-0.124468000	-4.761382000
S	4.535659000	-0.894456000	-2.914018000
S	-1.798217000	0.124468000	-4.761382000
S	-4.535659000	0.894456000	-2.914018000

5. Au[TPC(SCN)₄] anion

Au	0.000000000	0.000000000	0.661742000
C	0.000000000	0.000000000	4.018035000
C	0.000000000	0.000000000	5.507176000
C	0.000000000	0.000000000	8.314683000
C	0.327939000	-1.155109000	6.223609000
C	0.328305000	-1.156277000	7.614075000
C	0.715101000	-0.118950000	-2.104395000
C	1.233878000	-0.208881000	3.374585000
C	1.528377000	-1.623185000	-5.296355000
C	1.788257000	-0.283892000	-2.985866000
C	2.531582000	-0.352127000	3.956657000
C	2.599844000	-0.444744000	-0.827667000
C	2.749311000	-0.460745000	1.686963000
C	2.964363000	-0.507489000	-2.203659000
C	3.325405000	-0.548900000	0.403854000
C	3.443934000	-0.503325000	2.946495000
C	4.807766000	-0.710309000	0.365288000
C	5.260479000	0.501662000	-3.195008000
C	5.402509000	-1.941535000	0.650910000
C	5.633717000	0.378532000	0.077212000
C	6.784996000	-2.084866000	0.632927000
C	7.015832000	0.237429000	0.053004000
C	7.596184000	-0.995535000	0.329980000
C	-0.327939000	1.155109000	6.223609000
C	-0.328305000	1.156277000	7.614075000
C	-0.715101000	0.118950000	-2.104395000
C	-1.233878000	0.208881000	3.374585000
C	-1.528377000	1.623185000	-5.296355000

C	-1.788257000	0.283892000	-2.985866000
C	-2.531582000	0.352127000	3.956657000
C	-2.599844000	0.444744000	-0.827667000
C	-2.749311000	0.460745000	1.686963000
C	-2.964363000	0.507489000	-2.203659000
C	-3.325405000	0.548900000	0.403854000
C	-3.443934000	0.503325000	2.946495000
C	-4.807766000	0.710309000	0.365288000
C	-5.260479000	-0.501662000	-3.195008000
C	-5.402509000	1.941535000	0.650910000
C	-5.633717000	-0.378532000	0.077212000
C	-6.784996000	2.084866000	0.632927000
C	-7.015832000	-0.237429000	0.053004000
C	-7.596184000	0.995535000	0.329980000
H	0.000000000	0.000000000	9.398924000
H	0.577435000	-2.058049000	5.678798000
H	0.580303000	-2.064192000	8.150911000
H	2.736289000	-0.327215000	5.014936000
H	4.510200000	-0.622608000	3.049249000
H	4.769155000	-2.791604000	0.877592000
H	5.184757000	1.338841000	-0.147176000
H	7.229439000	-3.050155000	0.849424000
H	7.636381000	1.090938000	-0.194096000
H	8.674474000	-1.107630000	0.307684000
H	-0.577435000	2.058049000	5.678798000
H	-0.580303000	2.064192000	8.150911000
H	-2.736289000	0.327215000	5.014936000
H	-4.510200000	0.622608000	3.049249000
H	-4.769155000	2.791604000	0.877592000
H	-5.184757000	-1.338841000	-0.147176000
H	-7.229439000	3.050155000	0.849424000
H	-7.636381000	-1.090938000	-0.194096000
H	-8.674474000	1.107630000	0.307684000
N	1.252726000	-0.222413000	-0.838562000
N	1.353371000	-2.678187000	-5.741574000
N	1.415223000	-0.285132000	2.005001000
N	5.820141000	1.491909000	-3.415591000
N	-1.252726000	0.222413000	-0.838562000
N	-1.353371000	2.678187000	-5.741574000
N	-1.415223000	0.285132000	2.005001000
N	-5.820141000	-1.491909000	-3.415591000
S	1.788049000	-0.045192000	-4.728958000
S	4.504388000	-0.990750000	-2.895707000
S	-1.788049000	0.045192000	-4.728958000
S	-4.504388000	0.990750000	-2.895707000

6. Au[TPC(SCN)₄] cation

Au	0.000000000	0.000000000	0.687296000
C	0.000000000	0.000000000	4.032605000

C	0.000000000	0.000000000	5.508048000
C	0.000000000	0.000000000	8.305129000
C	0.275015000	-1.994771000	-4.630479000
C	0.600356000	-1.044856000	7.608449000
C	0.611542000	-1.041898000	6.221775000
C	0.704746000	-0.173472000	-2.054197000
C	1.254898000	-0.130239000	3.377132000
C	1.717254000	-0.639195000	-2.931175000
C	2.561447000	-0.111117000	3.957944000
C	2.574238000	-0.526401000	-0.799184000
C	2.764354000	-0.364322000	1.709196000
C	2.873208000	-0.862536000	-2.164440000
C	3.329506000	-0.521814000	0.406244000
C	3.475085000	-0.246407000	2.947049000
C	4.799821000	-0.600042000	0.323251000
C	5.106420000	-0.479042000	-3.567320000
C	5.494628000	0.362077000	-0.423165000
C	5.521508000	-1.591588000	1.002392000
C	6.878907000	0.338882000	-0.480044000
C	6.904928000	-1.625937000	0.919461000
C	7.586563000	-0.657746000	0.185614000
C	-0.275015000	1.994771000	-4.630479000
C	-0.600356000	1.044856000	7.608449000
C	-0.611542000	1.041898000	6.221775000
C	-0.704746000	0.173472000	-2.054197000
C	-1.254898000	0.130239000	3.377132000
C	-1.717254000	0.639195000	-2.931175000
C	-2.561447000	0.111117000	3.957944000
C	-2.574238000	0.526401000	-0.799184000
C	-2.764354000	0.364322000	1.709196000
C	-2.873208000	0.862536000	-2.164440000
C	-3.329506000	0.521814000	0.406244000
C	-3.475085000	0.246407000	2.947049000
C	-4.799821000	0.600042000	0.323251000
C	-5.106420000	0.479042000	-3.567320000
C	-5.494628000	-0.362077000	-0.423165000
C	-5.521508000	1.591588000	1.002392000
C	-6.878907000	-0.338882000	-0.480044000
C	-6.904928000	1.625937000	0.919461000
C	-7.586563000	0.657746000	0.185614000
H	0.000000000	0.000000000	9.388505000
H	1.056545000	-1.866320000	8.147552000
H	1.065183000	-1.865317000	5.683952000
H	2.772991000	0.019934000	5.005900000
H	4.547491000	-0.243447000	3.045099000
H	4.947000000	1.138271000	-0.943804000
H	4.992328000	-2.352953000	1.562691000
H	7.402893000	1.093000000	-1.053940000
H	7.454363000	-2.410776000	1.425131000
H	8.668201000	-0.682847000	0.129694000

H	-1.056545000	1.866320000	8.147552000
H	-1.065183000	1.865317000	5.683952000
H	-2.772991000	-0.019934000	5.005900000
H	-4.547491000	0.243447000	3.045099000
H	-4.947000000	-1.138271000	-0.943804000
H	-4.992328000	2.352953000	1.562691000
H	-7.402893000	-1.093000000	-1.053940000
H	-7.454363000	2.410776000	1.425131000
H	-8.668201000	0.682847000	0.129694000
N	0.647034000	2.692951000	-4.614787000
N	1.258721000	-0.160466000	-0.810680000
N	1.425144000	-0.276922000	2.024771000
N	5.687619000	0.352738000	-4.122641000
N	-0.647034000	-2.692951000	-4.614787000
N	-1.258721000	0.160466000	-0.810680000
N	-1.425144000	0.276922000	2.024771000
N	-5.687619000	-0.352738000	-4.122641000
S	1.607922000	-0.950226000	-4.666933000
S	4.300744000	-1.727393000	-2.756476000
S	-1.607922000	0.950226000	-4.666933000
S	-4.300744000	1.727393000	-2.756476000

5.5 Conclusions

The newly synthesized 2,3,17,18-tetra(thiocyano)corrolato-Au(III) complexes (**1–2**) are diamagnetic in nature as is evident from their sharp peaks with normal chemical shifts in their NMR spectra. Key features of the structure are similar to those observed in previously obtained structures for other corrolato-Au(III) complexes. Thus, the Au-N bond distances are 1.95 ± 0.01 Å. Unlike Cu corroles, which are invariably saddled, **2**, like other Au corroles, is essentially planar with C2-C1-C19-C18 and C8-C9-C11-C12 dihedrals around only 6.7° and 14.7° . The saddling of Cu corroles reflects ligand noninnocence, as noted elsewhere, a scenario that does not apply to Au corroles. The observed redox potentials are dramatically upshifted, by roughly half a volt, relative to those of the non-thiocyanated complexes. These upshifts are consistent with the Hammett σ_p and σ_m of the SCN groups, which are about the same as those of CN and CF₃ groups. Tetrathiocyanation has a dramatic impact on the UV-vis spectra of the corrolato-Au(III) complexes. The most notable effect is on the extinction coefficient of the Soret band,

which is dramatically weaker in the tetrathiocyano complexes. By comparison, the Q band intensities are much less affected. These differences translate to nearly equal intensities of both the Soret and Q bands for **1** and **2**, an uncommon occurrence for simple porphyrins and corroles, which follow the Gouterman four-orbital model. Compounds **1** and **2** exhibit a phosphorescence band peaked at ca. 900 nm in degassed toluene solution and corresponding to a lifetime of 10 μ s for both complexes. A strong solvent effect on the emission quantum yield was observed. Compounds **1** and **2** can efficiently sensitize singlet oxygen with singlet oxygen production quantum yields of 57% and 46 % respectively in chloroform solution. These results indicate that these molecules will have potential applications in the field of PDT and other bioimaging applications.

5.6 Experimental Section

5.6.1 Materials:

The precursor's pyrrole, *p*-chloranil, aldehydes were purchased from Aldrich, USA and gold acetate (99.99%) from Alfa Aesar. NH₄SCN (>98.5% purity), pyridine, acetonitrile (HPLC) was purchased from Merck chemicals. Other chemicals were of reagent grade. Hexane, CH₂Cl₂, CH₃CN were distilled from KOH and CaH₂ respectively. For spectroscopy studies, HPLC grade solvents were used. For the synthesis of FB corroles, a protocol developed by Gryko et al. was used.^[50] The synthetic methodologies and full spectroscopic characterization of free base corroles: 2,3,17,18-tetra (thiocyano) -10-(4-bromophenyl) -5,15-bis(4-cyanophenyl) corrole and 2,3,17,18-tetrathiocyano -10-(4,7-dimethoxynaphthalen-1-yl) -5,15-bis(4-cyanophenyl) corrole were reported earlier by us.^[45]

5.6.2 Physical Measurements:

The elemental analyses were carried out with a Euro EA elemental analyser. UV–Vis spectral studies were performed on a Perkin–Elmer LAMBDA-750 spectrophotometer. Emission spectra were performed on an Edinburgh FLS920 spectrofluorometer equipped with a Ge-detector for emission in the NIR spectral region, using optical cell of 1 cm path length. Luminescence lifetime were recorded with an Edinburgh FS5 equipped with a PMT980. Emission quantum yields were measured following Demas and Crosby method^[51] (standard used: HITCI (1,1',3,3,3',3'-hexamethyl-indotricarbocyanine iodide) in EtOH $\Phi = 0.30$).^[52] The singlet oxygen generation^[35] from the chloroform solutions was measured using a chloroform solution of 5,10,15,20-Tetraphenyl-21H,23H-porphine (TPP) as the reference with a singlet oxygen production yield of 55%.^[53] The three solutions have been excited in an isosbestic point (615 nm) and the singlet oxygen emissions were detected in a range from 1220 to 1330 nm and compared. FT–IR spectra were recorded on a Perkin–Elmer spectrophotometer with samples prepared as KBr pellets. The NMR measurements were carried out using a Bruker 400 MHz NMR spectrometer. Chemical shifts are expressed in parts per million (ppm) relative to residual chloroform ($\delta = 7.26$). Electrospray mass spectra were recorded on a Bruker Micro TOF–QII mass spectrometer. Cyclic voltammetry measurements were carried out using a CS350 electrochemical test system (China). A glassy carbon working electrode, a platinum wire as an auxiliary electrode, and an Ag–AgCl reference electrode were used in a three-electrode configuration. Tetrabutylammonium perchlorate (TBAP) was the supporting electrolyte (0.1 M), and the concentration of the solution was 10^{-3} M with respect to the complex. The half-wave potential E_{298}^0 was set equal to 0.5 ($E_{pa} + E_{pc}$), where E_{pa} and E_{pc} are anodic and cathodic cyclic voltammetric peak potentials, respectively. The scan rate used was 100 mV s^{-1} .

5.6.3 Crystal Structure Determination:

Single crystals of **2** were grown from the solution of **2** in dichloromethane-hexane mixture (1:1), followed by slow evaporation under atmospheric conditions. ORTEP diagram of **2** is shown in Figure 5.7 (hydrogen atoms are omitted for clarity). Ellipsoids are drawn at 50% probability. The crystal data of **2** were collected on a Rigaku Oxford diffractometer (Cu $K\alpha$ radiation) at 100 K. Selected data collection parameters and other crystallographic results are summarized in Table 5.1. All data were corrected for Lorentz polarization and absorption effects. The program package SHELXTL^[54] was used for structure solution and full matrix least squares refinement on F^2 . Hydrogen atoms were included in the refinement using the riding model. Contributions of H atoms for the water molecules were included but were not fixed. Disordered solvent molecules were taken out using SQUEEZE command in PLATON.^[55] CCDC 2122129 contains the supporting crystallographic data for **2**. These data can be obtained free of charge via www.ccdc.cam.ac.uk/data_request/cif.

5.6.4 Syntheses:

Synthesis of **2**, **3**, **17**, **18**-tetra (thiocyano) -**10**- (4-bromophenyl)- **5**, **15**-bis (4-cyanophenyl) corrolato- Au(III)}, **1**

25 mg (0.028 mmol) of 2,3,17,18-tetra(thiocyano)- 10- (4-bromophenyl)- 5,15-bis (4-cyanophenyl) corrole was dissolved in 5 ml of acetonitrile, and then 60 mg (0.16 mmol) of gold acetate was added to it followed by 12 ml of pyridine. The reaction mixture was stirred at room temperature for 1 h in air. After that, the solvent was evaporated, and the brown color crude product was subjected to column chromatography using a silica gel (100–200 mesh) column. The desired product (reddish blue) was eluted by using a mixture of 93% DCM and 7% acetonitrile. The final form of the compound was obtained as pinkish crystalline materials.

For 2, 3, 17, 18-tetra (thiocyano) – 10 – (4-bromophenyl)–5, 15-bis (4-cyanophenyl) corrolato-Au(III)}, 1

Yield: 33% (10 mg). Anal. Calcd for $C_{43}H_{16}AuBrN_{10}S_4$ (**2**): C, 47.92; H, 1.50; N, 13.00. Found: C, 47.81; H, 1.42; N, 13.16. λ_{\max}/nm ($\epsilon/M^{-1}cm^{-1}$) in CH_2Cl_2 : 403 (44014), 421 (40845), 537 (12233), 554 (17348), 578 (37719), 595 (44950) (Figure 5.9). 1H NMR (400 MHz, Chloroform-*d*) δ 8.50 (d, $J = 5.1$ Hz, 2H), 8.43 (d, $J = 5.1$ Hz, 2H), 8.23 – 8.08 (m, 8H), 7.93 (d, $J = 8.0$ Hz, 2H), 7.86 (d, $J = 8.1$ Hz, 2H) (Figure 5.1). HRMS (ESI) m/z : $[2+Na]^+$ Calcd for $C_{43}H_{16}AuBrN_{10}S_4Na$ 1098.9183; Found 1098.7538 (Figure 5.3).

Synthesis of 2, 3, 17, 18-tetrathiocyano – 10 – (4, 7-dimethoxynaphthalen-1-yl)-5,15-bis(4-cyanophenyl) corrolato-Au(III)}, 2

25mg (0.027 mmol) of 2,3,17,18-tetrathiocyano–10–(4,7–dimethoxynaphthalen-1-yl)-5,15-bis(4-cyanophenyl) corrole was dissolved in 4 ml of acetonitrile, and then 60 mg of gold acetate (0.16mmol) was added to it followed by 12ml of pyridine. The reaction mixture was stirred at room temperature for 1h in the air. After that, the solvent was evaporated, and the brown color crude product was subjected to column chromatography using a silica gel (100–200 mesh) column. The desired product (reddish pink) was eluted using a mixture of 95% dichloromethane and 5% acetonitrile. The final form of the compound was obtained as pinkish crystalline materials.

For 2, 3, 17, 18 – tetrathiocyano – 10 – (4,7–dimethoxynaphthalen-1-yl)-5,15-bis(4-cyanophenyl) corrolato-Au(III)}, 2

Yield: 34% (10 mg). Anal. Calcd for $C_{49}H_{23}AuN_{10}O_2S_4$ (**1**): C, 53.07; H, 2.09; N, 12.63. Found: C, 53.17; H, 2.16; N, 12.78. λ_{\max}/nm ($\epsilon / M^{-1}cm^{-1}$) in CH_2Cl_2 : 403 (45799), 422 (41020), 537 (13811), 554 (18997), 580 (43006), 596 (42058) (Figure 5.10). 1H NMR (400 MHz, Chloroform-*d*) δ 8.49 (d, $J = 9.3$ Hz, 1H), 8.31 – 8.23 (m, 4H), 8.18 (dd, $J = 15.4, 7.2$ Hz, 4H), 8.10 (d, $J = 8.3$ Hz, 4H), 7.83 (d, $J = 7.8$ Hz, 1H), 7.21 (d, $J = 2.4$ Hz,

1H), 7.05 (d, $J = 8.0$ Hz, 1H), 6.40 (d, $J = 2.7$ Hz, 1H), 4.22 (s, 3H), 3.24 (s, 3H) (Figure 5.2). HRMS (ESI) m/z : $[1+Na]^+$ Calcd for $C_{49}H_{23}AuN_{10}O_2S_4Na$ 1131.0446; Found 1131.0570 (Figure 5.4).

5.6.5 Computational Methodology:

All calculations employed scalar relativistic DFT, the ZPRA Hamiltonian, well-tested exchange-correlation functionals (OLYP,^[56,57] B3LYP,^[57,58] and B3LYP*,^[59] all-electron ZORA STO-TZ2P basis sets, tight criteria for SCF and geometry optimization cycles, fine integration grids, and, unless otherwise mentioned the COSMO solvation model and dichloromethane as solvent, all as implemented in ADF-2019.^[60-66] The solvent was omitted only in calculations of Ips^{[67-71][72]} and EAs.^[73,74] Because of the conformational flexibility of the SCN groups, great care was exercised to correctly identify the global minima of the molecules studied.

References

- [1] T. Itoh, *Chem. Rev.* **2012**, *112*, 4541–4568.
- [2] A. P. Savitsky, A. V Savitskaja, E. A. Lukyanets, S. N. Dashkevich, E. A. Makarova, in *Adv. Fluoresc. Sens. Technol. III*, SPIE, **1997**, 352–357.
- [3] F. Niedermair, S. M. Borisov, G. Zenkl, O. T. Hofmann, H. Weber, R. Saf, I. Klimant, *Inorg. Chem.* **2010**, *49*, 9333–9342.
- [4] Y. Amao, I. Okura, *J. Porphyr. Phthalocyanines* **2009**, *13*, 1111–1122.
- [5] R. P. Steer, *Dalt. Trans.* **2018**, *47*, 8517–8525.
- [6] Y. Fushimi, M. Koinuma, Y. Yasuda, K. Nomura, M. S. Asano, *Macromolecules* **2017**, *50*, 1803–1814.
- [7] M. Toganoh, T. Niino, H. Furuta, *Chem. Commun.* **2008**, 4070–4072.
- [8] K. Koren, R. I. Dmitriev, S. M. Borisov, D. B. Papkovsky, I. Klimant, *ChemBioChem* **2012**, *13*, 1184–1190.
- [9] H. Kurokawa, H. Ito, M. Inoue, K. Tabata, Y. Sato, K. Yamagata, S. Kizaka-Kondoh, T. Kadonosono, S. Yano, M. Inoue, *Sci. Rep.* **2015**, *5*, 1–13.
- [10] D. B. Papkovsky, G. V Ponomarev, W. Trettnak, P. O’Leary, *Anal. Chem.* **1995**, *67*, 4112–4117.
- [11] X. Wang, O. S. Wolfbeis, *Chem. Soc. Rev.* **2014**, *43*, 3666–3761.
- [12] S. Shao, V. Rajendiran, J. F. Lovell, *Coord. Chem. Rev.* **2019**, *379*, 99–120.
- [13] R. Bonnett, M. Berenbaum, *Photosensit. Compd. their Chem. Biol. Clin. use* **1989**, *146*, 40–53.
- [14] R. K. Pandey, T. J. Dougherty, D. Kessel, *Handbook of Photodynamic Therapy: Updates on Recent Applications of Porphyrin-Based Compounds*, World Scientific, **2016**.
- [15] R. Pereira, P.M., Tomé, J.P. and Fernandes, *Molecular Targeted Photodynamic*

Therapy for Cancer, Handbook Of Porphyrin Science, **2016**.

- [16] S. Patra, B.; Mondal, S.; Kar, **n.d.**, 1–24.
- [17] A. Mahammed, Z. Gross, *Coord. Chem. Rev.* **2019**, *379*, 121–132.
- [18] S. Nardis, F. Mandoj, M. Stefanelli, R. Paolesse, *Coord. Chem. Rev.* **2019**, *388*, 360–405.
- [19] A. B. Alemayehu, K. E. Thomas, R. F. Einrem, A. Ghosh, *Acc. Chem. Res.* **2021**, *54*, 3095–3107.
- [20] A. Ghosh, *Chem. Rev.* **2017**, *117*, 3798–3881.
- [21] R. Orłowski, D. Gryko, D. T. Gryko, *Chem. Rev.* **2017**, *117*, 3102–3137.
- [22] Y. Fang, Z. Ou, K. M. Kadish, *Chem. Rev.* **2017**, *117*, 3377–3419.
- [23] K. Fujino, Y. Hirata, Y. Kawabe, T. Morimoto, A. Srinivasan, M. Toganoh, Y. Miseki, A. Kudo, H. Furuta, *Angew. Chemie* **2011**, *123*, 6987–6991.
- [24] C. M. Lemon, *Pure Appl. Chem.* **2020**, *92*, 1901–1919.
- [25] J. F. B. Barata, M. G. P. M. S. Neves, M. A. F. Faustino, A. C. Tomé, J. A. S. Cavaleiro, *Chem. Rev.* **2017**, *117*, 3192–3253.
- [26] A. B. Alemayehu, A. Ghosh, *J. Porphyr. Phthalocyanines* **2011**, *15*, 106–110.
- [27] E. Rabinovich, I. Goldberg, Z. Gross, *Chem. Eur. J.* **2011**, *17*, 12294–12301.
- [28] K. Sudhakar, A. Mizrahi, M. Kosa, N. Fridman, B. Tumanskii, M. Saphier, Z. Gross, *Angew. Chemie Int. Ed.* **2017**, *56*, 9837–9841.
- [29] C. M. Lemon, D. C. Powers, P. J. Brothers, D. G. Nocera, *Inorg. Chem.* **2017**, *56*, 10991–10997.
- [30] K. E. Thomas, K. J. Gagnon, L. J. McCormick, A. Ghosh, *J. Porphyr. Phthalocyanines* **2018**, *22*, 596–601.
- [31] R. F. Einrem, E. T. Jonsson, S. J. Teat, N. S. Settineri, A. B. Alemayehu, A. Ghosh, *RSC Adv.* **2021**, *11*, 34086–34094.
- [32] X. Zhan, W. Lee, K. Sudhakar, D. Kim, A. Mahammed, D. G. Churchill, Z. Gross,

-
- Inorg. Chem.* **2021**, *60*, 8442–8446.
- [33] J. Turner, K. E. Thomas, H. Vazquez-Lima, A. Ghosh, *J. Inorg. Biochem.* **2022**, *231*, 111783.
- [34] A. Thomas, K. E.; Alemayehu, A. B.; Conradie, J.; Beavers, C.; Ghosh, *Inorg. Chem.* **2011**, *50*, 12844–12851.
- [35] K. E. Thomas, C. M. Beavers, A. Ghosh, *Mol. Phys.* **2012**, *110*, 2439–2444.
- [36] S. Lai, L. Wang, C. Yang, M. Chan, X. Guan, C. Kwok, C. Che, *Adv. Funct. Mater.* **2014**, *24*, 4655–4665.
- [37] R. D. Teo, H. B. Gray, P. Lim, J. Termini, E. Domeshek, Z. Gross, *Chem. Commun.* **2014**, *50*, 13789–13792.
- [38] A. B. Alemayehu, N. U. Day, T. Mani, A. B. Rudine, K. E. Thomas, O. A. Gederaas, S. A. Vinogradov, C. C. Wamser, A. Ghosh, *ACS Appl. Mater. Interfaces* **2016**, *8*, 18935–18942.
- [39] W. Sinha, M. G. Sommer, M. van der Meer, S. Plebst, B. Sarkar, S. Kar, *Dalt. Trans.* **2016**, *45*, 2914–2923.
- [40] J. Capar, J. Zonneveld, S. Berg, J. Isaksson, K. J. Gagnon, K. E. Thomas, A. Ghosh, *J. Inorg. Biochem.* **2016**, *162*, 146–153.
- [41] M. Soll, K. Sudhakar, N. Fridman, A. Müller, B. Röder, Z. Gross, *Org. Lett.* **2016**, *18*, 5840–5843.
- [42] R. W.-Y. Sun, C.-M. Che, *Coord. Chem. Rev.* **2009**, *253*, 1682–1691.
- [43] L. He, T. Chen, Y. You, H. Hu, W. Zheng, W. Kwong, T. Zou, C. Che, *Angew. Chemie* **2014**, *126*, 12740–12744.
- [44] A. D. Lammer, M. E. Cook, J. L. Sessler, *J. Porphyr. Phthalocyanines* **2015**, *19*, 398–403.
- [45] K. Sahu, S. Mondal, S. M. Mobin, S. Kar, *J. Org. Chem.* **2021**, *86*, 3324–3333.
-

-
- [46] H. Echizen, E. Sasaki, K. Hanaoka, *Biomolecules* **2021**, *11*, 1553.
- [47] K. E. Thomas, J. Conradie, L. K. Hansen, A. Ghosh, **2011**, 1865-1870
- [48] S. Ganguly, A. Ghosh, *Acc. Chem. Res.* **2019**, *52*, 2003–2014.
- [49] C. Hansch, A. Leo, R. W. Taft, *Chem. Rev.* **1991**, *91*, 165–195.
- [50] B. Koszarna, D. T. Gryko, *J. Org. Chem.* **2006**, *71*, 3707–3717.
- [51] G. A. Crosby, J. N. Demas, *J. Phys. Chem.* **1971**, *75*, 991–1024.
- [52] D. F. Eaton, *Pure Appl. Chem* **1998**, *60*, 1107–1114.
- [53] F. Wilkinson, W. P. Helman, A. B. Ross, *J. Phys. Chem. Ref. data* **1993**, *22*, 113–262.
- [54] G. M. Sheldrick, *Acta Crystallogr. Sect. A Found. Crystallogr.* **2008**, *64*, 112–122.
- [55] P. V Van der Sluis, A. L. Spek, *Acta Crystallogr. Sect. A Found. Crystallogr.* **1990**, *46*, 194–201.
- [56] C. Lee, W. Yang, R. G. Parr, *Phys. Rev. B* **1988**, *37*, 785.
- [57] N. C. Handy, A. J. Cohen, *Mol. Phys.* **2001**, *99*, 403–412.
- [58] A. Becke, *Chem. Phys* **n.d.**, *98*, 5648.
- [59] M. Reiher, O. Salomon, B. Artur Hess, *Theor. Chem. Acc.* **2001**, *107*, 48–55.
- [60] S. Grimme, J. Antony, S. Ehrlich, H. Krieg, *J. Chem. Phys.* **2010**, *132*, 154104.
- [61] A. Klamt, G. Schuurmann, *Klamt. AJ Chem. Phys* **1997**, *106*, 6622.
- [62] A. Klamt, *J. Phys. Chem* **1995**, *99*, 2224–2235.
- [63] E. van Lenthe, E.-J. Baerends, J. G. Snijders, *J. Chem. Phys.* **1993**, *99*, 4597–4610.
- [64] E. van Lenthe, E.-J. Baerends, J. G. Snijders, *J. Chem. Phys.* **1994**, *101*, 9783–9792.
- [65] E. Van Lenthe, A. Ehlers, E.-J. Baerends, *J. Chem. Phys.* **1999**, *110*, 8943–8953.
- [66] G. t Te Velde, F. M. Bickelhaupt, E. J. Baerends, C. Fonseca Guerra, S. J. A. van Gisbergen, J. G. Snijders, T. Ziegler, *J. Comput. Chem.* **2001**, *22*, 931–967.
- [67] J. Conradie, H. Vazquez-Lima, A. B. Alemayehu, A. Ghosh, *ACS Phys. Chem. Au* **2021**, *2*, 70-78.
-

- [68] A. Ghosh, J. Almlöf, *Chem. Phys. Lett.* **1993**, *213*, 519–521.
- [69] A. Ghosh, *J. Am. Chem. Soc.* **1995**, *117*, 4691–4699.
- [70] A. Ghosh, *J. Phys. Chem. B* **1997**, *101*, 3290–3297.
- [71] A. Ghosh, T. Vangberg, *Theor. Chem. Acc.* **1997**, *97*, 143–149.
- [72] A. Ghosh, *Acc. Chem. Res.* **1998**, *31*, 189–198.
- [73] H. Ryeng, E. Gonzalez, A. Ghosh, *J. Phys. Chem. B* **2008**, *112*, 15158–15173.
- [74] K. E. Thomas, H. Vazquez-Lima, Y. Fang, Y. Song, K. J. Gagnon, C. M. Beavers, K. M. Kadish, A. Ghosh, *Chem. Eur. J.* **2015**, *21*, 16839–16847.

Summary and Future prospects

Corroles are **tetrapyrrole macrocycles** having a 18π electron aromatic system as porphyrins have recently gained a lot of research interest for their interesting structural and spectroscopic properties. This thesis contains some of the less explored areas in the corrole field. The thesis mainly focused on β functionalization of corroles, and the corresponding metalated derivatives have been explored on the basis of their physical and biological significance. In separate studies, a synthetic protocol for the **regioselective** thiocyanation of corroles has been designed. The resulting thiocyanato appended corrole turned out to be a good corrole-based precursor for the facile synthesis of thiol-protected gold nanoparticles (**AuNPs**). A new method of activating corrole macrocycles via *in situ* generated SCN radical has been developed under very mild conditions in RT. This photo-redox reaction resulted in the generation of tetra-thiocyanated corrole. The photophysical properties of the newly synthesized tetra-thiocyanato corroles are dramatically altered from the parent corroles. The absorption feature of these modified corrole derivatives (both position and intensity) bears a nice similarity with the chlorophyll-*a* macrocycle. The tetrathiocyanatocorroles Ag(III) have been investigated for C-H \cdots Ag interactions. It was observed that the $\sigma_{\text{C-H}}$ orbital overlaps with the vacant d-orbital of Ag with interaction energy of 17.93 kJ/mol. The filled d-orbital of Ag overlaps with the $\sigma^*_{\text{C-H}}$ orbital with an interaction energy of 4.79 kJ/mol. Noncovalent interactions are frequently used to build various supramolecular structures with specific functions. These gold(III) corroles showed phosphorescence in the near-infrared region (at ca. 900 nm) at ambient temperature with relatively long phosphorescent lifetimes of 10 μs . In addition, these compounds can efficiently sensitize singlet oxygen with singlet oxygen production quantum yields of 57% and 46 %,

respectively, in chloroform solution are suitable windows for **PDT** and other bioimaging applications.

Currently, efforts are laid to investigate the corrole complexes of abundant and non-precious metals for their utilization as catalysts in the activation of small molecules such as water, oxygen, carbon dioxide, etc.